This dissertation is submitted for the degree of Doctor of Philosophy

Development of a method for estimating methane gas emissions at high resolution

Sarah Connors

St. Catharine's College

August 2015

Centre for Atmospheric Science

Department of Chemistry

University of Cambridge

Supervisor

Dr. Neil Harris

Examiners

Prof. Roderic Jones

Dr. Matthew Rigby

Declaration

This dissertation is the result of my own work and includes nothing which is the outcome of work done in collaboration except as declared in the Preface and specified in the text. It is not substantially the same as any that I have submitted, or, is being concurrently submitted for a degree or diploma or other qualification at the University of Cambridge or any other University or similar institution except as declared in the Preface and specified in the text. I further state that no substantial part of my dissertation has already been submitted, or, is being concurrently submitted for any such degree, diploma or other qualification at the University of Cambridge or any other University of similar institution except as declared in the Preface and specified in the text. It does not exceed 60 000 words (prescribed word limit set by the Degree Committee for the Faculty of Physics & Chemistry).

Sarah Connors August 2015

Acknowledgements

I would like to thank my funding body, the UK Natural Environment Research Council (NERC) for financing this PhD. I also thank the Department of Environment, Food and Rural Affairs (DEFRA) and the Royal Society for additional funding towards the GC-FID instruments. Thank you to the Haddenham Holy Trinity Church and the Tilney All Saints Church for allowing us to install the GC-FIDs into their church towers.

On a more personal level, I would like to thank my supervisor, Neil Harris for his support, guidance and advice. I would also like to thank Alistair Manning for his help with running InTEM. I would not have been able to write this thesis without the two of you.

My thanks go to the Centre for Atmospheric Science (CAS) which has been a great working environment. I have learnt so much about an area of science that I love. Thank you to Matthew Ashfold for his help with the coding, and for his patience whilst I got to grips with it! Thank you to Alex Archibald for helping me with the NAME model in the early days. My thanks go to Andrew Robinson and Stuart Riddick for all their support with the GC-FID instruments. Thank you, Stuart for driving us round East Anglia, before sunrise, to collect air samples. Finally, thank you to Jack Gibb and Arthur Zielinski for proof reading this thesis. I really appreciate it.

For my mum, my dad, and my brother.

Abstract

Methane is the second most important anthropogenic greenhouse gas, with a radiative warming of 0.97 [0.74-1.20] W m^{-2} (Stocker et al., 2013a) and a global warming potential of 21 times that of CO_2 over a 100 year timescale (Reay et al., 2010). Its significance to climate change is significant whereas our current understanding and quantification of its sources and sinks lack completeness.

This thesis explains the development of novel technique to estimate methane emissions at high spatial resolution. There is a growing need for comparisons between emission estimates produced using bottom-up and top-down techniques. In response to this, an inversion approach, InTEM, was adapted to estimate methane emissions for the East of England at high spatial resolution. InTEM incorporates in situ atmospheric methane measurements and computer dispersion modelling into a statistical technique. Methane emission estimates are inferred using cost function analysis within a simulated annealing method.

This thesis presents results covering a two year period (July 2012 - June 2014) in which atmospheric methane concentrations were recorded at 1 - 2 minute time steps at four locations within East Anglia. Precise measurements are obtained using gas chromatographs with flame ionisation detectors (GC-FID) for all sites except one, which uses a Picarro cavity ring down spectroscopy (CRDS) instrument. The UK Met Office's NAME dispersion model is used within InTEM to represent the physical atmospheric processes which occur throughout this period.

Methane concentrations are shown to vary over different time frames and are dependent on various meteorological variables, particularly boundary layer height and wind speed. A case study into methane concentration at the Haddenham site shows influence from local landfill sources. Isotopic analysis from whole air samples give a $\delta^{13}C$ isotopic signal of -58.3 $\pm$2 ‰ at the Haddenham site and -59.2 $\pm$2 ‰ at the nearby landfill.

Emission estimates for the East of England are calculated at varying spatial resolutions, on annual and seasonal time frames. County scale methane emission

estimates are produced and directly compared with the UK National Atmospheric Emissions Inventory (NAEI). Estimates between the InTEM inventory and the NAEI are shown to be similar in counties close to the observation sites. The Norfolk, Suffolk and Cambridge countries are estimated to produce 80.4 ±3.3 kt yr^{-1} of methane between June 2013 - May 2014 (NAEI equivalent of 89.6 kt yr^{-1}).

Multiple site sensitivity analysis shows that all four sites are necessary for the county methane estimates but coarser estimates can be observed using a sub-selection of sites. Individual site biases were shown to have an impact on 1 - 2 site inversions but the four site results minimised these biases.

Contents

Abbreviations

agl = Above Ground Level

agric = Agriculture

BL = Boundary Layer

CCM = Chemistry Climate Model

CRDS = Cavity Ring Down Spectrometer

DECC = Department for Energy and Climate Change

DEFRA = Department for Environment, Food and Rural Affairs

DJF = December, January, February (Winter months)

domcom = Domestic Combustion

EA = East Anglia

ENE = East North East

energyprod = Energy Production

EPA = Environment Protection Agency (US)

ESE = East South East

GC-FID = Gas Chromatography - Flame Ionisation Detector

GHG = Greenhouse Gas

GWP = Global Warming Potential

HAD, HD = Haddenham

HC = Hydrocarbon

indcom = Industrial Combustion

indproc = Industrial Processes

InTEM = Inversion Technique for Emissions Modelling

JJA = June, July, August (Summer months)

kt = Kilotonnes

L = Litre

LULUCF = Land Use, Land Use Change ad Forestry

MAM = March, April, May (Spring months)

ML = Mixed Layer

NAEI = National Atmospheric Emissions Inventory

NAME = Numerical Atmospheric-dispersion Modelling Environment

NBL = Nocturnal Boundary Layer

ND = Nafion Dryer

NNE = North North East

NNW = North North West

NOAA = National Oceanic and Atmospheric Administration

NPL = National Physical Laboratory

NSC = Norfolk, Suffolk, Cambridgeshire

O = Oxygen

Obs = Observations

RL = Residual Layer

rm = Rolling Mean

rsd = Rolling Standard Deviation

sd = Standard Deviation

SL = Sample Loop

SON = September, October, November (Autumn months)

SSE = South South East

SSW = South South West

TAC, TN = Tacolneston

Tg = Teragrams

TIL, TY = Tilney

UEA = University of East Anglia

UCAM = University of Cambridge

UM = Unified Model

W = Water

WEY, WY = Weybourne

WNW = West North West

WSW = West South West

yr = Year

1 Introduction to methane and the atmosphere

In this chapter, the scientific basis behind this thesis is introduced. The primary focus of this chapter is to discuss the current understanding of the greenhouse gas methane and the techniques used to estimate its atmospheric budget. It begins by briefly introducing the structure of the atmosphere, which includes an overview of the boundary layer. This is followed by an explanation of the major atmospheric processes involving methane throughout the troposphere and the stratosphere. A detailed review of methane's sources and sinks is then conducted. The major techniques used to produce emission inventories for methane are introduced followed by a discussion on how uncertainty is estimated within these techniques. Finally, an overview of the UK National Atmospheric Emissions Inventory (NAEI) for methane concludes this chapter.

1.1 The structure of the atmosphere

The Earth's atmosphere is divided into four major layers classified by the vertical temperature profile (Figure 1.1). The layer closest to the Earth's surface is the troposphere, which is highest at the equator (~18 km), lowest at the poles (~8 km) and can vary with season. The troposphere contains approximately 75 % of the atmosphere's mass and is defined as having a negative vertical temperature profile due to surface heating from the sun and convection. The next layer, the stratosphere, is found between 20 - 50 km in altitude and is separated from the troposphere by the tropopause. Here temperature stratifies and then increases with altitude. The ozone maxima is found in this layer where UV radiation is absorbed and re-radiated as thermal energy. This causes the continued temperature increase with altitude. The stratopause, which exhibits temperatures similar to the Earth's surface, separates the stratosphere with the mesosphere (50 - 90 km). Like the troposphere, the mesosphere also has a negative

vertical temperature profile although this is due to a decrease in solar heating and an increase in cooling by CO_2 radiation. The final layer, the thermosphere is separated by the mesopause and experiences high temperature fluctuations due to the impact of solar winds (Gabler et al., 2009). These layers can be further subdivided based on other defining features, some of which are described in the following section.

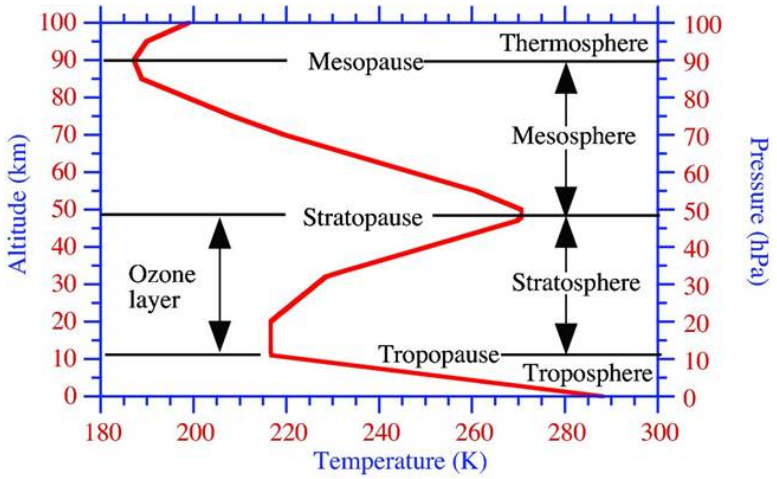

Figure 1.1: The vertical structure of the layers within the atmosphere (Jacobson, 2012). The vertical temperature profile is shown as a thick red line. x-axis shows temperature (K), y-axis shows altitude in km and hPa.

1.1.1 The boundary layer

The lowest layer of the atmosphere, found at the bottom of the troposphere is called the boundary layer (BL). It is defined as the layer that is "directly influenced by the Earth's surface, and responds to surface forcings with a timescale of an hour or less" (Stull, 1988). These surface forcings include processes like heat transfer, turbulence and pollutant emission. The BL height typically varies between 100-3000 m depending on the time of day and the region of the world, although ranges can be much higher. Marine boundary layers fluctuate less than land equivalents due to the large heat capacity of the ocean. The only exception to this being when two or more ocean currents of differing temperatures combine (Weller and Stage, 1988). BL heights found over land masses vary more with areas of high pressure usually exhibiting thinner layers than lower pressure regions. Lower pressure systems create less distinct BLs, which can be more arbitrarily defined using cloud top height. A clear and structured boundary layer, which evolves over time, can be observed in areas of relatively high pressure over land.

Figure 1.2 defines the two different structures of the BL during both day (left) and night (right). Three main sub-layers make up the BL: the mixed, the residual and the stable boundary or inversion layer. The convective mixed layer (ML) is sometimes further divided. Firstly, into the cloud and the sub-cloud layer if clouds are present. Other, less dominating, sections include a surface layer which makes up approximately 10 % of the bottom part of the BL (present in both the nighttime and daytime), and a micro layer which exists only in the bottom few centimeters above the surface. In the micro layer molecular transport is the main mixing process, whereas turbulence is considered the dominant source in other sections.

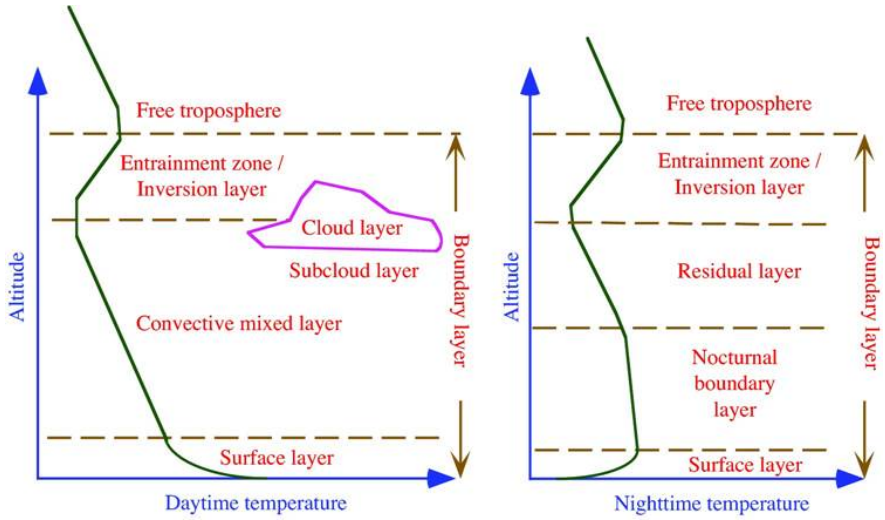

Figure 1.2: Daytime (left) and nighttime (right) boundary layer structures including vertical temperature profiles. Three main layers make up the daytime boundary layer: the convective mixed layer, the surface layer, and the inversion layer. A micro layer (not shown in this figure) is also found in the bottom few centimeters above the surface. The mixed layer can be further divided if clouds are present into the cloud layer and the sub-cloud layer. Above the BL is the entrainment zone, comprising more stable air. In the night the mixed layer splits into the residual and nocturnal boundary layer. Sourced from Jacobson, 2012.

The ML, which is convectively driven starts to form soon after sunrise and grows to a maximum height by mid-afternoon. ML height can also grow by entraining more stable air from above, known as the entrainment zone. On cloudier and colder days, the ML will reach lower heights due to less solar heating of the ground. On very cloudy days the ML can become non-turbulent or 'neutrally stratified' due to a lack of convection. Convective eddies transport pollutants vertically although they are too weak to penetrate the more stable layer above allowing emissions of pollutants to build up in concentration (Stull, 1988). Towards sunset

thermals stop and turbulence reduces causing the ML to split into a residual layer (RL) and a nocturnal boundary layer (NBL). The RL is a neutrally stratified air mass which contains the mixing concentrations from the ML during the daytime, but is no longer subject to the surface forcings. This layer does not conform to the original definition described at the beginning of this section but it is still considered part of the overall BL. Due to the neutral stratification of the residual layer, any pollutants entering this layer are subjected to weak, sporadic turbulence roughly equal in all directions, which produces cone-like shaped plumes. The NBL, which is found below the RL during the night, still experiences turbulence but on a much weaker scale than during the day. Pollutants that are emitted into this layer travel much further horizontally than vertically due it being capped by the RL. These emission plumes can be described as fanning plumes which meander more and allow concentrations to build up substantially (Stull, 1988).

1.2 A brief history of methane

Methane has been influencing climate throughout the Earth's history due to its radiative impact on the atmosphere. Energy from the Sun reaches the Earth in the form of visible and near-UV light. The Earth is approximated as a blackbody and can therefore absorb all radiation described. Some radiation is reflected back into space by the Earth's surface and atmosphere (the albedo effect). Figure 1.3 shows the expected blackbody radiance from the Earth's surface at certain temperatures (dashed lines), while the observed radiance shows some wavelengths have been absorbed (solid line). The 'troughs' at 12-17 µm, 9.6 µm and 8 µm correspond to vibrational frequencies of CO_2, O_3 and H_2O, respectively (Wayne, 1991). These gases, along with others found in the atmosphere, absorb the radiation emitted by the Earth and then re-radiate it as thermal energy. The extent of a molecule's radiative forcing is determined by their absorption properties. These are: a changing dipole when the molecule vibrates, the particular wavelength of absorption, and the degree of saturation of the wavelength. Methane has a strong radiative forcing due to its strong vibrational bend at 7.6 µm (~1 300 cm^{-1}). This wavelength is relatively unsaturated and thus is more effective at warming the atmosphere per molecule than CO_2 (Herzberg, 1945).

Methane is by far the most abundant hydrocarbon on Earth and its atmospheric concentration has been systematically measured since the 1960s when gas chromatography became a common analytical technique (Reeburgh, 2007).

Atmospheric concentrations before this time can be estimated using ice core data of which records are available for the last ~800 000 years.

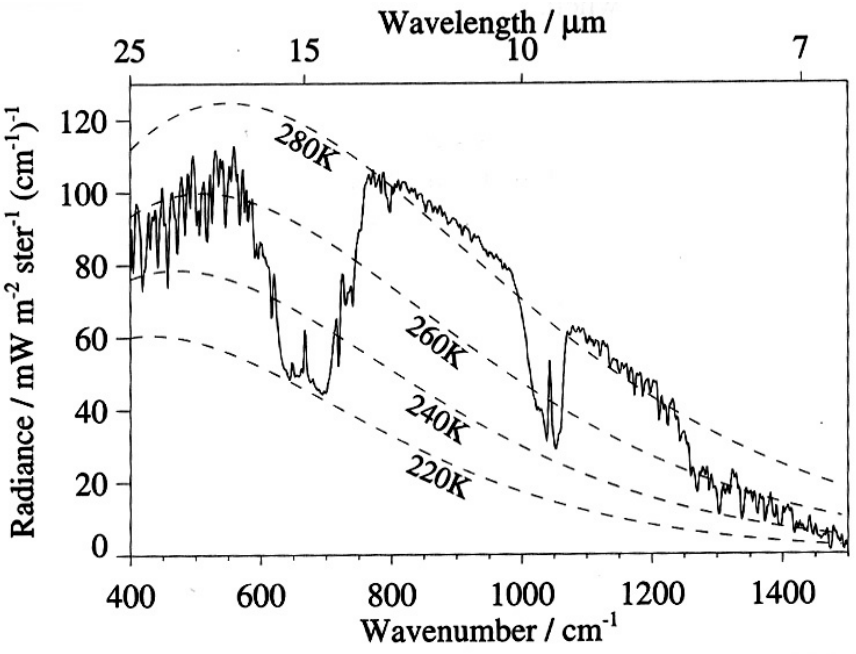

Figure 1.3: Theoretical (dashed lines set at specific temperatures) and observed (solid black line) radiance of the Earth's surface (Wayne, 1991).

Figure 1.4 shows ice core data of methane concentration over the past 10 000 years (Solomon et al., 2007). This graph demonstrates that levels have risen from ~700 part per billion by volume (ppbv) in the pre-industrial era to 1794 ppbv in 2009. Mole fractions for 2010 were 1893 / 1762 ppbv for the northern and southern hemispheres, respectively (Kirschke et al., 2013). Over this time period, the increase of more than double atmospheric methane concentrations has contributed an extra ~0.5 W m^{-2} radiative forcing (current total being 2.29 [1.13-3.33] W m^{-2}, Dlugokencky et al., 2011, Stocker et al., 2013a). Throughout the 20th century an average growth rate of ~1 % per year was observed (Badr et al., 1992). More recently, during the 1990s and 2000s, there has been reduction in the growth rate and emissions of methane seemed to be stabilising, but since 2006 rising emissions have resumed. Attribution to these changes include both varying anthropogenic and natural sources (fossil fuels and natural wetlands, respectively) although quantification of methane sources is still relatively unconstrained, which limits detailed understanding of trends on these timescales (Kirschke et al., 2013).

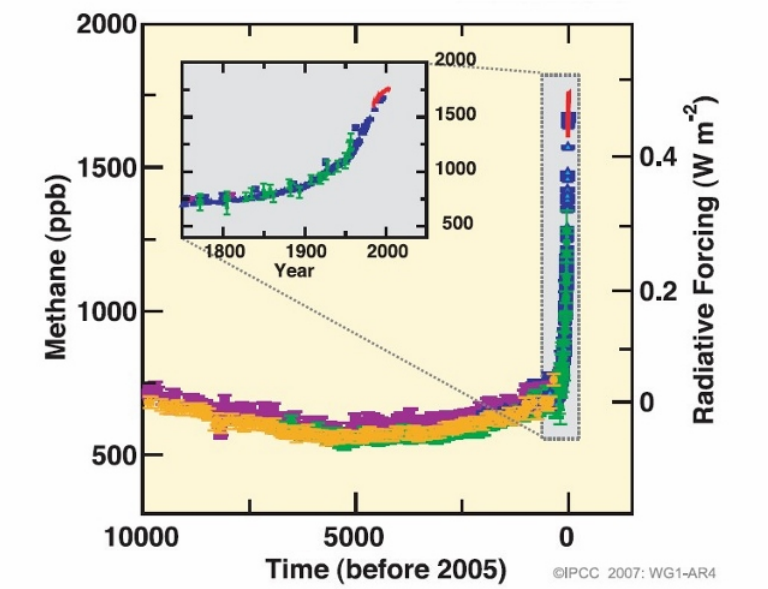

Figure 1.4: Concentration of atmospheric methane over the last 10 000 years deduced by Antarctic ice core data (Solomon et al., 2007).

The atmospheric concentration of methane is not equally distributed throughout the globe. Roughly 70 % of methane sources are found in the northern hemisphere. This gives a higher base concentration, a factor of 1.04 - 1.07 greater, than in the southern hemisphere (Badr et al., 1992). The global distribution and the season cycle of methane for the years 2000 - 2010 can bee seen in Figure 1.5. Seasonal cycles within the two hemispheres are out of phase. The southern hemisphere exhibits an annual minimum between February - March and a maximum during September - October. The northern hemisphere's annual cycle however is more complicated. Two minima at July - August and February, and two maxima at late winter and late summer, are usually observed. This is due to both sources and sinks. Both hemispheres experience a wintertime methane maxima and a summertime minima. This is due to the OH radical, methane's dominant sink, being present in higher concentrations during each hemisphere's summertime. The northern hemisphere late summer maxima is a result of wetland emissions, whereas the winter maxima is because of a rise in natural gas emissions from increased heating, and a lack of OH radical to act as a sink (Wilson et al., 2013). Methane's atmospheric lifetime is relatively short lived, estimated at 9.1 $\pm$ 0.9 years (Prather et al., 2012). Methane's vertical profile shows a stable concentration throughout the troposphere which steadily decreases once into the stratosphere because of increasingly dominant chemical reactions (more detail in the following section).

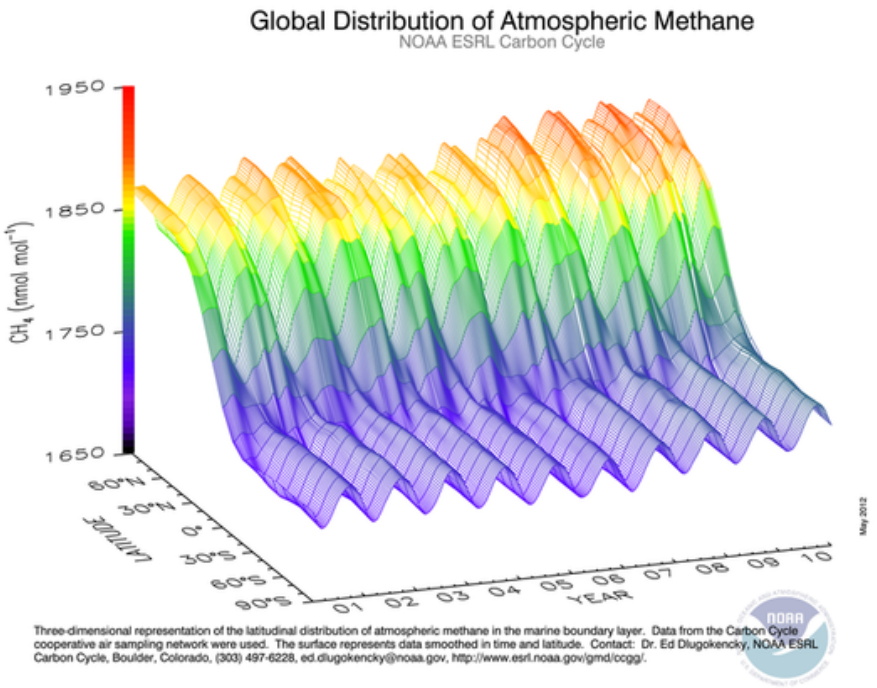

Figure 1.5: Methane 'flying carpet' figure representing global methane concentration in the marine boundary layer from 2001-2010. Figure taken from Manning et al. (2011a) but also can be sourced from E. Dlugokencky; NOAA/ESRL/GMD Carbon Cycle Greenhouse Gases Group, Boulder, CO, USA. Available at: http://www.esrl.noaa.gov/gmd/Photo_Gallery/ GMD_Figures/ccgg_figures/.

1.3 Atmospheric reactions involving methane

The chemistry of the atmosphere is largely dominated by radical reactions; predominantly OH and HO_2 (together known as HO_x). Equations 1.3.1 and 1.3.2 show the formation of the OH radical. Ozone will undergo photolysis to produce $O(^1D)$ at any wavelength reaching the Earth below 310 nm. Any higher wavelengths will produce $O(^3P)$ during ozone photolysis which does not form OH.

$$O_3 + h\nu \rightarrow O(^1D) + O_2(1\Delta g) \tag{1.3.1}$$

$$O^*(D) + H_2O \rightarrow 2OH \tag{1.3.2}$$

1.3.1 Methane in the troposphere

The OH radical is highly reactive and will oxidise many compounds, including methane. This reaction occurs throughout the troposphere and stratosphere (more dominant in the troposphere). It is thought to use up 30 % of the available OH in unpolluted atmospheres (Wayne, 1991). The first relatively stable product formed from methane oxidation is formaldehyde (CH_2O). The reaction pathway can be seen in Equations 1.3.3 - 1.3.8 (Houweling and Dentener, 2000).

$$CH_4 + OH \rightarrow CH_3 + H_2O \tag{1.3.3}$$
$$CH_3 + O_2 \rightarrow CH_3O_2 \tag{1.3.4}$$
$$CH_3O_2 + NO \rightarrow CH_3O + NO_2 \tag{1.3.5}$$
$$CH_3O + O_2 \rightarrow CH_2O + HO_2 \tag{1.3.6}$$
$$HO_2 + NO \rightarrow OH + NO_2 \tag{1.3.7}$$

OVERALL:

$$CH_4 + 2O_2 + 2NO \rightarrow CH_2O + 2NO_2 + H_2O \tag{1.3.8}$$

In this process HO_x is recycled although these reactions are highly dependent on the amount of NO_x (sum of NO and NO_2). Under low NO_x conditions Equation 1.3.5 may be out-competed by other termination reactions, for example Equations 1.3.9 and 1.3.10. As a result, if such reactions dominate in parts of the atmosphere where CH_4 levels are high and NO_x levels are low, then the concentration of OH will reduce (Houweling and Dentener, 2000). Of these two pathways, the reactions with higher NO_x dominates in the troposphere (Fiore et al., 2008).

$$CH_3O_2 + HO_2 \rightarrow CH_3O_2H + O_2 \tag{1.3.9}$$
$$CH_3O_2 + CH_3O_2 \rightarrow CH_2O + CH_3OH + O_2 \tag{1.3.10}$$

Most tropospheric OH exists in the tropics (80 %), and thus there is a geographical distance between the major methane source locations and its predominant sink (Bloss et al., 2005). Further tropospheric sinks include the oxidation via methanotrophic bacteria (discussed further in Section 1.5) and the reaction with chlorine in the marine boundary layer (Kirschke et al., 2013).

1.3.2 Methane in the stratosphere

While approximately 90 % of methane oxidation occurs in the troposphere, some oxidation reactions occur in the stratosphere. Chlorofluorocarbons (CFCs) are the main source of chlorine in the stratosphere, which will act as a catalyst in ozone destruction (Equations 1.3.11-1.3.17, Wayne, 1991)

FORMATION:

$$Cl_2 + hv \rightarrow 2Cl \tag{1.3.11}$$
$$Cl + O_3 \rightarrow ClO + O_2 \tag{1.3.12}$$

CATALYTIC CYCLE:

$$ClO + ClO + M \rightarrow (ClO)_2 + M \tag{1.3.13}$$
$$(ClO)_2 + hv \rightarrow Cl + ClOO \tag{1.3.14}$$
$$ClOO + M \rightarrow Cl + O_2 + M \tag{1.3.15}$$
$$2(Cl + O_3 \rightarrow ClO + O_2) \tag{1.3.16}$$

NET:

$$2O_3 + hv \rightarrow 3O_2 \tag{1.3.17}$$

Methane can terminate this catalytic reaction from occurring by reacting with chlorine to produce the relatively stable compound HCl. However, the methyl radical also produced can go on to activate another chlorine molecule (Equations 1.3.18 and 1.3.19).

$$Cl + CH_4 \rightarrow CH_3 + HCl \tag{1.3.18}$$
$$CH_3 + Cl_2 \rightarrow Cl_3Cl + Cl \tag{1.3.19}$$

Methane will also react directly with O(^{1}D) both in the troposphere and the stratosphere. This reaction is more dominant in the stratosphere than the troposphere due to O(^{1}D) being more abundant (Equations 1.3.20 and 1.3.21).

$$CH_4 + O(^1D) \rightarrow CH_3 + OH \tag{1.3.20}$$

$$CH_4 + O(^1D) \rightarrow CH_2O + H_2 \tag{1.3.21}$$

In regards to climate change, methane's reaction with OH (Equation 1.3.3) is the most significant of all the reactions mentioned in this section. The resulting water vapour produced from this reaction gives an additional positive radiative forcing in the atmosphere. It should also be noted that methane can photo-dissociate at high altitudes, which is the main methane sink above 65 km, although chemically this process occurs on a relatively small scale (Texier et al., 1988).

1.4 Methane sources

This section details an overview of the current understanding of methane sources. All anthropogenic and natural methane sources can be separated into three categories: biogenic, thermogenic and pyrogenic. Biogenic sources produce methane from bacteria (methanogens). Major sources include landfills, ruminants and wetlands. Thermogenic sources emit methane into the atmosphere that were formed thousands to millions of years ago underground. Emissions can be both natural (e.g. geothermal venting) and anthropogenic (e.g. fossil fuel mining). Pyrogenic sources occur during incomplete combustion events. Sources can include wildfires and fuel burning. All three sources have distinct δ^{13}C isotopic signatures spanning from -55 to -70 ‰, -25 to -55 ‰ and -15 to -25 ‰ for biogenic, thermogenic and pyrogenic, respectively (Kirschke et al., 2013). Biogenic sources of methane are more depleted of ^{12}C as bacteria will choose the lighter elements within their processes to reduce energy use. This results in an isotopic methane signal that is 'lighter' than other sources. Thermogenic methane sources are heavier than their biogenic counterparts but lighter than pyrogenic sources. This is because ^{13}C is gradually enriched through degradation and molecular diffusion over geological timescales (Bergamaschi et al., 1994). 1.4.1 shows how the δ^{13}C isotopic signal is calculated (Dlugokencky et al., 2011).

$$\delta^{13}C = \left(\left[\frac{\left(\frac{^{13}C}{^{12}C}\right)_{sample}}{\left(\frac{^{13}C}{^{12}C}\right)_{standard}} \right] - 1 \right) \text{x1000} \tag{1.4.1}$$

The following sections break down the major methane sources into natural and anthropogenic sub-categories. Table 1.1 shows a summary of all the sources and sinks (Section 1.5) including current emission and sink estimates. Table 1.1 also includes a detailed summary of the $\delta^{13}C$ isotopic signatures from these methane sources (Dlugokencky et al., 2011 and Kirschke et al., 2013).

Table 1.1: Summary of methane sources and sinks. Table adapted by Kirschke et al. (2013) with $\delta^{13}C$ values from Dlugokencky et al. (2011). Values labelled with * were taken from Reay et al. (2010) based on a study in 2007. **denotes inconsistent values to the sum of the sources / sinks but were the values reported by Kirschke et al. (2013).

2000-2009 (Tg CH_4 yr^{-1})	**Top-Down**	**Bottom-Up**	**$\delta^{13}C$ (%)**
Natural Sources	218 [179-273]	347 [238-484]	
Natural Wetlands:	175 [142-208]	217 [177-284]	
Swamps			-55 ±3
Bogs			-65 ±5
Other Sources:	43 [37-65]	130 [61-200]	
Fresh water		40 [8-73]	
Wild Animals		15 [15-15]	
Wildfires		3 [1-5]	
Termites		11 [2-22]	
Geological (inc. oceans)		54 [33-75]	
Hydrates		6 [2-9]	
Permafrost		1 [0-1]	-65 ±5
Anthropogenic Sources	335 [273-409]	331 [304-368]	
Agriculture and Waste:	209 [180-241]	200 [187-224]	
Rice agriculture		*54 [31-83]	-62 ±3
Landfills		*54 [35-69]	-53 ±2
Domestic Sewage			-57 ±3
Animal Waste:		*84 [76-92]	-58 ±3
Enteric Fermentation (C4)			-49 ±4
Enteric Fermentation (C3)			-70 ±4
Biomass Burning:	30 [24-45]	35 [32-39]	
C4 Vegetation			-17 ±3
C3 Vegetation			-26 ±3
Fossil Fuels:	96 [77-123]	96 [85-105]	
Coal			-35 ±3
Gas - North Sea			-34 ±3
Gas - Siberia			-50 ±3
Sinks			
Soils	32 [26-42]	28 [9-47]	
Total Chemical Loss:	518 [510-538]	604 [483-738]	
Tropospheric OH		528 [454-617]	
Stratospheric Loss		51 [16-84]	
Tropospheric Cl		25 [13-37]	
TOTALS			
Sources	**548 [526-569]	678 [542-852]	
Sinks	**540 [514-560]	632 [592-785]	
Imbalance	**8 [-4-19]	46 [40-243]	
Atmospheric Growth Rate	6		

1.4.1 Natural sources

Natural sources currently account for just under half of the total atmospheric emissions of methane. The largest single contributor of atmospheric emissions of methane is wetlands, which account for over half of the total natural emissions. Many natural sources vary largely on inter-annual timescales and can cause an impact on the Earth's climate. Natural sources can also contribute to climate feedback mechanisms, and this is discussed in more detail in the following subsections. The majority of the uncertainty associated with methane emissions are from natural sources (Kirschke et al., 2013).

1.4.1.1 Wetlands

Wetland emissions equate to roughly one quarter of all global methane emissions. These emissions have a high degree of variability. The sensitivity of this source is still relatively unknown; however the three main controlling factors that affect emission rates are: temperature (Christensen and Panikov, 2002), water table level and substrate availability (Christensen, 2003). A wetland is an environment of water-logged soil (usually high in organic matter) where anaerobic processes occur. Methane is produced through the microbial process of methanogenesis and emissions are at their highest in stagnant, warm wetlands that have a high water table and soils rich in organic matter. Wetlands can be found across the globe and their location greatly influences factors affecting emission sensitivity and variability. A summary of the main types of wetland and their seasonal variability can be seen in Figure 1.6. The northern wetlands found in the Arctic tundra are more susceptible to temperature variability than their tropical equivalents, which depend more on water table height and the length of the flooding period. It should be noted that the methane emissions from frozen tundra (Figure 1.6.e) are still under scientific debate as Mastepanov et al., 2008 have found that these annual emissions are inconsistent. Future emissions are difficult to confidently predict as they depend largely on response from soil processes. However, emissions would be expected to rise in areas where an increase in temperature will result in a wetter environment. There is already evidence of this occurring in places such as Siberia, Alaska and Canada where permafrost boundaries are receding (Reay et al., 2010). It is generally acknowledged that there will be an increase from Arctic tundra emissions as a result of climate change (Christensen et al., 1996).

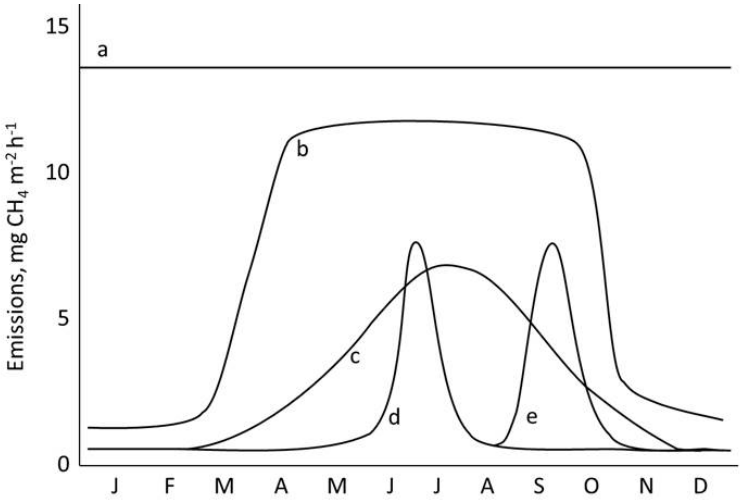

Figure 1.6: Seasonal variations of methane emissions from different types of wetlands. a) Constantly flooded tropical high methane emitting wetland. b) Tropical wetland with seasonal flooding. c) Northern latitudinal wetland which experiences seasonal flooding. d) Wetlands in permafrost regions. e) Permafrost wetlands plus methane emissions from initial freezing in winter. Sourced from Reay et al. (2010).

1.4.1.2 Hydrates

Methane hydrates or 'clathrates' are frozen water crystal structures that encapsulate methane molecules. They can be found in permafrost regions and also along continental margins under the sea bed (Kvenvolden, 1988). Kirschke et al. (2013) estimate that methane hydrates emit around 6 [2-9] Tg yr^{-1}. The estimate is expected to rise due to the sensitivity of permafrost regions to climate change (Christensen et al., 1996). Estimates of the quantity of methane stored as hydrates have been discussed within the scientific community, with estimates covering several orders of magnitude. Klauda and Sandler (2005) proposed around 1.2 x 10^{17} m^3 of methane existed as methane hydrates just in ocean sediments, while Milkov (2004) had a more cautious estimate of 1 - 5 x 10^{15} m^3. It must be noted that the majority of methane released from sea beds will not reach the atmosphere, as most will be converted into carbon dioxide by methanotrophic (bacteria performing methane oxidation) processes or be oxidised as it rises through the water column.

1.4.1.3 Geological sources

Geological sources are found in regions of tectonic activity and divide into two categories: emissions from sedimentary basins and geothermal / volcanic

emissions. Both categories obtain methane produced via methanogenesis or through thermogenic processes that occurred over 50 000 years ago. The IPCC AR4 reports a source strength of only around 9 Tg yr^{-1}, however current estimates are around 54 [33-75] Tg yr^{-1} according to 'bottom-up' inventories (Kirschke et al., 2013). Sedimentary basins release methane from underground gas reservoirs into the atmosphere via faults of fractured rocks. Fluxes from these sources are therefore highly driven by seismic activity. They are also dependent on underground pressures and the permeability of the rocks they pass through (Etiope et al., 2007). Volcanic methane emissions originate directly from magma whereas geothermal emissions can be released in hydrothermal solutions from plutonic or thermometamorphic environments (not from surface magma). It is thought that volcanic and geothermal methane emissions do not make a large contribution to methane concentrations in the atmosphere. Microseepage is estimated to contribute just under half of all the geological sources, which also include mud volcanoes, macro seepages and sub-marine emissions (Etiope et al., 2008). Submarine seeps are thought to only have a significant impact on atmospheric methane concentrations when sources are located at less than 100 - 300 m below sea level (Schmale, 2005). At any further depth the majority of methane is dissolved and then possibly oxidised to carbon dioxide via methanotrophy.

1.4.1.4 Termites

Termites produce methane via methanogenesis by microbes within their digestive system. They either feed on wood or soil and are found in parts of South East Asia, Australia, the Americas and Africa. Higher and lower subgroups of termites exist in all regions; higher termites being more socially and anatomically evolved. Global methane emissions estimates from termites have reduced significantly in recent years. Research produced by Zimmerman (1982) originally estimated that termites contribute between 75 - 310 Tg yr^{-1}, while estimates now stand at 11 [2-22] Tg yr^{-1} (Kirschke et al., 2013). Almost all assumptions made by Zimmerman have now been overturned as there is huge variability in flux size between types of termites, individual communities and different regions. Perhaps the most significant finding is that methane oxidation can occur in the soil used in the mounds that some termite communities live in (Sugimoto et al., 1998). In some cases these mounds can even act as a methane sink.

1.4.1.5 Vegetation

Keppler et al. (2006) proposed that vegetation was a direct methane source. The experiments were conducted in methane-free air, in temperatures too high for enzymes to function and with the samples treated with gamma radiation, thus proving the methane did not originate from microbes (Keppler et al., 2006). Since this fundamental paper, many others have researched into methane production from vegetation (e.g. Kirschbaum and Walcroft, 2008, Vigano et al., 2008). It has been proven that UV irradiation, not visible light, is required to produce methane emissions. In Keppler's original paper a rough extrapolation to calculate global emissions from vegetation estimated the figure to be between 62 - 242 Tg yr^{-1}. However, as this was calculated using a mean value for sunlight and did not take into consideration that only UV radiation produces methane emissions, Keppler has subsequently produced a lower extrapolation of between 0 - 50 Tg yr^{-1} (Keppler et al., 2009). This value does fit within the uncertainties of methane emissions quoted in the latest IPCC report AR5. Since the discovery of methane emissions from vegetation there has been discussion of its impact on science policy. However it is generally accepted that any negative impact on carbon sequestration will be negligible compared to the amount of carbon absorbed by vegetation in the form of carbon dioxide (Reay et al., 2010).

1.4.1.6 Wildfires

Wildfires are caused by lightning strikes and can occur in tropical regions as well as areas of Europe, America, Siberia and Australia. Current estimates of global methane emissions from wildfires stand at 3 [1-5] Tg yr^{-1} (Kirschke et al., 2013). Wildfires can account for up to 10 % of all substances emitted into the atmosphere from biomass burning (Section 1.4.2.2, Reay et al., 2010).

1.4.2 Anthropogenic sources

Anthropogenic methane sources account for over half of the total global emissions. Uncertainties are smaller than for natural emissions and there is better agreement between top-down and bottom-up inventory techniques (Table 1.1).

1.4.2.1 Rice agriculture

The cultivation of rice is a significant contributor to anthropogenic emissions of methane. Accurate emission values can be difficult to obtain due to a lack of experimental data in many of the countries producing the rice; however the IPCC AR5 report estimates 31 - 83 Tg yr^{-1}, which is roughly 11 % of global methane emissions (Bustamante et al., 2014). Around 90 % of rice paddies are grown in Asian monsoon countries where they provide a staple food resource for two thirds of the inhabitants there. Future emissions of methane are predicted to increase to help meet the demand for food of an increasing global population. Rice agriculture also produces methane via methanogenesis. The quantity produced is dependent on the type of paddy field and the cultivation techniques used. These techniques are classified according to their water regimes and summarised in Table 1.2 (Wassmann et al., 2000).

Table 1.2: Different agricultural cultivation systems. Methane emissions are thought to decrease in magnitude down the table (Reay et al., 2010).

Water Regime
Flooded
Continuously
Intermittently
Irrigated
Single Aeration
Multiple Aerations
Deepwater
Rain-Fed
Regular
Drought Prone
Upland

Other factors that can affect methane production from rice agriculture include the amount of fertilizer or manure used, aeration periods and the recycling of organic waste products. In general, low methane emitting paddy fields normally produce low crop yields (Wassmann et al., 2000).

1.4.2.2 Biomass burning

Biomass burning is the deliberate burning of dry vegetation to improve agricultural productivity (Crutzen and Andreae, 1990), or the burning of

agricultural waste and wood fuel; both produce similar emissions. Methane is emitted as a result of incomplete combustion, which occurs when there is an insufficient amount of oxygen present, or burning occurs at too low a temperature to produce purely carbon dioxide and water (Reay et al., 2010). Many compounds released during biomass burning have impacts on the climate. Carbon monoxide and methane will affect the oxidation of the atmosphere due to their reactivity with the OH radical. Nitrous oxide and many non-methane hydrocarbons will increase the concentration of ozone. Finally, particulate matter emitted can act as cloud condensation nuclei causing possible changes to the hydrological cycle and the atmosphere's radiation budget (Crutzen and Andreae, 1990).

It is thought that up to 90 % of biomass burning occurs in tropical regions and current estimated global methane emissions are around 35 [32-39] Tg yr^{-1} (roughly 5 % of total methane emissions, Kirschke et al. 2013). Future climates are expected to rise in temperature, which will have varying effects on the emissions from biomass burning. In some areas this will lead to an increase in the amount and size of fires (this applies to wildfires as well as biomass burning) thus causing an increase in methane emissions into the atmosphere. In other areas, soils will become more arid, meaning less vegetation will be produced and thus fewer fires will occur; reducing biomass burning emissions (Reay et al., 2010).

1.4.2.3 Ruminants

The farming of ruminants (cattle, sheep, goats and deer) for both meat and dairy products is the largest anthropogenic source of methane emitted into the atmosphere (Reay et al., 2010). Ruminants cannot digest cellulose themselves, so they have developed a symbiotic relationship with methanogens. These microbes break down the cellulose to produce carbohydrates that both the microbial community and the ruminants use as energy. Methane is produced as a by-product of this process. The vast majority of methane is emitted orally by the ruminant (92 - 98 %, Grainger et al., 2007). Total annual emissions of methane by ruminants are estimated at 76 - 92 Tg yr^{-1} (Stocker et al., 2013b). These estimates are based on Tier 1 and 2 calculations (for more information on this see Section 1.6).

Table 1.3 shows several suggested methods of methane reduction in ruminants. These have been classified into short term (available now), medium term (available in ten years) and long term (not commercially available for at least another ten years). Many of these suggestions have been disputed as they are

not economically viable, especially in developing nations. It has also been argued that with global populations expected to continue to rise the demand for meat will also increase. It is therefore considered that animal numbers will increase to meet this demand, along with methane emissions.

Table 1.3: Suggested methods for a reduction in methane emissions from ruminants. Definitions are short term (available now), medium term (available in ten years) and long term (not commercially available for at least another ten years).

Short Term	Medium Term	Long Term
Reduce animal numbers	Rumen Modifiers	Breed animals with low CH_4 yield
Increase productivity per animal	Select plants that produce lower CH_4 yield by the animals	Targeted manipulation of rumen ecosystem
Manipulate diet		
Rumen Modifiers		

1.4.2.4 Fossil fuels

The fossil fuel industry (natural gas, oil and coal) is estimated to emit 96 [85-105] Tg yr^{-1} of methane into the atmosphere (Table 1.1, Kirschke et al., 2013). Natural gas is composed of over 90 % methane (Wuebbles and Hayhoe, 2002). The majority of this is burned for energy production, but losses into the atmosphere can occur during extraction, handling, transport and combustion processes. These emissions are expected to rise 54 % between 2005 and 2020 (US EPA, 2006), mainly due to the economic growth of countries such as Brazil and China. Oil only contains trace quantities of methane, but methane gas deposits can be found in situ when drilling for oil. Therefore 97 % of all methane emitted from the oil industry comes from the oil fields. This too is expected to rise by ~100 % between 2005 and 2020 (US EPA, 2006). Mitigation techniques have been developed by capturing the methane emitted in the drilling process and injecting it back underground. This reduces methane emissions and aids further oil extraction. Ventilated methane can also be flared to convert it into carbon dioxide, thus reducing its radiative forcing.

The coal mining industry emits 30 - 46 Tg yr^{-1} of methane, which can be found in the seams of coal deposits and within the pores of the coal itself. The deeper

the coal deposit the higher the carbon content and the greater the amount of methane produced and stored. A surface mine is thought to emit 0.3 - 2 m^3 of methane per tonne of coal, whereas an underground mine can emit up to 10 - 25 m^3 of methane per tonne of coal (IPCC, 1996).

1.4.2.5 Landfills, waste and manure

Landfill and waste contribute between 35 - 69 Tg yr^{-1} of methane to the atmosphere (Kirschke et al., 2013). Methane is produced as a by-product of microbial processes occurring in organic matter within the waste. Recently a decrease in emissions has been observed within developed countries due to landfill gas recovery systems being installed in many landfills and waste treatment systems (US EPA, 2008, DEFRA, 2012). 98 % of landfill emissions are made up of methane and carbon dioxide at a 60:40 ratio. The remaining trace gases include ammonia and nitrogen (Hegde et al., 2003). Landfill emissions of methane are positively correlated with temperature although this is dependent on the depth of the landfill. Deeper landfills become insulated and a stabilising temperature between 25 - 45 °C can be reached. Bacterial activity decreases below 10 °C (ATSDR, 2001).

Landfills continue to produce methane for a number of years after dumping. This period varies for individual landfills. Einola et al. (2007) recorded emissions peaking between 2-3 years post dumping, with emissions after 5 years being 0.63 % of maximum recordings. Other landfills have been recorded to have longer methane emission periods. ATSDR (2001) states the majority of methane gas is emitted within 20 years of waste being dumped although smaller emissions may be recorded for 50 years or more. Future methane emissions from landfills are predicted to rise due to developing nations producing more waste (Reay et al., 2010).

Manure waste usually either remains on the farm where it is used as fertilizer or transported into storage. Waste water is either dumped into coastal waters or taken to be anaerobically treated. Anaerobic treatment is becoming more desirable, especially in developing nations, to actually enhance the production of methane for energy use. As long as the methane produced is not lost the overall emissions of methane are reduced and a new source of renewable energy is produced (Reay et al., 2010). Economic factors and the possibility of new policies will be key determinants for the future emissions of methane from landfills and other waste sources.

1.5 Methane sinks

The hydroxyl radical is the primary sink for methane in the atmosphere accounting for ~90 % of methane global removal. The remaining methane is removed by methanotrophic bacteria (~4 %), stratospheric reactions with oxygen and chlorine (~3 %) and in the marine boundary layer via chlorine reactions (~3 %, Kirschke et al., 2013).

Methanotrophy occurs aerobically in soils and water columns, and also anaerobically in anoxic water and sediment. According to Reeburgh (2007), over 50 % of all methane produced at depth in soils is oxidized through methanotrophy. Anoxic methanotrophy can occur under extreme temperature and energy conditions. It is therefore less responsive to temperature changes than methanogenesis. Aerobic methanotrophs use oxygen instead of sulphate to oxidise methane. In the water column most methane released from the sea bed will dissolve within a few hundred meters (Guinasso and Schink, 1973). Once dissolved, aerobic methanotrophs can oxidise methane, converting it to carbon dioxide and water.

Methane concentration is inversely proportional to the OH concentration due to the OH radical being methane's dominant sink. An inter-model comparison study by Voulgarakis et al. (2013) predicts that global sources of OH will remain relatively stable between now and 2100 under the RCP8.5 ('business as usual') scenario, but methane concentration will increase. This study stated that this will result in a reduction of global OH concentration by an average of 11.3 $\pm$7.7 % by 2100.

1.6 Quantifying the atmospheric methane budget

The global atmospheric methane budget is defined by assessing the difference between the total methane emitted and the total removed. These totals are produced using various inventories, which can be split into two basic categories: 'bottom-up' and 'top-down'. Both techniques can span spatial resolutions ranging from global to sub-national scales.

Bottom-up inventories are constructed using emission factors combined with scaling processes which consider spatial distributions. Top-down approaches take atmospheric measurements in combination with a process model to derive emission sources. The following subsections discuss these two methods in detail

and provide examples of current inventory results spanning global and regional spatial scales.

Uncertainties in relation to the global estimates are shown in Table 1.1. These values demonstrate how wide ranging the uncertainties for each source can be. Natural wetlands has the largest uncertainty range (107 Tg yr^{-1}) but smaller sources which are less constrained have higher relative uncertainties. Uncertainties on the regional, national and sub-national scale increase dramatically and become more difficult to quantify. It should be noted that in the review published by Kirschke et al. (2013) these uncertainties represent the spread in results from the inventories studied and not the uncertainties of the individual inventories. A closing request in the review asked for future estimates to be accompanied by a systematic uncertainty assessment.

1.6.1 Bottom-up inventories

By far the more established and detailed of the two methods, the bottom-up technique can produce finer spatial resolution and more detailed emissions for specific sources. In response to the United Nations Framework Convention for Climate Science (UNFCCC), the IPCC provides guidelines for countries to produce national inventories of anthropogenic emissions of the major greenhouse gases (GHGs). The IPCC defined a tiered system of bottom-up methods to create inventories of differing complexity. Tier 1 is the most simple, taking into account basic equations and emission factors. These can be as simple as emissions per animal multiplied by the number or animals, or the area of land used multiplied by the emission factor per area. Tier 2 uses country-specific parameters and more detailed calculations to produce the inventories. When estimating agricultural methane emissions for example, not only will animal population be considered, but also the average daily feed intake and the methane conversion rate as well as many other factors (Eggleston et al., 2006). Tier 3 is the highest and most complex method of calculating inventories. Specific energy equations are taken into account and regular use of complex models are incorporated where possible. Bottom-up techniques carry with them high uncertainties, particularly for fine spatial resolutions. This is because of the methodology for compiling these inventories. Full, global inventories require multiple datasets and emission factors. Datasets can be incomplete or compiled using different scaling methods, emission factors etc., which results in large uncertainties being placed on the final figures.

The National Atmospheric Emissions Inventory (NAEI) for the UK is compiled

using various bottom-up techniques (NAEI, 2006). It produces an inventory on a 1 x 1 km spatial scale annually, for more information please see Section 1.7.

Emissions from natural sources are estimated using these methods which result in comprehensive emission and sink budgets being obtained. For example, wetlands are the single largest source of methane and their intra/inter-annual emission can largely vary. For instance, Ringeval et al. (2010) used a global vegetation model and a process based emission model to estimate methane emissions from wetlands. Emissions were then calibrated against representative methane flux time series using eddy covariance techniques. Other such studies have been carried out.

1.6.2 Top-down approaches

Top-down approaches were developed in an attempt to reduce the high uncertainties associated with the bottom-up approaches. These 'inversion' techniques use atmospheric measurements along with a method to represent the origins of these concentrations (i.e. a Lagrangian dispersion model). Many inversion techniques have been developed over recent years and inventories are available at global (e.g. Rigby et al., 2008), regional and national scales (e.g. Manning et al., 2011b). There are currently no inversion techniques that can recreate the fine spatial resolution of the bottom-up techniques. This is because top-down approaches are also limited by the quantity and quality of the measurements, as well as the spatial resolution (and thus the accuracy) of the atmospheric transportation model. The spatial resolution produced by the bottom-up techniques could be theoretically matched if there was enough observational data and/or the resolution of the transport model was fine enough. Areas of the globe with fewer measurements are less restricted in the inversion process and thus produce estimates with larger uncertainties (Kirschke et al., 2013).

Source attribution is more problematic with inversion techniques. Estimates tend to be for total methane rather than specific sources. Isotopic measurements can be used to identify particular sources; however these measurement sites are a small subsection of the total number. So-called methane 'tracers' can be incorporated into CCMs to help estimate individual sources e.g. Bousquet et al., 2011, Houweling et al., 2014. In addition, land coverage maps can aid source attribution for areas where one source dominates (i.e. tropical wetland regions) but areas where several methane sources are found (i.e. urban areas) are more difficult to attribute individually.

Some top-down approaches quantify methane sinks by estimating OH concentration. A common technique for estimating global OH fields (the major sink of methane) is by proxy, using methyl chloroform measurements in an inversion method (Bousquet et al., 2011; Patra et al., 2014). These methods produce reliable global tropospheric OH fields, which can then give estimates of methane's chemical loss through its reaction with OH. Total estimates from bottom-up inventories of OH (and methane) have no upper limit as they lack a constraint on their global magnitude. They have been thought to overestimate global totals (Kirschke et al., 2013). Global estimates using top-down techniques are limited by the observed global growth rate (6 Tg yr-1 for 2000-2009, Table 1.1). Thus, the range between all the top-down emission estimates is smaller than the equivalent range using bottom-up techniques.

Lastly, a prior emission inventory can be used to reduce uncertainties in top-down approaches. These priors can have pre-defined uncertainties associated with them to quantify how much confidence should be given to them. NB: recent developments do not require the prior uncertainties to be rigidly defined (Ganesan et al., 2014).

1.6.3 Discrepancies between the inventories

The imbalance between methane sources and sinks differ in both inventory methods. Top-down calculates a difference between sources and sink of 8 Tg yr^{-1} whereas bottom-up produces a larger difference, of 46 Tg yr^{-1} (Table 1.1). Anthropogenic emissions agree well in both approaches, suggesting that the totals are well constrained in both top-down and bottom-up methods. Top-down techniques are limited by observed growth rates while bottom-up techniques have no upper limit. This is thought to result in over-predicting sources and sinks (Kirschke et al., 2013). Large differences between the top-down and bottom-up methods exist for the natural methane sources, particularly the wetland estimates (175 [142-208] Tg yr^{-1} compared to 217 [177-284] Tg yr^{-1}). Bottom-up techniques also estimate higher methane sinks (540 [514-560] Tg yr^{-1}compared to 632 [592-785] Tg yr^{-1}). Kirschke et al. (2013) postulates that the bottom-up global estimates of methane loss through OH are overestimated. This is because top-down estimates of OH (calculated using methyl chloroform measurements) are considered more reliable. The bottom-up methane sink estimates are more uncertain than the top-down estimates (28 Tg yr^{-1}compared to 245 Tg yr^{-1}). Voulgarakis et al. (2013) states the different temperature

and humidity fields used within the CCMs to calculate the OH sink produce wide-ranging values. The bottom-up estimates also suggest the OH radical has been increasing throughout the 2000s, yet observations of methyl chloroform show concentrations to be more stable. These errors lead to larger uncertainties in the bottom-up approach. An IPCC meeting in 2010 that discussed the 2006 report 'Guidelines for National Greenhouse Gas Inventories' stated that "while remote sensing, ambient measurement and inverse modelling techniques have been successfully demonstrated they are currently not sufficiently developed to provide comprehensive verification at the required accuracy". Both methods are required to develop and accurately quantify the global atmospheric methane budget (Eggleston, 2010), but more technique development and uncertainty reduction must be conducted to increase the current understanding.

1.6.4 Introduction to uncertainty

Understanding of the uncertainty in methane emission estimation techniques is vital in producing accurate and reliable results. The IPCC's 'Guidelines for National Greenhouse Gas Inventories' describe uncertainty as the "Lack of knowledge of the true value of a variable that can be described as a probability density function (PDF) characterising the range and likelihood of possible values. Uncertainty depends on the analyst's state of knowledge, which in turn depends on the quality and quantity of applicable data as well as knowledge of underlying processes and inference methods" (Eggleston et al., 2006). The points below list the major uncertainty types found in estimating emissions. These are primarily for top-down estimation methods but some are present in bottom-up techniques, which are highlighted in the text.

- Instrument uncertainty: Errors associated with the measurement instrumentation. This includes instrument precision and calibration gas errors. These errors are more easily quantifiable than most modelling uncertainties.
- Systematic modelling errors, or biases, are defined as consistent and repeatable errors, which have a mean of non-zero. They can be present in top-down and bottom-up emission estimation methods. Examples of these errors include measurement site biases (top-down) and inaccurate emission factors (bottom-up).
- Model representation uncertainty, which also carry systematic uncertainty (Ganesan et al., 2014), can refer to errors in the CTM. These include:

  - errors within the meteorology used, i.e the wind direction (Houweling and Dentener, 2000);
  - the assumption that a point observation is comparable to the mean simulated concentration on the corresponding grid box (top-down methods, Berchet et al., 2013);
  - model parametrisation or sub-resolution errors. These include uncertainties produced due to CTM resolution data being fixed. Any processes that are sub-scale must be paramaerised (i.e small-scale eddies) which then produce errors (Berchet et al., 2013).

- Aggregation uncertainties are concerned with errors from the resulting spatial resolution of the emissions estimates. This is discussed in Turner and Jacob (2015) who explain that errors can occur through the aggregation of the emission grid resolution. In inversion estimates, the most fine resolution is the same as the resolution used by the transport model. Aggregation errors occur when the emissions grid resolution is made more coarse, over space and time. This is done to reduce computational expense but the resulting resolution must assume the fixed emissions per gird box are correct (Ganesan et al., 2014). Some studies have attempted to reduce the aggregation errors using various statistical methods (Turner and Jacob, 2015, Kaminski et al., 2001). Similarly, in bottom-up estimates, finer resolution inventories may be scaled up or coarser estimate scaled down, causing similar error propagation.

An assessment of how uncertainty is attempted to be quantified in the experimental setup can be found in Chapter 3 and Chapter 5. A schematic for all uncertainty associated with the inversion approach is shown in Figure 1.7. The types of uncertainty discussed above have been divided into three main areas, those associated with the measurements, the dispersion model, and the inversion process itself.

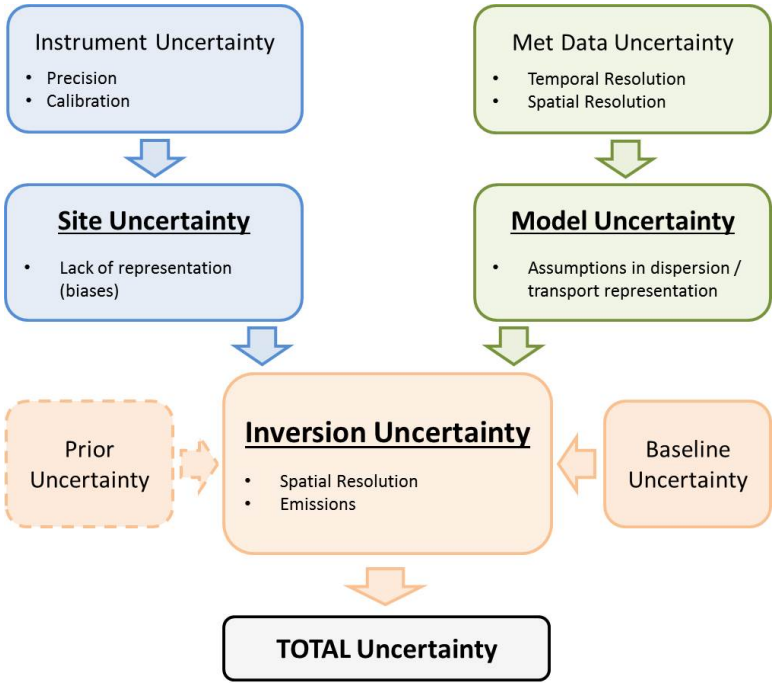

Figure 1.7: Schematic of uncertainty associated in the top-down emission estimate approach. Three main areas of uncertainty exist, those associated with the measurements, the dispersion model, and the inversion process itself.

The incorporation of a prior into the model setup can have both negative and positive implications. In top-down emission modelling, a prior is a defined as a previously produced estimate of emissions. Ideally with a rigorously assessed uncertainty associated with each value. A prior can help constrain the location and magnitude of emissions to within the known uncertainty ranges and can reduce uncertainties associated with representing transport. The uncertainties associated with these priors are not always quantifiable and so inaccurately low estimates can cause the propagation of these errors to the resulting emission estimates. Research conducted by Ganesan (2014; 2015) has developed a hierarchical Bayesian inversion method where absolute uncertainty values associate with the priors and model are not needed and an assessment of the uncertainty is conducted within the inversion setup.

The IPCC's guidelines issue two approaches to quantifying uncertainty: use of error propagation equations, or the use of a Monte Carlo or similar technique. The first technique can be used to estimate uncertainties for individual categories (i.e. emission factors) which can then build up an uncertainty estimate for the whole inventory (used in bottom-up approaches). It relies on the assumption that individual uncertainties (expressed as standard deviations) are not correlated and is normally used for relatively small uncertainty values. The Monte Carlo

approach is an alternative approach for estimating uncertainty which uses an iterative technique using sampled input values. This technique can be used when dealing with complex methods, larger uncertainties and when correlations between individual factors are present. The Monte Carlo process is iterated to produce a representative range of uncertainties for the model output. This approach is often used to reduce computer run time as only a subset of the potential input variables are used which still produces results which are considered representative. Results are generated using the PDFs specified for each input variable. For more information on the Monte Carlo approach please see (Morgan and Henrion, 1990).

1.7 The UK methane emissions inventory

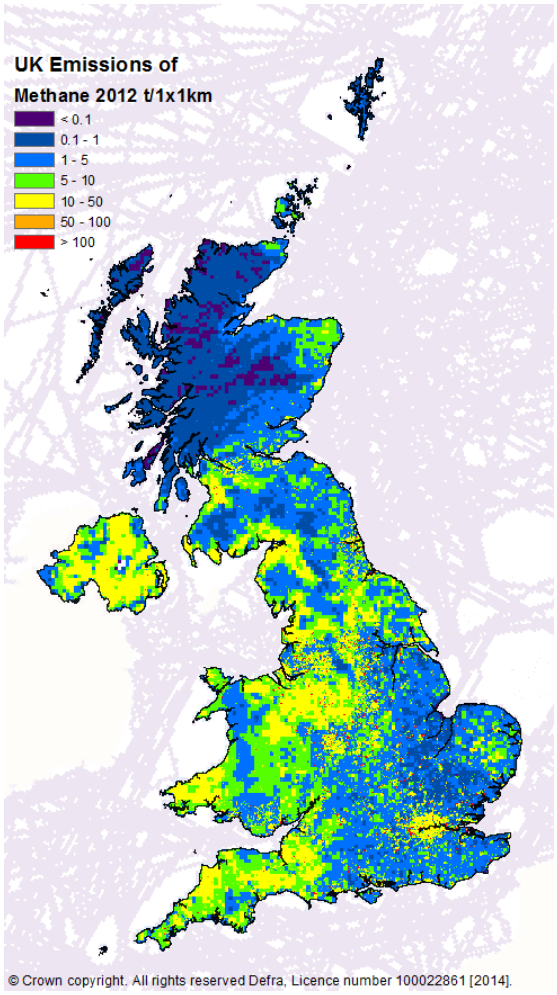

Figure 1.8: The UK 2012 NAEI for total methane emissions (t yr^{-1}). Emissions available on a 1 x 1 km spatial resolution. The maps are produced on a 5 x 5 km grid resolution and dis-aggregated to 1 x 1 km.

The NAEI for the UK is produced using extensive bottom-up techniques. Annual emission maps are produced for all six major GHGs (carbon dioxide, methane, nitrous oxide, hydroflurocarbons, perfluorocarbons and sulfur hexafluoride). All inventories are also available separated into the major source sectors. For methane this comprises agriculture, domestic combustion, energy production, industrial combustion, industrial production, natural, offshore, road transport, other transport and waste. The most recent NAEI map for all methane emissions (2012) is shown in Figure 1.8. Total emissions are estimated at 2.33 ±0.49 Mt for 2012. Methane is the UK's second largest GHG, making up 9.9 % of the total emissions (Sneddon et al., 2015). Individual nations' methane emissions

and percentage contributions to the total GHG emission can be seen in Table 1.4. England is responsible for 68 % of total UK methane emissions.

Each year, prior to the new inventory being compiled, current calculation methods are reviewed and improved where necessary. Industrial and commercial companies that produce pollutants are legally required to estimate and report emissions to contribute to the NAEI. These estimates are produced using methods described in Section 1.6.1. These sources usually reflect the larger, more pinpointed emissions in the NAEI. More diffuse and smaller sources are estimated using surrogate statistics for each sector. The methods used to compile these estimates for each GHG and source sector will vary according to the data available (DEFRA, 2015). All estimates are compiled using guidelines given by the IPCC and the UNFCCC (NAEI, 2013), which are also annually updated. The requested data are analysed for consistency and anomalies within different sources before the inventories are compiled.

Table 1.4: UK NAEI methane emission estimates (Mt CO_2-eq) and corresponding uncertainties (%). NB: CO_2-eq calculated on a 100 year GWP timescale. The values stated here would increase if shorter time scales were considered.

Region	Emission (Mt CO_2-eq)	% of region's total GHG emissions	Uncertainty (%)
UK	54.84	9.9	21
England	37.19	8.6	24
Northern Ireland	7.87	15.6	16
Scotland	5.40	10.6	23
Wales	4.38	19.6	17

Major emission source datasets include; industrial processes based on plant operator estimates, waste emissions based on waste disposal activity and agricultural emissions from UK emission factors and annual surveys. These emissions are then used in models with regional survey data (NAEI, 2013). The requested data produce a UK wide inventory estimate, although for some source sectors the national and sub-national statistics are available in less detail than others. Thus, the UK total emissions are sometimes dis-aggregated to produce smaller regional estimates. Each NAEI map is produced on a 1 x 1 km grid although the most recent maps (2012) show a 5 x 5 km grid resolution divided equally down to 1 x 1 km. This is due to high uncertainties associated at the finer resolution. Uncertainties are calculated for all GHGs emissions for the UK, England, Scotland, Wales and Northern Ireland. Total uncertainty is defined as $\pm 2 \times (\textit{standard deviation}) \,/\, \textit{mean emissions}$ and the methane values are shown

in Table 1.4 (NAEI, 2013). Uncertainties on a sub-national scale are not provided but are thought to be substantially higher than the national estimates.

Figure 1.9 shows the percentage contributions of each methane source sector in 2012 for the UK. The dominating sectors are agriculture and waste, both microbial sources of methane. The third largest contributor is offshore which is a geothermal source at the production site and within the pipeline. The remaining sectors contribute less, with the largest being domestic combustion which produces a little over 1 % of the total emissions.

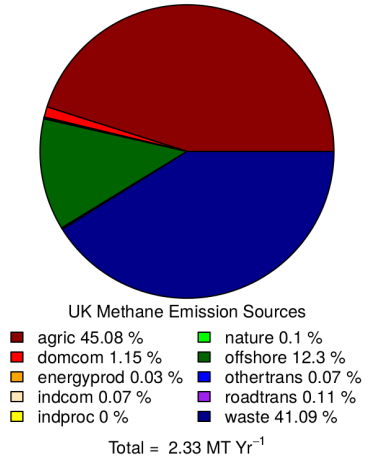

Figure 1.9: UK 2012 NAEI methane source sectors as a percentage of total methane. The ten sources sectors are: agriculture (45.08 %), domestic combustion (1.15 %), energy production (0.03 %), industrial combustion (0.07 %), industrial processes (<0.01 %), nature (0.10 %), offshore (12.30 %), other transportation (0.07 %), road transportation (0.11 %) and waste (41.09 %).

According to the NAEI, methane emissions have been steadily decreasing over the last two decades as highlighted in Figure 1.10 (Webb et al. 2014). A total reduction of 51 % has occurred since 1990. The dominating sector for this decrease is waste, which has reduced by 55 % over this period (46 % of the total methane emission reduction). Landfill capping to burn methane for electricity production is the main reason for this reduction. The energy sector has reduced by 74 % since 1990 as a result of a decrease in coal mining and improvements to the gas pipe network. Agriculture has reduced 21 % for this period due to livestock numbers being decreased (DEFRA, 2012). Contrary to the NAEI, Manning et al. (2011b) estimates much lower methane emissions for the UK during the 1990s. Both studies calculate similar estimates during the 2000s. Manning et al. (2011b) still estimates a drop in emissions over this time period but under half of that which

is reported in the NAEI (24 % compared to 51 %, respectively).

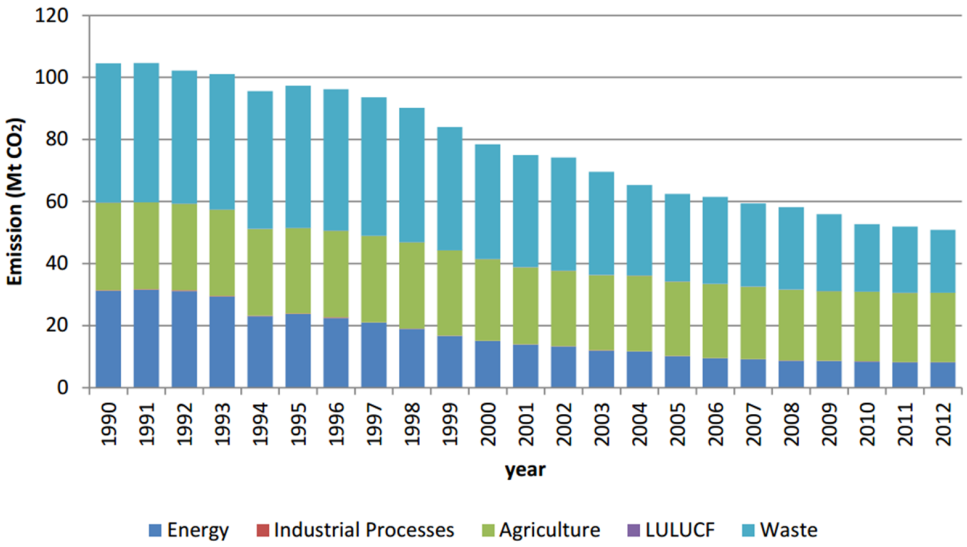

Figure 1.10: Trends in UK methane emissions by sector (Webb et al. 2014). Emissions have seen a 51 % decrease since 1990. NB: LULUCF = land use, land use change and forestry emissions.

1.8 Summary

This chapter aimed to provide an introduction to the importance of studying methane in the atmosphere. Its large GWP and strong radiative forcing makes it a powerful GHG. This chapter summarised the major methane reactions important in atmospheric chemistry and showed the diversity and variability of methane sources. The discrepancies between top-down and bottom-up inventory methods are thought to be explained by the bottom-up techniques being unconstrained to the global growth rate. Both methods are currently necessary due to the limited information obtained by top-down techniques at high spatial resolution. This chapter closed with an overview of how uncertainty is quantified in inventory techniques and the UK NAEI for methane was introduced. UK emissions of methane have been steadily decreasing this century although substantial uncertainties still remain for these estimates.

The following chapter introduces the project from which the results of this thesis are based. The major project aims and goals are described and a more detailed discussion of methane sources within the East of England is conducted.

2 Introduction to the project

The previous chapter gave an introduction to global and UK methane emissions. It highlighted the gap between top-down and bottom-up methane estimate methods and the growing need for top-down methods to increase their spatial resolution. This chapter introduces the major aims of this project and describes the processes conducted to achieve these aims. It then discusses the NAEI methane emission estimates in more detail, with a particular focus on the East Anglia emissions.

2.1 Project description and aims

This project has been developed in response to the growing need to achieve direct comparisons of top-down and bottom-up emission estimates. This section describes the major aims of the project, the reasons for choosing the locations for the project and the measurement sites, and which models are used in the top-down technique.

The principle aim of the project was to develop and test a novel approach for emissions modelling using a top-down method at high spatial resolution. This technique would achieve sub-national emission estimates and be directly comparable with the NAEI. The top-down technique used in this project was the 'Inversion Technique for Emissions Modelling' (InTEM - discussed in detail in Section 3.3), which incorporates atmospheric measurements and computer dispersion modelling within its setup. InTEM has previously produced UK methane emission estimates (Manning 2003; Manning and Derwent 2006; Manning 2011; Manning et al. 2011b) but has never been developed on a sub-national spatial resolution. An additional project aim was to investigate what spatial resolution could be achieved. This goal was dependent on the initial 'proof of concept' aim being successful. This project chose to pilot the InTEM development for a region within the UK rather than attempt a national scale inventory. This allows for a more thorough assessment of spatial resolution

sensitivity due to the limited number of measurement sites available for this project. Another aim of the project was to assess the sensitivity of resulting emission estimates using a varying number of observation sites. For this reason, four sites were installed for this project over the region of interest. Previous analysis by Manning et. al. (2003; 2011; 2011b) has used data from one measurement site (Mace Head, Ireland) for national emission estimates. Other national estimates have been conducted using a 4-site network from around the UK and Ireland (Ganesan et al., 2015, ODoherty et al. (2014)). These sites have not been used to explicitly estimate emissions at the county scale. The final aim of this project was to attempt emission estimates on a shorter temporal resolution than the NAEI, i.e. sub annual estimates. These estimates could give additional information for interested stakeholders, which are currently not available from the NAEI.

An appropriate region of the UK was needed to be identified, which could host suitable methane measurement sites. The East Anglia (EA) region of the UK was identified to trial this method for three particular reasons:

1. Its topography. The turbulence and vertical mixing of air generated by winds experiencing friction from the topography are greatly reduced in EA due to it being very flat. This reduces the presence of small scale meteorological events which have to be parameterised within the atmospheric model. This means that the modelled meteorological fields should be more accurate compared to areas of the UK with more complex topography. Additionally, flat land produces a much more stable boundary layer than compared to an uneven or elevated area. This, again, allows for the modelled meteorological data to be more representative.

2. Its broad range of methane emissions. Less methane is emitted in the north west, west and south of EA, where emissions are thought to be from natural sources rather than from agriculture / waste. The range of methane fluxes in this region allows the accuracy of the inversion system to be tested, for example, whether the emission gradient can be reproduced or not.

3. Its close proximity to Cambridge, and thus its ease of access.

The project saw the installation of three observation sites to measure methane. A fourth site is used in the analysis but was not installed by the University of Cambridge. The locations of these sites and a summary of the site details are shown in Figure 2.1 and Table 2.1, respectively.

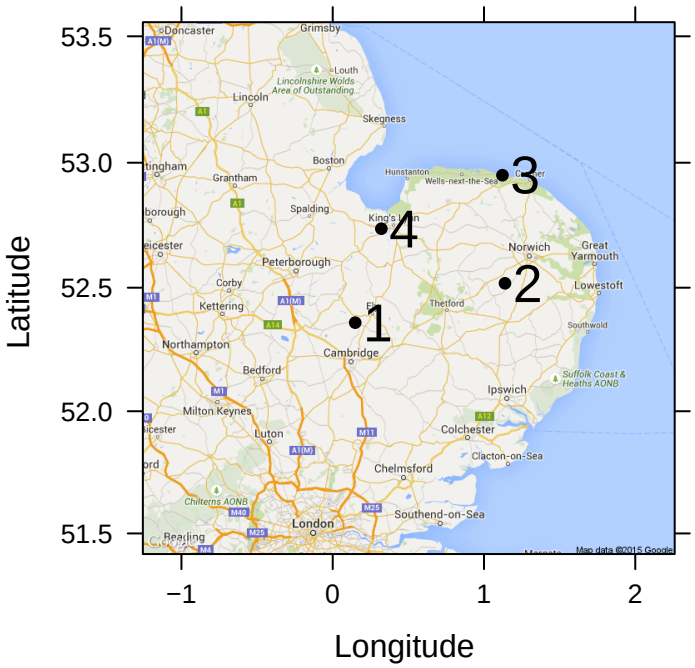

Figure 2.1: Chosen site locations for methane measurements in East Anglia. 1) Haddenham 2) Tacolneston 3) Weybourne 4) Tilney.

The Haddenham, Weybourne and Tilney sites use gas chromatography coupled with flame ionisation detectors (GC-FIDs) to measure methane. Tacolneston (location 2) is a tall tower site and uses a Picarro cavity ring down spectroscopy (CRDS) instrument. This site is funded by the Department of Energy and Climate Change (DECC) and run by the University of Bristol. Three inlet tubes measure atmospheric concentrations at 50 m, 100 m and 150 m in altitude. This project uses an average of the 50 m and 100 m observations (more information see Section 3.1.2).

All inlet tubes are desired to be above ground level (agl) to minimise influences from local sources. Haddenham and Tilney (locations 1 and 4) have GC-FIDs installed in churches with their inlet tubes positioned at the top of the towers (~25 m above ground level). To further minimise local influences on the inversion, sites were chosen away from gas pipelines and any known methane point sources where possible. Locations were also chosen so the individual sites were spread over East Anglia. This was with the aim to obtain as comprehensive representation of methane concentrations from East Anglia as possible (with four instruments).

To estimate emissions, concentrations measured at the sites must have upwind

air passing over the region of interest. A larger area can be monitored by placing the measurement sites throughout the region of interest, i.e. locations shown in Figure 2.1 rather than in a single straight line. The prevailing wind for East of England is south-westerly, this means the sites to the east (2 and 3) measure air exposed to EA's emissions more often. When the wind changes direction, other sites are suitably positioned to monitor emissions from EA.

Sites 1 and 2 were installed in July 2012, with sites 3 and 4 being installed in February 2013 and June 2013, respectively. This project assessed emissions over a variety of periods between July 2012 - June 2014. In addition to these measurements, another GC-FID instrument operated by the University of East Anglia recorded methane concentrations at the Weybourne site, using the same inlet tube. Both measurement datasets were combined in the analysis.

Table 2.1: Summary of the EA methane measurement sites used in this thesis. All sites off the gas grid.[a]Multiple landfills.

	Site Names	**Instrument**	**Coord-inates**	**Altitude (m)**	**Nearest Landfill (km)**	**Date Installed**
1	Haddenham, HAD, HD	GC-FID	52.359, 0.149	25	3-5[a]	July 2012
2	Tacolneston, TAC, TN	Picarro CRDS	52.518, 1.139	50, 100	10	July 2012
3	Weybourne, WEY, WY	GC-FID	52.950, 1.122	15	8	February 2013
4	Tilney, TIL,TY	GC-FID	52.737, 0.321	25	5	June 2013

The transport model used in this project is the Met Office's Numerical Atmospheric-dispersion Modelling Environment (NAME). More information on this model is found in Section 3.2. The methane measurements and modelled representations of air transport are then fed into the inversion technique to estimate emission fields.

2.2 Assessment of current East Anglian methane emission estimates

The NAEI produces methane emission maps for ten source sectors which represent a specific year's inventory. The most recent NAEI is for 2012 and is available on

a 1 x 1 km grid for the whole of the UK. Figure 2.2 summarises the 2012 NAEI methane emissions by sector for the EA region as percentages of the regional emission. For details into how this region was defined please see Section 3.2.4. Unlike the total emissions for the UK, this region experiences a higher percentage of waste emissions (65.66 % compared to 41.09 %) and less agricultural emissions (17.16 % compared to 45.08 %). All other sector emissions remain similar in both the UK and EA totals. The total methane contribution from EA is 14.2 % of the UK total.

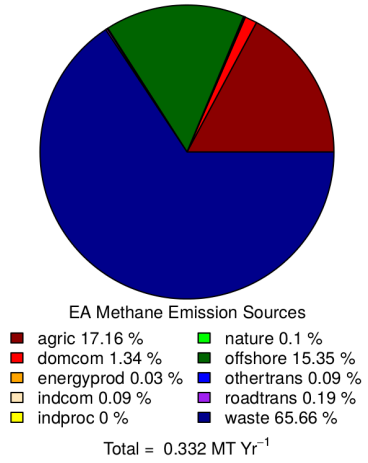

Figure 2.2: EA 2012 NAEI methane source sectors as a percentage of total methane. Ten sources sectors are: agriculture (17.16 %), domestic combustion (1.34 %), energy production (0.03 %), industrial combustion (0.09 %), industrial processes (<0.01 %), nature (0.10 %), offshore (15.35 %), other transportation (0.09 %), road transportation (0.19 %) and waste (65.66 %).

Emission maps of the source sectors are shown in Figure 2.3 for the EA region (NB the colour scale is logarithmic). Agricultural emissions dominate towards the centre and east of EA. Waste sector emissions, predominately landfill emissions, are shown as red/orange point sources. These two emissions sources dwarf other sectors with the exception of some re-distributed offshore emissions (originating from pipeline leaks).

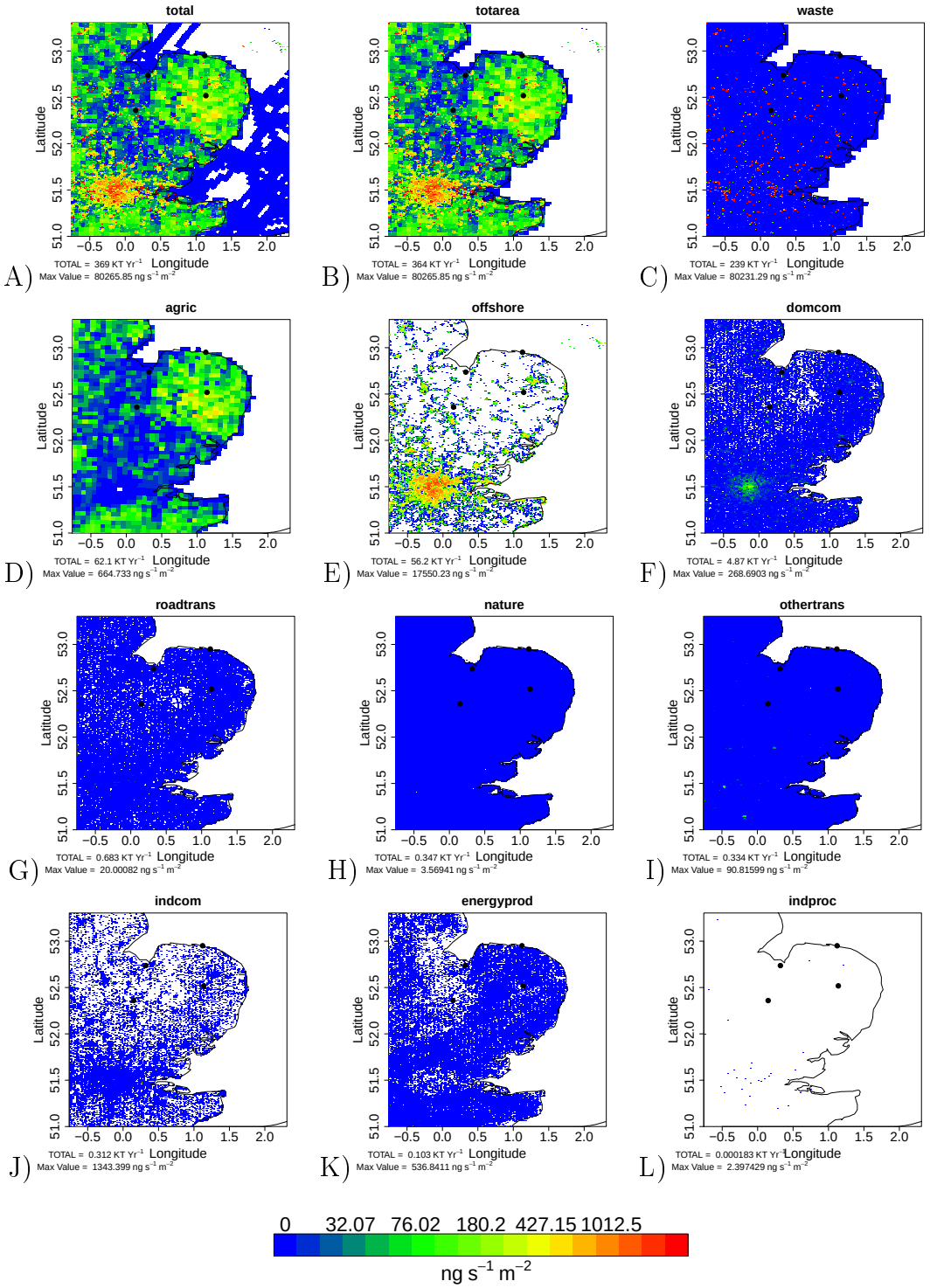

Figure 2.3: EA methane emission maps of the 2012 NAEI total, total area and ten source sectors (total area does not include emissions from shipping). Ten sources sectors are labelled in order of total magnitude for the EA region: A) total B) total area C) waste D) agriculture E) offshore F) domestic combustion G) road transport H) nature I) other transport J) industrial combustion K) energy production L) industrial processes. NB: Emission scale is logarithmic. Measurement site locations shown as black points.

Each measurement site is influenced by nearby methane sources. This 'footprint' of emissions that each site is influenced by can be estimated using the NAME model. NAME can track the movement of air backwards in time and calculate any influence this air has had with the surface (defined as the bottom 100 m of the atmosphere). This can be calculated for a given location over multiple instances and is represented as a time integrated concentration (units of g s m^{-3}). These estimations of surface influence can then be incorporated with the EA NAEI source sector maps to produce an estimate of each source sectors' contribution to the four sites, which is represented as a modelled concentration, or 'pseudo-observation'. The synthesis of these pseudo-observations is not described in this section but a detailed explanation of this technique can be found in Section 4.4.

A summary of the influence each methane source sector has on the four observation sites can be seen in Figure 2.4. This figure is split into three sections. Figure 2.4.A shows the contribution of each methane source sector's pseudo-observations to the measurement sites (as a percentage of total concentration). Figure 2.4.B shows the range of these pseudo-observations as boxplots (units of ppb). Figure 2.4.C shows the range in 'surface influence' NAME has calculated for each site (units of g s m^{-3}). Haddenham and Tilney experience a higher waste contribution than the other two sites. This observation is reflected in the pie charts and the pseudo concentrations boxplots (parts A and B). These boxplots also highlight that Haddenham and Tilney have higher methane concentrations compared to the other sites. These two sites are in closer proximity to landfills (shown in the waste emission map in Figure 2.3). Prevailing south westerly winds suggest these could be the source of the high methane concentrations. It is also expected that Tacolneston would experience a larger fractional contribution from the agricultural sector, as emissions for this region are at a maximum to the south west of this site (agricultural emissions map in Figure 2.3).

Lower interquartile ranges (IQRs) of the pseudo-observations at Tacolneston and Weybourne (Figure 2.4.B) can be explained by the equivalent NAME integrated concentration boxplots (Figure 2.4.C). Similarly to the pseudo-observation boxplots, Tacolneston and Weybourne have lower values than Haddenham and Tilney, implying that these sites experience less surface influence. For Weybourne, this is simply due to the site being at close proximity to the edge of the region and thus, when the wind blows from the north, NAME will record a lower influence. Measurement sites at higher altitudes experience a larger free tropospheric air

contribution, and are less dominated from air within the boundary layer. Their higher altitude also means that nearby methane sources have had a longer time to mix/dilute before being measured, therefore lowering the measured concentration. Tacolneston's inlet is located at a higher altitude than the other sites and thus will have a lower surface influence and experience lower methane concentrations on average.

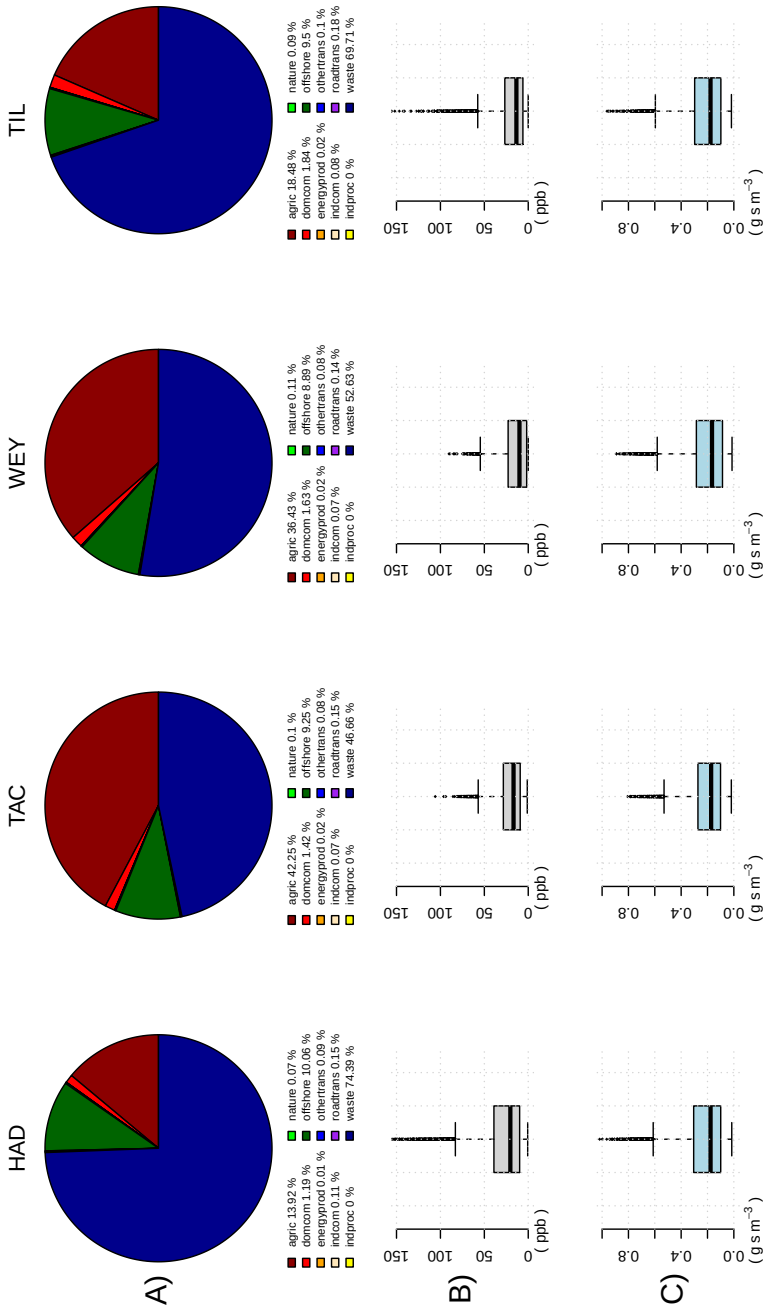

Figure 2.4: A) Measurement sites' influence from the methane source sectors as a percentage. B) Pseudo-observations as boxplots (units of ppb). C) NAME 'surface influence' as boxplots (units of g s m^{-3}). Boxplots show the inter-quartile range (IQR) represented as the coloured section, with the mean value as a dark horizontal line. The whiskers show 1.5 times the IQR with any outliers plotted as individual points. All data used are from 01 June 2013 - 31 May 2014. Calculation method is explained in Section 4.4.

2.3 Summary

This chapter gave an overview of the major logistical processes of the project. This included a description of how the pilot region for the development of this novel technique was chosen, and consequently where the measurement sites were installed. Sites were chosen away from large methane sources with inlet tubes installed above ground level to reduce local biases and spread out across the region of interest to incorporate a wide-ranging footprint of emissions. The chapter then discussed the current methane estimates within EA, which is dominated by three main source sectors: waste, agriculture and offshore. The four sites are influenced by these sectors differently. Haddenham and Tilney experience larger waste contributions whereas Tacolneston and Weybourne have a larger agricultural contribution. The following chapter introduces and discusses the experimental protocol of the methane instruments, the atmospheric dispersion model, and the inversion method.

3 Methods

This chapter describes the experimental overview and modelling setup used throughout the analysis in this thesis. This chapter is split into three parts. The first introduces the gas chromatography instruments and their sampling capabilities, including data selection and calibration procedures. The second section introduces the dispersion model used to represent the physical atmospheric processes occurring at each instrument site throughout the measurement period. Finally the inversion technique, InTEM, is introduced and the model setup which determines the resulting methane emission estimates is explained.

3.1 Gas chromatography

Gas chromatography allows for the separation of compounds within a sample by passing the gas mixture through a column. An inert carrier gas (the mobile phase) is passed through a packed column (the stationary phase). The principles of GC lie in the fact that compounds can be separated depending on their affinity towards the stationary phase. Compounds with a greater affinity will elute more slowly through the column. The separated compounds can then be passed to a detector to be identified and quantified.

For this project, atmospheric methane was measured using commercially available 200 Series gas chromatographs (GCs) sourced by Ellutia Ltd. (Ellutia, 2011a). A schematic of the instrumental setup is shown in Figure 3.1 where the GC was coupled to a flame ionisation detector (FID) for sample analysis. Nitrogen was used as a carrier gas between samples. Two other gases, pressurised air and hydrogen, were used in the FID to fuel the combustion of the flame (Section 3.1.1). All three gas cylinders first passed through a molecular sieve to filter out water and hydrocarbons (labelled W and HC in Figure 3.1). The nitrogen carrier gas was also scrubbed for oxygen to protect the column from oxidation (labelled O in Figure 3.1). Inlet and calibration tubes were filtered using a desiccant-based

Nafion dryer (ND) to avoid contamination and destruction of the column's stationary phase. A stainless steel mesh (2 μm) was fitted to the inlet tube to filter any larger impurities from damaging the GC and reducing the air flow. The GC was run at an internal temperature of 100 °C and a column pressure of 34 psig. The columns used in the 200 Series GCs are 3 m in length and packed with a polar macroporous resin known as 'Hayesep Q Polymer'. A compound's retention time (how quickly it elutes) is determined by its polarity, with non-polar compounds eluting first. Retention times for non-polar compounds are determined by boiling point. With a boiling point of -161.5 °C, methane elutes quickly under these column conditions (<1 minute).

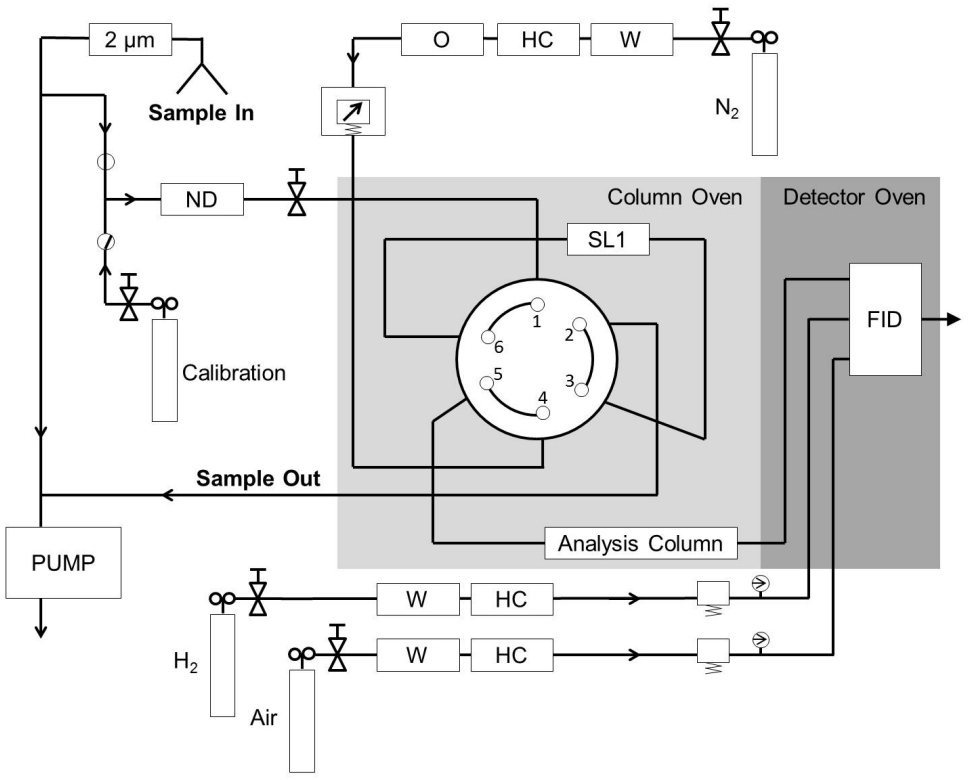

Figure 3.1: Ellutia GC-FID 200 Series system flow diagram. Nitrogen carrier gas is filtered for water (W), hydrocarbons (HC) and oxygen (O) before entering the column. Hydrogen and compressed air are used to fuel the flame ionisation detector (FID). These are filtered for W and HC. The inlet tube is attached to a funnel filled with stainless steel-mesh (2 μm) and faced down to protect from rain and large particulates. Solenoid valves allow the GC to sample either the inlet air of the calibration gas. A pump is attached to draw in the inlet air and draw out the sample from the GC-FID. NB: SL1 = sample loop 1. ND = Nafion dryer. (Ellutia, 2011b)

3.1.1 Flame ionisation detector (FID)

Flame ionisation enables the detection and quantification of target organic compounds through analysis of the ions produced using a hydrogen flame. The fraction of hydrogen ions from the sample with respect to the hydrogen flame allows for easy identification of hydrocarbons. The quantity of ions generated is proportional to the compound concentration. Carbon monoxide and carbon dioxide cannot be directly measured using an FID as they possess no hydrogen. Furthermore, no other hydrocarbons elute at the same time as methane (no co-elution). The detector was set to an internal temperature of 200 °C. Figure 3.2 shows a typical chromatogram produced by the GC-FID. The initial peak is due to a disruption to air pressure when the injector pump is used and is therefore ignored. Due to the fast retention time of methane, air samples were taken every 1 - 2 minutes. Frequent calibration gas sampling allowed the quantification of air samples by comparison and the achievement of high precision, both are explained in more detail in the following section.

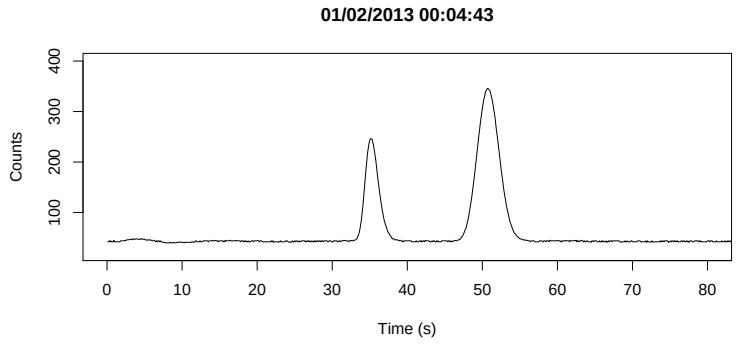

Figure 3.2: Ellutia 200 GC series raw data of a single chromatogram. The first peak shows a disruption due to air pressure when the injector pump is used, which is ignored. (Ellutia, 2011b)

3.1.2 Sampling and calibration

Each GC is capable of recording air samples every 1 - 2 minutes. This produces over 3000 chromatograms per day when all three sites are considered. It is therefore necessary to automate the analysis. This is done using the commercially available software 'Igor' (Wavemetrics, 2012) which automatically detects and measures the desired peak height. Each GC site has a Brin's Oxygen Company (BOC) methane calibration gas which has been cross calibrated with a

National Physical Laboratory (NPL) standard calibration gas to give an increased accuracy. Precision is defined as either the coefficient of variation (%) or the relative standard deviation (%) (AirLiquide, 2015). The latter was used for this thesis, specifically defined as $rsd5\,/\,rm5 \times 100$ where rsd5 is the five point rolling standard deviation and rm5 is the five point rolling mean. Calibration timesteps of 15, 30 and 60 minutes were explored. The resulting precisions proved that running calibration gas samples every 30 minutes gave optimum results without unnecessary gas usage.

As mentioned in Chapter 2, additional data used in this thesis were recorded at the Weybourne and Tacolneston sites using a GC-FID and a Picarro CRDS, respectively. These sites have been calibrated onto the NOAA scale (Schnell et al., 2004). Intercalibration results between the Cambridge NPL and NOAA calibration gases for three separate instances are shown in Table 3.1. Both the stated and derived calibration concentrations for the NPL standard were within the ranges of the calibration gas uncertainties plus GC-FID precision. However, the NPL standard consistently showed a lower reading than the NOAA derived concentrations. This is further demonstrated in Figure 3.3 which shows methane concentrations of both the University of Cambridge (UCAM) and the University of East Anglia (UEA) GC-FIDs at Weybourne. Outliers between the two datasets are thought to be due to either time-varying instrument precisions or sampling frequency. As stated before, the Cambridge GC-FID sampled every 1-2 minutes allowing for the majority of fluctuations in methane concentrations to be resolved. The University of East Anglia GC-FID had a sampling resolution of ~20 minutes which, when averaged down to hourly values, could sometimes cause discrepancies between the two datasets. In response to this, Haddenham, Weybourne and Tilney were transferred onto the NOAA scale by adding the averaged concentration difference from the three inter-calibration experiments (+4.9 ppb).

Table 3.1: Intercalibration results of NPL and NOAA gas cylinders. Initial NPL methane concentration was 1802 ±5 ppb. The NPL concentrations shown are derived using multiple point calibration analysis using NOAA gas cylinders with uncertainties of ±0.2 ppb. Calibration 1 was run through the UEA GC-FID located at Weybourne. Calibration 2 was run through the UCAM GC-FID located at Weybourne. Calibration 3 was run through the UCAM GC-FID located in the Cambridge laboratory. The three GC-FID sites were transferred to the NOAA calibration scale by adding the averaged ppb difference from the three inter-calibration experiments (1806.9 - 1802 = 4.9 ppb)

	Location-Instrument	NPL (ppb)	Instrument Precision (ppb)
1.	Weybourne - UEA GC-FID	1804.7	1.3
2.	Weybourne - UCAM GC-FID	1806.5	3.1
3.	Cambridge - UCAM GC-FID	1809.5	4.3
	Avg.	1806.9	2.9

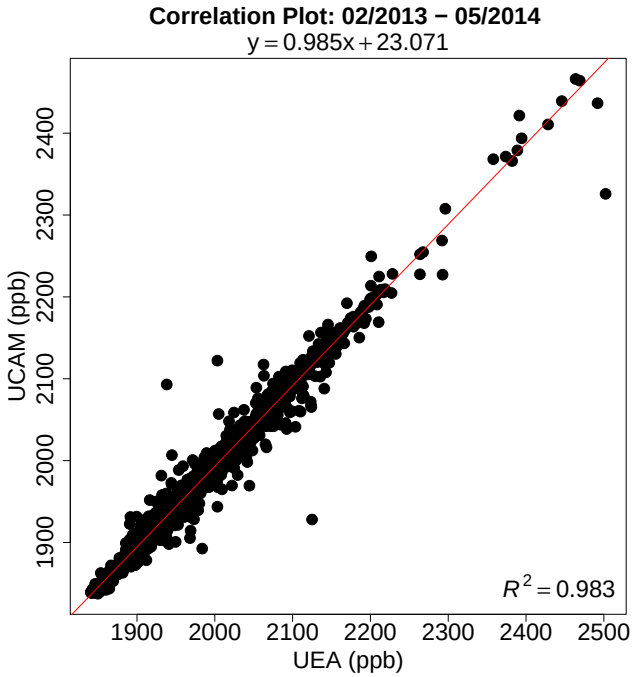

Figure 3.3: Correlation plot between the Weybourne East Anglia (NOAA calibration, x-axis) and Cambridge (NPL calibration, y-axis) GC-FID concentrations measured between February 2013 and May 2014. Plot shows hourly averaged methane data for time periods when both instruments recorded concentrations.

3.1.3 Data selection

Raw concentration values were averaged to hourly timesteps and corresponding precision values were also calculated. In addition, statistical information,

including 5^{th} and 95^{th} percentiles, and an observation 'uncertainty' were derived. The observational uncertainty was defined as the total of the calibration gas uncertainty range, the GC instrument precision and the standard deviation within the hourly observation. There are strengths and limitations to this chosen method of estimating uncertainty, which is discussed in detail in Section 5.7, for example, the chosen metrics infact double counts for the repeatability. InTEM (Section 3.3) produces an estimated emission field for the particular time period (i.e. one year). If an observation has a high standard deviation then this implies a varying source emission, or a rapid change in meteorological conditions. By including the variability of each hourly observation this helps to estimate any errors in transportation within the model timestep.

3.2 Numerical Atmospheric-dispersion Modelling Environment (NAME)

3.2.1 Eulerian and Lagrangian modelling

There are two main types of atmospheric numerical models: Eulerian and Lagrangian. These models differ in their perspective of atmospheric motion. This project uses data from both model types to run the inversion system. A Eulerian model defines specific reference points in a gridded system that monitors atmospheric properties (e.g. pressure, temperature, chemical concentration) over time.

A Lagrangian model takes the perspective of a finite element or 'air parcel'. The position and the properties of this air parcel are calculated over time using the constructed meteorological fields. The path that the air parcel travels along is called its trajectory, which can be expressed by Equation 3.2.1, where: X = particle position, u = wind velocity, t = time.

$$X_{t+\Delta t} = X_t + u(X_t)\Delta t \tag{3.2.1}$$

The particle trajectories are calculated by recording their coordinates over a repeated model timestep (Δt). Particles can have finite or infinite lifetimes, can be assigned radioactive half-lives and are subject to the modelled physical atmospheric processes.

The Numerical Atmospheric-dispersion Modelling Environment (NAME) is a

Lagrangian numerical model developed by the UK Met Office used to calculate and predict physical atmospheric processes (Maryon and Smith, 1991). Its original purpose was to monitor the emergency response of pollutant dispersion and air quality forecasting but now is used in source assessment (Kourtchev et al., 2013) and emissions modelling (Manning, 2003). Global meteorological information (i.e. gridded winds, temperature, cloudiness etc.) required for running NAME is calculated using the Unified Model (UM, Davies et al., 2005). The UM is an Eulerian model, also developed by the UK Met Office, which divides the world into 3D grid cells. It constructs 3D meteorological fields by incorporating a large amount of observational data (i.e. satellites, balloon data etc.) into a forecasting system. From these data, a short-term forecast one hour into the future is produced, which is then re-constrained using the data, as it becomes available. This process is repeated to produce the 3D state of the atmosphere, which is represented by meteorological variables. This is stored and the meteorological variables can be then incorporated into NAME. For more details please read Davies et al., 2005. Various different spatial and temporal resolution meteorological data can be used in NAME, as explained in Section 3.2.4.

3.2.2 Representation of turbulence in NAME

The atmosphere is in a constant state of mixing, or turbulence. This is caused by many complex processes, including the movement of unstable air masses and winds experiencing friction along the Earth's surface. It is therefore necessary to represent turbulence within Lagrangian particle dispersion models in order to calculate reasonable trajectories. Equation 3.2.2 states that the particle position, X, after each timestep is dependent on the wind velocity vector, $u(X_t)$, the turbulent velocity vector for small-scale turbulence, $u'(X_t)$, the low-frequency horizontal meandering, $u'_l(X_t)$, and the timestep, Δt (Ryall and Maryon, 1998).

$$X_{t+\Delta t} = X_t + [u(X_t) + u'(X_t) + u'_l(X_t)]\Delta t \tag{3.2.2}$$

The turbulent velocity vector, u', is a random walk term which has horizontal, u'_t, and vertical, w'_t, components that depend on velocity variances, σ^2, Lagrangian timescales, τ, and a random Gaussian variable, r, (Ryall and Maryon, 1998). Their mathematical relationships are shown in Equations 3.2.3 and 3.2.4. The final component in Equation 3.2.4 represents a "drift velocity", which stops

particles from gathering together when the standard deviation is small.

$$u'_{t+\Delta t} = u'_t(1 - \frac{\Delta t}{\tau_u}) + (\frac{2\sigma_u^2 \Delta t}{\tau_u})^{\frac{1}{2}} r_t \tag{3.2.3}$$

$$w'_{t+\Delta t} = w'_t(1 - \frac{\Delta t}{\tau_w}) + (\frac{2\sigma_u^2 \Delta t}{\tau_u})^{\frac{1}{2}} r_t + \frac{\Delta t}{\sigma_w} \frac{\partial \sigma_w}{\partial z} (\sigma_w^2 + w'^2_t) \tag{3.2.4}$$

3.2.3 Accuracy of trajectory models

Trajectory models that incorporate 3D wind fields and consider the turbulent mixing that occurs under the boundary layer produce a better representation of transportation than conventional trajectory models, although errors of around 20 % of the distance that the particle has travelled can be expected (Stohl, 1998). Errors can be higher for forecasting trajectories, reaching higher than 30 % in some cases, but Stohl (1998) emphasises that trajectory error varies greatly on an individual basis. The accepted way to assess trajectory model accuracy is to compare it with a reference trajectory whose origin is known and whose quantity can be easily measured. Tracer experiments are usually carried out with 'tracers of opportunity' rather than with artificially deployed tracers which require pre-planning an extra cost (Stohl, 1998). Specific examples of these tracer experiments using NAME include biomass burning emissions in Russia being traced to the UK (Witham and Manning, 2007) and emissions of sulphur dioxide from the eruption of Eyjafjallajökull in Iceland which were then measured by satellite (Heard et al., 2012). In a study by Ryall and Maryon, 1998 NAME was described as "successfully predicting the overall spread and timing of the plume" although the vertical dispersion scheme was described as "insufficient" in the two experiments conducted in this paper (this is discussed further in Section 6.5).

3.2.4 NAME configuration

NAME releases 'particles' that represent air-parcels at any x, y, z coordinate location. These particles' trajectories can be monitored either forwards or backwards in time. In this study, the model setup at each site was identical except for the source release location and height. The three sites which measured between 15-25 m (Haddenham, Weybourne and Tilney) had a release altitude of 25 m (±25 m). Tacolneston, which recorded at 50 m and 100 m was assigned a release altitude of 75 m (±25 m). For this study, NAME produced a modelled representation of the contributing surface influence to a particular source location

over a defined period of time. For example, particles can be released for a set duration and periodically monitored. NAME produces a time integrated particle density map for each source, which shows, on a gridded output, how many particles, and for how long have they been in each grid cell over the determined time period.

For this project, NAME was run in backwards mode, releasing 10 000 particles over each hour of the day. There were therefore 24 different sources released per day. Each source had an emissions rate of 1 g s^{-1} and an internal timestep of one minute was used to recalculate particles' trajectories. A source's overall mass remains constant throughout the run as the particles are defined as inert. Only surface influence (defined as the 100 m above ground level in NAME) is recorded for this study as the objective is to calculate emission rates. Particle lifetimes were set at five days as this period was considered long enough for the vast majority of particles to leave the domain of interest, therefore recording all surface influence within the domain. This duration also accounts for any trajectories re-entering and re-exiting due to a change of wind direction. Results were processed on a horizontal grid, which can be seen in Figure 3.4 and the dimensions stated in Table 3.2.

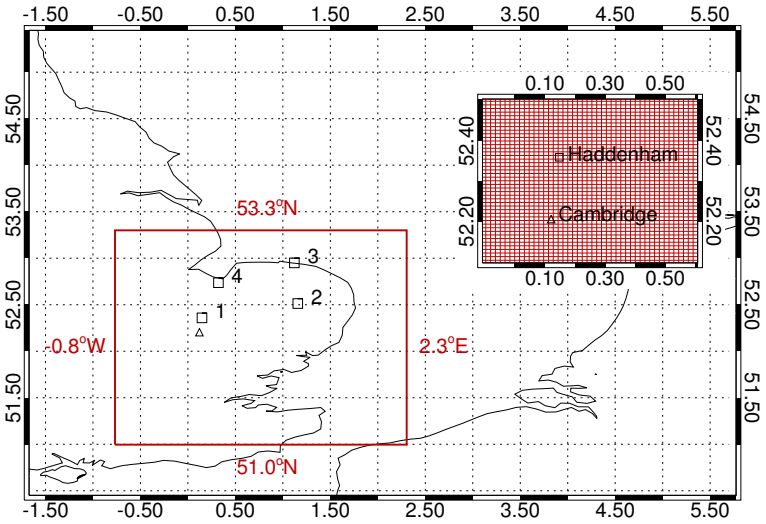

Figure 3.4: NAME output grid boundaries and spatial resolution. Site locations are labelled as squares and numbered accordingly: 1) Haddenham, 2) Tacolneston, 3) Weybourne, 4) Tilney. Cambridge is labelled as a triangle for spatial reference (~17 km from Haddenham). The subplot to the top right shows the resolution of the grid (~1.5 x 1.5 km).

Figure 3.5 shows an example of a NAME 'air history map'. This figures shows the surface contribution (0 - 100 m agl) of a single source released over a one

Table 3.2: NAME output grid spatial resolution details. All units are in degrees.

	***X* Start**	***Y* Start**	**Number of *X***	**Number of *Y***	**d*X***	**d*Y***
1.5 km resolution	-0.76	51.00	192	256	0.016	0.009

hour period. The particles are released from the Haddenham measurement site and tracked backwards in time for five days. This particular source release shows a change of wind direction where recent air comes from the south east while older air was from the north west. Areas with the highest integrated particle density throughout the 'surface' are shown in red. Note that a log scale is used where grid boxes shaded purple show a surface influence difference of five orders of magnitude less than red.

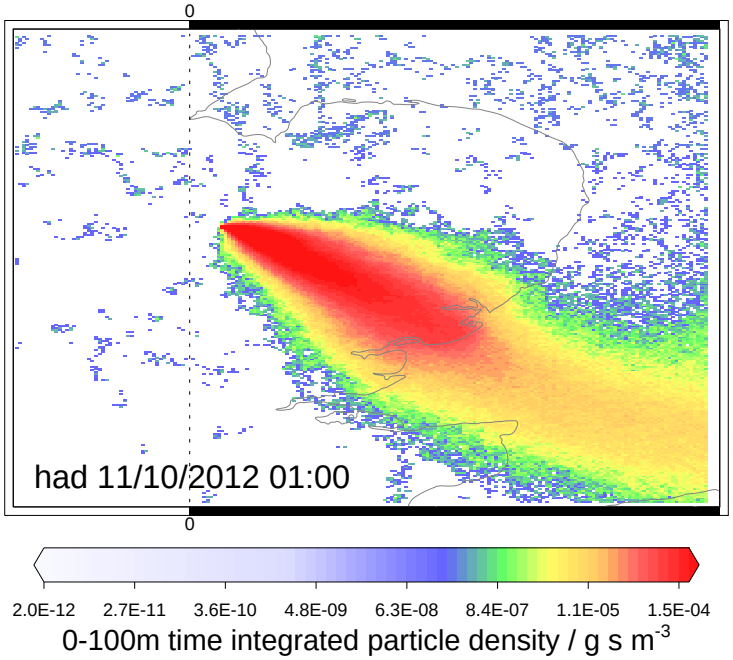

Figure 3.5: Single site NAME backward trajectories map (air history map) of a one hour source release from Haddenham on 11 December 2012 01:00-02:00. The surface influence (0 - 100 m agl) is recorded as a time-integrated concentration (g s m^{-3}). The meteorological data used were UM nested UK regional at 1.5 km resolution within global 25 km resolution (Section 3.2.4.1). This air history map shows a south easterly wind with the majority of the surface influence being from the Suffolk region.

3.2.4.1 NAME meteorological data resolution

As described in Section 3.2.1, NAME requires meteorological data from the UM. These meteorological data are available on different spatial and temporal resolutions depending on the area of the globe and the year NAME runs at.

Prior to August 2014, global meteorological data were available at 25 km spatial resolution. This was calculated using the N48 L60 UM configuration, which divides the world into grid cells of 0.375 degrees longitude by 0.234 degrees latitude and 60 vertical grids that reach an altitude of 85 km. Current meteorological data spatial resolution is available at 17 km. This is produced using the N96 L85 UM configuration, which has grid cells of 0.255 degrees longitude by 0.159 degrees latitude and 85 vertical grids that reach an altitude of 85 km. Both these configurations produce meteorological data at three hour intervals. Additionally, since July 2012 regional meteorological data, covering the UK only, are available at 1.5 km horizontal resolution and at an hourly temporal resolution. This is produced by the N96 L85 UM configuration described above (Met Office Website, 2015b). Figure 3.6 shows the difference between using the high and low resolution meteorological data. Minor differences in wind speed, direction and turbulence propagate through the backwards trajectories producing 'fan-like' effects in the difference plots (Figure 3.6.C). Due to the small regional scale of this project the 1.5 km meteorological data were used in order to represent regional wind flow more accurately.

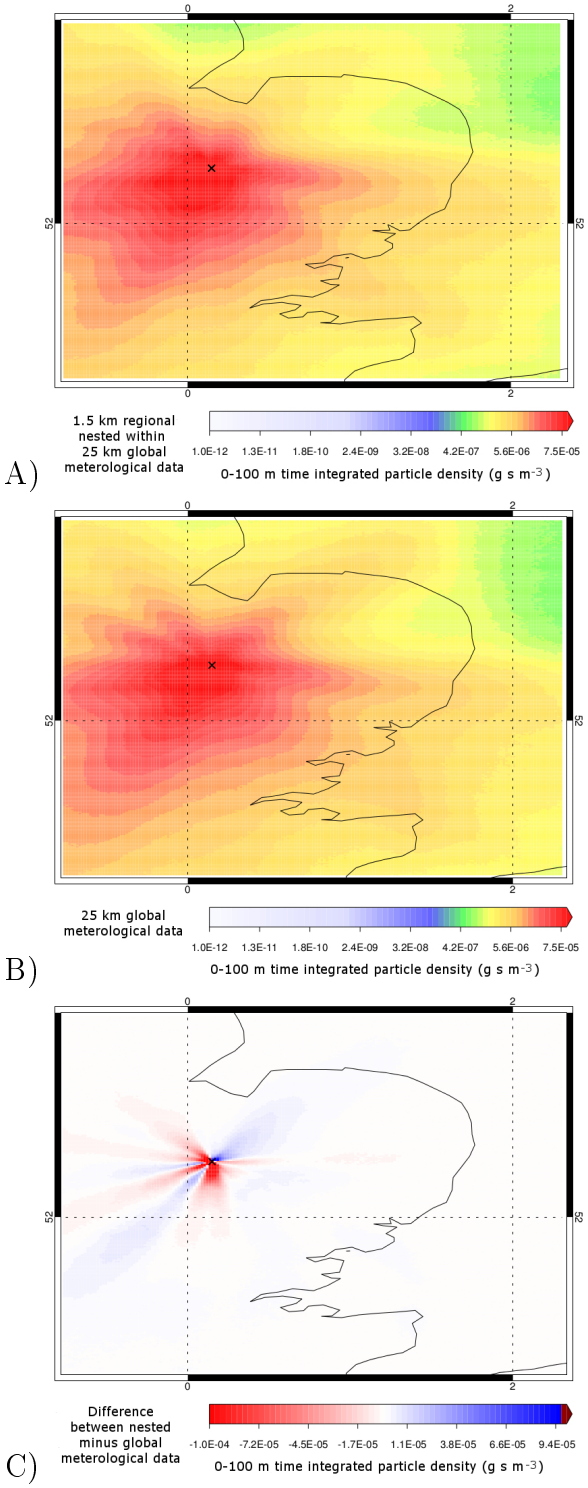

Figure 3.6: Single site NAME backward trajectories maps. Sources are released from Haddenham (labelled X) for a one hour duration period, every hour throughout August 2012. All particles released are tracked backwards in time for five days. The surface influence (0 - 100 m agl) is recorded as a time-integrated concentration (g s m^{-3}). A) Uses 1.5 km resolution regional EA meteorological data nested within 25 km global resolution data within NAME, whereas B) uses solely 25 km resolution meteorological data. C) shows the differences between the two (A-B). All plots shown on the NAME output grid of 1.5 km box resolution shown in Figure 3.4.

3.3 Inversion Technique for Emissions Modelling (InTEM)

3.3.1 Introduction

In this section the specific inversion method used for all analysis in future chapters is described. The inversion process combines the observational time series produced from the GC data and the NAME air history output, which were explained in the previous sections. This process produces estimate methane emission fields for a pre-defined domain of interest. The Inversion Technique for Emissions Modelling (InTEM) was developed by A. Manning at the UK Met Office and has typically been used to estimate regional emissions for long lived gas species (Manning, 2003; Manning et al., 2011b; Manning, 2011; Manning and Derwent, 2006). In some instances, this technique has been used to estimate emissions of very short lived species (Ashfold et al., 2014). InTEM requires several variables to be determined prior to running, all of which are explained in this section.

The principles of inverse modelling provide an estimation method for a driving variable of a system. This variable, normally defined as the state vector (and for this project is the emission rates), can be estimated using our understanding of the surrounding physical driving forces and by measuring some observed variables which have evolved from this system e.g. atmospheric concentrations (Jacob, 2007). Equation 3.3.1 explains this relationship in its simplest form where y is the measured observations, x is the state vector, k is the forward model and σ_ϵ is the representation of error. This error is a sum of both the modelled, σ_m, and measured errors, σ_i, (Equation 3.3.2). The major assumptions undertaken with this formulae are that the relationship between x and y is linear and that all errors are uncorrelated and therefore additive.

$$y = kx \pm \sigma_\varepsilon \tag{3.3.1}$$

$$\sigma_\varepsilon^2 = \sigma_i^2 + \sigma_m^2 \tag{3.3.2}$$

A crude overview describing the relationship between the NAME air history maps, the measured observations and how InTEM links these variables is shown in Equation 3.3.3.

$$emission\,(g\,s^{-1}\,m^{-2})\;\times\;dilution\,(s\,m^{-1})\;=\;concentration\,(g\,m^{-3}) \tag{3.3.3}$$

InTEM synthesises the resulting emission fields by producing a modelled time series of observations (pseudo-observations) which is compared to each measurement site's concentration time series. More information about how these pseudo-observations are generated can be found in Section 4.4, but essentially, a starting emission field is multiplied with a manipulated formulation of the NAME air history maps (called the dilution matrix - Section 3.3.2). These two observation time series are compared using cost function analysis (Section 3.3.5) through a process called simulated annealing, which iterates between different emission fields to find the optimal result. Simulated annealing, named due to its similarities with annealing in metallurgy, aims to locate a good approximation to the optimum result. A large search space results in the derived output often being an acceptable conclusion rather than the best possible solution. The iterating process is split into so-called 'temperature' steps which each have a number of internal iterations. For this thesis 100 temperature steps and 20 000 internal iterations were used. A detailed explanation into this decision can be found in Section 5.1.

3.3.1.1 Why InTEM was chosen

Many different inversion techniques exist for emissions modelling. InTEM was chosen for this project due to the long-standing relationship with the UK Department for Energy and Climate Change (DECC) where it has been used to produce annual national methane emissions estimates dating back to 1990 (Manning et al., 2011b). An initial aim of this project was to establish a 'proof of concept' that InTEM could be used at the regional scale, and thus was a development of the ongoing work confuted by Manning *et al.* for DECC. Other inversion methods differ in three main ways: by using different observations, model, and/or cost function. Most other methods use an alternative cost function than the one described in Section 3.3.5 named the Bayesian approach. The strengths and weaknesses associated with these cost functions are described in Section 3.3.5.1. Alternative meteorology used in other top-down approaches include European Centre for Medium Ranged Weather Forecasting (ECMWF) data, as opposed to UM data. These data have been used in work such as

Meirink et al. (2008); Bergamaschi et al. (2005, 2009). The major differences between these two datasets are the spatial resolution. The UM data are on a finer resolution of ~1.5 x 1.5 km hourly as opposed to ~60 x 60 km in the ECMWF available every three hours (Berchet et al., 2013). The finer spatial and temporal resolution should capture smaller scale meteorological movements and more accurately estimate the methane emission distributions on the regional scale. The observational data used for this project is from four instrument sites within EA. Other inversion techniques that have estimated methane emission in the UK have used single and multiple measurement sites, for example, Manning et al. (2011b) uses data from the Mace Head site in Ireland, and Ganesan et al. (2015) uses four tall tower sites situated in Mace Head, Tacolneston (EA), Ridgehill (West of England), and Angus (Scotland). The four measurement sites used in this project are located much closer together (<100 km) as this project focuses on a smaller, more regional area of the UK.

3.3.2 Dilution matrix

The dilution matrix (s m^{-1}) is used to link surface emissions (g m^{-2} s^{-1}) to a modelled or measured concentration (g m^{-3}). This is derived by manipulating the hourly NAME air history maps by firstly dividing by the mass released (g) and then multiplying by a surface area matrix (m^2). Figure 3.7 shows the dilution matrix averaged over all source releases in 2013 and 2014 for the Haddenham site. The site experienced a dominating air origin from the south west (the prevailing wind direction). This was also the case (although not shown) for the other sites and other years studied in this thesis.

3.3.3 The solution grid

InTEM produces the resulting emission field on a pre-determined spatial grid or 'solution' grid. A more finely resolved solution grid allows InTEM a greater degree of freedom when estimating emission fields, however this flexibility is at a cost of computer time. The solution grid can be as fine as the NAME output grid resolution (0.016 x 0.009 degrees, 1.5 x 1.5 km), however this results in 49 152 grid boxes in which the emissions can be varied within InTEM. This far exceeds the computer power and time that is available for this study. It is therefore necessary to define a more coarse solution grid resolution (which has fewer degrees of freedom) for InTEM to solve on. To start, the inversion

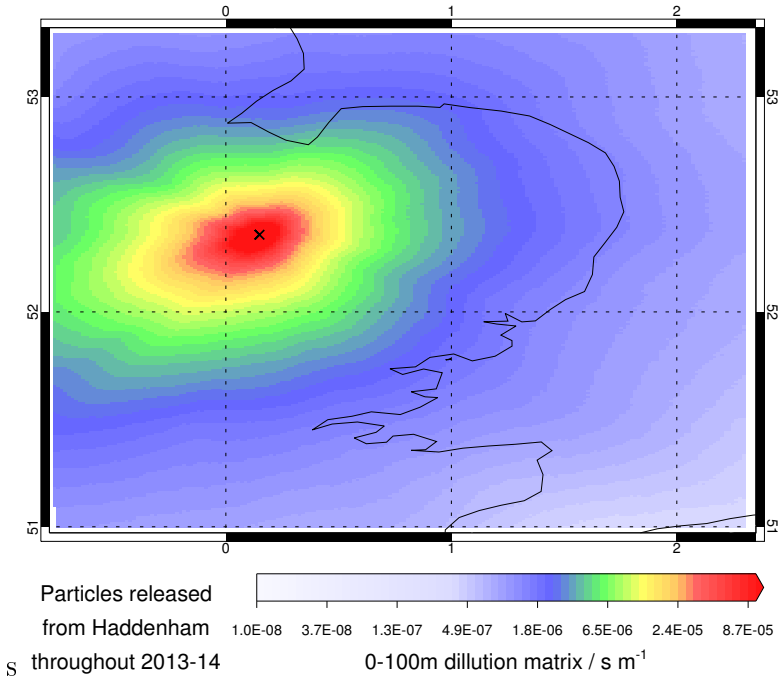

Figure 3.7: Mean dilution matrix for the Haddenham site (location marked with a X) for the years 2013 and 2014. Sources are released for a one hour duration period, every hour from 01 January 2013 to 31 December 2014. Meteorological data used to run NAME were 1.5 km regional resolution nested within 25 km global resolution.

domain must be manually divided into coarse 'regions'. This project chose to define the coarse regions based roughly upon the East Anglian county boundaries. Figure 3.8.A shows the inversion domain split into these 15 regions of varying sizes. The regions making up the edges of the domain are usually disregarded when analysing emission fields due to baseline issues (explained in Section 5.10). InTEM produces statistical information for each separate region, which gives valuable information relating to emission uncertainty values. The solution grid can then be formed via one of two methods (described below), but is always based around these original regions. The resulting solution grids have a spatial resolution in between the original regions and the NAME output grid resolution.

- The NAME-based solution grid. This method created a solution grid with a varying spatial resolution which was determined using the NAME dilution maps. The method is similar to that described in Manning et al. (2011b) where areas within the inversion domain that have a larger 'surface influence' will have a finer spatial resolution. A large surface influence refers to when the released NAME particles from each measurement sites' x, y, z coordinates have remained in the bottom 100 magl for relatively long period of time. For example, from Figure 3.7 it can be seen that areas

around the measurement site location, or upwind of this location have larger surface influences. Conversely, areas where air has spent relatively little time i.e. north-east of the sites (opposite to the prevailing wind) have a lower surface influence. A pre-defined dilution threshold subdivides regions into more finely resolved grids based on the dilution matrix and produces the resulting solution grid, which is in the same units as the dilution matrix (s m^{-1}). A region is repeatedly split into two equally contributing sub-regions if it reaches this threshold. Areas nearer to the observation site will reach this threshold many times over and thus create finely resolved regions while areas where little information is known will remain coarser (Manning et al., 2011b).

- The NAEI-based solution grid. This alternative method also used the described method above however, additionally, it incorporates the methane NAEI emissions to also determine the solution grid resolution. For each subdivided area the NAEI emission magnitudes are used as a scaling factor to the dilution threshold in determining the solution grid resolution. In this method areas of the inversion domain where point sources of methane can be found in the NAEI (e.g. landfills) will be be more finely resolved than areas where low methane emissions are found.

These methods are discussed in more detail in Section 5.4 and Section 5.5. Figure 3.8.B and Figure 3.8.C show the resulting solution grids used in this analysis for the NAME-based and NAEI-based methods, respectively. Both grids are ~150 grid boxes. Areas with smaller grid boxes correspond to having a higher surface influence (calculated from the NAME air history maps) and, for Figure 3.8.C, higher sources of methane according to the NAEI.

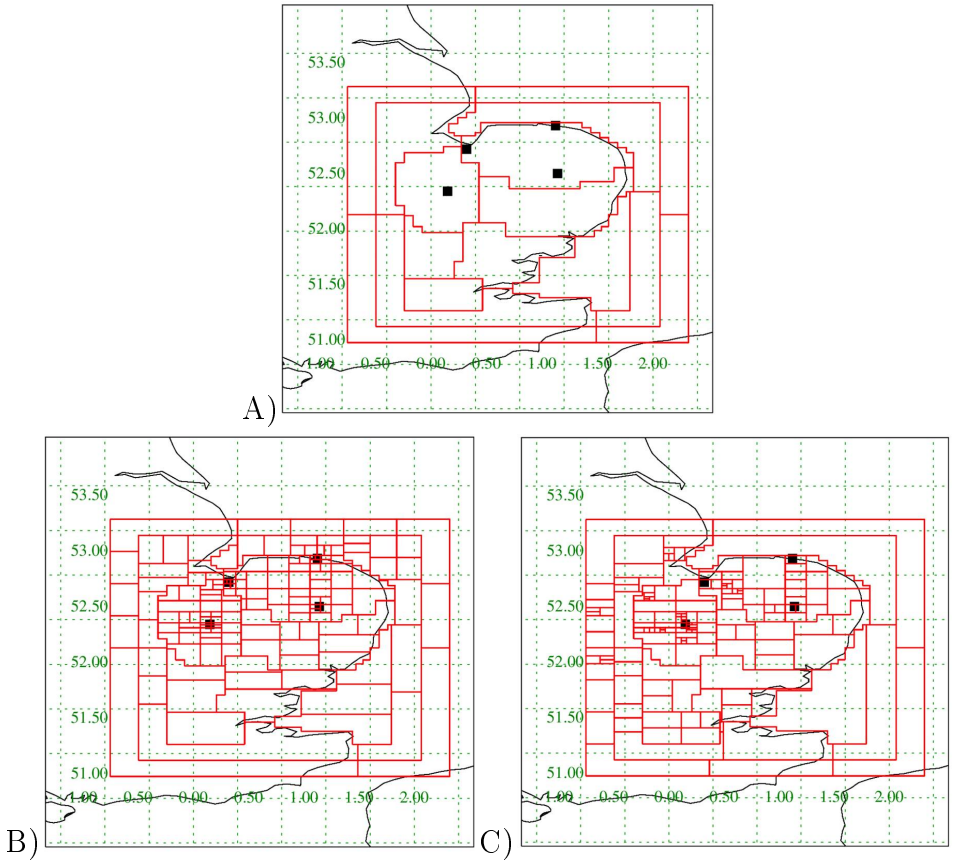

Figure 3.8: InTEM solution grids at various spatial resolutions. A) shows the most coarse resolution of 15 regions based loosely upon the UK county borders (e.g. Norfolk, Suffolk, Cambridgeshire and Essex). Other regions are more loosely defined. B) shows the NAME method's resulting solution grid. C) shows the corresponding NAEI method's solution grid. Both grids have ~150 grid boxes. Black squares represent the measurement site locations.

3.3.4 Baseline representation within InTEM

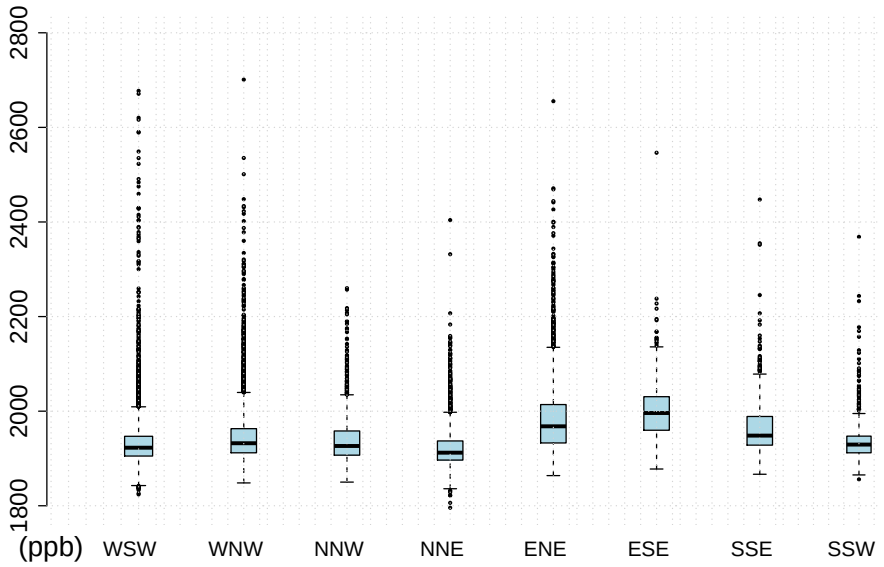

Figure 3.9: Boxplots showing the range in concentrations (ppb) of all four sites across the full two year dataset (July 2012 - May 2014) separated by wind direction. Lower and upper box limits refers to the 25^{th} and 75^{th} percentiles, respectively, and the mean is shown as a thick horizontal black line. Whiskers show 1.5x the interquartile range with outliers marked as individual points.

The NAME air history maps are only subject to surface contributions from the previous five days and from within the domain itself. Any outside emissions must therefore be removed from the observational time series. The method developed here to produce these baselines uses the NAME air history maps as an indication of the air origin and was conducted on the full dataset (July 2012 - May 2014). Firstly, the edges of the NAME domain were split into octiles representing different wind directions (NNE, ENE, ESE etc.). For each hourly air history map the time integrated concentrations for all eight edge sections were converted into percentages. When a backmap had a dominating air origin, i.e. one octile had over 80 % of the mass, this methane concentration was subselected. This was repeated for all four observation sites to produce separate time series representing concentrations from the eight different wind sectors. Figure 3.9 displays the subselected time series as boxplots. Air originating from the east and south east typically have larger contributions from European emissions than the other edge regions, while air from the west has more high outliers. This implies nearby, time-varying methane sources. Eight individual baselines were then calculated

for each wind section. This was done using a rolling 18^{th} percentile spanning one week, which produced a smooth baseline. Sensitivity analysis where the rolling percentile was varied showed this baseline produced emission results with consistently stable emissions with the lowest cost score of all baselines tested. Analysis of these sensitivity studies is found in Figure 3.10. A time window of one week was chosen because the baseline is flexible enough to respond to long term polluted periods of elevated methane levels but will not vary over shorter time periods from more local influences. Diurnal variability, which is strongly related to boundary layer height, is modelled in NAME and thus should not be removed in the baseline. Individual baselines for the four observation sites were then constructed by taking the percentage that each edge contributes for every hour timestep. Figure 3.10 shows an example of the resulting baselines for a one month period. Further justification for this baseline can be found in Section 5.10.

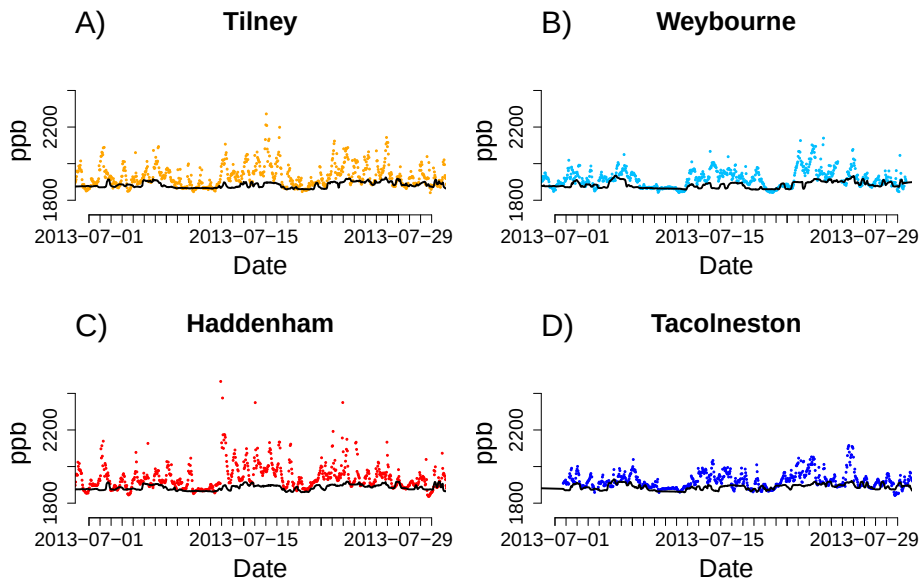

Figure 3.10: Time series of methane data (coloured points) and the resulting baselines (black lines) throughout July 2013 for A) Tilney B) Weybourne C) Haddenham and D) Tacolneston. All concentrations in ppb. Baselines calculated by separating methane concentrations into eight time series based on wind direction. Rolling 18^{th} percentile spanning one week then filter each time series. Individual baselines for the four measurement sites are then created using the percentage contribution of each wind direction for every hourly concentration (wind direction percentage contributions were calculated using the NAME air history maps).

3.3.5 Cost functions

The cost function provides a quantitative assessment of the different state vectors being tested. Multiple cost functions exist in InTEM and a near unlimited amount could be defined. For this thesis an uncertainty weighted cost function was used (Equation 3.3.4) that is similar to the traditional least squares approach. K_i is the forward model and x_i is the measured concentration, at a particular timepoint. For all timesteps the difference between the simulated-observation (Kx) and the measured observation (y) is squared and then divided by the uncertainty variance (σ_ϵ^2). This uncertainty is a sum of all assumed errors in observations, modelling and baselines for each particular hourly timestep. The specific uncertainty quantities and their derivations are explained in Chapter 5. Dividing by the total uncertainty de-weights uncertain observations. The resulting score (r_i) at each timestep (i) is then adjusted to a final cost score depending on its value (Table 3.3 and Figure 3.11).

$$r_i = \sum_{i=1}^{n} \left(\frac{(y_i - (Kx)_i)^2}{(\sigma_\varepsilon)_i^2} \right) \tag{3.3.4}$$

Table 3.3: Cost Score Table

Initial Score	Cost Score (m_i)
$r_i < 2$	r_i^2
$2 \leq r_i \leq 8$	$r_i + 2$
$r_i \geq 8$	$10 + \log_{10}(r_i - 8 + 1)$

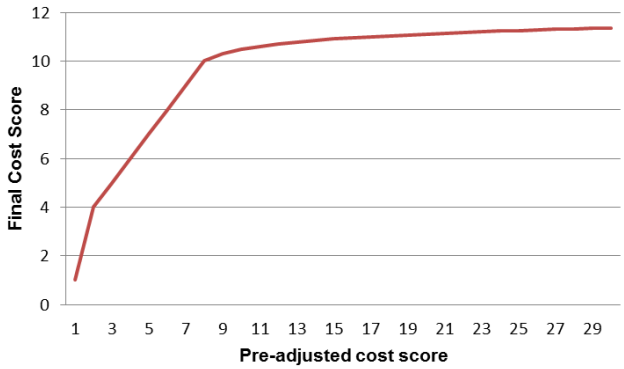

Figure 3.11: Graphical figure of the pre- and post-adjusted cost scores used within InTEM.

The final cost score (J, 3.3.5) is the sum of m_i. This non-linear approach is arbitrarily defined and is adopted to reduce the impact of outliers on the cost score.

$$J = \sum_{i=1}^{n} (m_i) \tag{3.3.5}$$

Other cost functions were considered for this project, for example, a cost function exists in InTEM which uses three statistical metrics to compare the pseudo- and measured observations (correlation coefficient, normalised mean square error and within a factor of two). This cost function was used in the analysis published in Ashfold et al., 2014. Previous analysis, not presented in this thesis, showed this cost function weighted reltively certain and uncertain observations equally and thus it was deemed the uncertainty weighted cost function more appropriate to be used for this project.

3.3.5.1 Weaknesses of the cost function

As stated before, a near-unlimited number of cost functions can be created and used for this application. This cost function was used in this thesis as the previously cost function used in Manning et al. (2011b) and Ashfold et al. (2014) did not incorporate quantifiable uncertainty values to be used within its formula and thus could not de-weight more uncertain observations. This new cost function is not without its limitations however, and the following bullet points highlight the main weaknesses.

- The use of uncertainty: Although this cost function incorporates uncertainty estimates for every timestep this value is only used to proportionally de-weight the residual at each timestep. These values are not used in calculating a final uncertain metrics within the emissions themselves. Other cost functions, for example the Bayesian approach (explained below and in Chapter 7), allows a prior, and its associated uncertainties, to be included within its cost function to produce to produce more robust uncertainty estimates of the emissions.
- Arbitrary de-weighting of high-scoring observations: The cost score used has an arbitrary method of de-weighting the outlier observations so that they don't disproportionately increase the final value.
- Resulting uncertainty estimates: The final estimation of uncertainty is defined as the resulting methane emissions' standard deviation after InTEM

has been repeated 25 times. This is justified in Section 5.3 but a remaining issues is that this is an arbitrary definition which has little mathematical basis. The resulting uncertainty estimates are likely to be incomplete. This issue is discussed more in this thesis' results chapters 5-6.

An alternative cost function, which is more commonly used within the inversion community, is the Bayesian cost function. This cost function incorporates a prior emission field to more rigorously assess uncertainties within the inversion system. More details about this method can be found in Chapter 7. An initial aim of this project was to compare emission results the uncertainty-weighted cost function together with results from the Bayesian technique but time constraints prevented this goal from being achieved. Reasons for choosing to use the uncertainty-weighted cost function as the primary analysis method were two-fold. Firstly, as described in Chapter 2, this project aimed to simulate an alternative methane emissions inventory to compare to the NAEI. Areas of similarity and differences were to be highlighted and discussed. It was concluded that, to produce an independent inventory, the Bayesian cost function (in which the NAEI would be used as a prior) should not be initially used to produce the emission estimates. Other methane emissions inventories, which could have been used as a prior, exist, for example, the EDGAR inventory, however this is available on a more coarse resolution and does not resolve point sources as finely as the InTEM system is able to. Interpolating the prior inventory to a finer spatial resolution than its available resolution can be a source of error. Additionally, assigning uncertainties to these prior emissions (a necessary step in Bayesian inversions) can be arbitrary and un-robust. Secondly, the Bayesian cost function was not available for use in InTEM at the beginning of this project. When the cost function did become available there was too little time for a thorough assessment of assigning associated uncertainties to the given prior. Thus, the uncertainty-weighted cost function was used to produce the results discussed in this thesis.

3.4 Summary

This chapter provided an overview of the experimental methods used in this thesis. The GC instruments are capable of taking atmospheric methane samples every 1-2 minutes. Raw data are analysed using the commercially available software 'Igor'. The processed data are then calibrated and formatted to hourly

timesteps. Equivalent precision and uncertainty values which are used within the InTEM setup are defined as the sum of the instrument precision, the calibration gas uncertainty, and the hourly standard deviation of the observations.

Following this, the NAME particle dispersion model was introduced and the major variables used to produce the model results were discussed. So-called 'air history maps' are calculated for each instrument site for every hour observation throughout the measurement time period (July 2012 - June 2014). Inert particles are released from each site's x, y, z coordinates and tracked backwards in time for five days. The 'surface influence' (0-100 m above ground level) of these hourly air history maps are recorded as a time integrated concentration (g s m^{-3}) on a gridded format. These air history maps are then re-formatted into a dilution matrix (units s m^{-1}) to be used within the inversion technique.

The final section of this chapter then described the InTEM setup. Various factors which need to be set for InTEM to run were described and the cost function which quantitatively assess the emissions fields was explained. More detail into the sensitivity experiments conducted to achieve these specific parameters can be found in Chapter 5. The InTEM solution grid which determines the spatial resolution of the methane emissions had a resolution of 150 individual grid boxes. Two solution grids were determined, one using solely the NAME air history maps to determine the spatial resolution, the other also incorporated the 2012 NAEI emissions field.

A baseline method to represent methane concentrations from outside the specified domain was then described, which incorporated the observation sites NAME air history maps to determine which wind direction the concentrations originated from. A rolling 18^{th} percentile averaged over one week was then used to create eight time dependent baselines based on wind direction. Each site's percentage contribution of each wind direction at each hour timestep then created the individual baselines. Finally, a least-squares cost function was introduced, which is used within InTEM to determine the most appropriate resulting methane emission field.

The next chapter explores the observations measured at the four locations in more detail. Their relationship with meteorology and their variability over time is assessed. To conclude, a case study at the Haddenham site (location 1) is discussed, which attempts to attribute the local sources experienced at this site.

4 Methane measurement analysis

This chapter is the first of the three results chapters. It discusses analysis of the atmospheric methane concentrations measured at the four sites. The measurements' variability with respect to different time periods is analysed and its relationship with modelled meteorological variables is assessed. The modelled meteorological data used in this section are from the UK Met Office's Unified Model (UM) which outputs 3D meteorological fields on hourly time frames (for more detail see Section 3.2.1). These meteorological data are used to run trajectory analysis in the NAME model but can also be directly interpolated to a given x, y, z coordinate to produce time series. These meteorological data are used to assess methane's dependance with each meteorological variable. This chapter then introduces modelled pseudo-observations, which are calculated using the NAME air history maps and the 2012 NAEI methane emission field. A case study focusing on the Haddenham measurement site including an analysis of its local sources concludes this chapter.

4.1 The measurements

A time series of the raw data measurements for all sites can be seen in Figure 4.1 - Figure 4.8. Summer months (JJA) show a clear diurnal pattern in contrast to winter months (DJF) where this pattern is less defined. Sharp, short lived peaks of methane can be seen at both Haddenham and Tilney, with occasional peaks of smaller magnitudes experienced at Weybourne. Long periods of elevated methane measured at all sites indicate large, distant sources. The potential factors driving these variations are discussed in more detail in Section 4.2 and Section 4.3.

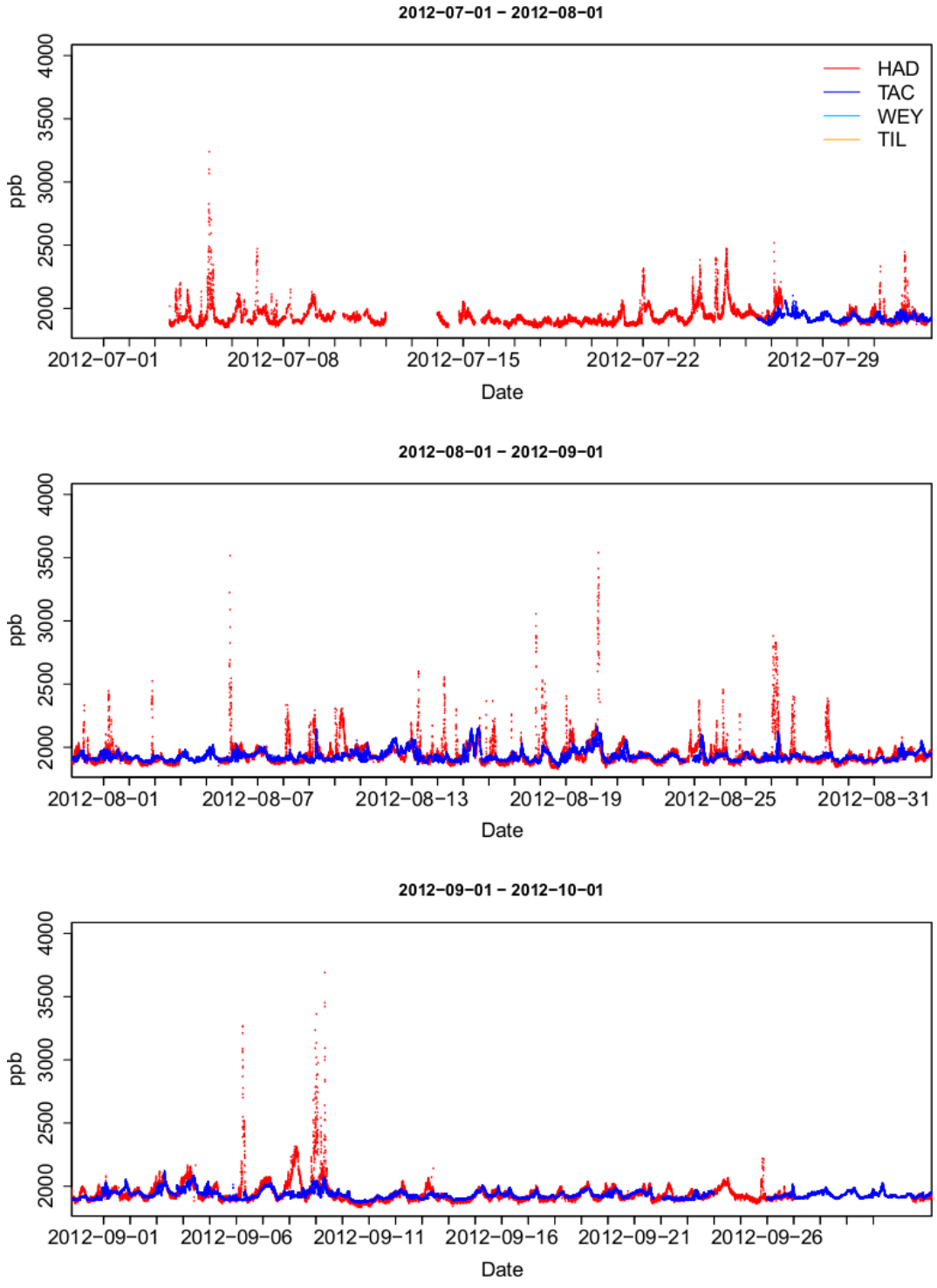

Figure 4.1: Time series of raw methane measurements collected from July - September 2012 for the Haddenham and Tacolneston sites, in ppb. Haddenham start date: 03 July 2012. Tacolneston start date: 26 July 2012.

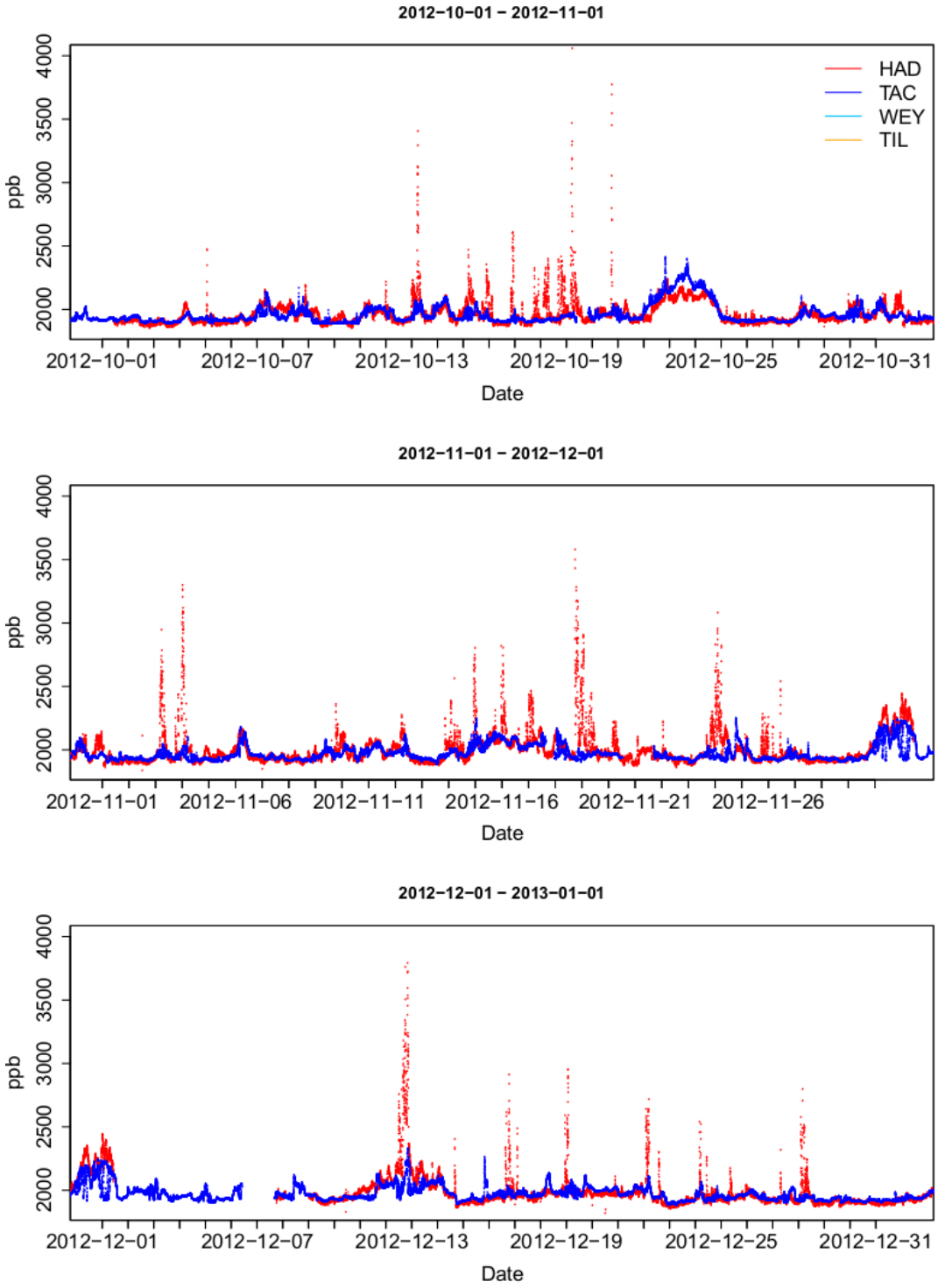

Figure 4.2: Time series of raw methane measurements collected from October - December 2012 for the Haddenham and Tacolneston sites, in ppb.

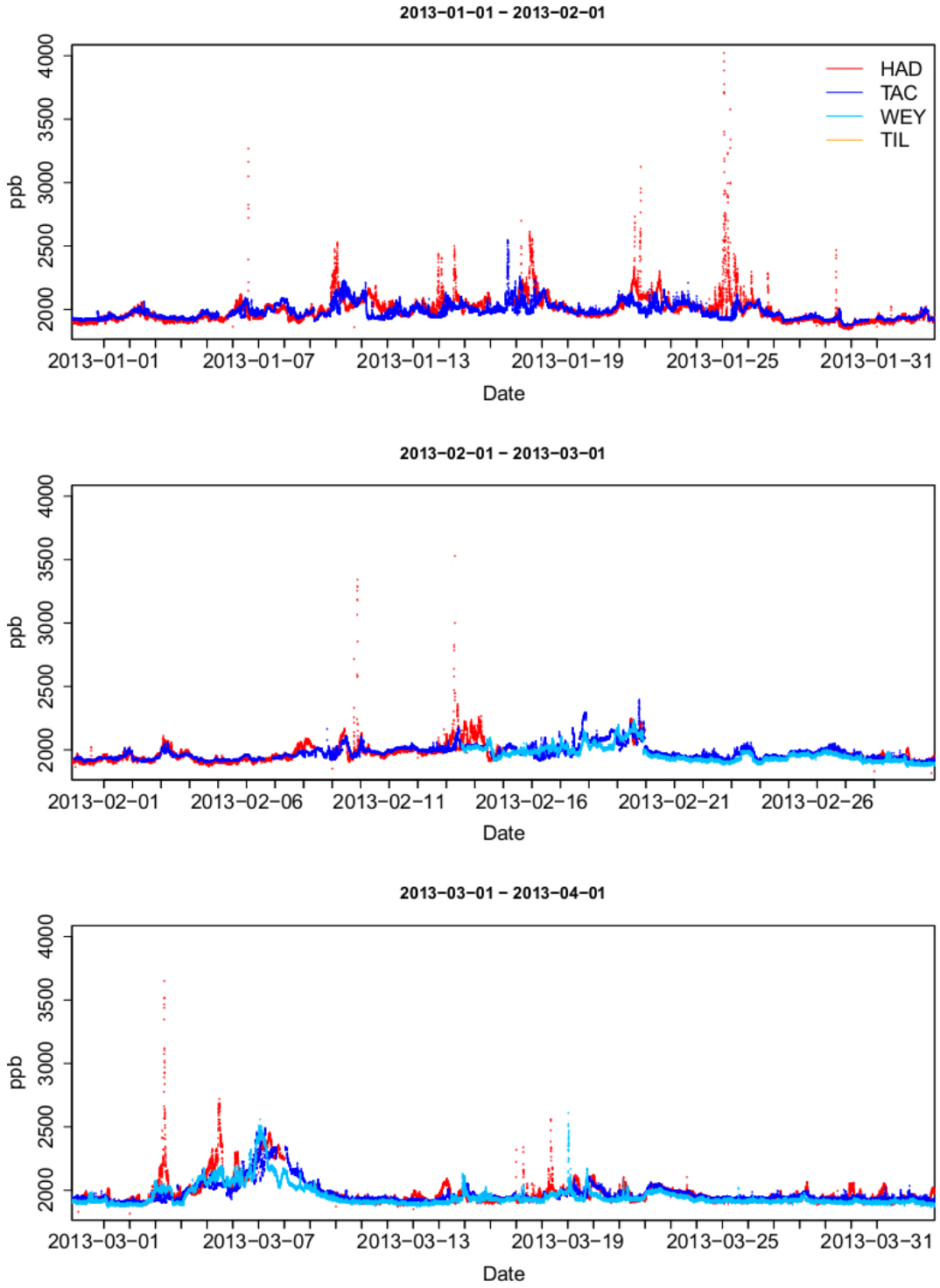

Figure 4.3: Time series of raw methane measurements collected from January - March 2013 for Haddenham, Tacolneston and Weybourne sites, in ppb. Weybourne start date: 13 February 2013.

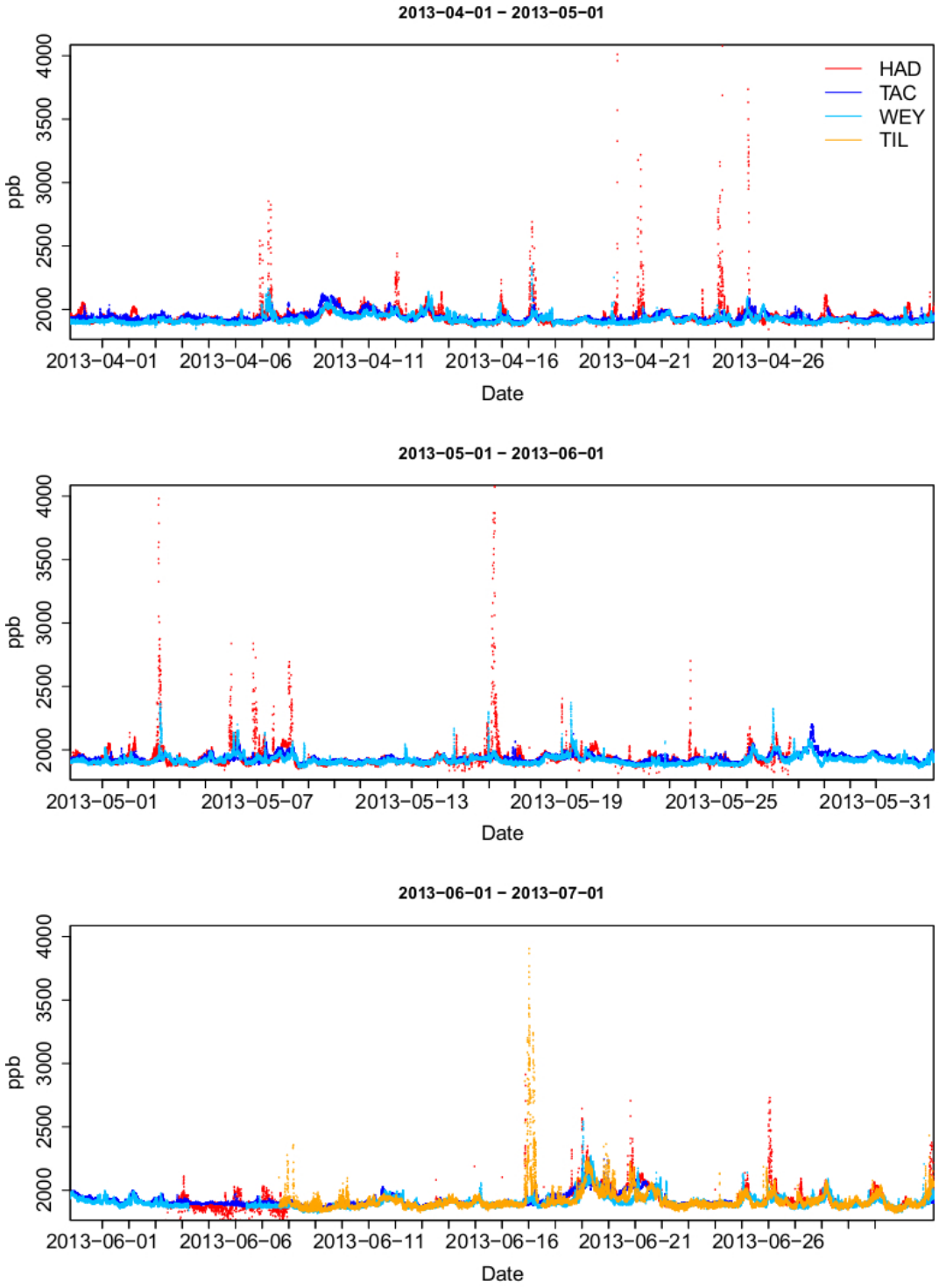

Figure 4.4: Time series of raw methane measurements collected from April - June 2013 for all four sites, in ppb. Tilney start date: 07 June 2013.

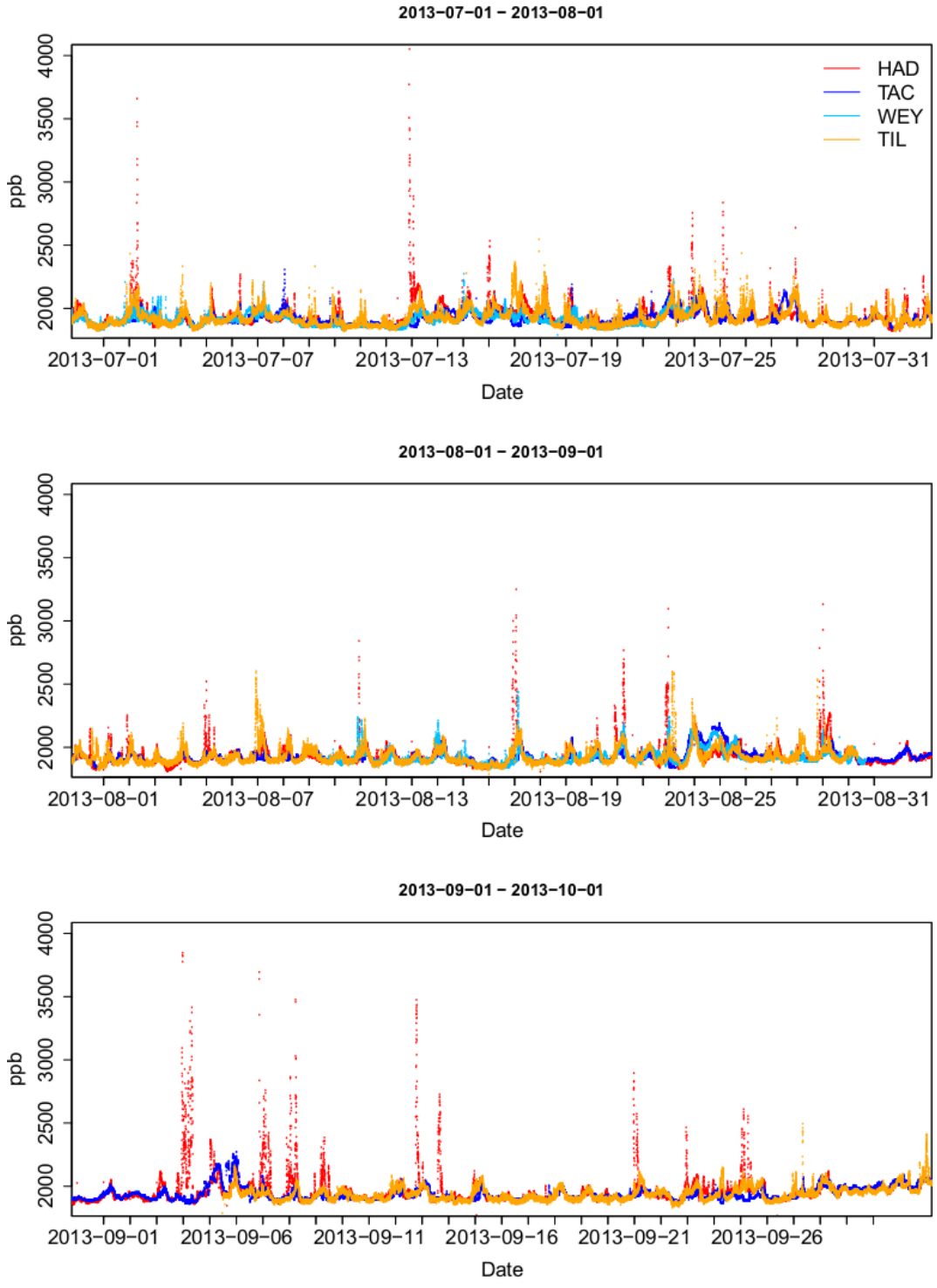

Figure 4.5: Time series of raw methane measurements collected from July - September 2013 for all four sites, in ppb.

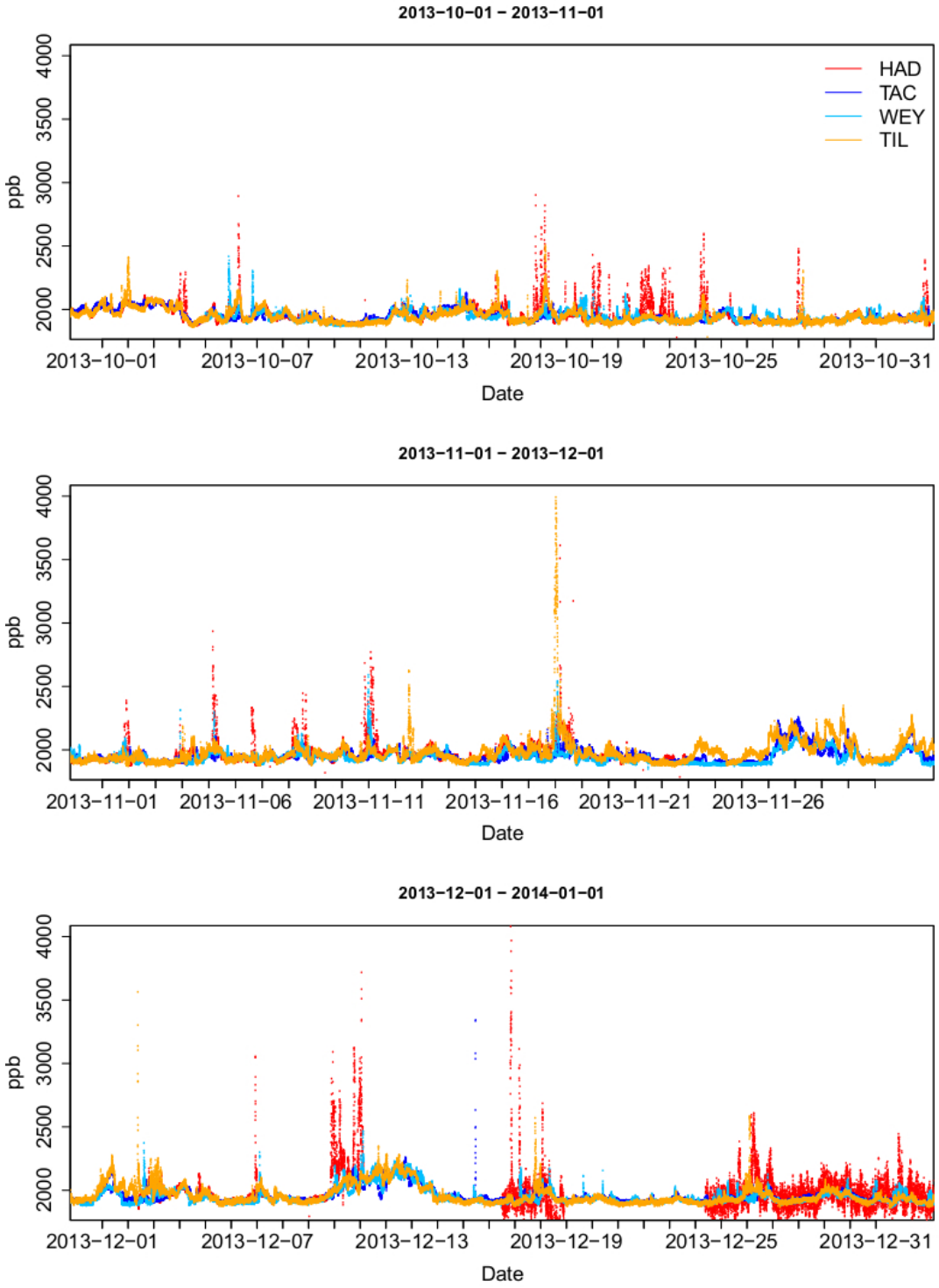

Figure 4.6: Time series of raw methane measurements collected over from October - December 2013 for all four sites, in ppb.

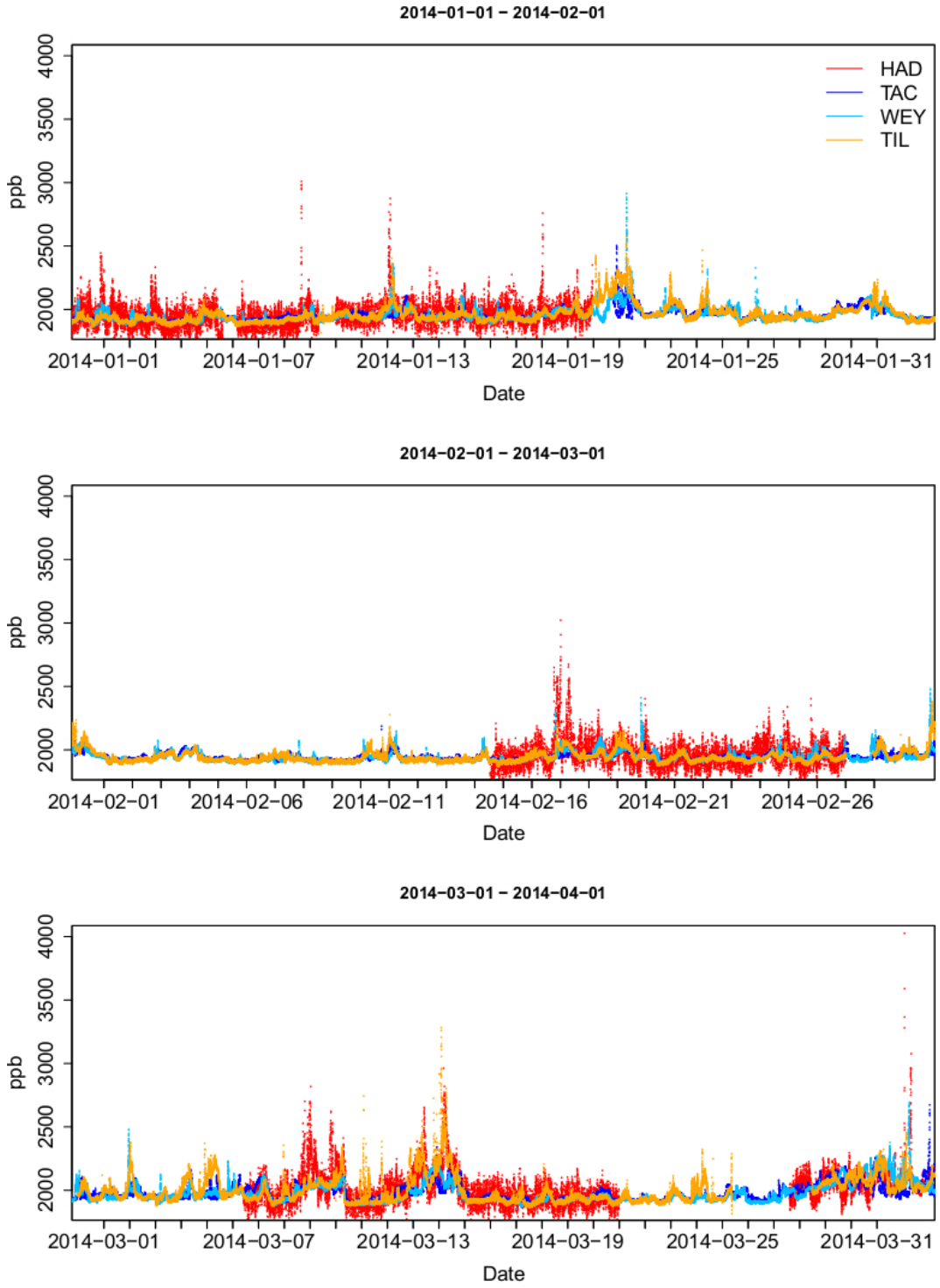

Figure 4.7: Time series of raw methane measurements collected from January - March 2014 for all four sites, in ppb.

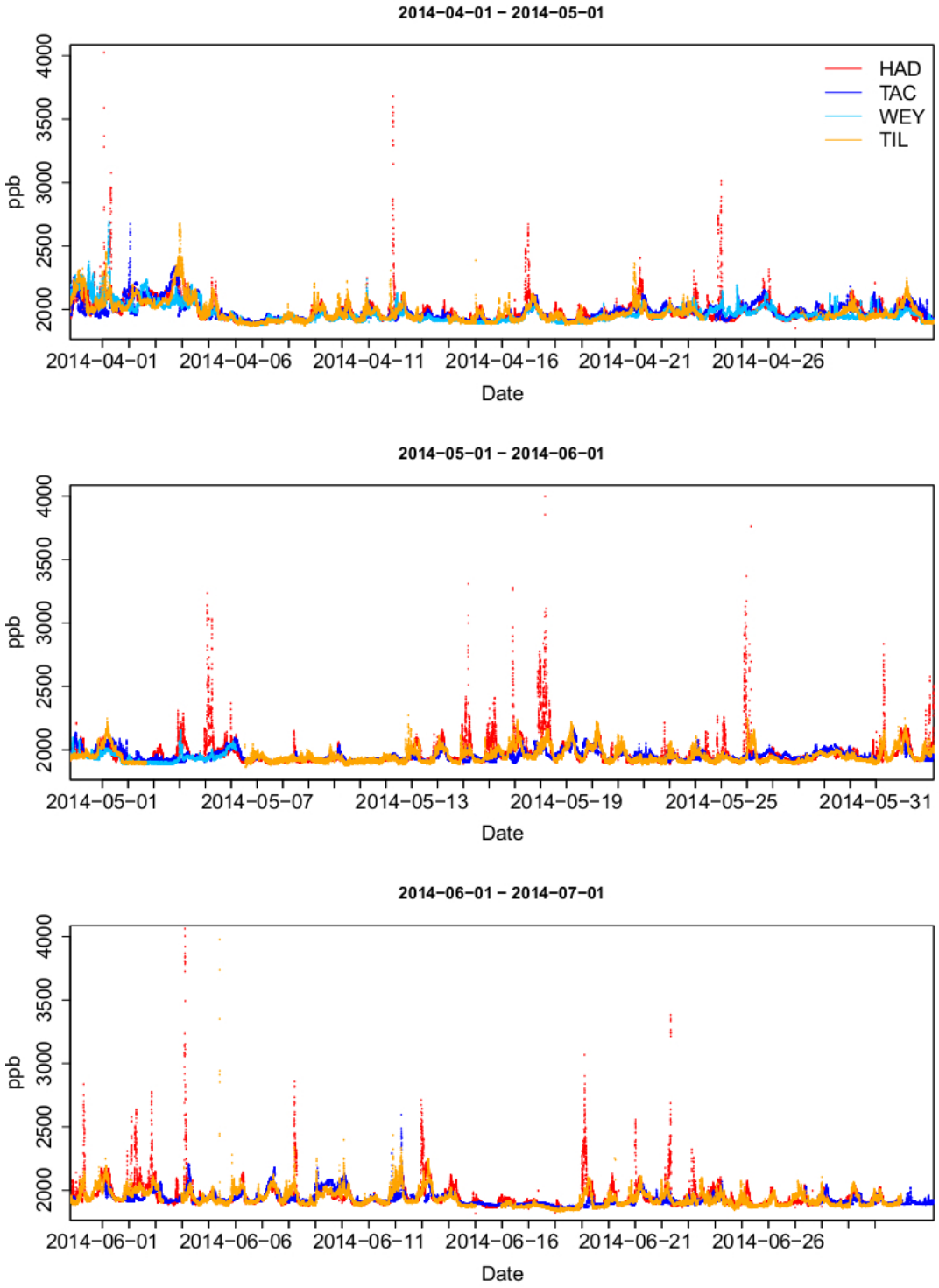

Figure 4.8: Time series of raw methane measurements collected from April - June 2014 for all four sites, in ppb.

A malfunction occurred in the Haddenham GC-FID during 10 December 2013 - 01 April 2014 resulting in significantly less precise measurements being taken.

The resulting methane concentration ranges increase considerably for this period, as can be seen in Figure 4.6 and Figure 4.7. This period of Haddenham data were removed for this chapter's analysis. The InTEM setup however, allows for instrument precision to be incorporated into the analysis and so it could still be used in the inversion process.

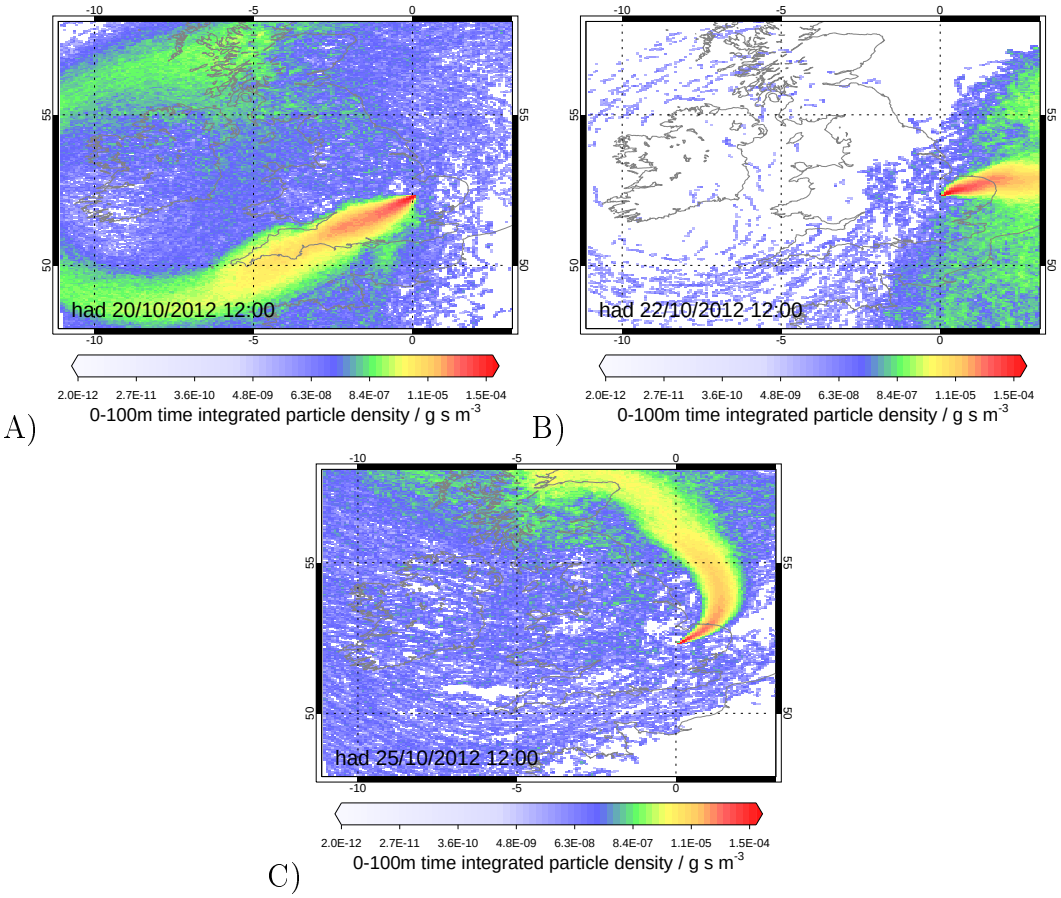

Figure 4.9: Haddenham NAME air history maps for three periods during 20 - 25 October 2012, where above baseline methane concentrations were observed. Particle release times between A) 12:00-13:00 20 October 2012 B) 12:00-13:00 22 October 2012 and C) 12:00-13:00 25 October 2012. Sources are released from Haddenham (0.149 longitude, 52.359 latitude) for a one hour duration period and tracked backwards in time for five days. Their surface influence (time spent in the bottom 100 m agl) is recorded and shown as a time integrated density map (units g s m^{-3}).

The hourly NAME air history maps can be used to explain some of the data's measured concentration changes. One example of this is the period between 20 October 2012 and 25 October 2012 (Figure 4.2) where background methane levels quickly rise and remain high for 3 - 4 days. Figure 4.9 shows three hourly NAME air history maps from before (20 October 2012 12:00), during (22 October 2012 12:00) and after (25 October 2012 12:00) this event. The sites experience easterly

winds during this elevated period, sourcing methane from North-Eastern Europe. The extensive spread of the NAME plume (Figure 4.9.B) suggests relatively low wind speeds. The Met Office's synoptic weather charts for this period also supports this conclusion (Wetter Zentrale, 2015). Before (Figure 4.9.A) and after (Figure 4.9.C) this period the wind originates primarily from the west and the North Sea, respectively, resulting in lower methane concentrations. The NAME spatial domain used here does not include continental Europe so no information on the methane source-type can be drawn. One hypothesis, when examining the EDGAR inventory, suggests Scandinavian sources are dominated by wetlands (Olivier and Berdowski, 2014), although more traditional anthropogenic sources (natural gas, waste etc.) tend to dominate Eastern Europe. The contribution is likely to be a mixture of multiple sources due to the spread of the observed plume. Large sources from outside the inversion domain

4.2 Methane concentration and its variation with time

This section describes how the measured methane concentration varies over different time periods. Figure 4.10 shows all four measurement sites' daily, weekly and intra-annual variability. Clear diurnal cycles are shown at all sites, particularly in Haddenham and Tilney. Accumulated methane concentration over periods of more stagnant meteorological conditions (nighttime) usually imply local sources. Both Haddenham and Tilney have nearby landfill sites which can be large point sources of methane, whereas Tacolneston and Weybourne are in more remote areas and do not experience such dynamic diurnal cycles. In addition to this, an apparent weekly cycle is observed in all sites with the possible exception of Haddenham. This trend is assessed in more detail in Section 4.2.1. Each site's relative distribution to each other is shown in Figure 4.10. Haddenham and Tilney experience higher concentrations than the other two sites on average. This seems to be primarily driven by the large nighttime values experienced. Weybourne experiences the lowest range of concentrations, which could be due to its coastal location and its distance from large methane sources.

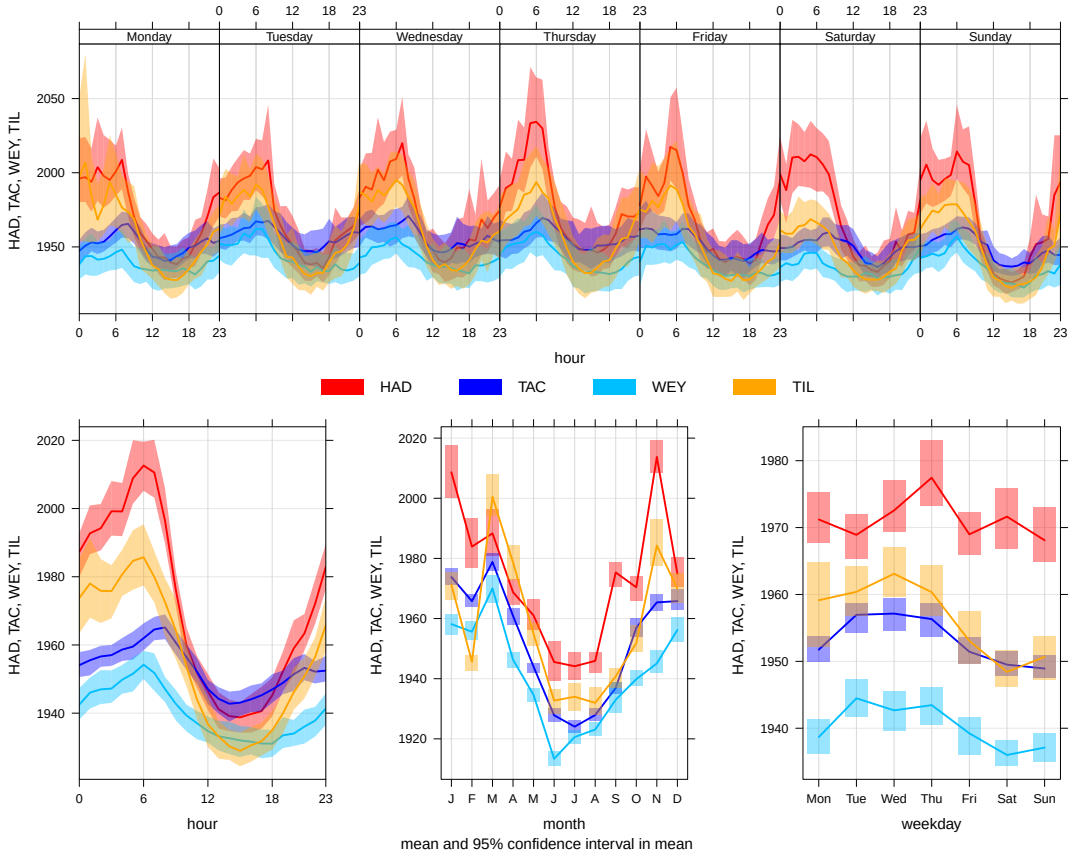

Figure 4.10: Methane variations over time for all four sites using full two year dataset (July 2012 - June 2014). Top plots show time variations over each hour of the day for each day of the week. The bottom-left plot shows the two year dataset averaged over hour of the day. The bottom-centre plot shows monthly averages and indicates an annual cycle. The bottom-right plot shows daily averages and indicates any weekly cycles. The graphs portray mean values with one standard deviation shown in the corresponding shaded colours. Plotting software sourced from Carslaw and Ropkins (2012).

The lower central plot in Figure 4.10 shows the monthly averages for each site over the two year dataset. Annual cycles can be observed with a minima in the summer months and a maxima in the winter/spring months, however all sites show an anomaly in the DJF months with a reduction in concentration values. This is most prominent in the Tilney and Haddenham data. Figure 4.11 shows these annual cycles split into the two separate years (June 2012 - May 2013 and July 2013 - May 2014). As stated earlier, the Haddenham data from 10 December 2013 to 01 April 2014 were removed for this analysis due to the low instrument precision. The 2012-2013 year observed a more usual annual cycle, however December still experiences a reduced monthly average compared to November

and January. The 2013-2014 annual cycle shows a larger than expected winter decrease in methane concentrations across all sites. Local sources cannot fully account for this observation as it is reflected across all four sites. This means that either more distant sources have affected the observations during this period, or other factors (meteorological for example) have caused this change.

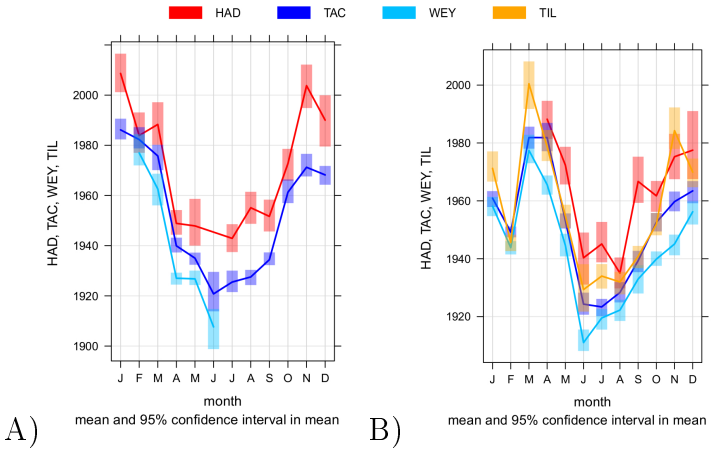

Figure 4.11: Intra-annual cycles of methane concentration (ppb) variability for all four sites. The two year dataset has been split into two separate years: A) July 2012 - June 2013 and B) July 2013 - June 2014. Plotting software sourced from Carslaw and Ropkins (2012).

Figure 4.12 shows the seasonal wind roses for Tacolneston split into the two separate years. The meteorological data used here are from the UK Met Office's UM, which have been interpolated to the measurement sites' locations. This analysis was conducted on all sites and produced similar results throughout. The prevailing wind direction for this region is from the south west (Met Office Website, 2015a). The spring, summer and autumn seasons look relatively similar in both years although summer 2013-2014 experiences more north-easterly winds than 2012-2013. Average wind speeds are similar for both years for all sites, but there is a large difference between the winter wind roses. The 2013-2014 winter is dominated by the prevailing wind direction, whereas the 2012-2013 winter season has more variability. Winter 2013-2014 also experiences much higher average wind speeds (8.7 m s^{-1} compared to 7.1 m s^{-1}). Very little wind is from the south east, which observes higher baseline concentrations of methane on average due to European sources (Section 4.3). In addition to this, faster wind speeds produce lower atmospheric concentrations compared to the same emission at lower wind speeds. Thus it can be assumed that the significant decrease in methane concentrations over the winter months in 2013-2014 was due to meteorological

conditions rather than a change in emissions.

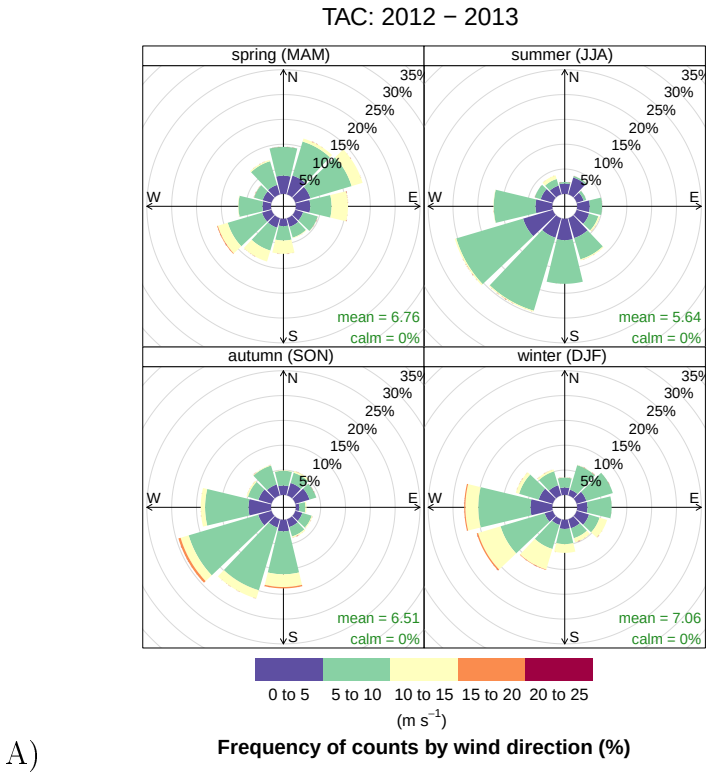

A)

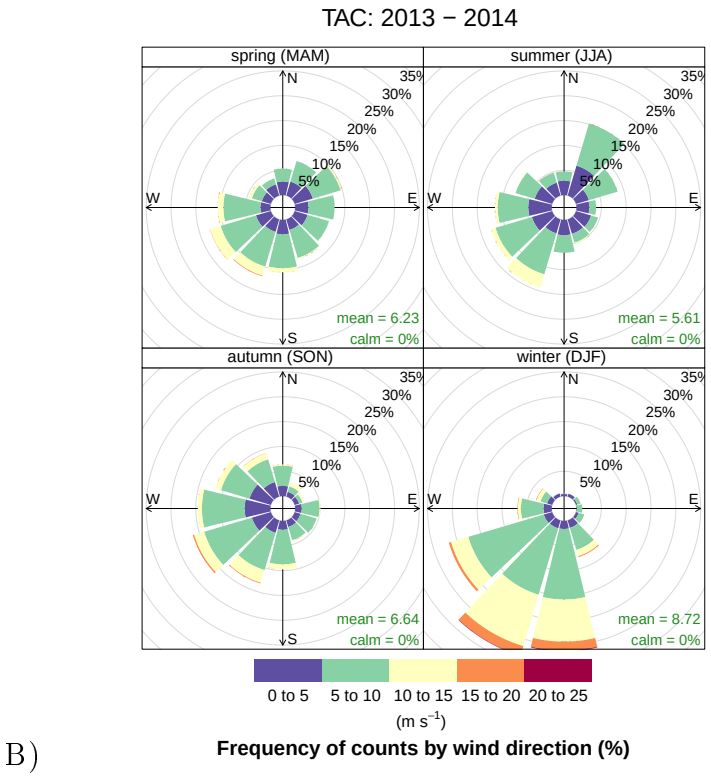

B)

Figure 4.12: Wind rose plots for Tacolneston for A) July 2012 - June 2013 and B) July 2013 - June 2014. Plotting software sourced from Carslaw and Ropkins (2012).

4.2.1 Weekly cycles

This section investigates the apparent weekly cycle seen in Figure 4.10. Figure 4.13 shows polar bivariate plots of the methane concentration two year dataset (July 2012 - June 2014) for each measurement site split into weekday and weekend observations. The axes indicate wind direction and the distance from the origin shows wind speed. High concentrations at low wind speeds indicate local sources. All sites experienced elevated methane concentrations to the east at medium-high wind speeds, which further indicates European sources.

An attempt to quantitatively analyse the differences between the weekday and weekend polar bivariate plots involved the application of a 'Mann-Whitney-Wilcoxon' statistical significance test (U-test, 95 % confidence) to the dataset. A U-test is much the same as a T-test, which tests two datasets of being different to a statistically significant level. A U-test is applied here to compensate for the positive skew to the concentration data (whereas T-tests are used on normally distributed data). A U-test compares the differences between each individual element of one dataset with all of the other elements in the second set.

Table 4.1 shows the summary of the U-test analysis. Any differences between weekday and weekend values were assessed for the whole time period as well as for the individual years for each site (U-test results under the column 'all' in Table 4.1). This difference was also analysed when the weekday and weekend data were split further into different wind quartiles. Only Haddenham and Tacolneston have results for the 2012-2013 period as only full year datasets were analysed.

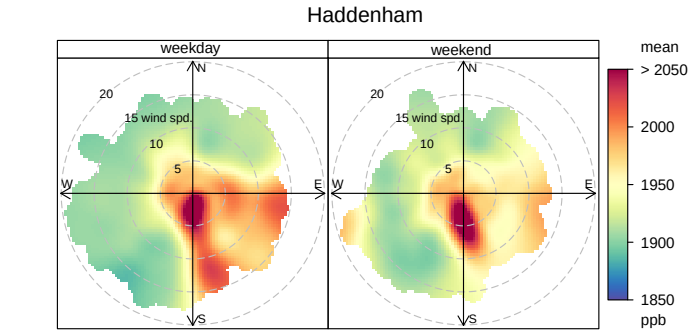

A)

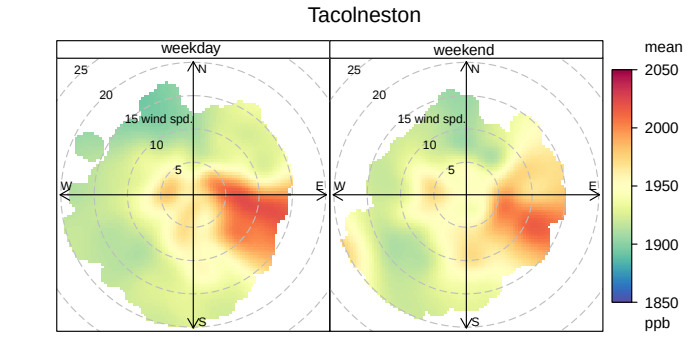

B)

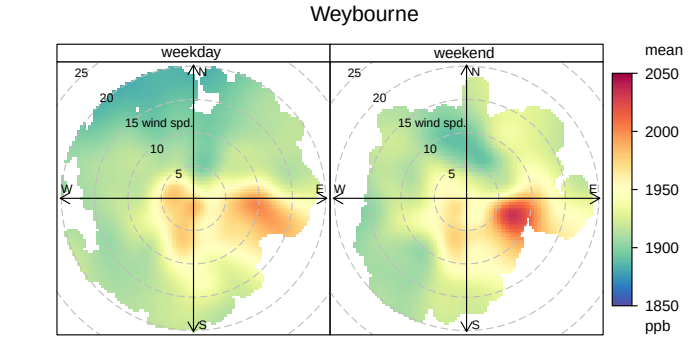

C)

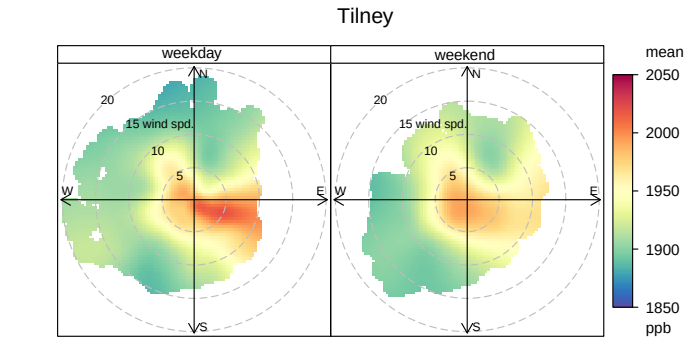

D)

Figure 4.13: Polar bivariate plots of methane concentrations for each site showing differences between weekday (left) and weekend (right) data. Plots using the two year dataset (July 2012 - June 2014). The axes indicate wind direction and the distance from the origin shows wind speed. Plotting software sourced from Carslaw and Ropkins (2012).

Table 4.1: Mann-Whitney-Wilcoxon statistically significance test (U test - 95 % confidence) comparing weekday and weekend methane concentrations at each measurement site. Tick indicates a statistically significant difference between weekday and weekend methane concentrations (p-value smaller than 0.05). A cross indicates the opposite (p-value greater than 0.05).

	North (315-45°)	**South (135-225°)**	**East (45-135°)**	**West (225-315°)**	**All**
2012-2014					
HAD	X	✓	✓	✓	X
TAC	X	X	X	✓	X
WEY	X	X	X	✓	✓
TIL	X	✓	✓	✓	✓
2012-2013					
HAD	✓	✓	✓	✓	X
TAC	✓	✓	✓	✓	X
WEY	-	-	-	-	-
TIL	-	-	-	-	-
2013-2014					
HAD	✓	✓	X	✓	✓
TAC	✓	✓	X	✓	✓
WEY	✓	✓	X	✓	✓
TIL	X	✓	✓	✓	✓

The results for the two year period shows no clear conclusions, with some sites' wind sectors appearing significantly different whereas others do not. Testing the datasets without separating by wind sector increases the internal variance within the two individual datasets. This will more likely produce a statistically insignificant result as there is now more overlap within the two sets. If the reasons for this internal variance are independent from the parameter being tested for, then this should be taken into account before the U-test is applied. For example, wind direction has a large influence on methane concentrations which may dwarf any variation otherwise observed in the weekly variation. Similarly this also applies if the two different years tested have very different meteorological conditions. This could be why insignificant results were found when testing the sites' whole datasets in the 2012-2014 and 2012-2013 periods.

If the data are split into the two individual years however, clearer trends can be observed. Almost all of the four wind sectors show statistically significant differences between weekday and weekend methane concentrations for the two individual years. The exceptions to this are the 2013-2014 eastern quartile for Haddenham, Tacolneston and Weybourne, and the northern quartile for Tilney. It should be noted that a U-test was conducted on each site's datasets split only

by the year they were observed (July 2012 - June 2013 and July 2013 - June 2014) showed a statistically significant difference between the two years.

The analysis described here suggests a weekly cycle is significant when data are split into different wind directions and individual years. Due to methane's long atmospheric lifetime the observed weekly cycles are more likely to derive from local sources as further afield sources would have had more time to become mixed. Local sources in East Anglia are dominated by waste (65.66 %) and agriculture (17.16 %), which are heavily dependent of farm and landfill management. Local landfills are managed to receive waste 5 - 6 days a week, usually being closed on Sunday (Riddick et al., in prep) whereas farming practices are less rigidly defined. If less work occurs during the weekends then this would reduce the methane emission magnitudes. It is therefore possible that the weekly cycles could be due to the waste / landfill management practices.

4.3 Methane concentration and its relationship with meteorology

As previously described at the beginning of this chapter, analysed wind fields and other meteorological data calculated by the Met Office's Unified Model are used for the running of NAME. These can be extracted to produce a meteorological time series at a given x, y, z location. The meteorological data are available on a 1.5 x 1.5 km spatial resolution at hourly timesteps. A site's meteorological influence is defined as a 1.5 km square box centered on each measurement location's x, y, z coordinates. The following section's analysis uses these modelled meteorological data to establish whether these variables influence methane concentration. The following meteorological variables are used in this analysis: wind speed (m s^{-1}), wind direction (°), temperature (°C), pressure (Pa), and boundary layer height (m). Since these variables are available on a one hour timestep the methane concentrations are averaged to fit this duration. Linear regression analysis is applied comparing methane concentration to all meteorological variables, except wind direction. The results are described below. Poor linear correlations were found between methane concentration and boundary layer height and wind speed. A stronger correlation was found when when compared to the logarithm of each quantity, for example, R^2 between boundary layer height and concentration increased from 0.138 to 0.213 when logging was applied. For this reason all three variables are subjected to a natural logarithmic

function before linear regression is applied.

- Wind speed and boundary layer height: All sites show slight negative correlations with wind speed and boundary layer height. The p-value, which is a standard measure of the correlation's statistical significance, for all sites is less than 2.2 x 10^{-16}. R^2 values are below 0.12 and regression gradients are below -0.025x. Variables are calculated using the core statistical package within the R software (R Core team,2013). Both variables are expected to have a negative correlation with concentration due to dispersion.

- Pressure: Less conclusive results are found for the four sites as Haddenham and Tacolneston produce statistically insignificant negative correlations. Weybourne also produce a slight negative relationship with pressure (p-value $<$ 3.7 x 10^{-05}, $R^2 = 0.0005$, regression gradient = -0.002x), however Tilney experiences a slight positive trend (p-value $<$ 4.5 x 10^{-07}, R^2 of below 0.004, regression gradient of 4.9x). All pressure correlations observe a lower degree of significance than the other meteorological variables, and as no uncertainties of the measurements and meteorological data have been included in these calculations, it can be concluded that the results show no clear correlation can be identified between these two variables.

- Temperature: Shows a statistically significant slight negative correlation at all sites (p-value $<$ 2.2 x 10^{-16}, R^2 of below 0.08, regression gradients below -4.0x). Most sources of methane have a positive correlation with temperature, for example, microbial methane production is positively related to temperature within the observed temperature ranges of the measurement sites (Reay et al., 2010). However, the sinks or methane also have a positive relationship with temperature. This is particularly important for waste sector sources of methane as methanotropic bacteria will oxidise greater amounts of methane to carbon dioxide at higher temperatures (between 2 and 25 °C, Maurice and Lagerkvist, 2004; Scheutz and Kjeldsen, 2004; Scheutz et al., 2004). Methane emissions from waste dominate this area of the UK and so this could be why a negative trend is observed. The negative correlation could also be enhanced due to the simplistic regression approach using direct correlation analysis and not incorporating other dependent variables (discussed below).

The measured changes in temperature and boundary layer height both vary with respect to time. Figure 4.14 shows how methane concentration and boundary layer height vary when averaged over each hour of the day. Methane

concentrations are highest in the early or late hours of the day (Figure 4.14.A). The opposite is seen with boundary layer height (Figure 4.14.B).

Figure 4.15 separates the Weybourne methane concentrations by wind direction and then correlates with wind speed and boundary layer height. A clear positive trend can be seen between boundary layer height and wind speed. High methane concentrations (>2100 ppb) are always associated with low boundary layer heights (<400 m) and conversely, high boundary layers always (>1000 m) are always associated with low methane concentrations (<2000 ppb). The prevailing wind direction (south west) is indicated by the density of the individual plots. The complex dependent nature of each meteorological variable's relationship with methane concentration highlights the limitations of a simplistic linear regression analysis and suggests a multivariate analysis could better explain the observed dependencies.

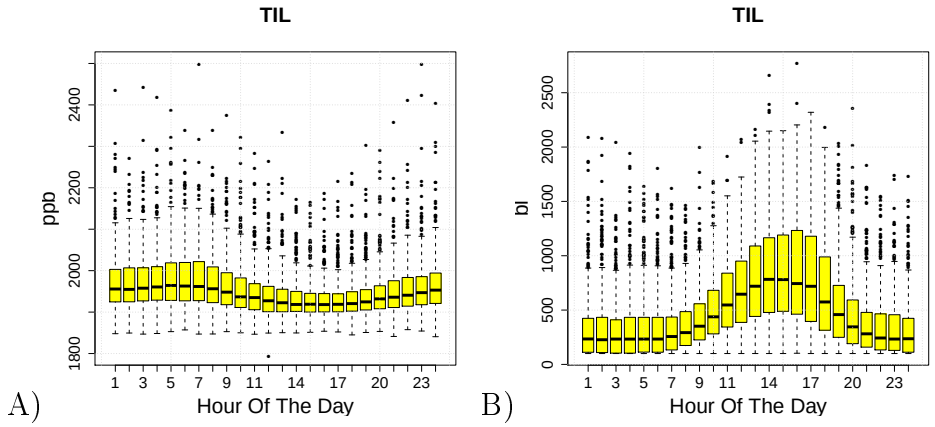

Figure 4.14: Boxplots showing A) Tilney methane concentration and B) boundary layer height data averaged over each hour of the day. A negative relationship between concentrations (ppb) and boundary layer height (m). A lower boundary layer height induces a rise in atmospheric methane concentration.

Different wind sectors experience different variations of methane concentration. Winds from the south, south west and east see elevated methane values at higher wind speeds (~10 m s^{-1}) whereas other wind sectors (e.g. north, north west) only experience these values below ~7 m s^{-1}. Weybourne is located on the north east coast of East Anglia and so methane sources from the east would be from Europe. North east sources could potentially be from offshore oil rigs (shown in the NAEI as large point sources). The NAEI indicates very few sources of methane north west of Weybourne but to the south and south west there are many anthropogenic sources, including agriculture, waste and emissions from

major cities (i.e. Norwich, Ipswich and London).

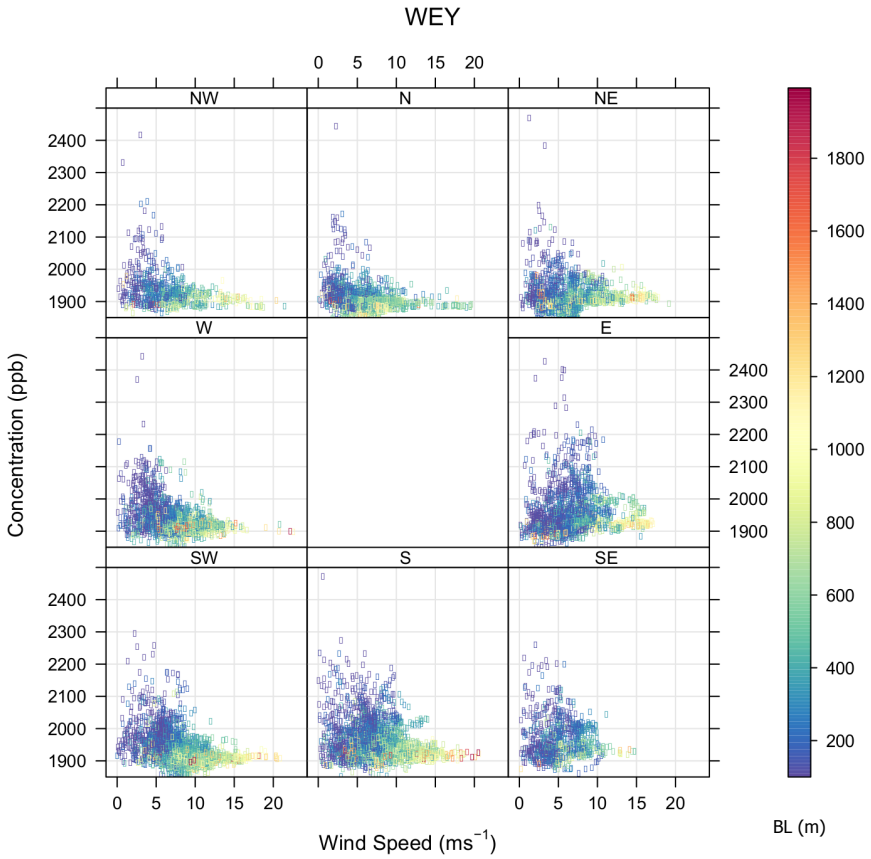

Figure 4.15: Scatter plot showing wind speed (m s^{-1}) vs. methane concentration (ppb) with boundary layer height (m) on the z-axis. Plotting software sourced from Carslaw and Ropkins (2012).

The concentration ranges for all sites separated by wind direction and shown as boxplots can be seen in Figure 4.16. Strong local sources are clearly prevalent to the south of Haddenham. The plot also shows the influence of south, south east and east wind directions in giving higher baseline values of methane. Weybourne experiences lower distributions of methane from the east compared to the other sites. This suggests that not all elevated concentrations of methane originate from Europe.

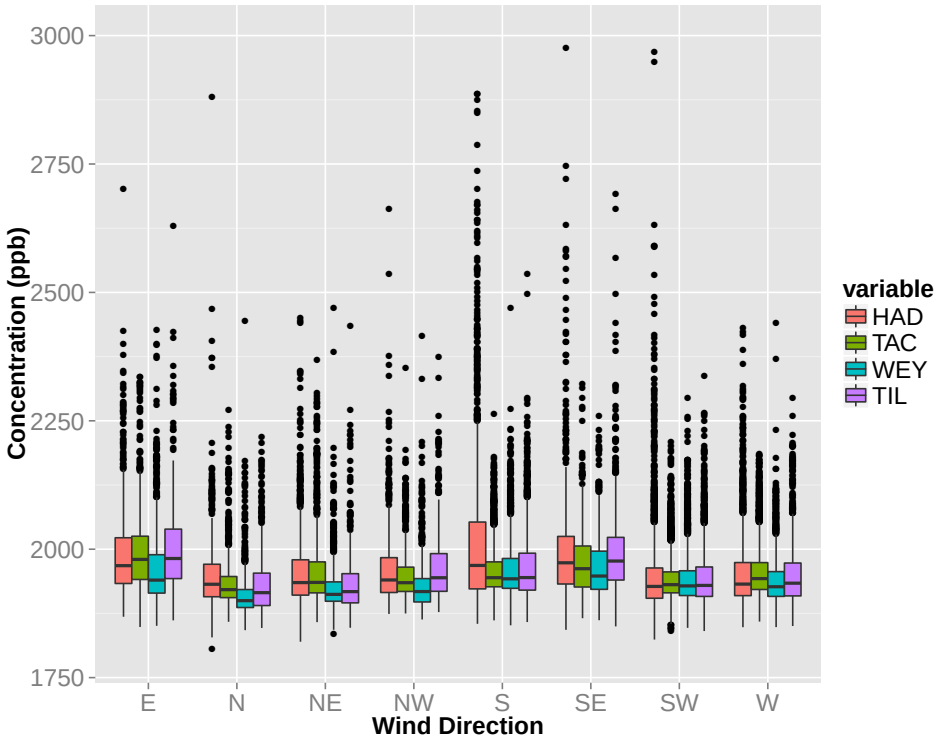

Figure 4.16: Boxplots of methane concentrations (ppb) from Haddenham (red), Tacolneston (green), Weybourne (blue) and Tilney (purple) split by wind direction.

4.4 Pseudo-observations

The NAME model produces a time-integrated particle density (g s m^{-3}) map which represents the surface influence (bottom 100 m agl) of air experienced at a particular measurement site (as explained in Section 3.2). When this metric is multiplied by the gridded surface area (m^2) and divided by the NAME particles' mass (g) from the duration of release, a dilution metric with the units m s^{-1} can be calculated. This can be used with a defined scenario of emissions, for example the NAEI, to create a modelled, or pseudo-, concentration. NAME air history maps are available for each hour, so an hourly time series of pseudo-observations can be created and directly compared with the measured concentrations. The NAEI (g s^{-1} m^2) is regridded to the NAME dilution map spatial resolution (1.5 x 1.5 km) and the two products multiplied to produce these pseudo-concentration time series. Figure 4.17 shows these time series for all four sites throughout August 2013. A baseline must be added to the pseudo-observations to represent methane sourced from outside the domain of interest. The baseline used was calculated for the inversion system. Its calculation method is described in Section 5.10.

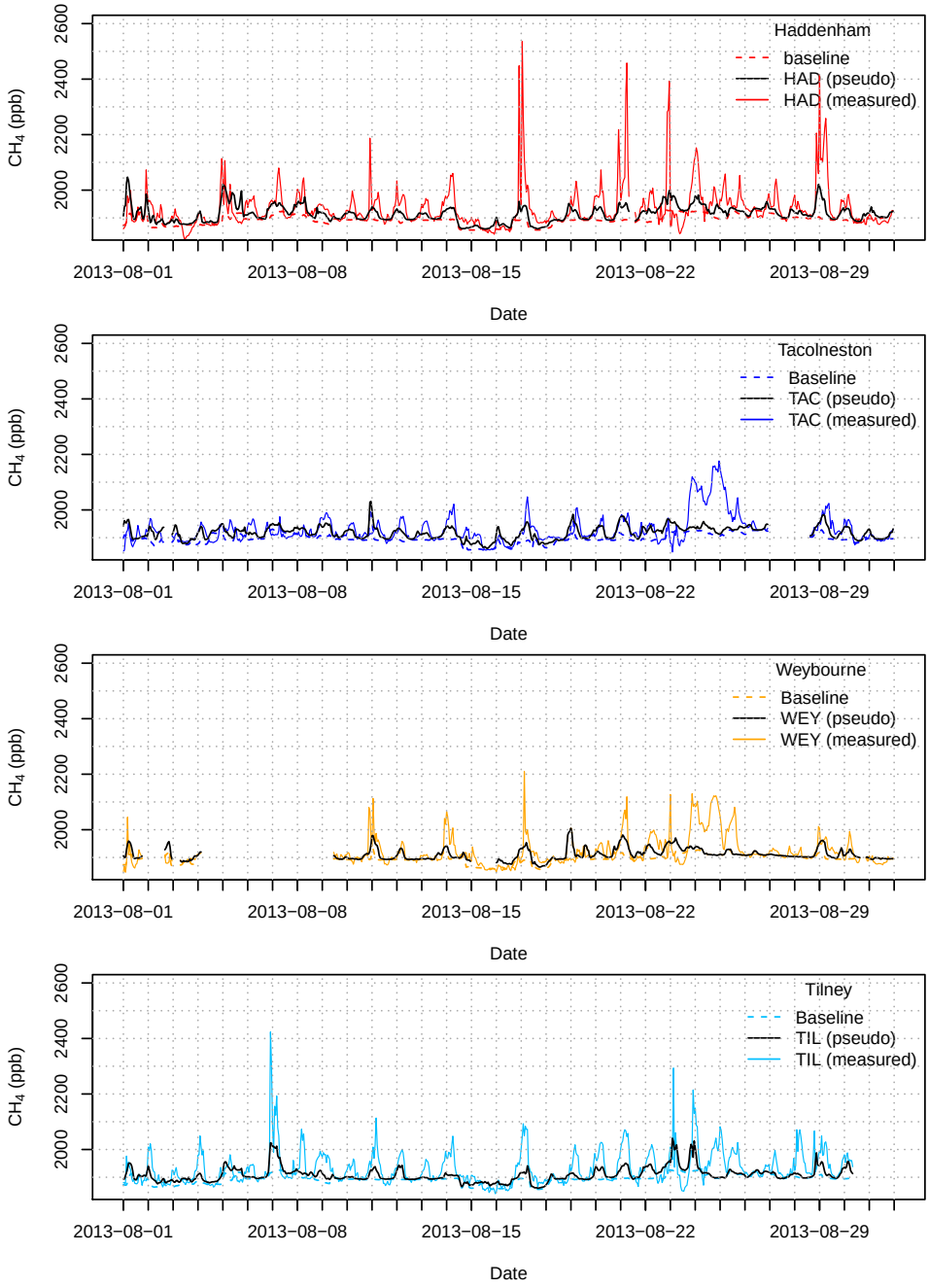

Figure 4.17: Time series of measured and pseudo-concentrations of methane at all four sites for August 2013. Pseudo-observations calculated by multiplying the NAME dilution matrix (s m^{-1}) by the NAEI methane emission field (g s m^{-3}).

Figure 4.17 shows the variations between the modelled and measured observations correlate well. Sharp peaks seen in the measured concentrations are often also seen in the pseudo-observations, however the differences in these magnitudes can vary significantly. Several potential reasons for these differences exist. The NAEI is available as an annual total for a specific year (2012). To produce hourly

values, these totals are averaged down to the desired hourly period. The NAEI therefore assumes a constant emission from every source throughout the defined time period.

The NAEI publishes ten source sector emission maps for methane which include agriculture, waste and offshore sources. The offshore source sector, rather confusingly, incorporates emissions from the natural gas pipelines situated in-land. These maps can be used to calculate pseudo-concentrations specific to the source sector. Figure 4.18 shows a fractional time series of all sectors for the same time period as Figure 4.17. When large peaks of methane are measured the fractional contribution of the waste sector (primarily landfill emissions) also increases. These sources are known to be extremely variable over time (Scheutz and Kjeldsen, 2004). This is exemplified further at the Haddenham site, which is situated close to several landfills and experiences variable methane concentrations over relatively short time periods. Time varying sources will cause aggregation and systematic errors within the inversion as InTEM solves assuming that emissions are static over the observation time period (1 year is most commonly used within this thesis). These can be reduced by increasing the spatial and temporal resolutions to a finer scale.

Another possible reason for the observed differences between measured and pseudo-observations could be due to the NAEI being year specific. Different practices adopted by the local landfills could have been implemented since 2012, and hence not accounted for in the NAEI, although this is unlikely given measurements commenced only six months after the NAEI was published. The NAEI methodology for the inventory compilation was renewed for the 2012 inventory, and the emissions differ with the previous inventory assembled for the year 2009. The major difference between the two inventories was the waste sector, which saw more pinpointed emission estimates in the 2012 inventory. Methane capture techniques across many landfills were also incorporated into the 2012 inventory (European Environment Agency, 2012). Figure 4.19 compares the two NAEI inventories (2009 and 2012) with the measured observations at Haddenham. The other three sites were analysed but are not shown here due to there being less obvious differences. The 2009 NAEI is less able to create the sharp peaks of methane seen in the measured time series, and seems to underestimate the emission sources. Additionally, there are instances where peaks are not observed in the 2009 inventory (23 and 29 August 2013). This shows additional sources have been added to the 2012 inventory. Changes to the waste emissions are more prevalent in the Haddenham time series due to its local source influences. A less

striking difference is shown for the other sites' time series as previous analysis showed they were less influenced by the waste sector (Figure 2.4).

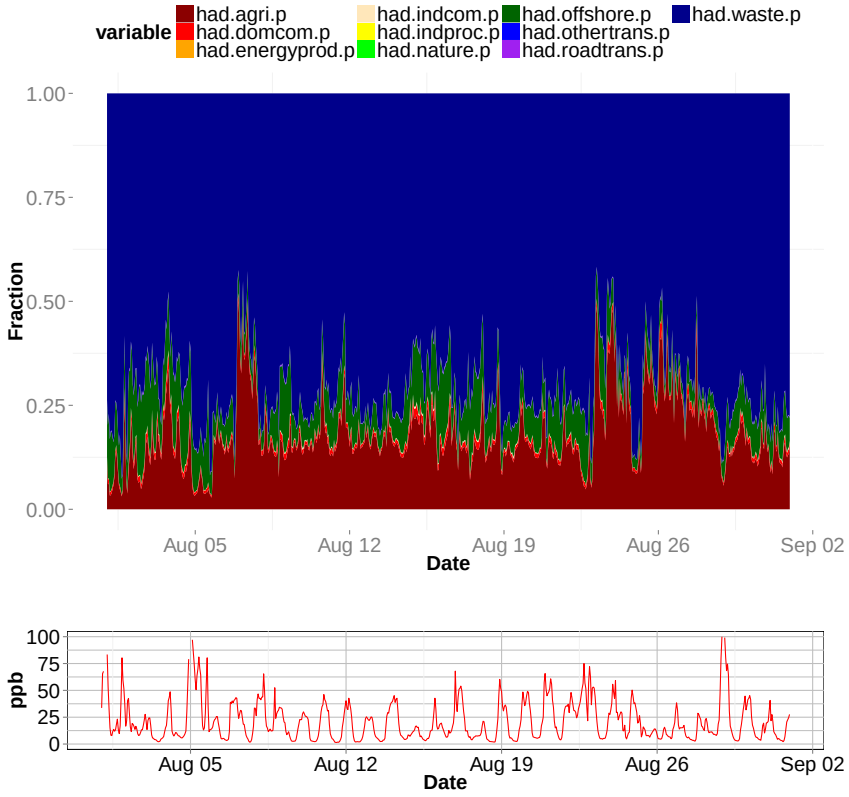

Figure 4.18: Time series of the fractional contribution of each NAEI methane source sector as pseudo-observations for Haddenham during August 2013 (top), and the equivalent pseudo-observations (ppb) with no baseline included (bottom). Source sectors are: agriculture, domestic combustion, energy production, industrial combustion, industrial processes, nature, offshore, other transport, road transport and waste.

There are some periods in Figure 4.17 where peaks are seen in the measurements but not in the pseudo-observations. For example, there is a period from 23 - 26 August 2013 where the Tacolneston and Weybourne sites show elevated methane levels, however these do not appear in either of the pseudo-observations, nor in the other two measurement sites. If all sites have seen this increase then the elevated concentrations could be due to large sources from outside of the spatial domain. Analysis of the NAME air history maps show air to have come from the north but then from the east (Europe) when not over land. This could imply a European source that, for some reason, is not being picked up at Haddenham or Tilney, or it could be a temporary source unaccounted for in the NAEI.

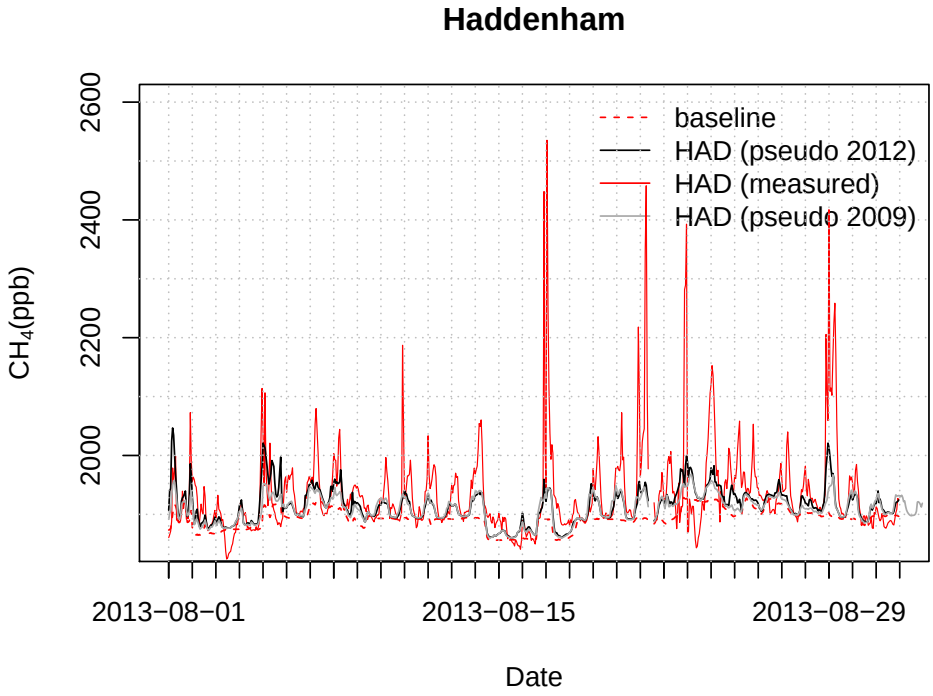

Figure 4.19: Time series of measured and pseudo methane concentrations at Haddenham for August 2013 (ppb). Pseudo-observations for the 2009 and 2012 NAEI are both shown. 23 and 29 August 2013 show instances where additional sources have been added to the 2012 inventory as peaks are not observed in the 2009 inventory.

Scatter plots of the pseudo- and measured observations for each individual site can be seen in Figure 4.20. All sites show a shallower gradient between the two variables than compared to the 1:1 line. The pseudo-observations as they never replicate the large peaks seen in the measurements. Tacolneston has the greatest correlation with an R^2 value of 0.42. This site measures at a higher altitude than the other three sites (50 - 100 m rather than 15 - 25 m) and hence is less influenced by local point sources. This could mean that Tacolneston is experiencing a less biased 'view' of the East Anglian emissions. Further discussions regarding this and the influence of the different sites in the inversion system can be found in Chapter 6.

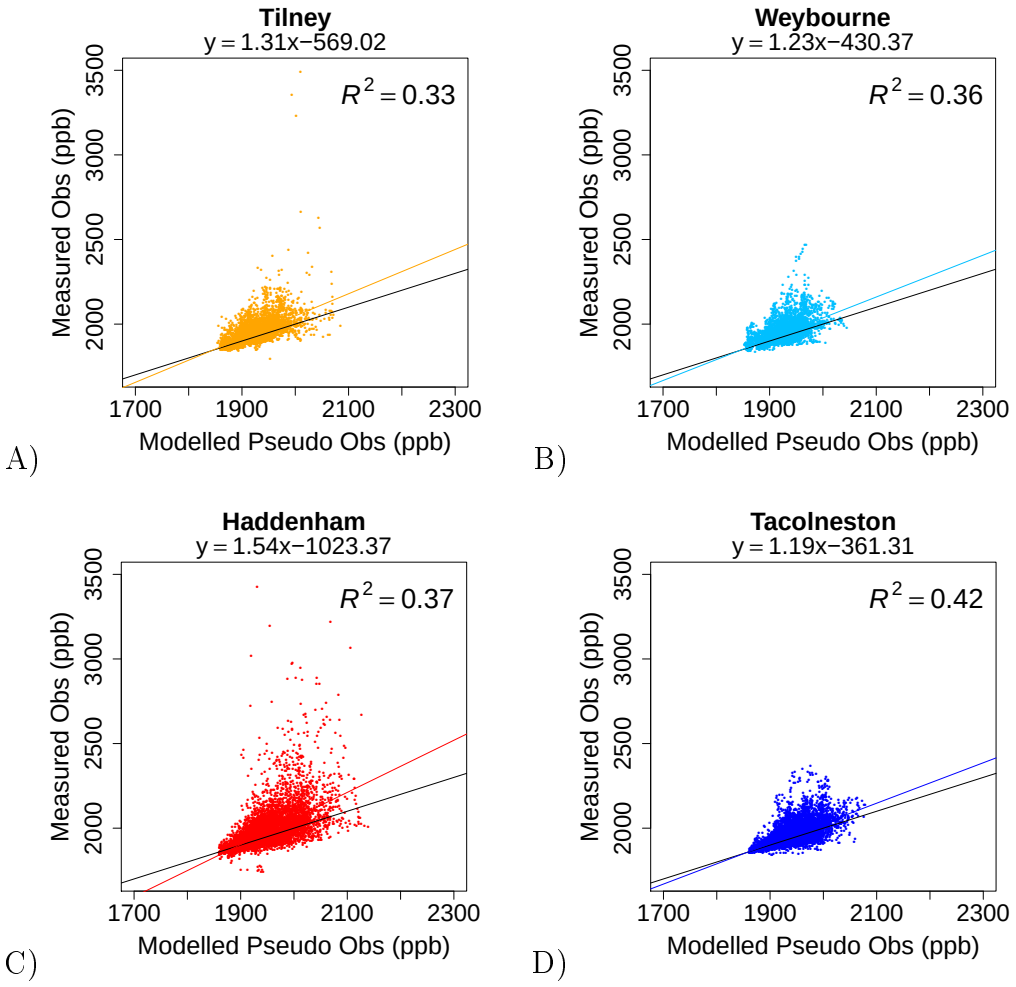

Figure 4.20: Correlation analysis of the measured and pseudo-observations at all four sites A) Tilney B) Weybourne C) Haddenham D) Tacolneston. Linear regression lines have been added to each plot shown in the corresponding site colours and a 1:1 line is shown in black has been added for reference.

4.5 Haddenham measurements and modelling case study

This section is split into two different analysis techniques which focus specifically on the Haddenham measurement site. The first concentrates on a month-long period of data collected from November – December 2012. Data were collected using a Sensor Networks for Air Quality (SNAQ) instrument in addition to the methane GC-FID measurements. The aim of this installation was to compare measured meteorological data with the modelled equivalents produced by NAME, and to attempt to attribute potential local methane sources. The second part of

this section describes methane isotopic analysis carried out in collaboration with Royal Holloway. In this, whole air bag samples were collected with the aim of identifying the source responsible for the large short-lived peaks regularly seen in the GC-FID data at Haddenham.

4.5.1 The SNAQ instruments

The SNAQ-Heathrow project has developed multiple low-cost portable sensors to measure pollutants and meteorological data that influence air quality. The sensors were developed and produced at the University of Cambridge as part of a collaborative project with Imperial College London, University of Hertfordshire, University of Manchester, National Physical Laboratory and Cambridge Environmental Research Consultants Ltd (Mead et al., 2013). The SNAQ deployment covered the entirety of London Heathrow Airport with almost 50 sensors being installed. The species measured were NO, NO_2, CO, CO_2, SO_2, O_3, VOCs, size-speciated particulate matter, as well as meteorological data such as wind speed, wind direction and temperature. The sensor was installed on the west side and at the top of the church tower next to the GC inlet tube. It was attached to a horizontal hand rail and the anemometer was free from any immediate and obvious interference. The sensitivity of the SNAQ sensor is estimated to be of the order of the ppm level for carbon dioxide and the ppb level for carbon monoxide (Mead et al., 2013).

4.5.2 Meteorological analysis

Three meteorological variables are measured by the SNAQ node: wind direction, wind speed and temperature. Comparison of these values with modelled NAME meteorological data is shown as probability density functions (PDFs) in Figure 4.21 parts A-C. Parts D-F in Figure 4.21 show the difference between the measured minus modelled data. Both modelled and measured temperature values correlate well with an R^2 of 0.93 although Figure 4.21.F shows a slight positive bias. Wind direction is also reasonably correlated although there is a discrepancy in the northerly wind directions with the SNAQ node registering only a couple of hours in this direction over the whole month dataset. This correlation has a lower R^2 of 0.74. Although no immediate objects of interference could be seen when the sensor was installed at Haddenham, nearby obstacles could have been affecting the local winds surrounding the church tower. For example, several

tall trees were located to the north-west of the tower (5-7 m away). Rather than an error in the modelled values it is expected that there was an obstruction towards the north north-west direction of the sensor. This discrepancy is also highlighted in Figure 4.21.D which shows an overall negative bias between the measured and modelled variables. Wind speed is less well correlated compared to the temperature values, with an R^2 of 0.78 and shows a negative bias in Figure 4.21.E. The PDF (Figure 4.21.B) shows that the modelled wind speeds have a more Gaussian distribution (with a slight positive skew), whereas the measured wind speeds have a more prominent positive skew. This is reflected in the mean wind speeds for the two datasets, which are 4.6 m s^{-1} and 6.7 m s^{-1} for measured and modelled, respectively. This low correlation is due to an overestimation of wind speeds in the modelled dataset (or an underestimation in the measured) however this is not a constant offset, nor does it occur over a particular wind direction. The most likely reason for this discrepancy will be the Met Office model being unable to resolve high enough spatial resolution to capture local gusts of wind. The meteorological parameters fed into NAME are available at 1.5 km square resolution. Sub-grid scale changes in orography and meteorology will be less well represented and could therefore cause discrepancies between the two datasets. The correlation between modelled and measured meteorological data is still reasonable enough for the NAME data to be used in the inversion analysis. However, the uncertainty associated with the modelled data should be incorporated into the inversion analysis.

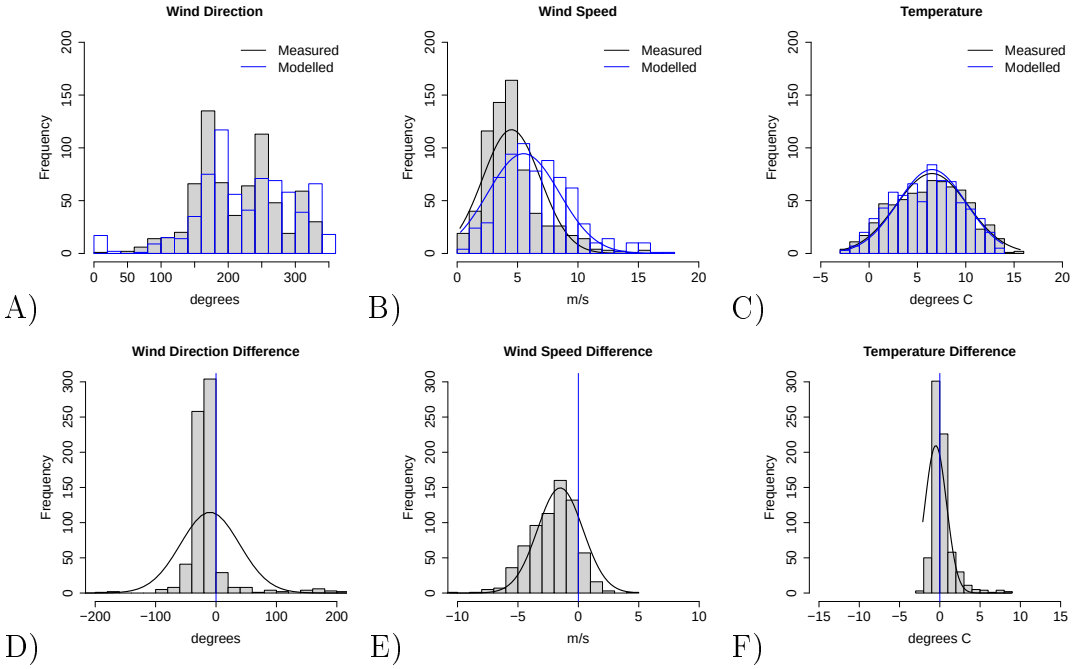

Figure 4.21: Histograms comparing the Haddenham site's A) wind direction (°) B) wind speed (m s^{-1}) and C) temperature (°C) using measured (SNAQ) and modelled (NAME) data, respectively. Figures D), E) and F) show the corresponding differences of the meteorological variables (measured minus modelled).

4.5.3 Source attribution analysis

The SNAQ instrument ran between 09 November – 08 December 2012. The methane GC instrument was not running for the first week of December. Figure 4.22 shows the methane concentration time series of both Haddenham and Tacolneston for this period. Equivalent time series for CO_2, CO, wind speed, wind direction and boundary layer height are also shown for comparison. Some correlations can be seen in this figure, i.e. a low boundary layer height implies a higher methane concentration.

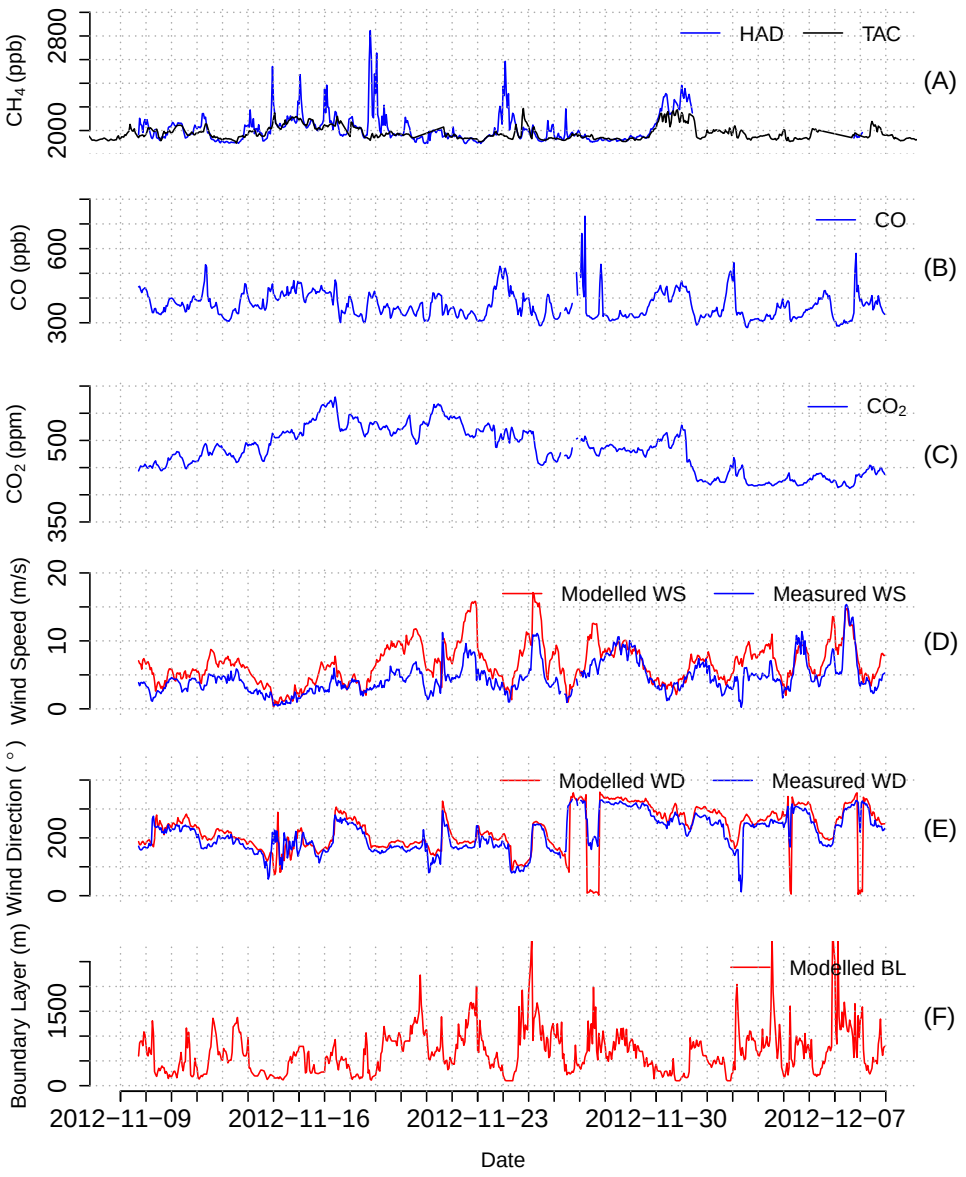

Figure 4.22: Time series showing A) methane concentration at Haddenham and Tacolneston (ppb), B) carbon monoxide measured using the SNAQ node (ppb), C) carbon dioxide measured using the SNAQ node (ppm), D) modelled and measured wind speed (m s^{-1}), E) modelled and measured wind direction (°), F) boundary layer height from the NAME model (m). All data measured at the Haddenham site or modelled using Haddenham location co-ordinates (with the exception of Tacolneston methane concentration in A).

NAME can be used to help attribute different source regions to the measured time series. The first few days show varied concentrations of methane at both Haddenham and Tacolneston which can be attributed to both boundary layer effects and the air mass history coming from over the UK (Figure 4.23.A).

The wind direction then changes so that the air comes from over Europe, and wind speed drops (Figure 4.23.B). This accounts for above baseline methane concentrations observed at both sites from 15 - 19 November 2012. The short lived high levels of methane at Haddenham correlate with nighttime periods and most likely come from local sources. The NAME air history map in Figure 4.23.C shows an increased surface influence south of Haddenham at the time of the large methane spike observed in the early hours of 21 November 2012. The air history map suggests both local and London sources could contribute to this observation. Methane concentrations remain low due to a prevailing wind direction coming from over the English Channel or Atlantic Ocean (Figure 4.23.D), with the exception of 23 November where reduced wind speed and a low boundary layer height contribute to this high peak. The low methane concentrations after this period are due to a change in wind direction to come from over the North Sea (Figure 4.23.D) where relatively few sources are seen compared to on land. The final above baseline observations of methane seen on 30 November 2012 could be attributed to air coming from north west England where large industrial methane sources are located.

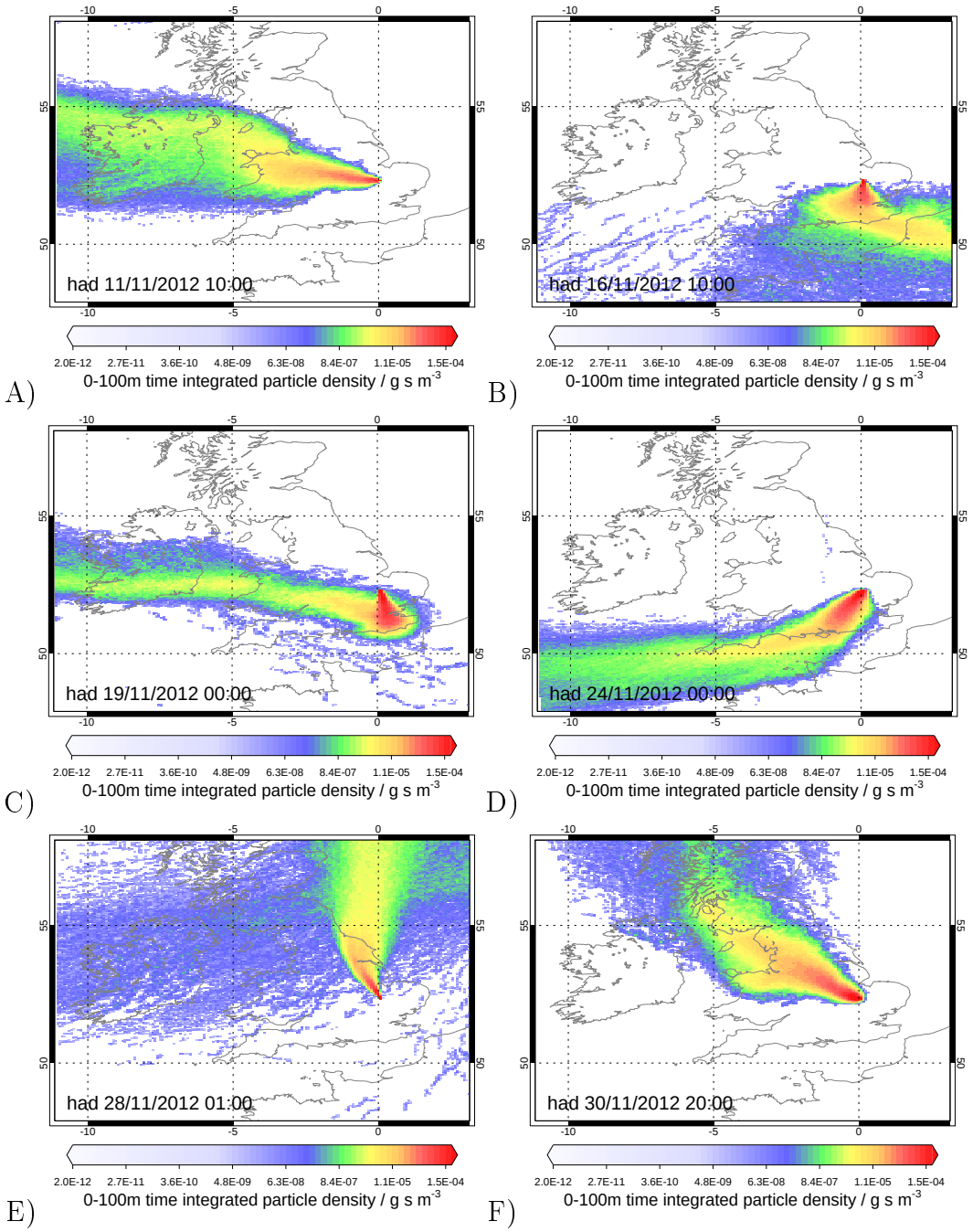

Figure 4.23: NAME air history maps with source release from Haddenham between 11-30 November 2012. Maps show the time integrated density of the surface influence (bottom 100 m) for a one hour source release released at A) 11-11-2012 10:00 B) 16-11-2012 10:00 C) 19-11-2012 00:00 D) 24-11-2012 00:00 E) 28-11-2012 01:00 F) 30-11-2012 20:00.

Relationships between methane and carbon dioxide or carbon monoxide can give an indication of the sources of these gases. A positive correlation between methane and carbon monoxide implies a source of incomplete combustion.

Anthropogenic sources of incomplete combustion can be found in the UK, for example oil and gas industry plants or domestic gas usage. Methane's relationship with carbon dioxide is much more diverse than with carbon monoxide as it depends on available sources and sinks for both compounds. Various methanogens reduce the amount of carbon dioxide in the surrounding area and produce methane (Chapter 1). Conversely, landfills are known sources of carbon dioxide as well as methane (60 % methane to 40 % carbon dioxide) due to the decomposition of organic matter (Hegde et al., 2003). This suggests that a positive correlation between these two gases could be a landfill source signal, as well as the other incomplete combustion sources mentioned.

Figure 4.24 show correlation plots for methane and carbon monoxide split into different wind directions (determined by NAME). Modelled boundary layer heights are shown on the z-axis. The prevailing wind for this period (south west) is reflected in the correlation plots. Active landfills around Haddenham can be found to the west and (more closely) to the south. These are on the outskirts of Huntingdon and Cambridge, respectively. Methane sources from landfills and incomplete combustion would be expected from both these quadrants.

Figure 4.24 shows that northerly winds seem to be associated with fewer sources of methane for this period, while carbon monoxide concentrations rise to over double their baseline value. Observations of carbon monoxide without methane could imply shipping emissions from the North Sea (Endresen, 2003).

The other wind direction plots show a positive correlation, particularly from the west (C) and the south (D), with the west appearing more linear than the south. A negative relationship between these concentrations and boundary layer height can be seen, where higher ppb values are associated with lower heights ($<$ 600 m). This implies that this positive correlation can be partially attributed to dispersion effects, although the time series of carbon monoxide (Figure 4.22.B) shows a variation of only ~50 ppb (from boundary layer maximum to minimum). Since the methane and carbon monoxide ranges are larger than this diurnal fluctuation, this could be showing an incomplete combustion source of methane. This correlation can be seen in Figure 4.24.D however many methane outliers can be seen which do not have the expected carbon monoxide concentration for an incomplete combustion source. The equivalent correlation plots for carbon dioxide and methane are not shown here but, in general, show similar correlations for the north and east quadrants. Less defined correlations can be seen for the other two wind directions, however the high methane concentrations observed from the south also show above baseline carbon dioxide concentrations ($>$ 500 ppm). This

analysis suggests that the high methane concentrations could have come from landfill sources. The following section discusses this source attribution in more detail.

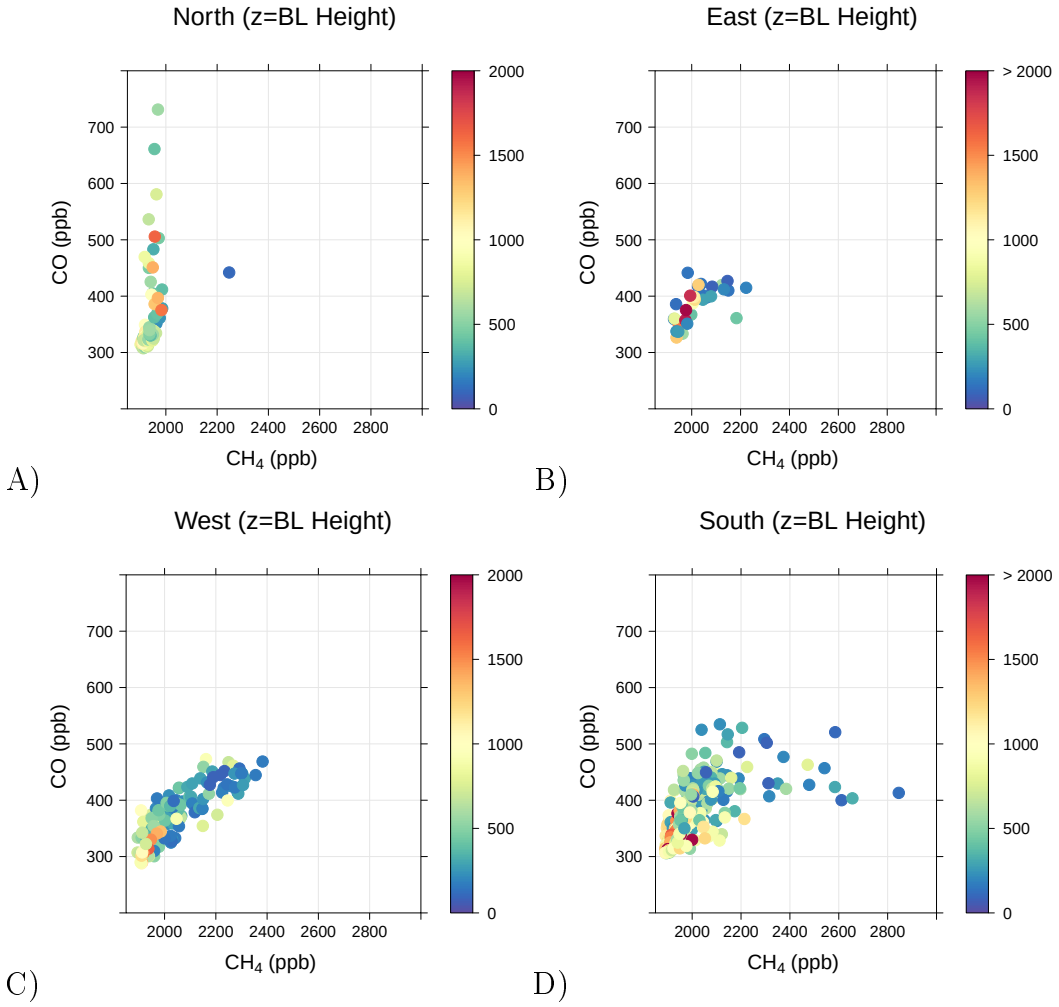

Figure 4.24: Scatter plots showing correlations between carbon monoxide (ppb) and methane (ppb) concentration. z-axis shows boundary layer height (m). Total dataset from 09 November 2012 – 08 December 2012 has been subdivided into four wind quadrants: A) North ($\geq$ 315 °, $<$ 45 °), B) East ($\geq$ 45 °, $<$ 135 °), C) West ($\geq$ 135 °, $<$ 225 °), D) South ($\geq$ 225 °, $<$ 315 °). Plotting software sourced from Carslaw and Ropkins (2012).

4.6 Methane isotopic measurements

Different methane sources have different δ^{13}C isotopic signatures (as discussed in Section 1.4). Biogenic methane formation will have a δ^{13}C isotopic signature between -55 to -70 ‰ (Kruger et al., 2008). This section describes analysis conducted from whole air samples taken using 3L Teflon bags at Haddenham

and two of its nearby landfills to the south. The nearest landfill is situated approximately 6 km to the south, with the other roughly 12 km in the same direction. These samples were taken over one day (11 February 2015) when the wind was from the south / south east. Air samples were taken at Haddenham in the early morning with the hope to capture an accumulated concentration of landfill emissions within the nocturnal boundary layer. Isotopic analysis was carried out by the Nisbet Group at Royal Holloway using a GC-IRMS (Isotope Ratio Mass Spectrometry, Fischer et al., 2008). Figure 4.25 shows the measured methane time series from the GC-FID at Haddenham for 11 February 2015. The whole air samples' methane concentration taken at Haddenham have been added as red points. Several large methane plumes, potentially from the landfills, were measured at Haddenham during this period. Four whole air samples can be seen to not correlate with the GC concentrations in Figure 4.25. This could be due to cross contamination within the Teflon bags as they had been reused. In addition to this three air samples had noticeably high carbon dioxide concentrations ($>$ 600 ppm) than all other samples. These three also corresponded to the higher methane concentration anomalies. Royal Holloway (Zazzeri et al., 2015) have adopted an approach to remove samples with unexplained carbon dioxide levels, and for this reason these four air samples were removed from the analysis. Whole air samples from the two landfills (six samples for each landfill) were taken in between the measuring periods at Haddenham.

Figure 4.26 shows two Keeling plots produced from the whole air samples. Keeling plots identify a compound's source by applying a linear regression between its δ13C isotopic signature and the inverse of its atmospheric concentration. These values are obtained from atmospheric measurements taken from within the vicinity of the potential source (Keeling, 1958). A Keeling plot assumes that atmospheric samples contain a combination of the background compound concentration and additional concentrations from local sources. Assuming a conservation of mass between source and sample the compounds source can be identified (Pataki et al., 2003). Figure 4.26.A uses air samples taken at Haddenham from 07:00 to 12:00 (shown as red points in Figure 4.25). Figure 4.26.B shows samples taken from the Milton landfill (12 km south of Haddenham and 1 km north of Cambridge). Air samples taken at the nearer landfill were too close to the site to create a useful Keeling plot and could not be used in this analysis. If samples are taken too close to large landfill methane sources then the isotopic signal can become contaminated by the different landfill cells. Older cells tend to be more $\delta^{13}C$ heavy due to the oxidising capacity of the

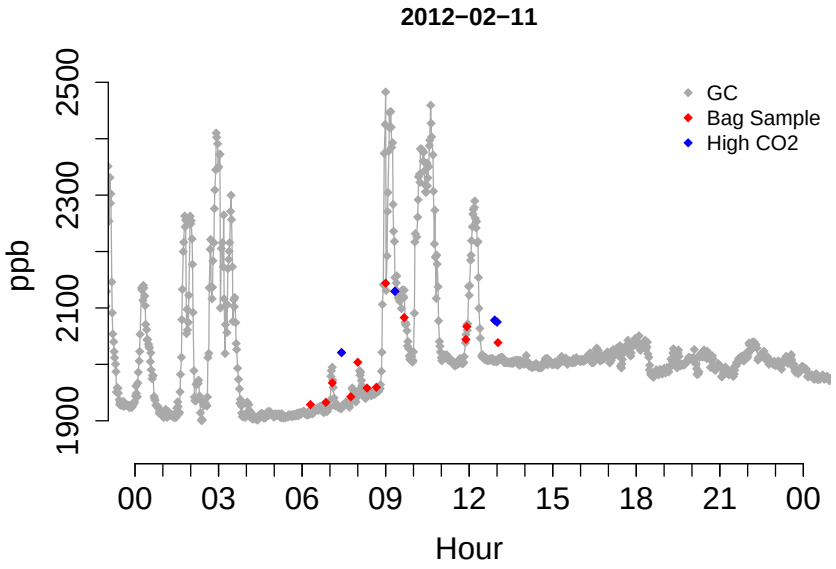

Figure 4.25: Time series of Haddenham GC-FID measurements for 11 February 2015. Whole air samples' methane concentration taken at Haddenham have been added as red points. Blue points show whole air samples which have unusually high CO_2 concentrations. These samples were removed from the isotopic analysis. NB: The whole air bag samples were measured using a GC-FID at Royal Holloway, which was calibrated onto the NOAA calibration scale. $\delta^{13}CH_4$ was measured using a GC-IRMS at Royal Holloway.

topsoil (Hegde et al., 2003). South Eastern UK landfills have been measured by Zazzeri et al. (2015) at Royal Holloway to have a $\delta^{13}C$ isotopic signature of -58 ±3 ‰. The y-axis intercept shows $\delta^{13}C$ ‰ of the methane source. Both Keeling plots in Figure 4.26 show clear signals within this stated range (-58.3 ±2 ‰ at Haddenham, -59.2 ±2 ‰ at the Milton landfill). Uncertainty was calculated as twice the standard deviation to be consistent with Zazzeri et al. (2015). More recent work conducted at Royal Holloway includes air samples taken from the nearer of the two landfills south of Haddenham. This analysis calculated an isotopic signal of -59.8 ‰, which corresponds to the signal calculated in this analysis (Lowry, D., 2015 - personal communication). This helps to certify the assumptions made in Section 4.5.3 that Haddenham's measured concentrations are dominated by landfill emissions.

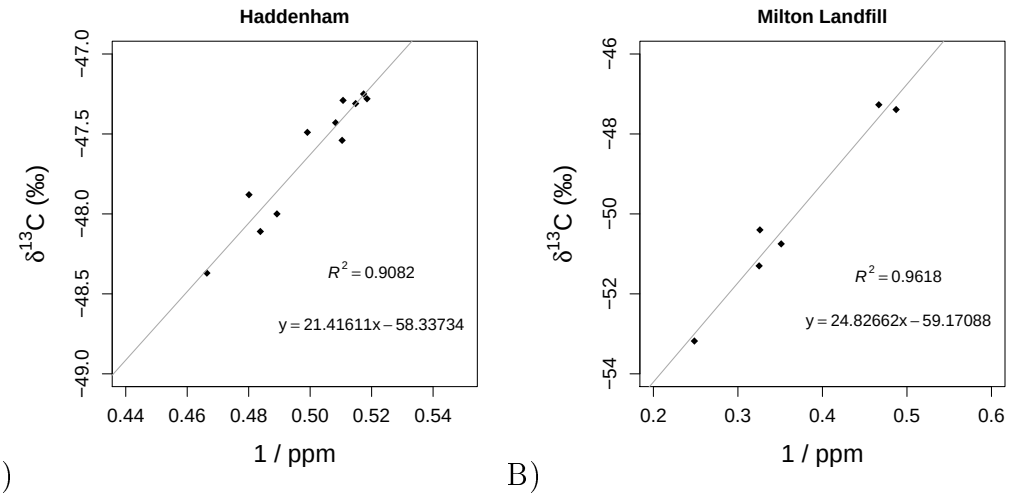

Figure 4.26: Keeling plots of whole air samples taken at A) the Haddenham GC-FID measurement site and B) the Milton landfill. x-axis shows 1/methane concentration (ppm) with y-axis showing δ^{13}C ‰. y-axis intercept shows δ^{13}C ‰ of the methane source.

4.7 Summary

This chapter provided an overview of the atmospheric methane measurement analysis. Initial analysis looked at methane's variation over different time periods. Strong diurnal cycles were observed at all four sites but greater variations were seen at Haddenham and Tilney due to local point sources being prevalent at these sites. Seasonal cycles were observed with a maxima in winter and a minima in summer. This corresponds to global annual cycles. A possible weekly cycle is observed at the sites which may be due to management practices of local methane sources (assumed to be from waste sector sources).

Methane's relationship with the meteorological variables wind speed, wind direction, temperature, pressure, and boundary layer height were assessed. All sites had strong negative correlations with wind speed and boundary layer height.

The following section compared the measured methane time series at each site with modelled equivalents formed using the NAME air history maps and the 2012 NAEI for methane. These pseudo-observations recreated the variability of the methane concentrations with respect to time well, however the magnitudes of the measured methane could not be reproduced. This could potentially be due to either NAME dispersion modelling errors or due to the NAEI being an annual average. The NAEI could not therefore recreate the large methane sources which are very variable over shorter time periods, e.g. landfills. The

pseudo-observational analysis then compared the 2009 and the 2012 NAEI. The latter inventory appeared to give a more accurate recreation of the measured observations. This implied that the changes made to this inventory methodology created a more realistic and accurate inventory.

The final section of this chapter looked at a case study of the Haddenham site. This section was split into two parts. The first concentrated on a one month period where a SNAQ node was installed at the site. This sensor measured carbon dioxide, carbon monoxide, wind speed, wind direction and temperature. Analysis between SNAQ-measured and UM-modelled meteorological data showed a relatively strong positive correlation, although modelled wind speed was higher than measured on average (6.7 m s^{-1} compared to 4.6 m s^{-1}). Wind direction saw a discrepancy between northerly values, which could have been due to an unknown obstruction at the measurement site. The SNAQ analysis also looked at methane's relationship between carbon monoxide and carbon dioxide to ascertain information on source attribution. It was thought that sources of biogenic and incomplete combustion sources of methane exist.

The second half of this section looked at whole air samples taken from Haddenham and its two nearest landfills on 11 February 2015. Isotopic analysis from these samples conducted at Royal Holloway showed Haddenham was dominated by landfill emissions. An isotopic signal of -58.3 ± 2 ‰ was observed at the Haddenham site and -59.2 ± 2 ‰ was observed from the Milton Landfill.

The next chapter looks into the sensitivity of the InTEM technique. Various factors must be predefined within the InTEM setup which may have an effect on the emission results. The following chapter assess these variables' impacts on the methane emission estimates and creates a final setup which is both robust and able to produce consistent results.

5 Development of the inversion approach

This chapter aims to describe the variables within the InTEM setup that influence the emission results. Various sensitivity studies have been undertaken to ascertain the impact of these variables with the aim to establish a robust final setup. These factors include:

- the optimum number of internal iterations to produce the emission fields;
- how many times InTEM should be repeated to create a consistent result;
- how the InTEM solution grid should be defined and at what resolution;
- how important are the predefined regions in changing the emission results;
- whether all observations should be included in the InTEM setup;
- which observational and modelling uncertainties should be incorporated into the setup;
- how sensitive are the InTEM results to the defined baseline.

All experiments within this chapter use a one year, four site inversion setup covering the period from June 2013 to May 2014 (inclusive), with hourly observations. All experiments, with the exception of those in Section 5.6, use the 15 predefined regions shown in Figure 5.1 as subtotals of the emission results. The more central regions approximately correspond to the county boundaries of East Anglia (Norfolk-10, Suffolk-4, Cambridgeshire-15 and Essex-5). Border regions (3, 7, 8, 13) are used to assess baseline issues (Section 5.10). An approximate central London area is represented in region 11, and the remaining regions' boundaries (1, 2, 6, 9, 12, 14) are less rigidly defined. It should be noted that resulting emission totals in the sections preceding Section 5.11 (InTEM Final Setup) should not be considered absolute, but rather used as a relative comparison to each other to assess the sensitivity.

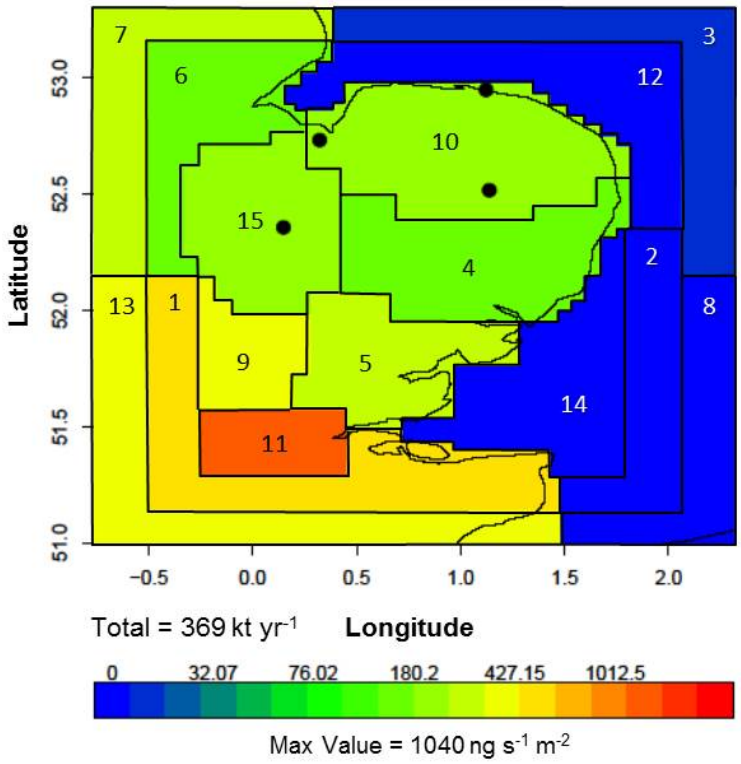

Figure 5.1: The inversion domain with 2012 NAEI total methane emissions regridded to the 'county based' regions (15 regions in total). Defined counties in East Anglia are: Norfolk (10), Suffolk (4), Cambridgeshire (15) and Essex (5). Region 11 represents central London. Regions 6 and 9 are loosely based around Lincolnshire and Bedfordshire / Hertfordshire. Region 1 comprises the south west area in the inner domain. Regions 3, 7, 8 and 13 make up the border. Regions 9, 12 and 14 divide the North Sea. Measurement site locations are shown as black points.

5.1 InTEM internal iterations and temperature steps

The simulated annealing methodology produces emission estimates that have been iteratively produced by cost function analysis (as described in Section 3.3.5). This particular method requires a set number of 'temperature' steps and internal iterations which vary the emission fields being tested. These variables are defined prior to running the inversion. The values chosen are somewhat arbitrary as a balance must be found between computer time and cost score reduction. When considering the metallurgy annealing analogy, from which the simulated annealing concept was created, temperature steps represent the system temperature.

During the simulated annealing, different potential emissions fields are compared

using cost function analysis. The amount each emissions field can vary is determined by the temperature step. In this instance, the temperature step is defined as the magnitude the individual emissions within a potential a posterior emissions grid can vary between the old and subsequent emissions grid. This reflects the amount of random noise added to individual grid cells of a potential emissions map. This magnitude reduces as the temperature step is progressed. This isolates a resulting emissions grid with the lowest cost score. In addition to this, the temperature steps can be lowered linearly (lowering at a constant rate), quadratically (gradual reduction of the temperature step magnitude) or cubically (gradual increase of temperature step magnitude followed by a decrease towards the end of the overall temperature change). This is illustrated in Figure 5.2. Within each temperature step, the potential a posterior emissions field is compared a specific number of times before the temperature is 'lowered'. This number of iterations is described as the internal iterations number.

Increasing the number of temperature steps and internal iterations is known to impact the computational expense. In this project, many different combinations of the number of temperature steps and internal iterations were explored ranging from 50 to 500 temperature steps and 5 000 to 50 000 internal iterations. Results suggested an increase in the number of temperature steps and iterations reduced the cost score and modified the regional emission quantities but only slightly. The cost score reduced by ~2 % between the two extreme experimental setups. No experimental setup produces results that were outside of the corresponding standard deviations. Increasing the number of internal iterations and temperature steps also came at a large computational expense. There was a five-fold difference in computer time between 5 000 and 50 000 internal iterations. A final setup using 100 temperature steps and 20 000 internal iterations was decided as it was deemed a compromise between cost of computer time and cost score reduction. A quadratic fit to the change in temperature steps was found to decrease cost scores more than a linear or cubic fit, and thus was applied to all future inversion experiments.

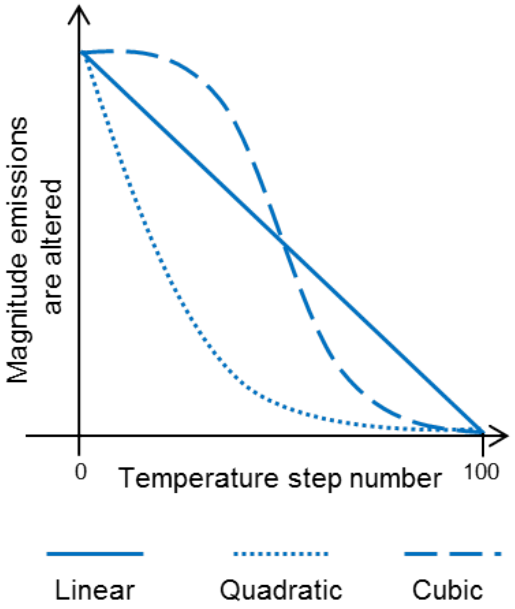

Figure 5.2: Illustration of how the magnitude of each emission can vary depending on the temperature step. The three different approaches used in InTEM's simulated annealing are A) Linear B) Quadratic and C) Cubic. NB: Purely illustrative and does not show exact values.

5.2 InTEM testing using pseudo-observations

The accuracy of InTEM can be tested using pseudo-observations constructed for the measuring sites. Using these pseudo-observations aims to re-create the underlying NAEI emissions. The general method for pseudo-observations generation using the NAME dilution matrices and the NAEI are described in Section 4.4. In this section the 2012 NAEI inventory is regridded to the county regions shown in Figure 5.1 and the resulting pseudo-observations are generated using this emission field. InTEM is then run using the pseudo-observations instead of the measured concentrations to test if the resulting emission field are similar to the regridded NAEI. The InTEM resulting region totals are shown in Table 5.1. InTEM recreates the NAEI emission totals to within a few kilotonnes in all regions. The cost score reflects the slight discrepancy between the two totals. A perfect fit between the inversions modelled observations and the pseudo-observations would produce a cost score of zero; however here a score of 0.112 was recorded. These differences are a result of the chosen number of temperature steps and internal iterations. The exact NAEI totals could be recreated with increased computational power or increasing the computer run

duration. However this was not available for this project. It appears InTEM cannot reproduce regions with small emission totals and thus the percentage differences for these in Table 5.1 are relatively high. It is reassuring that all other region totals can be recreated to within 10 % of the 2012 NAEI totals, with most being within 5 %.

Table 5.1: InTEM county regional emission totals (kt yr^{-1}) using pseudo-observations generated from the NAEI. Region label abbreviations: CBG - Cambridge, SFL - Suffolk, NFK - Norfolk, LDN - London, ESX - Essex, LCS - Lincolnshire, BHS - Bedfordshire / Hertfordshire, SW - Region to the south west (L-shaped). Regions 3, 7, 8 and 13 make up the border. Regions 9, 12 and 14 divide the sea. % difference is relative to the NAEI. Total does not include border regions.

	CBG	**SFK**	**NFK**	**LDN**	**ESX**	**LCS**	**Sea Regions**		
	15	**10**	**4**	**11**	**5**	**6**	**2**	**12**	**14**
2012 NAEI	26.5	38.9	24.1	51.2	24.5	17.6	0.1	0.1	0.3
InTEM	25.5	37.4	23.3	50.4	25.9	16.9	0.0	0.0	0.0
% difference	3.8	3.9	3.3	1.6	-5.7	4.0	100.0	100.0	300.0
	BHS	**SW**	**Border Regions**				**Total**		**Cost**
	9	**1**	**3**	**7**	**8**	**13**			**Score**
2012 NAEI	20.5	75.0	1.6	29.9	0.1	55.2	369.4		
InTEM	20.3	69.8	0.0	31.2	0.0	53.0	353.8		0.1
% difference	1.0	6.9	160.0	-4.3	100.0	4.0	4.7		

5.3 Optimum number of inversion repeats

Repeating the inversion method gives slightly different cost scores and emission totals. This is due to the stochastic nature of the changes made during the iteration process and the model setup, which constrains iterations to a limited number. Figure 5.3 displays the cost scores produced for an inversion repeated 104 times when using the real observations within InTEM (not pseudo observations). Figure 5.3.A shows the accumulated mean cost score for each repetition number with its known standard deviation. It can be seen that a more constant mean cost score and standard deviation appears at ~25 inversion repeats. Prior to that the mean values vary more dramatically, but all scores are within their standard deviations. The probability distribution function (PDF) of these scores is shown in Figure 5.3.B. There is a slight positive skew to the data due to the rare higher-scoring outliers that are calculated. As these outliers posed no significant

change to the results they were not removed. In addition to this, the individual region totals (shown above in Figure 5.1) were also analysed and showed very similar resulting patterns. It was decided that all analyses should be repeated a minimum of 25 times to produce reliable results. The standard deviation within the results of InTEM's 25 repeats is the sole representation of uncertainty for the final emission estimates.

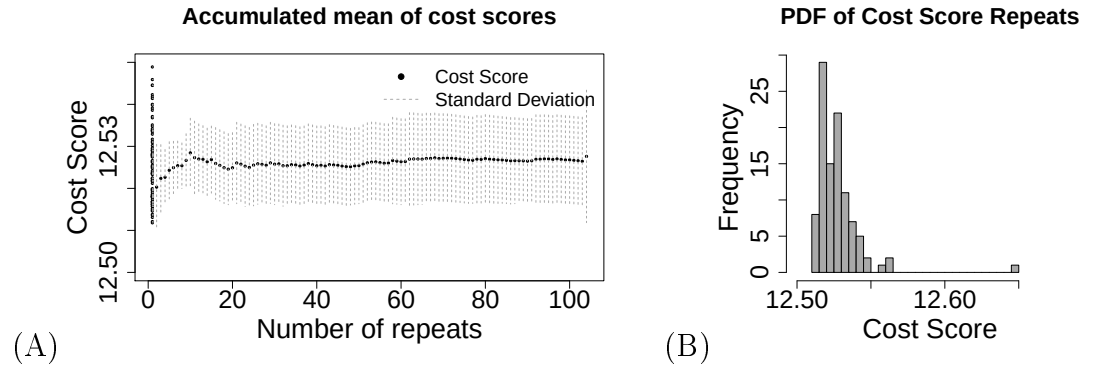

Figure 5.3: The effect the number of InTEM repeats has on cost score. A) Number of InTEM repeats vs. resulting cost scores and standard deviations. B) PDF of cost scores for all 104 InTEM repeats.

5.4 Solution grid creation method

As highlighted in Section 3.3.3, two different methods are used to create the inversion solution grids based on either the NAME air history maps or a combination of the former and the 2012 NAEI emission field. These two techniques are referred to as NAME-based and NAEI-based methods throughout this section. Here the results are shown for both methods based on a 150 grid box resolution solution grid (more information on how this was defined in Section 5.5).

There are many other methods for defining the solution grid structure and resolution, for example, Rigby et al. (2011) who creates the sub-regional grid resolution from the product of the footprint of the observation sites and the emissions prior. It is also dependent on the country that they resided in.

Figure 5.4 shows the resulting emission maps at this fine spatial resolution. All four figures are shown with the border regions removed but their totals can be found in Table 5.2. The reasons why the border regions are removed are given in Section 5.10. Some regions exhibit significant differences between the two techniques although many of the regions have overlapping emissions (within

one standard deviation). Both methods have similar cost scores and the regions near to the observation sites show little difference in their emission totals. The regions which do not overlap (9, 12, 14) correspond to the regions just north of London and the two coastal sea regions around East Anglia, respectively. Region 9 (BHS) emits far less methane in the NAME-based method than the NAEI-based technique (2.6 ±3.8 compared to 30.6 ±7.3 kt yr^{-1}). This seems to be due to the number of subdivided boxes with regions 9 and 11. The air history maps having relatively low influence from the London area compared to the observation sites because of the distance from the sites. The NAME-based method only subdivides region 9 once, and the London region (11) is left as one box. NAME trajectory analysis shows that particles increasingly originate from the free troposphere further back in time. Thus, regions further away from the observation sites will have less surface influence. The NAEI-based method divides the London region, due to the large emissions stated in the 2012 NAEI around this area. This finer resolution allows greater flexibility in the emissions resulting in a diffusion of the emissions, whereas the NAME method creates more polarised regional totals in this area. The London totals show the NAME-based method calculating larger emissions than the NAEI-based method (66.9 ±14.8 kt yr^{-1} compared to 45.7 ±18.0 kt yr^{-1}). Although neither method matches the 2012 NAEI emissions for this region the NAEI-based technique is closer. An addition of another site to the south of the inversion domain would be an interesting experiment to investigate if these regional totals would converge when using the two techniques. More information and a discussion of the effects of changing the observational site number can be found in Section 6.3.

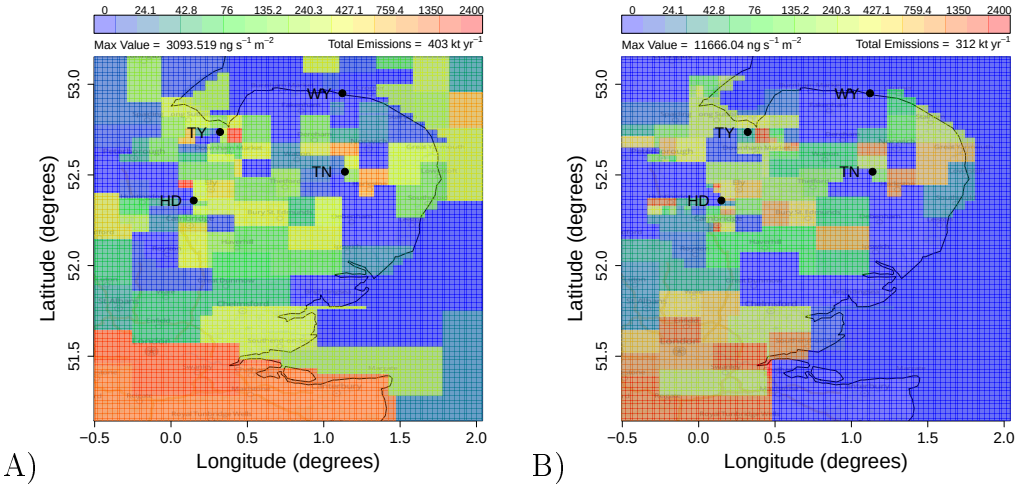

Figure 5.4: InTEM emission fields showing emissions generated using A) NAME-based solution grid and B) NAEI-based solution grid. Both maps show fine spatial resolution (150 grid boxes). Corresponding regional emission totals (kt yr^{-1}) can be found in Table 5.2.

The coastal regions (12 and 14) show larger emissions in the NAME-based technique, which may be due to these regions being subdivided only in this method. As in the previous example, an increased resolution compared to a coarse grid leads to more diffuse distribution of emissions. For these regions however, this seems to have a negative effect on the emission results. According to the 2012 NAEI, both solution grid methods would be expected to produce small methane emissions in this region. The NAME-based method produces emissions which overestimates the 2012 NAEI. The inversion technique has no indication of land or sea and this, along with uncertainty in the meteorology (Section 5.5), can produce unexpectedly large emissions over areas of little methane activity. In addition to this, the inversion domain could be causing the NAME method to overestimate region 12 emissions. The 2012 NAEI shows point sources of methane to the east of region 12 which are close to the border region 3. Any 'excess' emissions resulting from uncertainty in the baseline are put in the border regions (Section 5.10). The close proximity of these sources to the border region, as well as the meteorological uncertainty, can confuse emissions from the oil rig with boundary / baseline emissions. In summary, it is likely a combination of both the inversion domain edges and the meteorological uncertainties that result in region 12 being overestimated. These biases can be addressed to a certain extent using the NAEI-based solution grid technique, but not with the NAME-based method. For these reasons the NAEI-based solution grid creation method was chosen as part of the final InTEM setup.

Table 5.2: InTEM county emission totals (kt yr^{-1}) for the NAME and NAEI solution grid emission results. Region label abbreviations: CBG - Cambridge, SFL - Suffolk, NFK - Norfolk, LDN - London, ESX - Essex, LCS - Lincolnshire, BHS - Bedfordshire / Hertfordshire, SW - Region to the south west (L-shaped). Regions 3, 7, 8 and 13 make up the border. Regions 9, 12 and 14 divide the sea. NSC = Norfolk (10) + Suffolk (4) + Cambridgeshire (15). Total does not include border regions.

	CBG	**NFK**	**SFK**	**LDN**	**ESX**	**LCS**	**Sea Regions**		
	15	**10**	**4**	**11**	**5**	**6**	**2**	**12**	**14**
2012 NAEI	26.5	38.9	24.1	51.2	24.5	17.6	0.1	0.1	0.3
NAME-method	21.7	31.1	27.5	66.9	18.3	15.6	2.1	36.9	11.7
sd	*3.3*	*3.3*	*4.8*	*14.8*	*9.0*	*8.9*	*2.9*	*8.7*	*8.8*
NAEI-method	20.5	37.1	22.8	45.7	19.6	9.1	0.2	0.1	0.4
sd	*2.1*	*1.7*	*1.9*	*18.0*	*8.1*	*4.1*	*0.6*	*0.1*	*1.2*
	BHS	**SW**	**Border Regions**				**Total**	**NSC**	**Cost**
	9	**1**	**3**	**7**	**8**	**13**			**Score**
2012 NAEI	20.5	75.0	1.6	29.9	0.1	55.2	369.4	89.6	**-**
NAME-method	2.6	173.1	83.7	232.0	51.9	225.5	407.5	80.3	12.6
sd	*3.8*	*37.2*	*14.7*	*13.0*	*14.3*	*49.0*	*44.6*	*6.7*	*0.0*
NAEI-method	30.6	124.5	116.1	240.0	53.6	294.9	310.5	80.4	12.5
sd	*7.3*	*59.2*	*1.0*	*7.1*	*16.1*	*43.1*	*63.0*	*3.3*	*0.0*

5.4.1 Temporal aggregation errors

The section evaluated the effect of spatial aggregation on emissions results. A flaw of this chapter's sensitivity analysis is that temporal aggregation is not assessed to the same extent. Temporal aggregation error describes the error formed from having a fixed a posteriori throughout the calculated time period. This technique assumes constant emissions over the inversion time period (in this thesis this period ranges from 3 months to 2 years) but in reality methane emissions will be changing near-continuously. Shortening the inversion time period helps to minimise this error, however increasing the temporal resolution also decreases the number of observations available to constrain the fluxes within this period (Thompson et al., 2011). This is problematic, as fewer observations can lead to an under-representation of the diversity and magnitude of emissions within the spatial domain. Thompson et al. (2011) states that "if the aggregation error is

ignored, then a significant bias error in the retrieved fluxes ensues." It is therefore necessary that future experiments be conducted to analyse the impact of temporal aggregation error on these methane emission estimates.

5.5 Solution grid spatial resolution

As mentioned in Section 5.4, InTEM produces emission values on a predefined solution grid, which is created from a coarser regional grid split into specific regions. Spatial aggregation errors within this solution grid (discussed with both this and the previous section) can impact the resulting emission estimates. The defined spatial resolution of the solution grid assumes that the emission magnitude per grid cell is representative and do not significantly differ from the area mean (Thompson et al., 2011). Minimising this spatial aggregation error is important as when errors are large they can significantly bias the inversion results. Unfortunately, InTEM's cost function allows no aggregation error estimation to be included. Finer spatial solution grids will have smaller associated aggregation errors but this comes at a cost of computer running time. In addition, the finer the spatial resolution the more significant any errors with the prescribed meteorology become.

The two techniques used to create the solution grids are based on the method described in Manning et al. (2011b) in which the spatial resolution of the solution grid is determined by two metrics: a dilution threshold (defined as 3.4 s m^{-1}), and a number of times (set at 360) that a grid cell must contribute this dilution threshold before its size is reduced. As stated in Section 3.3.3, the solution grid resolution is determined using the NAME output grid spatial resolution divided into the 'regions' shown in Figure 5.1 from as a starting point. Manning's methods explains that these coarse regions can be subdivided down to produce the solution grid. A region is halved if the two metrics described above are satisfied, i.e. a dilution threshold of 3.4 s m^{-1} is reached over 360 times during the period of interest (one year). This method describes how the NAME-based solution grid is determined. The alternative method, the NAEI-based solution grid, incorporates a prior emissions field (NAEI) into the creation technique. The NAEI is aggregated onto the NAME output grid resolution (1.5 x 1.5 km) and divided into the coarse regions shown in Figure 5.1. The magnitudes of the NAEI emissions are used as a scaling factor to the dilution threshold. Regions which have larger NAEI emissions will be subdivided more to produce a finer solution grid resolution.

Some of the assumptions in Manning et al. (2011b) are somewhat arbitrarily defined and so the method described above was changed slightly. Here, the impact of varying the grid resolution upon resulting emissions was investigated. This involved varying the dilution threshold to change the resulting solution grid resolution. Emission dilution thresholds were calculated to produce solution grids with varying resolutions, nine grids were investigated with the number of boxes ranging from 15 (the most coarse consisting solely of the county boundaries region grid) to 250. Resulting maps for four of these resolutions are shown in Figure 5.5. The high emissions shown in the border regions are due to resulting baseline issues which are discussed in Section 5.10. Increasing the grid resolution allows the identification of inversion point sources - the locations of which generally correspond to point sources in the 2012 NAEI. Some differences do exist, for example, the point source south of the Weybourne site (north east) appears in a different box (1 - 3 km away) compared to the equivalent 2012 NAEI emission map on the same solution grid resolution. This particular point source corresponds to a landfill and thus its location is known. This suggests that although the InTEM method is able to identify point sources at fine spatial resolution, errors in the meteorology can propagate through to these emission locations.

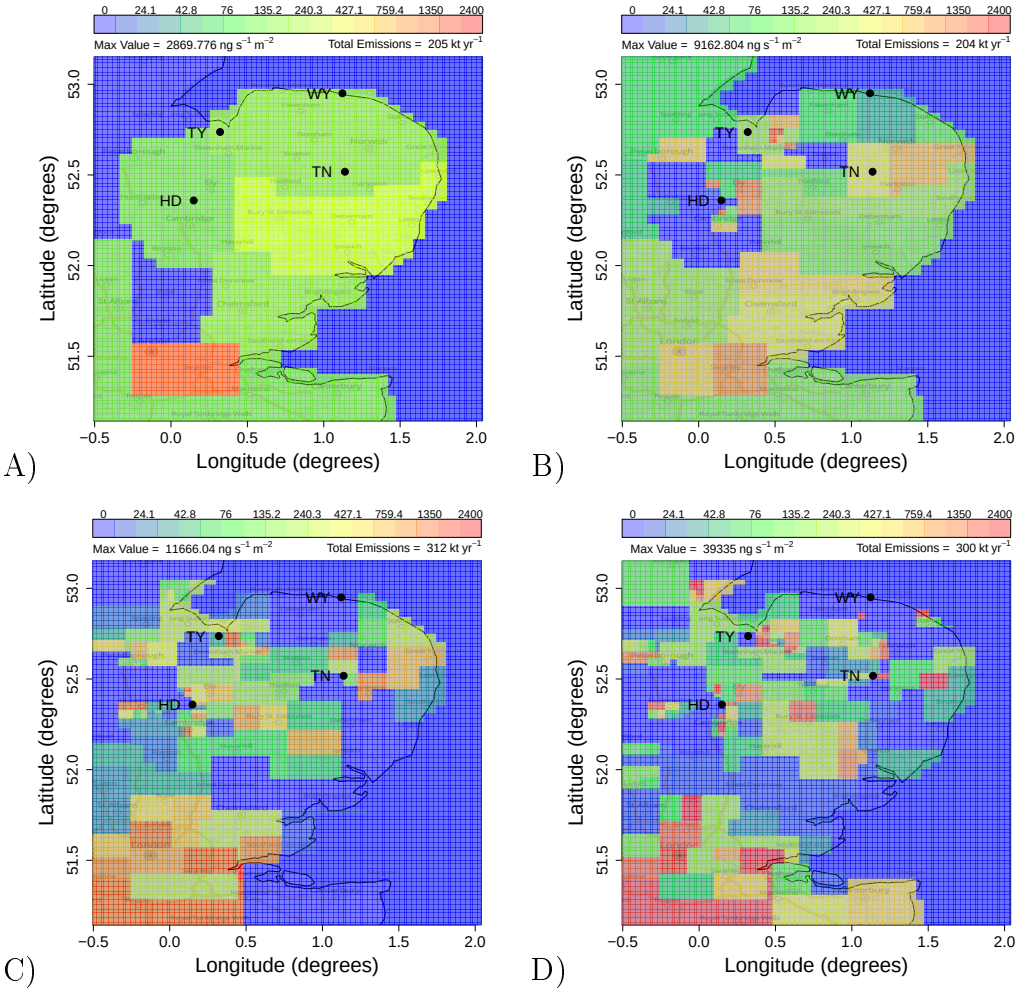

Figure 5.5: InTEM emission maps showing the effect on varying the spatial resolution of the solution grid. Number of grid boxes in each map are A) 15 B) 64 C) 150 D) 250.

To allow direct comparison, emissions (on each particular solution grid spatial resolution) were aggregated together onto the coarser county-scale resolution (15 regions) for each of the nine solution grid resolutions investigated, as shown in Figure 5.6. With the exception of the 15 grid box resolution all totals for the different regions are similar and overlap when the standard deviations are considered. Several regions show a significant step change in the emission totals for the 15 grid boxes which are normally further away from the 2012 NAEI totals. This suggests the resolution is too coarse to resolve the regional emission totals. The emissions from the three regions closest to the observation sites show very little variation at any spatial resolution (with the exception of the 15 region grid). Other, more distant regions show larger fluctuations in emissions (i.e. regions 1, 5, 9, 11, 12).

Analysis of the resulting cost scores for each grid resolution showed a gradual decrease with increasing resolution. This is to be expected as a more finely resolved grid has additional degrees of freedom. This grid can then produce a pseudo-observational time series which more accurately replicates the measured observations. However, increasing resolution comes at a computational cost, taking ~4 times as long to run at 250 grid boxes than at 15 boxes. It was decided to choose 150 grid boxes as the final solution grid resolution for future analysis as this was deemed high enough resolution to identify major point sources without being prohibitively computationally intensive. Solving on the finer solution grid spatial resolution helps to minimise aggregation error. Aggregating the emission magnitudes to the region spatial-resolution is one method to reduce trajectory uncertainties from meteorological data errors. The resulting dilution thresholds were found to be 15.0 s m^{-1} and 19.5 s m^{-1} for the NAME-based and the NAEI-based methods, respectively. The threshold derived in Manning et al. (2011b) is lower than the chosen thresholds, and produced a much finer solution grid resolution. The solution grids which were closest to Manning's threshold (250 grid boxes) were too computer intensive and did not produce results that were statistically significant.

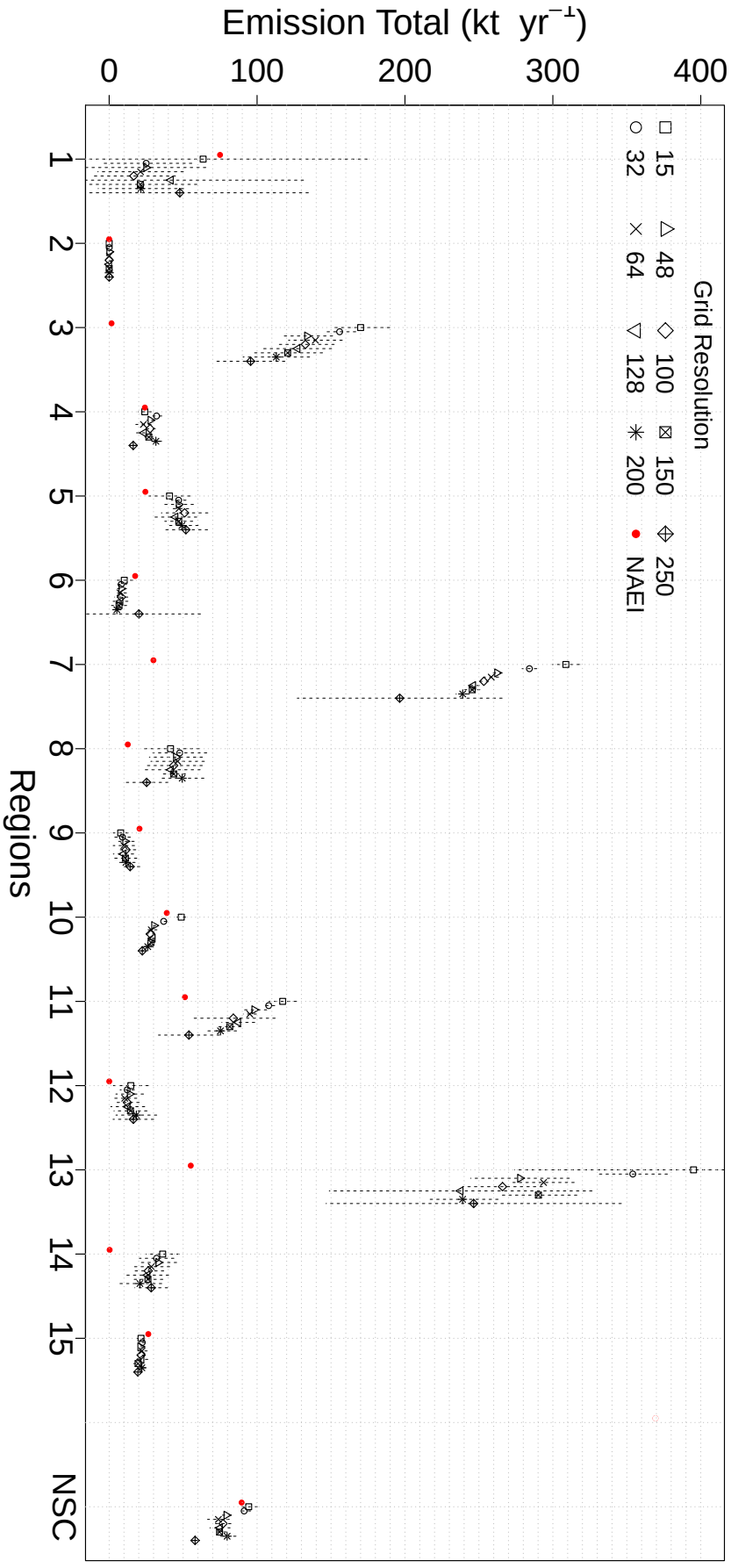

Figure 5.6: Summary figure of all 15 regional emission totals (kt yr^{-1}) for nine grid resolutions tested. For reference, NAEI emissions for the corresponding regions are shown as red circles. Grey dashed lines show one standard deviation for the 25 inversion repeats. Region numbers shown in the x-axis correspond to the labels in Figure 5.1. 1 = L-shaped region to the SW, 4 = Suffolk, 5 = Essex, 6 = Lincolnshire, 9 = Hertfordshire / Bedfordshire, 10 = Norfolk, 11 = Central London, 15 = Cambridgeshire. Regions 2, 12 and 14 make up the North Sea. Regions 3, 7, 8 and 13 make up the border regions. NSC = Norfolk (10) + Suffolk (4) + Cambridgeshire (15)

5.6 Different starting regions grid

Analysis previous to this section has seen InTEM using a solution grid created using the county-based region grid (Figure 5.1). A listed description of all three grids used in InTEM is shown below. This section explores whether an alternative starting 'regions grid' would have an effect on the resulting emission estimates.

- NAME-output grid: This grid is the spatial resolution of the model output from the NAME model. The resolution and dimensions is also the same in the dilution matrix (Section 3.3.2). This is a regularly spaced grid of 1.5 x 1.5 km resolution.
- Regional grid or starting regions grid: This grid sees the NAME-output grid boundary limits and resolution divided into irregular and arbitrarily defined regions. An example of this is Figure 5.1, which shows regions based loosely on the UK county boundaries.
- Solution grid: This grid also has the same boundary limits as the previous two grids, however it has a variable spatial resolution which fits around the regional grid and whose individual grid cells will never be finer than the NAME-output grid resolution. The solution grid is created using the methods described in Section 5.4 and Section 5.5. The solution grid resolution and arrangement of grid cells will be different if a different regional grid is used. NB: Post analysis of InTEM results (produced on the solution grid resolution) are sometimes aggregated back to the regional grid resolution to compare different model setups. This is because statistical data for each individual region is outputted with InTEM (as described at the beginning of this chapter on page 107).

This section assesses if the resulting methane emission estimates differ if an alternative regional grid is used to create the solutions grid. Figure 5.7 shows the 2012 NAEI on a more regularly defined regional grid, as opposed to the county-based regions shown in Figure 5.1. Results from this section show analysis using both the NAME-based and the NAEI-based methods of producing solution grids (explained in Section 5.4), based on this new region format. These runs used a 150 solution grid box resolution.

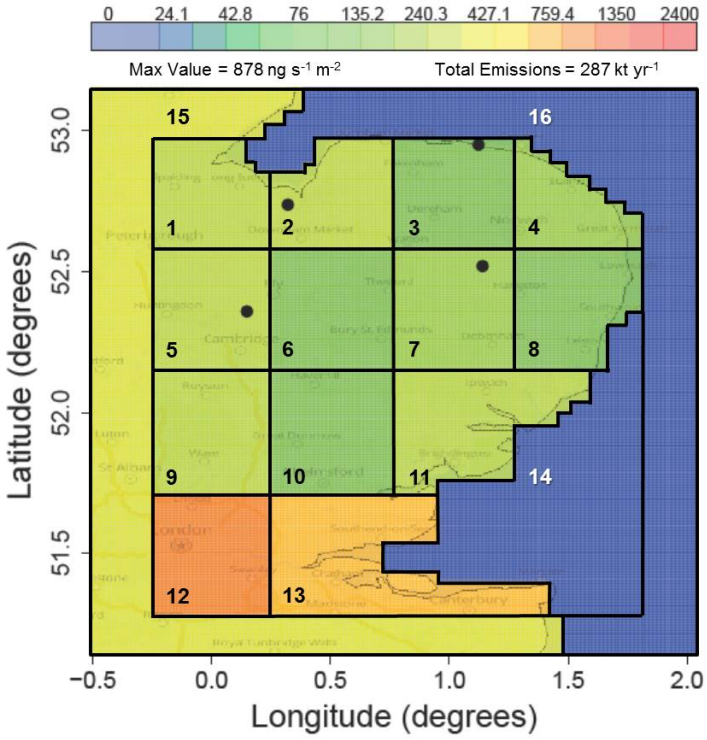

Figure 5.7: 2012 NAEI regridded to alternative region domains. Regions are more arbitrary. Two thick border regions exist (15 and 16) to remove excess emissions from baseline errors (Section 5.10). The inner regions are more regular shaped than the county boundaries region grid in Figure 5.1. The only region to appear in both grids tested is number 14. Measurement site locations shown as black points.

The resulting emission maps for both solution grid methods are shown in Figure 5.8 and the regional totals, along with the equivalent emissions of the NAEI, can be found in Table 5.3.

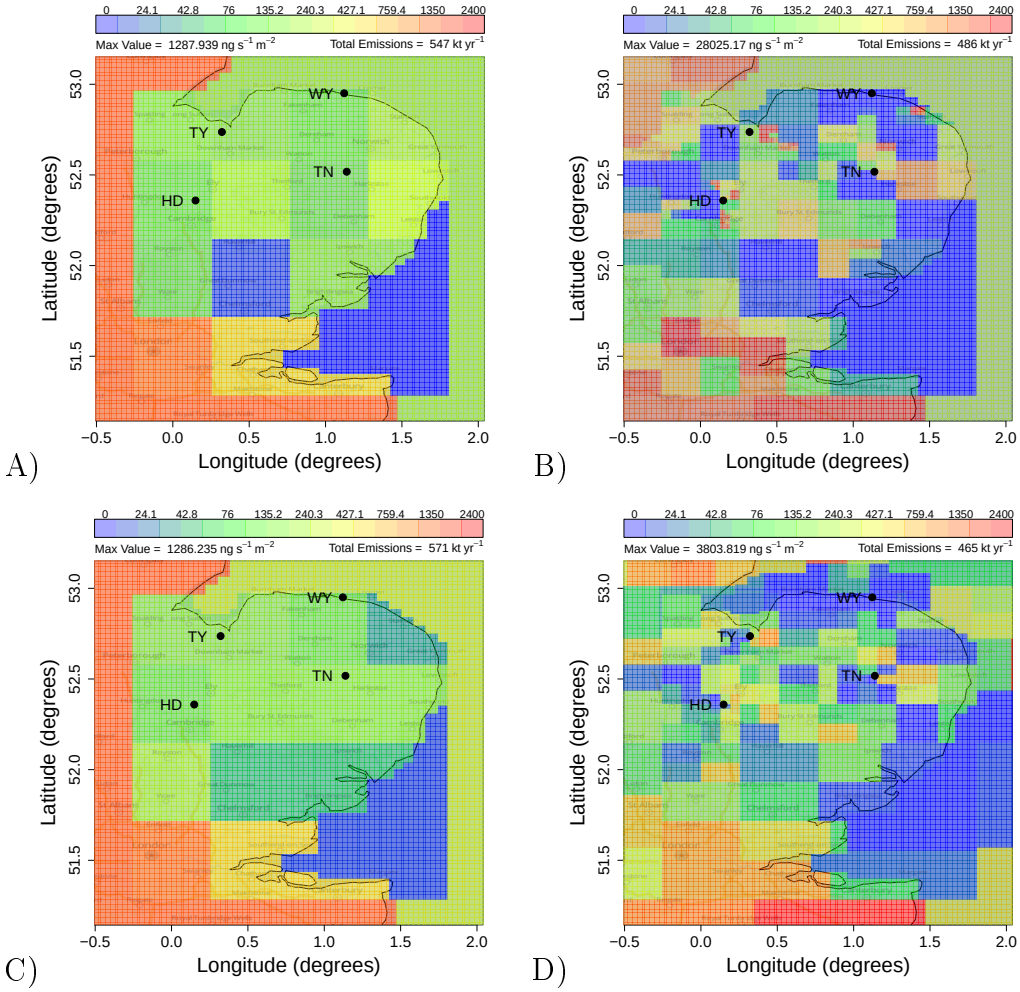

Figure 5.8: InTEM emission fields based on the alternative region structure showing emissions generated using A) NAEI-based solution grid (fine spatial resolution) B) NAEI-based solution grid (coarse spatial resolution) C) NAME-based solution grid (fine spatial resolution) D) NAME-based solution grid (coarse spatial resolution).

The major differences and similarities between the NAME-based and NAEI-based emission maps formed from the alternative starting regional grid are summarised below.

- Both solution grid methods produce similar emission distributions in the East Anglia area. This is observed within the county boundaries regional grid as well.
- Most regions overlap with each other's standard deviations apart from three: regions 4, 8 and 11.
- The NAEI-based solution grid method shows a fine point source to the south east of Weybourne in region 4, which is not resolved in the NAME

method. The result shows the NAME method emissions are more spread out over this region and over the nearby coast which underestimates region 4 with respect to the 2012 NAEI.

- The NAEI-based grid emits more in region 8 (east of the Tacolneston site) resulting in a larger emission total for this region than both the 2012 NAEI and the NAME-based method. There is no obvious reason for this discrepancy between the two methods. The NAEI-based solution grid in the county boundaries regional grid also puts larger emissions to the east of Tacolneston than the NAME solution grid method.

- Both solution grid methods produce lower estimates for regions 10 and 11 compared to the 2012 NAEI. The NAEI-based solution grid method puts almost all emissions in region 11, whereas the NAME-based technique has a more homogenous distribution, making both regions lower than the 2012 NAEI. This underestimation is also present in the finely resolved county based regions, although the overall county estimate is increased by including emissions from the south of region 5 (Figure 5.1).

- London emissions (region 12) are slightly overestimated compared to the 2012 NAEI but the values still overlap within one standard deviation. This could be a further example of emissions being polarised in regions where they are too constrained.

This analysis shows that the starting regional grid can have an impact on the resulting solution grid. Taking the example of the point source to the south east of Weybourne, this point source is only resolved in the 16-box (the alternative, more arbitrarily defined) regional grid using the NAEI-based solution grid method (Figure 5.8.C). This is not seen in either of the solution grids formed from the county-boundaries regional grid. This is because of how the regions are subdivided. A region is only divided if it reaches the defined dilution threshold. For the NAME-based solution grid this threshold is in the same units at the dilution matrix (s m^{-1}). Areas nearer to the observation site will reach this threshold many times over and thus create finely resolved regions while areas where little information is known will remain more coarse. The NAEI-based method incorporates the 2012 NAEI as a multiplying factor to the dilution threshold to determine the solution grid resolution. Once this threshold is reached the region is split into two equally contributing subregions. This will differ depending on the area of the starting regional grid and thus can result in differing solution grids.

Similar cost scores are produced for the starting regional grids and the solution grid methods used. The regions in this section which are close to the observation sites (1, 2, 3, 5, 6, 7) all agree well with the 2012 NAEI. Overall, changing the starting regions does not appear to have a significant impact on these emission totals, despite relatively different solution grids being produced. The county-based regions were chosen as part of the final InTEM setup as these totals could aid policy makers, and are easier to visualise when communicating emission totals.

Table 5.3: InTEM coarse regional emission totals (kt yr^{-1}) for the NAME-based and NAEI-based solution grids. Solution grids are based on the alternative 16 box starting region grid. Total does not include border regions (15 and 16).

	1	**2**	**3**	**4**	**5**	**6**	**7**	**8**	**9**
2012 NAEI	11.3	12.9	8.0	6.5	14.2	8.9	12.0	7.2	13.4
NAME-method	9.7	6.9	8.5	1.5	9.0	12.1	12.5	11.5	13.2
sd	*2.5*	*0.9*	*0.6*	*1.2*	*1.7*	*2.6*	*2.8*	*3.1*	*4.9*
NAEI-method	10.3	7.6	7.2	8.3	9.0	15.9	7.2	17.9	7.3
sd	*2.5*	*0.7*	*0.7*	*1.5*	*1.4*	*1.5*	*2.2*	*1.73*	*5.4*
	10	**11**	**12**	**13**	**14**	**15**	**16**	**Total**	**Cost Score**
2012 NAEI	8.8	14.9	46.9	49.59	0.3	152.9	1.7	369.4	-
NAME-method	3.6	3.7	58.6	55.22	2.0	580.0	189.8	206.1	12.5
sd	*4.6*	*4.1*	*18.6*	*15.59*	*3.4*	*50.0*	*1.7*	*26.4*	*0.0*
NAEI-method	0.8	12.0	60.2	58.08	0.2	560.0	107.2	242.2	12.7
sd	*1.1*	*2.0*	*14.5*	*12.90*	*0.3*	*30.0*	*1.4*	*20.8*	*0.0*

5.7 Observational uncertainty and variability

As mentioned in the methods chapter (Section 3.3), uncertainties associated with both the measurements and the modelling can be incorporated into InTEM to influence the resulting emissions produced. This section describes two different approaches which can represent observational uncertainties, i.e. uncertainties associated with the instrumentation and the measured observations. Both approaches incorporate hourly instrument precision and calibration uncertainties. These values range between 5 and 10 ppb on average. One method also includes

the standard deviation within each hourly observation. This measure of the hourly observational variability is a method of paramertising 'random' errors within the dispersion model (explained in greater detail in Section 5.8). These ppb values are larger than the instrument uncertainties, ranging from a few ppb to over 100 ppb in some instances. High, short lived methane spikes are inconsistently seen at two of the sites (Haddenham and Tilney) resulting from local methane sources. If a large methane concentration is observed, which has relatively low uncertainty associated with it, InTEM will try to recreate this magnitude. It was therefore considered that these instances could bias the inversion, and thus the hourly standard deviation was used as a measure of variability / uncertainty.

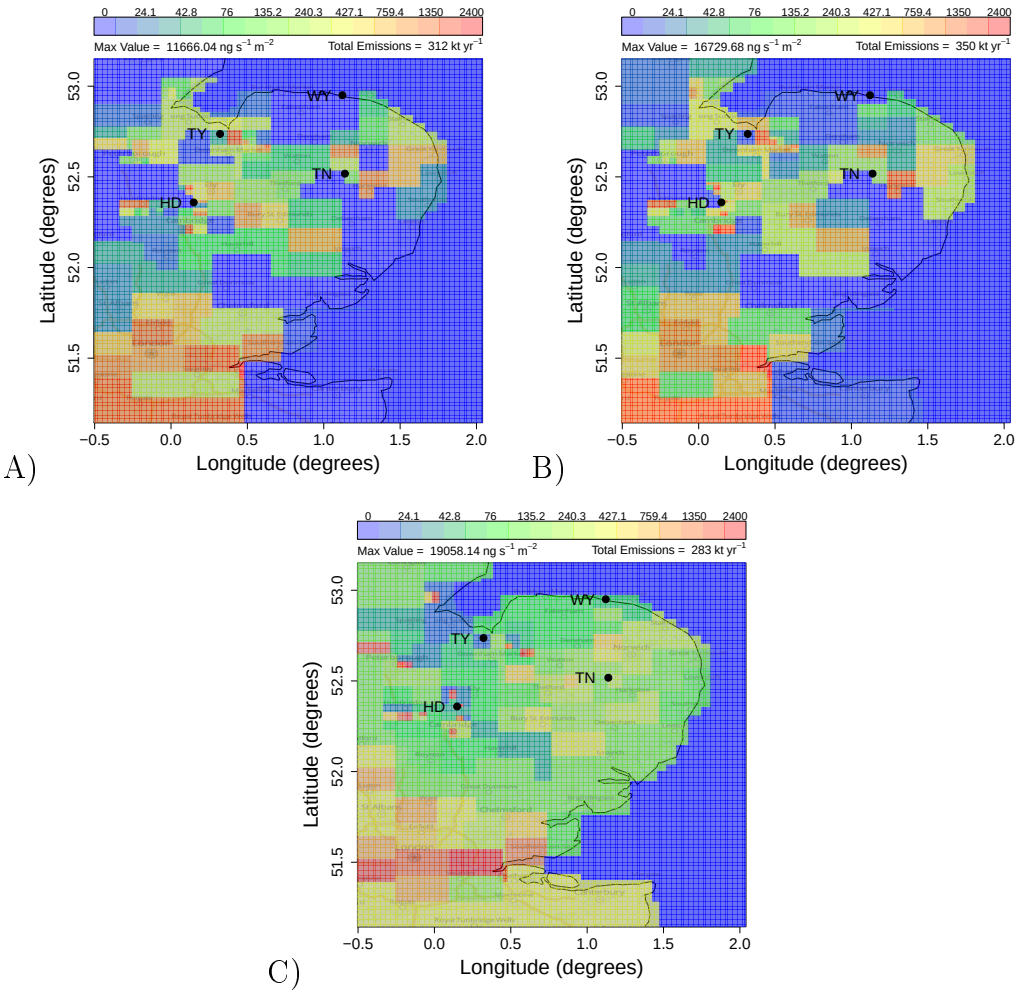

Figure 5.9: InTEM emission fields comparing two setups assessing observational uncertainty. A) Observational uncertainty defined as hourly instrument precision and calibration uncertainties. B) Observational uncertainty defined as hourly instrument precision, calibration uncertainties and hourly concentration standard deviations. C) NAEI regridded onto 150 box solution grid. All uncertainties expressed in ppb.

Figure 5.9 shows the fine spatially-resolved emission maps when hourly standard deviations are not included (Figure 5.9.A) and are included (Figure 5.9.B) within InTEM. The NAEI at the same resolution is also included for reference (Figure 5.9.C). The county regional totals for all three maps are shown in Table 5.4. The overall totals for both methods are similar, however some of the regions differ significantly. The region totals near to the observation sites (4, 10 and 15) increase when no standard deviation is included. Additionally, more methane is placed in region 3 (border box to the north east). There is significantly less methane emitted in regions 5 and 8 however, which correspond to the Essex county region and the border box to the south east, respectively.

Table 5.4: InTEM county emission totals (kt yr^{-1}) for experiments comparing observational uncertainty. Region label abbreviations: CBG - Cambridge, SFK - Suffolk, NFK - Norfolk, LDN - London, ESX - Essex, LCS - Lincolnshire, BHS - Bedfordshire / Hertfordshire, SW - Region to the south west (L-shaped). Regions 3, 7, 8 and 13 make up the border. Regions 9, 12 and 14 divide the sea. NSC = Norfolk (10) + Suffolk (4) + Cambridgeshire (15). Total does not include border regions.

	CBG	**NFK**	**SFK**	**LDN**	**ESX**	**LCS**	**Sea Regions**		
	15	**10**	**4**	**11**	**5**	**6**	**2**	**12**	**14**
2012 NAEI	26.5	38.9	24.1	51.2	24.5	17.6	0.1	0.1	0.3
SD Included	20.5	37.1	22.8	45.7	19.6	9.1	0.2	0.1	0.4
sd	*2.1*	*1.7*	*1.9*	*18.0*	*8.1*	*4.1*	*0.6*	*0.1*	*1.2*
SD Not Included	27.7	42.6	29.3	55.0	7.7	9.9	0.2	0.1	0.1
sd	*2.2*	*2.9*	*4.2*	*25.9*	*5.3*	*9.7*	*0.5*	*0.1*	*0.3*
	BHS	**SW**	**Border Regions**				**Total**	**NSC**	**Cost**
	9	**1**	**3**	**7**	**8**	**13**			**Score**
2012 NAEI	20.5	75.0	1.6	29.9	0.1	55.2	369.4	89.6	-
SD Included	30.6	124.5	116.1	234.0	53.6	294.9	305.5	80.4	12.5
sd	*7.3*	*59.2*	*1.0*	*7.1*	*16.1*	*43.1*	*63.1*	*3.3*	*0.0*
SD Not Included	34.0	134.0	125.5	223.8	17.1	290.9	357.7	99.6	29.7
sd	*5.1*	*57.9*	*1.5*	*17.2*	*9.1*	*38.7*	*64.8*	*5.6*	*0.0*

In other comparisons explained in this chapter cost scores have been used to identify a more relevant experimental setup, for example Section 5.4. However, in this section, cost score cannot be used as a metric to justify one experimental setup over another. This is because the fundamental mechanics of the chosen cost

score in this analysis is based upon uncertainty. The cost score is calculated by dividing the residual by the associated uncertainty at each timestep and thus the resulting scores would have to be normalised in order to be used as a comparison.

Previous analysis showed the elevated, short lived methane peaks to be from local point sources (Section 4.6). Therefore, an increase in methane emission totals in the regions close to the observation sites is to be expected when no hourly standard deviation is included in the InTEM setup. Less obvious reasons exist for the decrease in regions 5 and 8. This could be due to the distance these regions are from the observation sites as more distant regions seem to be consistently less resolved than regions which contain the observation sites. More importantly the inclusion of hourly variability acts as a pseudo-modelling uncertainty. This is described in further detail in the next section. For these reasons the hourly standard deviations were chosen to be used in the final inversion setup.

5.8 Additional modelling uncertainty

This section describes the modelling uncertainty experiments conducted to assess its impact on the InTEM results' sensitivity. This is in addition to the variability experiments described in the previous section. A modelling uncertainty, which represents errors in the NAME model and baseline, can be included in InTEM in addition to uncertainty associated with the measurements and observations (described in Section 5.7). Table 5.5 summarises the experiments in this section.

Experiment 1 sets a modelling uncertainty of 5 ppb for each timestep. This value increases by 5 ppb for each experiment shown in Table 5.5 until run 7. All experiments, with the exception of experiment 8, define observational uncertainty as the total of the instrument precision, the calibration gas uncertainty, and the standard deviation of the hourly concentration values. Experiment 8 sets all sites' observational uncertainty as a constant number throughout the period of interest (15 ppb). Modelling uncertainty can either be added to the respective observational uncertainty, or combined as a multiple. All experiments add modelling and observational uncertainty, with the exception of experiment 9 which applies a multiplying factor of two. NB: The term observational uncertainty includes the hourly variability described in the section before. This variability actually attempts to capture the 'random' errors within the dispersion model. In experiment 9, the doubling the observational uncertainty and variability examines the incorporation of this variability in more depth.

Table 5.5: Summary of the InTEM experiments assessing model uncertainty sensitivity. Table is split into three sections. The left section states the observational uncertainty with ✓ denoting values described in Section 5.7. Experiment 8 has a default observational uncertainty of 15 ppb for each timestep at all sites. The central section describes the modelling uncertainty which is either added to the observational uncertainty or applied as a multiple. Experiment 9 in effect is 2x the observational uncertainty. The right section gives the mean total uncertainty for each experiment at every site, for reference. All values are in ppb.

#	Observational Uncertainty	Modelling Uncertainty		Total Mean Uncertainty (ppb)			
		Additive	Multiple	HAD	TAC	WEY	TIL
1	✓	5	-	40.4	14.1	19.9	26.9
2	✓	10	-	45.4	19.1	24.9	31.9
3	✓	15	-	50.4	24.1	29.9	36.9
4	✓	20	-	55.4	29.1	34.9	41.9
5	✓	25	-	60.4	34.1	39.9	46.9
6	✓	30	-	65.4	39.1	44.9	51.9
7	✓	35	-	70.4	44.1	49.9	56.9
8	15	15	-	30.0	30.0	30.0	30.0
9	✓	-	Obs	70.8	18.2	29.8	43.9

The mean observational uncertainties associated with each of the four observation sites are shown in Table 5.5. The observational uncertainties dominate the mean total uncertainty values in experiments 1-3, although this ratio changes as more modelled uncertainty is added to the inversion system. It appears that a constant modelling uncertainty value set at all timesteps has a different impact on the individually weighted observations (which vary with time due to the observational uncertainties). A large modelling uncertainty added onto an already uncertain observation will have relatively little impact on the contribution of this observation, while the addition of a large model uncertainty to an otherwise precise observation will be larger. Therefore, an increase in model uncertainty should be expected to have an impact on the resulting emissions. This can be seen in Figure 5.10 where certain regions show trends in emission totals as the model uncertainty is increased. It appears that regions closest to the observation sites exhibit increasing totals when model uncertainty is also increased. Regions further away (1, 5, 9) seem to decrease their total emissions, although the London region (11) also increases its methane emissions.

The instances where observations have large uncertainties are when concentrations exhibit large standard deviations within the hourly average value. These occasions usually occur during periods of more stagnant meteorological

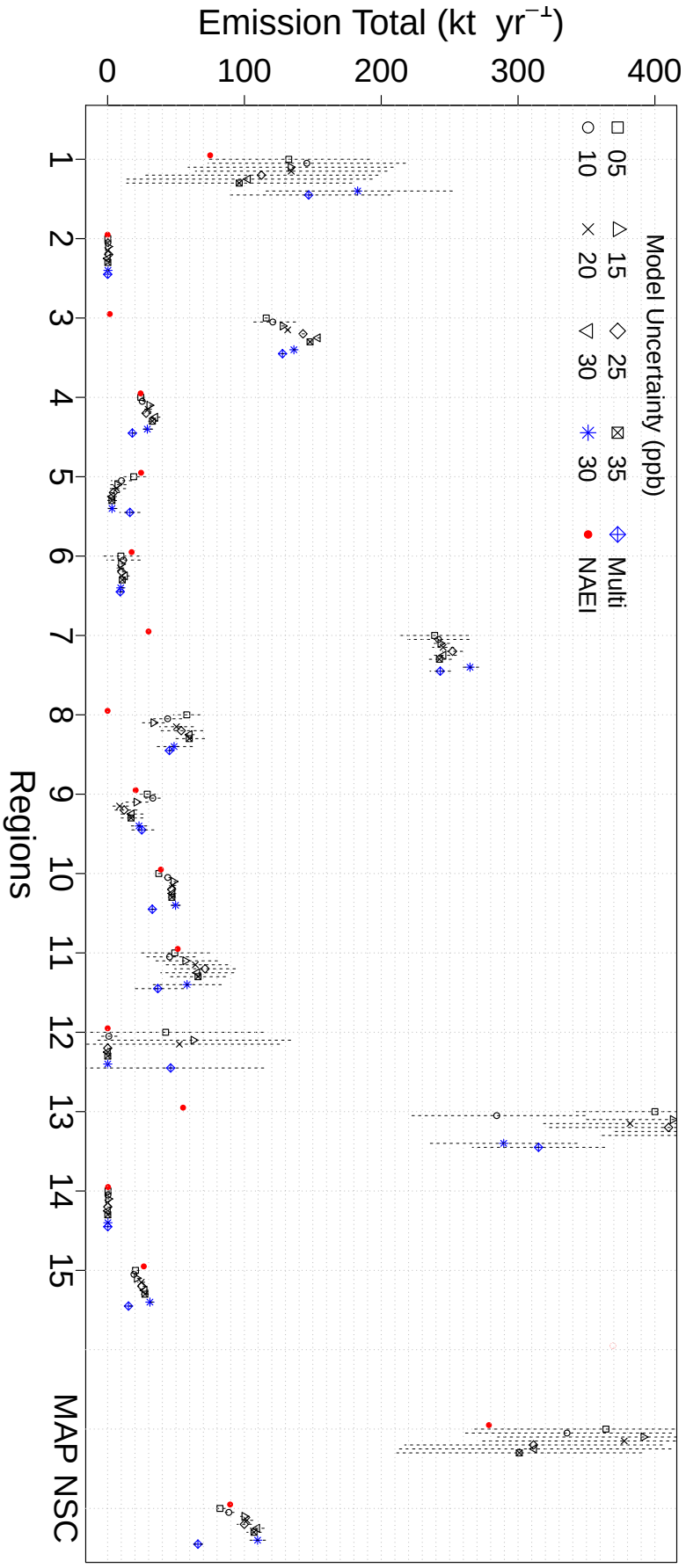

Figure 5.10: A summary of the InTEM region totals for the model uncertainty experiments. Figure key refers to assigned model uncertainty in ppb. Blue star refers to experiment 8. Blue diamond refers to experiment 9. NAEI is shown as a red point for reference. x-axis refers to the county region number in Figure 5.1. 1 = L-shaped region to the SW, 4 = Suffolk, 5 = Essex, 6 = Lincolnshire, 9 = Hertfordshire / Bedfordshire, 10 = Norfolk, 11 = Central London, 15 = Cambridgeshire. Regions 2, 12 and 14 make up the North Sea. Regions 3, 7, 8 and 13 make up the border regions. NSC = Norfolk (10) + Suffolk (4) + Cambridgeshire (15).

conditions (nighttime - low boundary layer height, low wind speeds etc.) which allows a build up of methane concentrations. These instances are difficult to model and thus should have larger associated model uncertainties. This is why the incorporation of variability can be a relevant model to help capture time-dependent modelling errors. Applying a large, additive uncertainty which is set at a constant value de-weights the more certain observations. This results in the inversion assuming larger, more local sources. This suggests adding a constant value to represent model uncertainty is not an effective method to capture this error. Further experiments using pseudo observations could be conducted to better understand the differences within these results. Experiment 9, keeps the relative distribution of uncertainties over the duration of the inversion, but still has almost double the uncertainty amount of experiment 1. The resulting regional emissions are similar. It appears that there are limitations to the additive method to create overall uncertainty. Addition of a constant model uncertainty desensitises the more precise observations giving a bias to the less precise observations. By including the standard deviation of the hourly concentrations acts as an indirect parameter to model uncertainty as the larger, short lived concentrations of methane usually occur at nighttime, when modelling uncertainty is higher.

The other aspects of measurement uncertainty are not correlated with errors in the model. Other metrics should be incorporated into the InTEM setup to represent modelling uncertainty to be more inclusive/representative. For example, continuous meteorological measurements could be made at all sites so when the measured and modelled values diverge (for example if the timing of an incoming front is wrong) additional uncertainty could be incorporated into the inversion setup. Results shown in Section 4.5 found that modelled winds can differ from measured values in the Haddenham case study. For these reasons a default value of 5 ppb was adopted to represent model uncertainty for the final InTEM setup.

5.9 Daytime and nighttime inversions

To assess if there are optimal measurement times for the inversion setup, InTEM is run using observations split into daytime or nighttime values. These are defined as measurements between 10:00 - 16:00 UTC for daytime and 22:00 - 04:00 UTC for nighttime values. The resulting emission maps and region totals can be found in Figure 5.11 and Table 5.6, respectively.

The InTEM solution grid resolution maps look like near-opposites to each other in the EA region. Both maps still place large emissions over point sources and cities (London, Cambridge, Ipswich etc.) but the nighttime map (Figure 5.11.B) places more emissions in region 6 (Lincolnshire) and to the west of Weybourne. Although the nighttime emissions seem more detailed in the EA area, the Norfolk and Suffolk region totals are much less than the equivalent daytime values. The daytime maps place much larger emissions in the point sources but resolve few of the smaller emissions.

The dilution matrices used within the InTEM setup can explain why these differences occur. Figure 5.12 shows the daytime (A) and nighttime (B) dilution matrices for the Haddenham site over a one year period (June 2013 - May 2014). The spatial extent of the region of high sensitivity is larger for the dilution matrix for nighttime (Figure 5.12.B) than the daytime (Figure 5.12.A). This is due to the nighttime meteorological conditions, which usually experience lower wind speeds and more stagnant conditions. The lower nocturnal boundary layer heights and wind speeds will result in a less diffuse dilution matrix compared to daytime equivalents. This could be why the nighttime maps produce a more detailed spatially distributed emission map.

Nighttime meteorology is more challenging to model in NAME due to localised subgrid scale influences which are not fully captured in the UM's meteorology. This is seen in several inversion studies which use different meteorological data, e.g. Geels et al. (2007); Chevillard et al. (2002); Elbern et al. (2007). Geels et al. (2007) states that when running experiments similar to those described in the section (i.e. running inversions using solely day- or nighttime observations "daytime values are quite well predicted, nighttime values are generally underpredicted.". Similarly, the results shown here produce much lower estimates using just nighttime observations. Nighttime timesteps should therefore be assigned a larger modelled uncertainty. As discussed in Section 5.8, specific, time-dependent modelling uncertainty has not been adopted into the InTEM setup, which could mean that the nighttime local sources may be being modelled incorrectly. However, one alternative method of representing this increase model uncertainty in the nighttime observations can be to de-weight nighttime observations within the uncertainty cost function (Section 3.3.5). This pseudo-model uncertainty helps to represent the nighttime meteorological error.

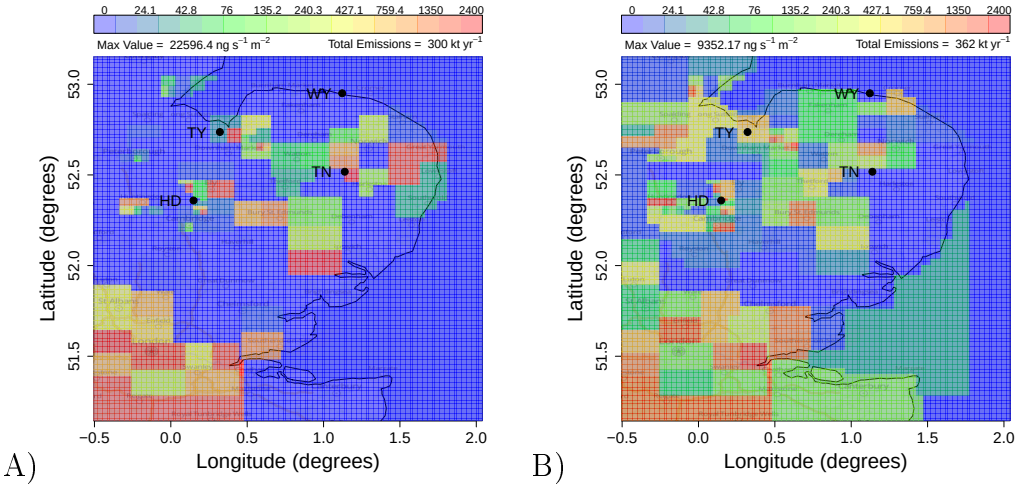

Figure 5.11: InTEM emission maps for the Haddenham site over a one year period (June 2013 - May 2014) using A) daytime (10:00-16:00) and B) nighttime (22:00-04:00) observation measurements.

Table 5.6 shows the regional daytime emission estimates are higher than the 2012 NAEI and the nighttime are lower, whereas emission maps produced using all measurements produce maps which are more similar to the NAEI. It was decided to incorporate all observations within the InTEM setup, as the resulting nighttime emission maps showed no obvious errors which could be identified as resulting from nocturnal meteorological uncertainty. The failure to fully capture the diurnal variability is a systematic error found in most inversion setups. By attempting to de-weight the nocturnal observations by increasing their associated uncertainties tries to asses this error but the method is not fully comprehensive.

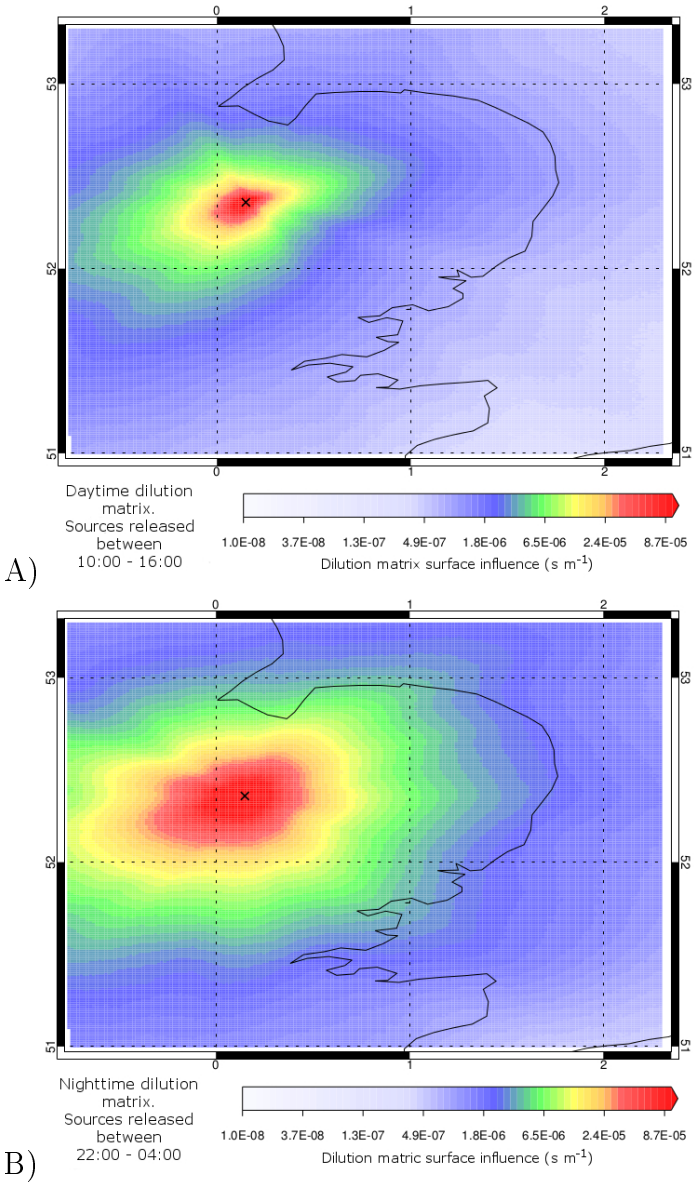

Figure 5.12: Daytime and nighttime dilution matrices for the Haddenham site over a one year period (June 2013 - May 2014). Figures show the average 'dilution' values throughout 2013 and 2014 (s m^{-1}). The Haddenham site location is marked with an X.

Table 5.6: InTEM county emission totals (kt yr^{-1}) using daytime and nighttime observation measurements. Region label abbreviations: CBG - Cambridge, SFL - Suffolk, NFK - Norfolk, LDN - London, ESX - Essex, LCS - Lincolnshire, BHS - Bedfordshire / Hertfordshire, SW - Region to the south west (L-shaped). Regions 3, 7, 8 and 13 make up the border. Regions 9, 12 and 14 divide the sea. NSC = Norfolk (10) + Suffolk (4) + Cambridgeshire (15). Total does not include border regions.

	CBG	**NFK**	**SFK**	**LDN**	**ESX**	**LCS**	**Sea Regions**		
	15	**10**	**4**	**11**	**5**	**6**	**2**	**14**	**12**
NAEI	26.5	38.9	24.1	51.2	24.5	17.6	0.1	0.3	0.1
Day	12.6	50.8	42.4	73.4	9.1	0.8	0.1	65.9	0.04
sd	*1.7*	*1.9*	*3.3*	*30.3*	*8.4*	*0.7*	*0.3*	*121.7*	*0.07*
Night	24.2	27.4	15.4	24.4	27.5	19.7	0.2	6.0	1.4
sd	*3.0*	*1.5*	*1.8*	*14.8*	*6.6*	*4.1*	*0.4*	*6.4*	*6.0*
	BHS	**SW**	**Border Regions**				**Total**	**NSC**	**Cost**
	9	**1**	**3**	**7**	**8**	**13**			**Score**
NAEI	20.5	75.0	1.6	29.9	0.1	55.2	369.4	89.6	-
Day	11.5	103.8	140.4	266.7	40.0	241.0	370.4	105.7	11.8
sd	*8.5*	*49.7*	*1.4*	*4.8*	*75.0*	*18.0*	*135.5*	*4.1*	*0.0*
Night	39.3	174.9	85.7	151.1	74.7	322.5	360.5	67.0	12.2
sd	*7.7*	*63.8*	*13.6*	*5.9*	*15.7*	*60.3*	*67.1*	*3.8*	*0.0*

5.10 Baseline formulation

In InTEM, a baseline must be calculated to represent the atmospheric methane concentration arriving at the edge of the inversion domain. There are many different approaches to formulating baselines but here a statistical technique is used. Hourly concentrations at each measurement site are divided into eight individual time series based upon wind direction origin. This is calculated using the NAME air history analysis. A rolling 18^{th} percentile spanning one week is used to create eight baselines. Tailored baselines for the measurement sites are then produced using the percentage contribution of each wind direction for every timestep (explained in more detail in Section 3.3.4). This section aims to demonstrate how this method was chosen for the final InTEM setup. These experiments used a slightly coarser solution grid of 64 boxes to reduce computational time. The remainder of the experimental setup was identical to the description at the beginning of this chapter.

Earlier analysis explored the possibility of individual baselines for all sites, where statistical filtering was used based solely on the measurement sites' concentration time series. These results were compared with a combined baseline and showed

very little differences. It was decided however, that this statistical filtering approach could filter out potential emissions from within the inversion domain. The individual baselines mostly overlap with each other, but during some periods of high methane they diverge. The baselines for all sites should only be different if they are experiencing wind coming from different directions. A simple filtering method does not take into consideration air origin at these times and therefore there are no means of confirming if these baseline differences arise from this or if they filter out potential sources from within the domain. Consequently, the chosen method was decided to create time-dependent baselines which represent the different domain edges. Individual baselines for each site could then be created based upon their air mass history contribution to each of the octiles for each time stamp. As this area of the UK can have different baselines depending on wind direction, the domain edges were split into octiles rather than quadriles to capture these differences.

The baseline method described here is a simpler version than is described in Ganesan et al. (2015), which uses a total of 21 so-called boundary conditions to derive time-dependent baselines for each of the measurement sites. These 21 boundary conditions use the NAME backward trajectories to consider the vertical and horizontal air origins, whereas the method described in this thesis only uses 8 boundary conditions which are only represent the surface origins of the NAME particles. Additionally, derived baselines described here use the observation site concentrations but in Ganesan et al. (2015) baselines are calculated using polynomial equations. One flaw of the method chosen for this thesis is the failure to represent the fraction of air coming from the 'upper-atmosphere', which at times could represent a significant fraction of the air's origin.

Figure 5.13 shows the InTEM results where different rolling percentiles are fitted through the eight different time series which represent air from each particular wind direction (the same percentile is used for each time series). If the inversion technique calculates that some measured methane has actually originated from outside the inversion domain (and has not been correctly filtered out in the baseline), then these emissions are placed in the boxes furthest away from the observation sites, i.e. the border boxes. This makes the border boxes (regions 3, 7, 8 and 13) inaccurate in their emissions and explains why all results place large emissions in the eastern border regions (regions 3 and 8) where very little methane would be expected. The border regions show a decrease in magnitude with increasingly elevated percentiles. It appears that regions in close proximity to the observations sites have more stable emission totals than those further

away. This leads to the encouraging conclusion that dramatically changing the baseline does not significantly change many of the regional totals. In addition to this, when analysing the highly resolved emission maps, all baseline experiments consistently show the same distribution of emissions. However, individual peak magnitudes of some regions do slightly reduce with an increasing baseline.

In InTEM, above-baseline excursions have been set to have a minimum value of zero as a way of avoiding negative emissions. Other authors, for example Ganesan et al. (2015), apply log-normal distributions (rather than Gaussian used in InTEM) to ensure no negative emissions can occur. The minimum zero value can be problematic if a baseline is set too high as it results in reducing peak sizes in the observed data and thus results in an under-estimation of emissions. This is seen in the results for the high baseline InTEM runs described above and shown in Figure 5.13.

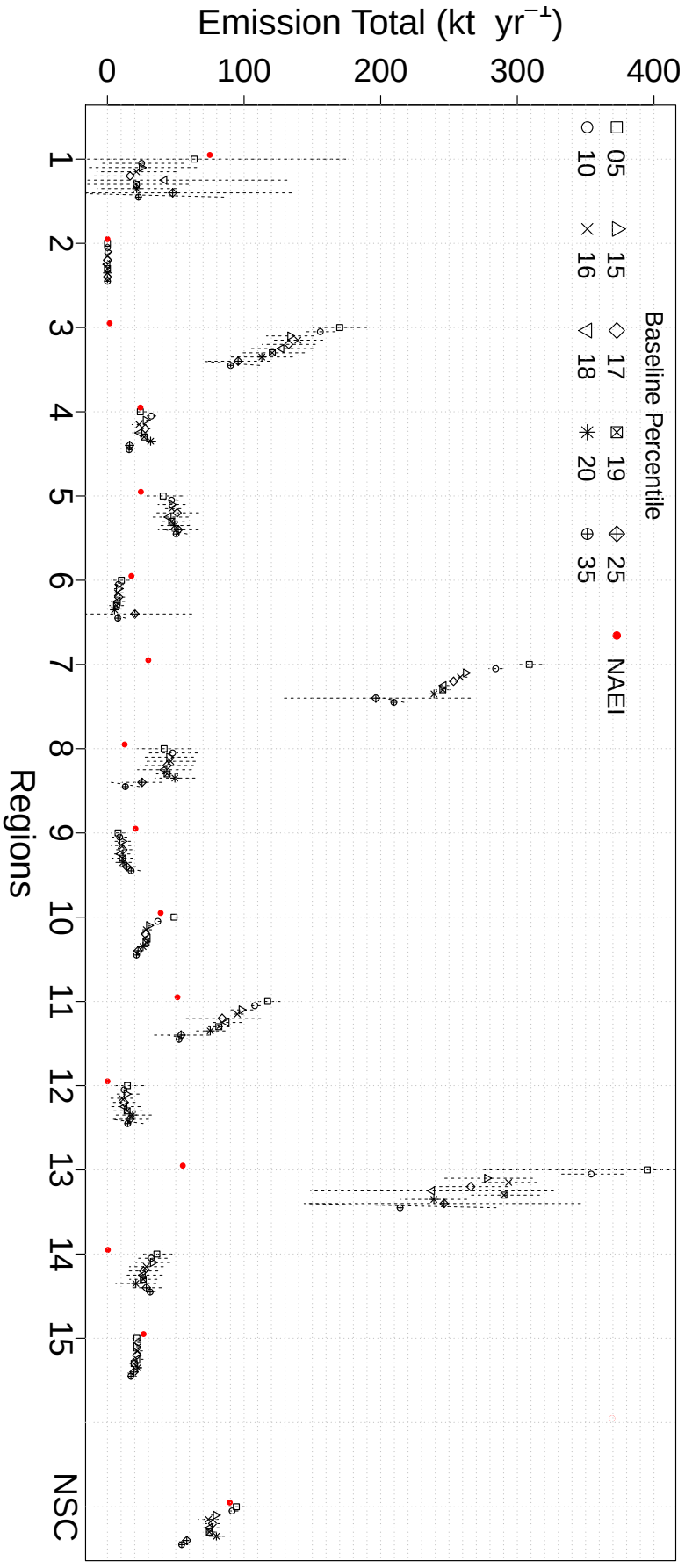

Figure 5.13: A summary of the InTEM region totals for the baseline experiments. The rolling baseline percentile used to filter the eight wind direction concentration time series are given in the inset legend. NAEI is shown as a red dot for reference. x-axis refers to the county region number in Figure 5.1. 1 = L-shaped region to the SW, 4 = Suffolk, 5 = Essex, 6 = Lincolnshire, 9 = Hertfordshire / Bedfordshire, 10 = Norfolk, 11 = Central London, 15 = Cambridgeshire. Regions 2, 12 and 14 make up the North Sea. Regions 3, 7, 8 and 13 make up the border regions. NSC = Norfolk (10) + Suffolk (4) + Cambridgeshire (15).

Figure 5.14 shows a plot of the cost scores for each percentile analysed. There is a minima at the 18th percentile, although the 17th overlaps when considering the standard deviation. An increasing score with an increasing baseline would be expected if the baseline is too high. In InTEM, the baseline is subtracted from the observational time series, defaulting at zero rather than becoming negative. If the baseline is prohibitively high then more periods of 'zero' methane will be present. This makes the observed time series incorrect and more difficult to re-create in the pseudo-observational time series. Similarly, if the baseline is too low, the inaccurate, high observations will become more difficult to model.

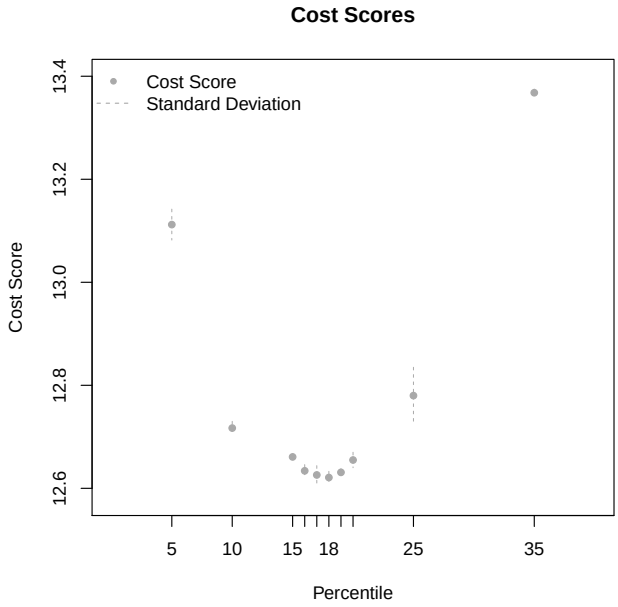

Figure 5.14: Baseline rolling percentile used to create baselines that are fed into InTEM vs. the resulting InTEM cost score. Standard deviations (dotted lines) are from each InTEM set up being repeated 25 times. The minimum cost score is found at the 18th percentile.

Figure 5.15 shows the ranges of the constructed baselines for Haddenham. There is a difference of 24 ppb from the lowest to the highest mean concentration of the different baseline percentiles. The highest percentile's (35) mean concentration is 43 ppb lower than the average methane observation at Haddenham (1969 ppb) over the two year dataset.

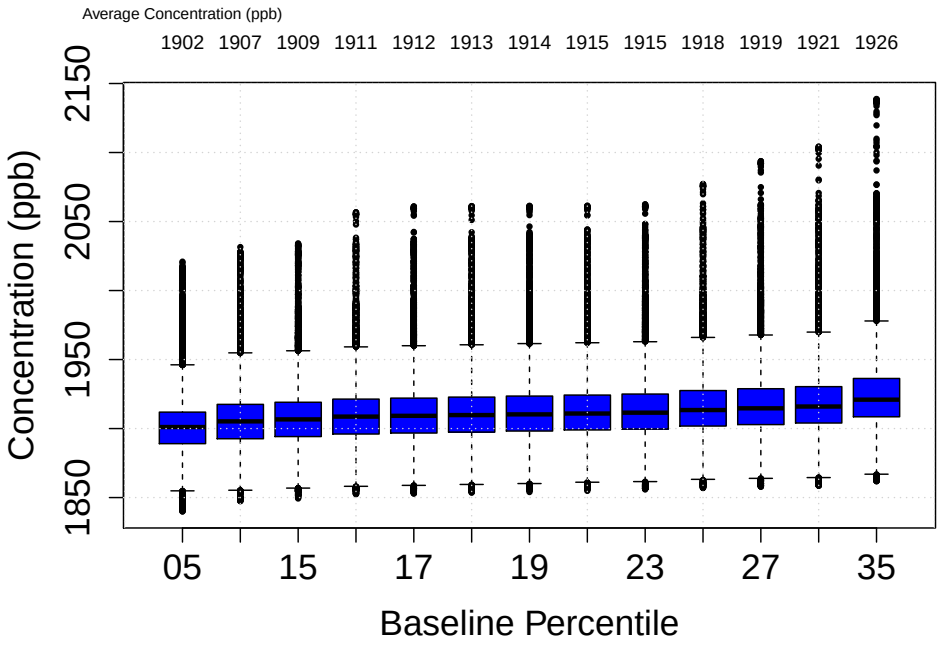

Figure 5.15: Boxplots of the baselines calculated for the Haddenham measurement. x-axis shows the rolling percentile used for baseline filtration. The mean is depicted as the bold horizontal line. The box limits show the 25^{th} and 75^{th} percentile with the whiskers delimiting 1.5x the interquartile range. Outliers are then shown as individual points. Average concentration (ppb) for each baseline is stated at the top of the plot.

5.11 Final setup and summary

This chapter aimed to address the sensitivity of the InTEM methodology. The accuracy of the InTEM method was successfully tested using pseudo-observations which had been constructed using the NAME dilution matrix and the 2012 NAEI. Several sensitivity experiments were then conducted to produce a final InTEM setup which can be trusted to produce consistent and reliable emission results. The posteriori of the final setup is assessed in Section 6.1.3.

The final setup includes the simulated annealing methodology to have 100 temperature steps and 20 000 internal iterations. InTEM is repeated 25 times to produce a representative range in emission variation which becomes stratified when the number of repeats are raised. The solution grid has a resolution of 150 grid boxes defined using the NAME air history maps and the NAEI as a prior to help locate point sources. This solution grid is derived from the county based regions. InTEM incorporates observation and modelling

uncertainty. Observation uncertainty is defined as the total of the hourly instrument precision, the calibration gas uncertainty and the standard deviations of the hourly concentrations. Model uncertainty has been set at a constant value of 5 ppb for every timestep. Finally, the baseline has been defined by splitting each measurement sites' time series into eight sectors based on wind direction origin. A rolling 18^{th} percentile spanning one week then filters these time series to to produce eight different baselines. An individual baseline for each site is then constructed using the percentage contribution of each wind direction per timestep (one hour).

The following chapter, and final result chapter in this thesis, uses this setup to create methane emission estimates for the East of England. InTEM is run for different time periods and uses varying number of measurement sites. This analysis aims to answer the main project aims, which were explained in Section 2.1.

6 East of England methane emission estimates

This chapter aims to answer the main goals of this project described in Section 2.1. The final InTEM setup described in Section 5.11 is run for a one year period (June 2013 - May 2014) and compared with the 2012 NAEI. Major similarities are highlighted and possible explanations for the differences are discussed. InTEM is then run at shorter time periods and seasonal emission estimates are assessed. Following this, the sensitivity of the emission results when fewer than four sites are used is analysed to understand the necessity of a multiple site network. InTEM emission estimates are then deduced and assessed for the year period from June 2012 to May 2013 and compared with the subsequent year. A two year inversion is also analysed and compared to the single year results. This chapter concludes with a sensitivity assessment of the Tacolneston site using the NAME model.

The results discussed in Section 6.1 and Section 6.3 use an InTEM setup which uses all four sites' methane measurements for an equal period of time (June 2013 - May 2014). This is purposefully devised to fairly assess the contribution of each site to the emissions described in Section 6.3 (Multiple site sensitivity analysis).

6.1 Resulting InTEM emission maps

This section explores the methane emission estimates calculated for the East of England using the InTEM setup described in Section 5.11. The one year period from June 2013 to May 2014 represents the longest duration that all four sites ran in parallel. Emission estimates shown in this section result from an InTEM setup derived from the various sensitivity tests conducted in the previous chapter. These results are the most justifiable to determine a proof of concept for the technique.

The one year (June 2013 to May 2014), four site methane emission map for the EA region is shown in Figure 6.1.A. The NAEI has been regridded from its 1

km resolution to the InTEM solution grid resolution (Section 5.5) and is shown in Figure 6.1.B. Striking similarities can be seen between the InTEM and NAEI results, although some major differences are also present. Both maps have totals within 15 % of each other (NAEI estimates 283 kt yr^{-1}, InTEM estimates 312 kt yr^{-1}). Similar area totals provide some reassurance that the InTEM inversion method can give realistically estimated values. Additionally, similarities between the spatial emission distributions can be seen, with both maps showing large emissions in the London area, point sources around Haddenham, and lower emissions along the southern EA coast.

Discrepancies appear between some of the magnitudes in the finely resolved emissions maps. The inversion method appears to produce a 'dipole effect' in some areas. For example, a large source is shown to the SSW of Tacolneston but low emissions are estimated in the surrounding area. The NAEI also shows an increased emission level SSW of Tacolneston, but the overall emission ranges are less extreme. Although it cannot be proved that these dipoles are not 'true' signals, they are mostly likely a product of InTEM's methods being unable to fully resolve emissions on this spatial scale (A. Manning - personal communication). Conversely, the NAEI's maximum emission value is greater than the InTEM results (19 058 ng s^{-1} m^{-2} compared to 59 928 ng s^{-1} m^{-2}). InTEM appears to create more diffuse emissions sources rather than produce precise point sources like the NAEI. This can be seen east of Tilney and north of Haddenham in Figure 6.1. Uncertainty in the modelled meteorology used to run NAME could account for InTEM being unable to pinpoint emission sources. In addition to this, during the nighttime, when a more stable boundary layer and lower wind speeds are observed, concentrations can build up and spread out horizontally making sources appear to be located over a larger area. This can result in the methane sources being incorrectly located. In these instances, local flows and local orography start to dominate the meteorological driving forces. These sub-scale influences are not fully captured in the UM's meteorology used within NAME. Thus, nighttime meteorology is thought to be more uncertain.

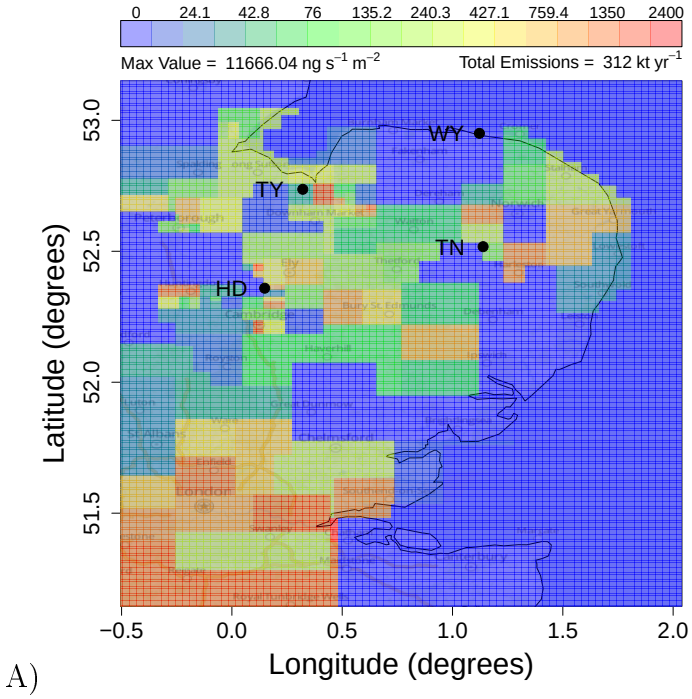

A)

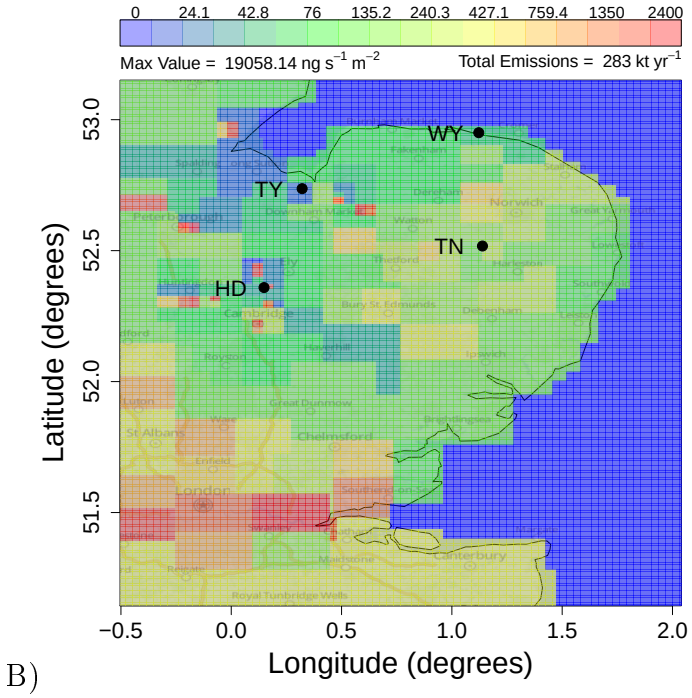

B)

Figure 6.1: A) InTEM four site, one year methane emission map from June 2013 to May 2014. B) 2012 NAEI regridded to the InTEM solution grid resolution. Sites are labelled for reference: HD = Haddenham, TN = Tacolneston, WY = Weybourne, TY = Tilney. NB: Logarithmic colour scale. Difference between orange / red is roughly a factor of 100 larger than the difference between blue / green.

6.1.1 Methane emission estimates surrounding Haddenham

Emissions in areas closely surrounding measurement sites are on a finer spatial resolution than areas further away. This is due to the methods used to calculate the InTEM solution grid resolution explained in Section 5.4. Figure 6.2 shows a magnified subsection of the emission maps in Figure 6.1, focusing on the Haddenham observation site. Two aspects should be noted from this figure. Firstly, all point sources in the NAEI (Figure 6.2.B) correspond to landfill, with the exception of the most southerly point source, which represents Cambridge. These sources also appear in the InTEM emission grid, although all emissions west of Haddenham are lower than the NAEI. InTEM also places far fewer emissions in the area between Huntingdon (labelled "1" in Figure 6.2) and Haddenham. Modelled meteorological uncertainty could explain the emission discrepancies as InTEM has placed a larger methane source further west. The two locations could be too close for InTEM to resolve these emission sources correctly. If the NAME meteorology is to be believed, the area of interest actually corresponds to 'historic' landfills which are no longer in use (Environment Environment Agency, 2015) and thus InTEM is assigning lower emissions from these unused landfills than the NAEI. It is difficult to determine which hypothesis is correct with the current inversion method but Figure 6.2 infers that the historic landfills west of Haddenham are emitting less than the NAEI estimates. Hegde et al. (2003) investigated methane emissions from a landfill in Taiwan. They observed that buried waste had a peak emission between two and three years and that emissions after five years were 0.63 % of the maximum values measured. The historic landfills to the west of Haddenham were decommissioned in late 1980s and early 1990s (Environment Environment Agency, 2015) and would be expected to be producing much less methane than when they were active.

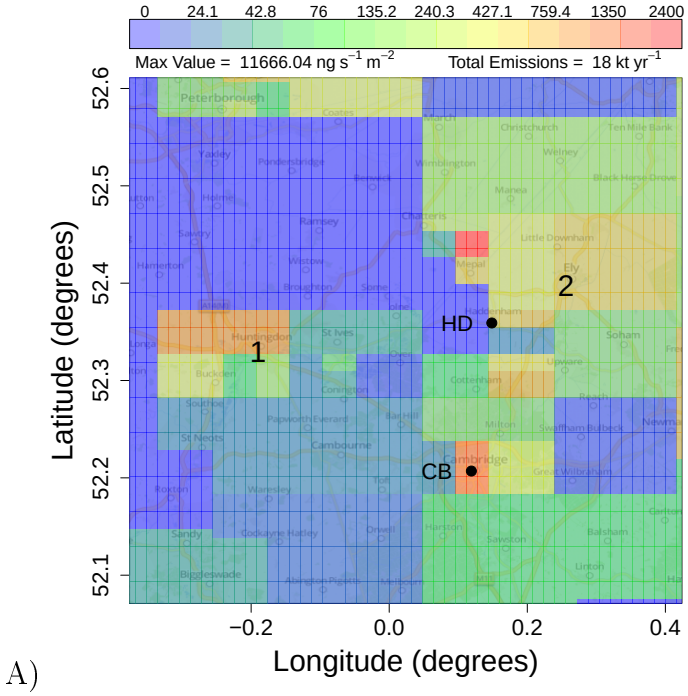

A)

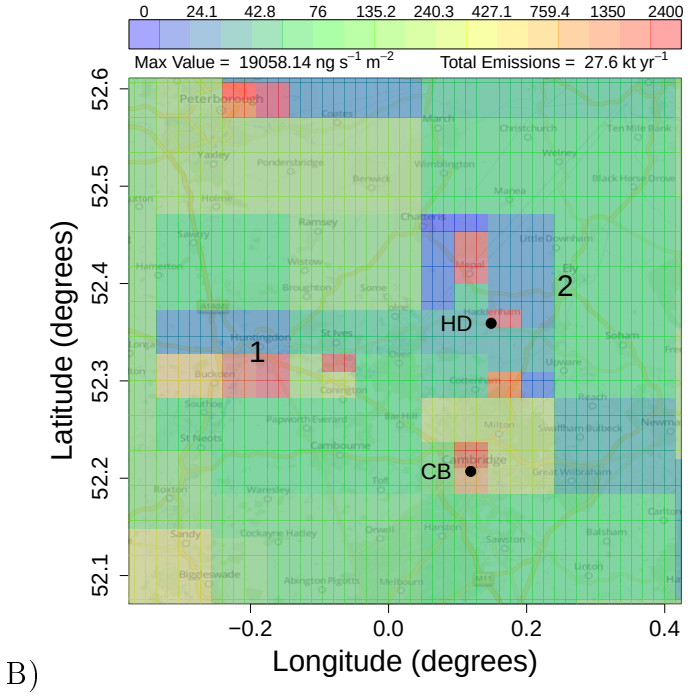

B)

Figure 6.2: A) InTEM four site, one year methane emission map from June 2013 to May 2014, magnified onto Cambridgeshire area. B) NAEI equivalent regridded to the InTEM solution grid resolution. Haddenham (HD) and Cambridge (CB) are labelled for reference. The area labelled "1" refers to Huntingdon which includes a large amount of active landfills. The area just east (high lighted as a methane point source in the NAEI - plot B) shows an area of 'historic' landfills. The area labelled "2" shows Ely. The surrounding area is made up of manufactured irrigation channels, where stagnant water can accumulate.

The second difference between the two emission maps is the area to the north east of Haddenham (labelled "2" in Figure 6.2). This wind sector, unlike the emissions to the west, has few other local methane sources. This area corresponds to fenland (including the 'Great Fen') with multiple irrigation channels structured throughout. Areas of near-stagnant water can potentially be large methane emitters (see Chapter 1 Section 1.4.1.1). It is thought that the NAEI does not include wetland emissions. The 'Nature' source sector (SNAP 11) is shown as a standard fixed emission factor throughout the UK, which makes up 0.1 % of total methane emissions (DEFRA, 2012). Smith and Butcher (English National Park 2010) report that the 'Nature' sector is comprised of five sources of wildfires and that the current "state of research into LULUCF (Land Use, Land Use Change and Forestry) emissions and removals for methane and nitrous oxide is not well enough advanced for estimates to be included in the UK's international submission of greenhouse gases". The signal shown here is more likely to be 'real' signal, providing evidence toward to incorporation of wetland representation within the NAEI. Further local analysis, including measurements, of this area would help to confirm this finding.

6.1.2 Spatially coarse methane emission estimates for the East of England

The large uncertainties associated with the fine emission maps allows for differences between the NAEI and InTEM to be identified but the emission magnitudes are less reliable. Aggregating the InTEM emission maps to a coarser spatial resolution can reduce the modelling uncertainty. InTEM is still solved on the finer solution-grid spatial resolution but the individual emissions are aggregated to the coarser county-regional resolution. This produces a less spatially resolved map but more confidence can be placed in the emission values. Figure 6.3 and Table 6.1 show the corresponding emission results aggregated into regions based on the UK counties (Figure 5.1). The aggregated emission maps show strikingly similar InTEM and NAEI region totals in the counties located close to the observation sites. Table 6.1 shows that regions 4, 10, 15 (Suffolk, Norfolk and Cambridgeshire) are within one standard deviation of NAEI values. InTEM and NAEI regional estimates become less similar as the distance from the observation site increases. InTEM also seems to be unable to resolve the Greater London area, this is shown with larger standard deviations for the corresponding regions (1, 11). This implies that observation sites have a particular footprint of

no more than a ~50 km radius. The sites' footprints are discussed in more detail in Section 6.3.

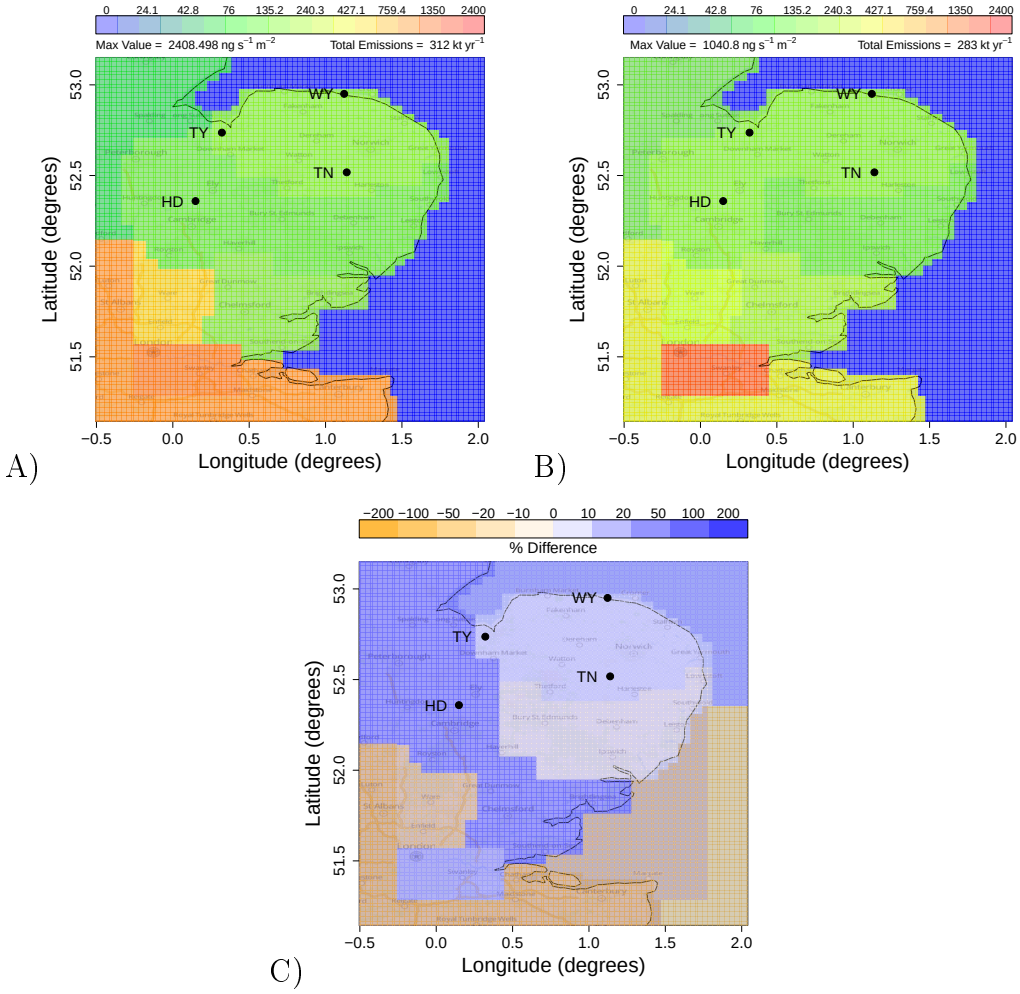

Figure 6.3: Regridded InTEM methane emission maps (Figure 6.1) to coarse regional estimates based upon the UK county boundaries. A) InTEM emission estimates B) NAEI emission estimates C) Percentage difference of B-A. All emissions in units of kt yr^{-1}. Border regions have been removed from this figure but their totals can be found in Table 6.1. HD = Haddenham, TN = Tacolneston, WY = Weybourne, TY = Tilney.

Table 6.1: Regional emission totals (kt yr^{-1}) comparing InTEM four site, one year inversion results to the NAEI. One standard deviation (sd) is shown below regional estimates. Regional percentage differences using NAEI as a base are shown below the sd values. [a]Percentage differences using emissions not rounded to one decimal place. [b]Total is the sum of all regions except the four border regions (3, 7, 8, 13). Region label abbreviations: CBG - Cambridge, SFL - Suffolk, NFK - Norfolk, LDN - London, ESX - Essex, LCS - Lincolnshire, BHS - Bedfordshire / Hertfordshire, SW - Region to the south west (L-shaped). Regions 9, 12 and 14 divide the sea. NSC = Norfolk (10) + Suffolk (4) + Cambridgeshire (15).

	CBG	**NFK**	**SFK**	**LDN**	**ESX**	**LCS**	**Sea Regions**		
	15	**10**	**4**	**11**	**5**	**6**	**2**	**12**	**14**
NAEI	26.5	38.9	24.1	51.2	24.5	17.6	0.0	0.1	0.3
InTEM	20.5	37.1	22.8	45.7	19.6	9.1	0.2	0.1	0.4
sd	*2.1*	*1.7*	*1.9*	*18.0*	*8.1*	*4.1*	*0.6*	*0.1*	*1.2*
% difference	22.5	4.7	5.6	10.8	19.9	48.3	-1808.8[a]	14.0[a]	-23.7
	BHS	**SW**	**Border Regions**				**Total[b]**	**NSC**	**Cost**
	9	**1**	**3**	**7**	**8**	**13**			**Score**
NAEI	20.5	75.0	1.6	29.9	0.1	55.2	369.4	89.6	**-**
InTEM	30.6	124.5	116.1	240.0	53.6	294.9	310.5	80.4	12.5
sd	*7.3*	*59.2*	*1.0*	*7.1*	*16.1*	*43.1*	*63.0*	*3.3*	*0.0*
% difference	-49.1	-66.1	-7153.8	-702.1	-325.0	-434.5	-11.4	10.2	

The percentage difference between the NAEI and the InTEM emission estimates are shown in Table 6.1. Border estimates should be discounted due to the baseline issues described in Section 5.10. Sea regions also have a high percentage difference due to their relatively small totals. Norfolk and Suffolk have low percentages whereas InTEM's estimate for Cambridgeshire is 22.5 % lower than the NAEI estimate (14.6 - 30.6 % when *sd* is included). Percentage differences for regions that are further away from the measurement sites range from 10.8 % (region 11, LDN) to 66.1 % (region 1, SW). All land regional estimates are within a factor of two of each other.

6.1.3 InTEM pseudo-observations

Section 4.4 describes how InTEM produced a modelled time series of methane concentration using a dilution matrix and an emission field. This emission field can be synthesised by InTEM or it can be a previously defined set of emissions, i.e. the 2012 NAEI. Figure 4.19 in Chapter 4 shows that when the 2012 NAEI is used to create these pseudo-observations their temporal variability

fits the observed methane concentrations relatively well. The magnitudes were less similar, with the observed concentrations normally exceeding the modelled observations (especially at the Haddenham and Tilney sites). Figure 4.19 also supported that the previous 2009 NAEI's pseudo-observations were less accurate than the 2012 NAEI. This was due to a major reassessment of the methane sources' emission factors in between these inventory years (DEFRA, 2015).

Figure 6.4 shows the measured and pseudo-observations for all four sites between 01 July 2013 and 10 July 2013. The 2012 NAEI pseudo-observations have also been added. Please note that these modelled concentrations differ slightly from the ones shown in Section 4.4 as the emissions used for calculating these values were on the InTEM solution grid resolution (i.e. 150 boxes of varying sizes - Figure 3.8.C). Regridding the emissions fields will change the resulting pseudo-observations. The pseudo-observations shown in Section 4.4 were calculated using the 1.5 km regular grid resolution NAEI.

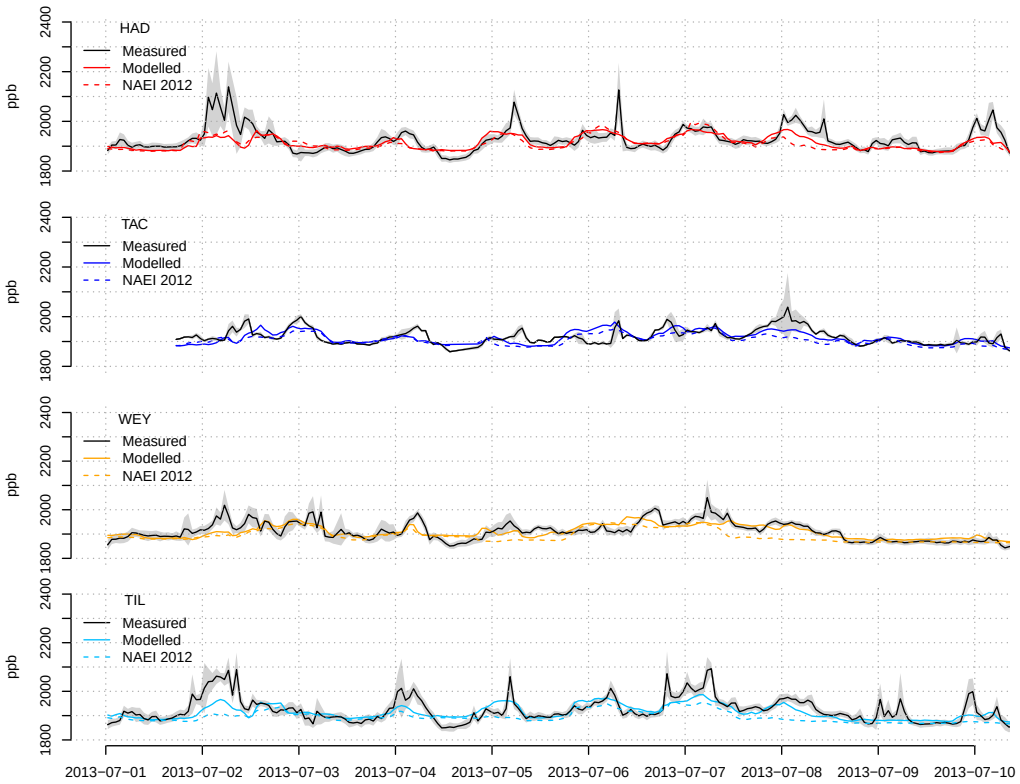

Figure 6.4: Time series of measured and pseudo- methane concentrations for all four observations sites between 01 July 2013 and 10 July 2013. Pseudo-observations based on the InTEM emissions field shown in Figure 6.1.A and the 2012 NAEI. Pseudo-observations created from emission fields regridded to the 150 box solution grid resolution to allow for a direct comparison.

Figure 6.4 highlights the similarities and differences between the measured

concentrations and the InTEM and NAEI pseudo-observations. A large fraction of the a posteriori observations outside of the uncertainty range of the measured observations. This implies that either the prescribed uncertainties are not substantial enough or that the resulting emission field should be more resolved. One reason for this could be the compromised spatial resolution of the emission grid being too coarse to fully capture the peaks and troughs of the measured timeseries. It should be noted that the NAEI is also substantially outside the shown uncertainty ranges.

Like the NAEI, InTEM's selected emission field also does not replicate the high concentrations observed at Haddenham and Tilney. Additionally, Figure 6.4 shows where the InTEM and the NAEI pseudo-observations differ, for example, during 02 July 2013 in Tilney and 08 July 2013 in all sites. Possible explanations for these differences are explored using the NAME air history maps. During 02 July 2013 air appears to stagnate during the evening, allowing local sources to build up. This period could imply that if NAME is not modelling nighttime dispersion correctly then the InTEM emissions field could be overestimating the emission that corresponds to this peak. This is difficult to decipher without knowing the methane sources this peak corresponds to.

NAME air history maps show the wind coming from the east during 08 July 2013 with concentrations reducing once the wind direction changes towards the south (after 15:00 08 July 2013). This implies this period of elevated methane originates from European sources and has not been filtered out in the baseline. Both pseudo-observation datasets have the same baseline described in Section 5.10. The NAEI includes no emissions from Europe and thus would not be able to recreate this peak in its pseudo-observations. In contrast, InTEM uses the outer border regions to allow for uncertainties in baseline filtration, and thus uses these 'excess' emissions to replicate the measured observations. Although this period shows the NAEI and InTEM pseudo-observations diverging, it will correspond to small differences within the central inversion domain. A suggestion for future experiments would be to recreate pseudo-observations using different emission inventories, for example, the EDGAR methane emissions inventory is available at 0.1 x 0.1 degree resolution over all of Europe. Additionally, pseudo-observations created from the NAEI nested within the EDGAR inventory could be directly compared to the modelled and measured observations experiment described above.

Table 6.2: Cost scores comparing the measured concentrations with the resulting InTEM emission field shown in Figure 6.1.A and the two NAEI inventory years (2012 and 2009). All emission fields are on the InTEM solution grid resolution of 150 grid boxes.

Emissions Field	Cost Score
InTEM	12.53
NAEI 2012	14.90
NAEI 2009	15.81

The InTEM emissions field has a lower cost score than the NAEI, which is shown in Table 6.2. The 2009 NAEI is higher than both the InTEM and the 2012 NAEI emission fields. This analysis shows the methane emission map produced by InTEM fits the measured observations better than the 2012 NAEI. Both datasets fit better than the 2009 NAEI. These cost scores are dependent on the uncertainties assigned to each timestep. If these were to change, for example, an incorporation of a time dependent modelled meteorology, then this would effect the resulting costs scores and potentially change this result. That being said, this final setup, with current assumptions on uncertainty indicates that the InTEM emissions field is more realistic than the 2012 and 2009 NAEIs. Although, this doesn't completely guarantee that the solution is better due to the associated, and uncharacterised, modelling errors.

6.2 Seasonal inversions

The NAEI is limited by being produced to represent one specific year. InTEM has a greater flexibility and can be run for any time period. This section describes the analysis of seasonal inversions using all four measurement sites to assess if robust sub-annual information can be determined. The 2013-2014 dataset was split into four seasonal subsets (Summer: JJA, Autumn: SON, Winter: DJF, Spring: MAM) and the same inversion method was applied. Figure 6.5 shows the seasonal fine spatial resolution emission maps. The coarse, county scaled emission maps and region totals can be seen in Figure 6.6 and Table 6.3.

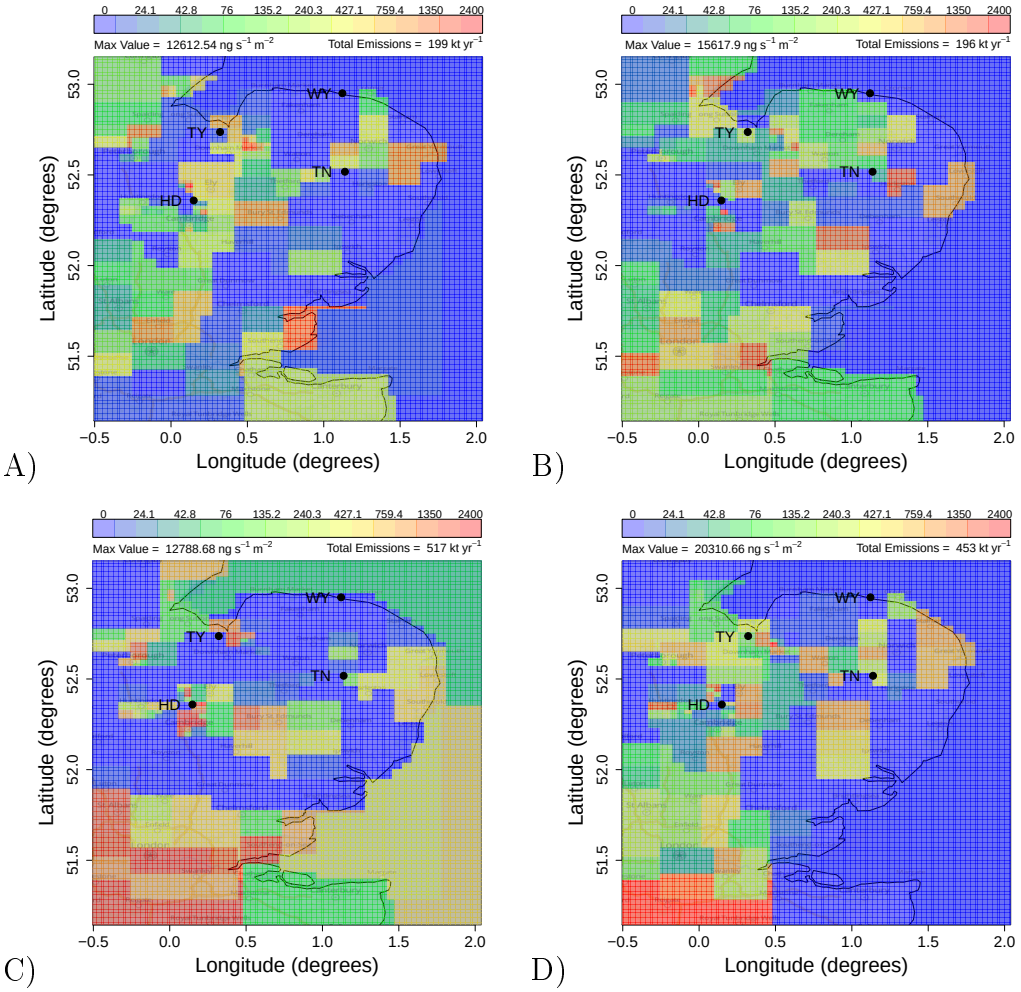

Figure 6.5: Seasonal InTEM methane emission maps on the InTEM solution grid spatial resolution. A) Summer: JJA 2013 B) Autumn: SON 2013 C) Winter: DJF 2013-2014 D) Spring: MAM 2014. HD = Haddenham, TN = Tacolneston, WY = Weybourne, TY = Tilney.

The fine spatial resolution maps are more qualitative than quantitative, although interesting signals can still be identified. Emission totals are higher during winter and spring than summer and autumn, which is predominantly due to the London area (regions 1 and 11). Emissions appear to decrease during the winter months in the fenland area to the north east of Haddenham. Similarly, emissions over the fenlands and the Norfolk Broads (east of Tacolneston) dominate these emissions in summertime. The winter map shows more point source emissions of methane from city locations (Cambridge, Norwich etc). The winter map also places significant emissions over the sea and is the only season to do so. Figure 4.12 previously showed that over 75 % of the wind came from the south or south west during the winter of 2013-2014. The devised layout of the four measurement sites (square

shape rather than linear) ensures surface influence information can be obtained for the EA area whichever direction the wind blows. If there is very little change in wind direction however, the domain edges situated upwind (i.e. in the north and east), will have relatively little data to constrain the estimated emissions from InTEM. This could be a reason why only this season places emissions over the sea, to the east and south east of the inversion domain. This theory gives further evidence to believe estimates nearer to the measurement sites are more robust than areas further away. The county totals should be used to infer a more quantitative assessment of seasonal variations.

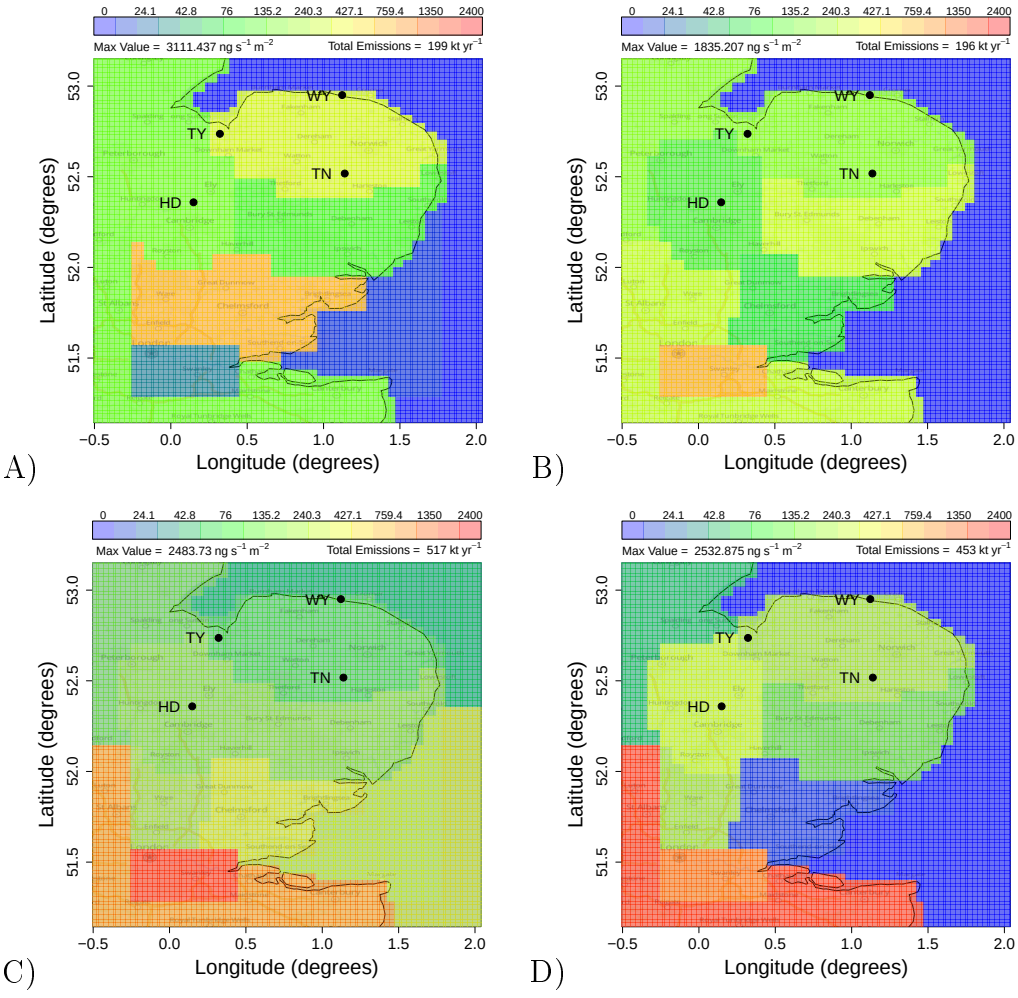

Figure 6.6: Seasonal InTEM methane emission maps on county scaled spatial resolution. A) Summer: JJA 2013 B) Autumn: SON 2013 C) Winter: DJF 2013-2014 D) Spring: MAM 2014. HD = Haddenham, TN = Tacolneston, WY = Weybourne, TY = Tilney.

Norfolk, Suffolk and Cambridgeshire (NSC, counties closest to the measurement sites) see a seasonal cycle with a summer maxima and a winter minima. This

cycle is dominated by the Norfolk region. The London region, which is less constrained due to its distance from the measurement sites, still shows a distinct cycle. This, in contrast to the NSC region, has a clear maxima in the winter and spring periods. The summer estimates for the London and 'SW' region are too low to be a reasonable estimate. The southern regions (1, 5, 9, 11) have been summed together and are shown in Table 6.3. These show a similar seasonal cycle compared to London, with larger emissions in the winter and spring months than the summer and autumn.

Table 6.3: NAEI and InTEM seasonal regional emission totals (kt yr^{-1}). (Summer: JJA 2013, Autumn: SON 2013, Winter: DJF 2013-2014, Spring: MAM 2014). Region label abbreviations: CBG - Cambridge, SFL - Suffolk, NFK - Norfolk, LDN - London, ESX - Essex, LCS - Lincolnshire, BHS - Bedfordshire / Hertfordshire, SW - Region to the south west (L-shaped). Regions 3, 7, 8 and 13 make up the border. Regions 9, 12 and 14 divide the sea. NSC = Norfolk (10) + Suffolk (4) + Cambridgeshire (15). The regions making up the south of the domain (1, 5, 9, 11) have also been grouped together. Total does not include border regions.

	CBG	**NFK**	**SFK**	**LDN**	**ESX**	**LCS**	**Sea Regions**		
	15	**10**	**4**	**11**	**5**	**6**	**2**	**12**	**14**
NAEI	26.5	38.9	24.1	51.2	24.5	17.6	0.1	0.1	0.3
Summer	20.1	51.0	23.4	1.8	43.3	15.8	0.1	0.5	1.6
sd	*3.4*	*1.2*	*3.3*	*3.2*	*11.8*	*4.2*	*0.1*	*0.6*	*2.1*
Autumn	14.3	31.7	37.3	24.1	9.7	19.2	0.2	0.0	0.1
sd	*2.5*	*2.0*	*6.2*	*12.6*	*8.1*	*11.0*	*0.3*	*0.0*	*0.1*
Winter	25.3	21.3	23.9	88.2	49.4	14.8	42.0	9.7	49.5
sd	*3.9*	*4.7*	*7.3*	*27.8*	*11.9*	*5.3*	*27.8*	*8.3*	*9.3*
Spring	41.3	43.1	25.3	64.6	2.2	6.5	0.1	0.0	0.1
sd	*3.5*	*1.3*	*2.0*	*34.3*	*2.0*	*3.3*	*0.1*	*0.1*	*0.2*

	BHS	**SW**	**Border Regions**				**Total**	**NSC**	**South**	**Cost**
	9	**1**	**3**	**7**	**8**	**13**			**region**	**Score**
NAEI	20.5	75.0	1.6	29.9	0.1	55.2	369.4	89.6	171.2	-
Summer	23.3	24.9	95.3	310.1	0.4	276.4	205.8	94.5	93.3	10.8
sd	*9.1*	*46.7*	*1.5*	*7.7*	*0.5*	*46.4*	*49.5*	*4.9*	49.1	*0.0*
Autumn	13.6	43.0	174.7	182.9	147.9	138.3	193.2	83.4	90.3	12.7
sd	*9.8*	*24.8*	*3.4*	*20.6*	*7.6*	*31.0*	*33.2*	*7.0*	90.6	*0.0*
Winter	13.2	172.1	32.0	247.5	26.6	61.3	509.3	70.5	322.9	9.2
sd	*8.7*	*41.7*	*18.9*	*12.4*	*35.1*	*43.0*	*61.5*	*9.5*	52.3	*0.0*
Spring	14.5	257.8	112.9	228.8	48.2	420.0	455.4	109.6	339.1	14.0
sd	*4.9*	*78.3*	*1.7*	*7.6*	*3.7*	*40.0*	*85.9*	*4.3*	85.7	*0.0*

A possible explanation for these cycles could be the dominating source sectors in each county. The different methane source sectors' contribution to the regions stated above (NSC, London and 'southern' region) can be seen in Figure 6.7. All

pie charts in Figure 6.7 have a large contribution from the waste sector. The bacteria found in landfill of which make up most of the waste emissions, have a positive correlation with temperature (Reay et al., 2010 and Einola et al., 2007). However, an increase in temperature results in an overall decrease in landfill emissions, as more methane-oxidation reactions occur from methanotropic bacteria at higher temperatures (Maurice and Lagerkvist, 2004; Scheutz and Kjeldsen, 2004). In addition to this, London has a larger contribution from the 'offshore' sector, which includes all expected leakages from natural gas pipelines. An increased demand during winter months would see this source sector rise (Wilson et al., 2013). This is assuming there is a link between demand and emissions. These reasons support the London seasonal cycle. The cycle observed in the NSC region is less obviously attributable than the London seasonal cycle. The NSC region has a larger contribution from the agricultural sector but this sector does not have a clear trend in seasonal emissions.

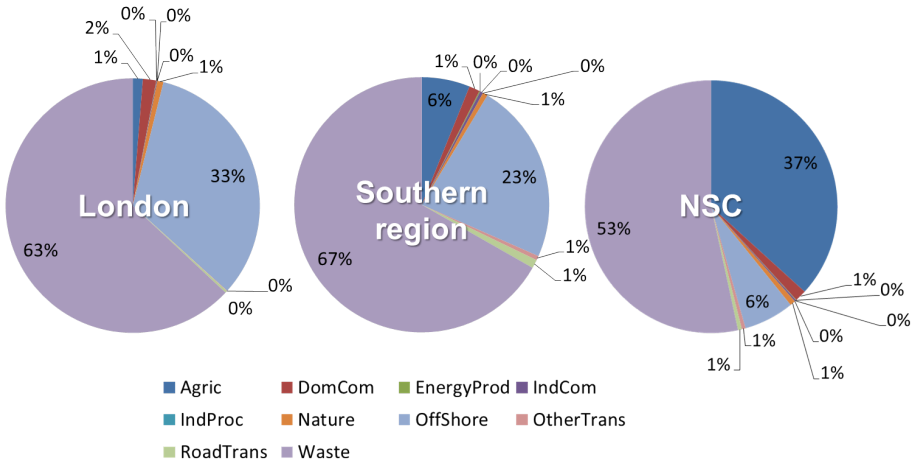

Figure 6.7: Percentage contributions of the methane source sectors for London, the 'Southern Region' and NSC (Norfolk, Suffolk, Cambridgeshire). Source sector data from the 2012 NAEI. Created using the NAME air history maps for a two year duration (July 2012 - June 2014).

6.2.1 Estimation of uncertainty

Throughout this section, uncertainty has been estimated as one standard deviation (1sd) of the emissions from 25 InTEM repeats. This was justified in Section 5.3 which shows regional emission totals and their corresponding standard deviations stabilise when InTEM is repeated a minimum of 25 times. A limitation with the chosen InTEM setup is that no specific uncertainty metric is produced

as a result. Other cost functions, for example, a Bayesian cost function is able to produce this (Section 7.2.2). The results in this chapter imply that 1sd is too conservative to represent uncertainty for the regional estimates. This is highlighted in the seasonal emission results. Seasonal uncertainties would be higher than the annual estimates due to the smaller dataset used to restrict the inversion but these estimates are only slightly higher. This implies that the seasonal variation may be less prominent than is displayed in Table 6.3. The London seasonal cycle however, is large enough to be considered a signal despite the distance from the measurement sites, although absolute values remain too uncertain.

6.3 Multiple site sensitivity analysis

One of the main aims of this project was to investigate the sensitivity of using multiple sites within InTEM on the emission estimates (as described in Section 2.1). The significance and the necessity of using more than one site is valuable information which can be used when future experiments are planned.

For this investigation, InTEM was repeatedly run for the one year 2013-2014 duration using all combinations of 1 - 3 site's measurements. Figure 6.8 shows the single site emission maps regridded to the coarse, county-scale regions. The corresponding region totals are shown in Table 6.4. Each map (Figure 6.8) shows a local 'footprint' experienced by the individual site. The single site inversions suggest the emission estimates are close to the NAEI for the county each site is situated in, or the nearby county which is upwind of the prevailing wind direction.

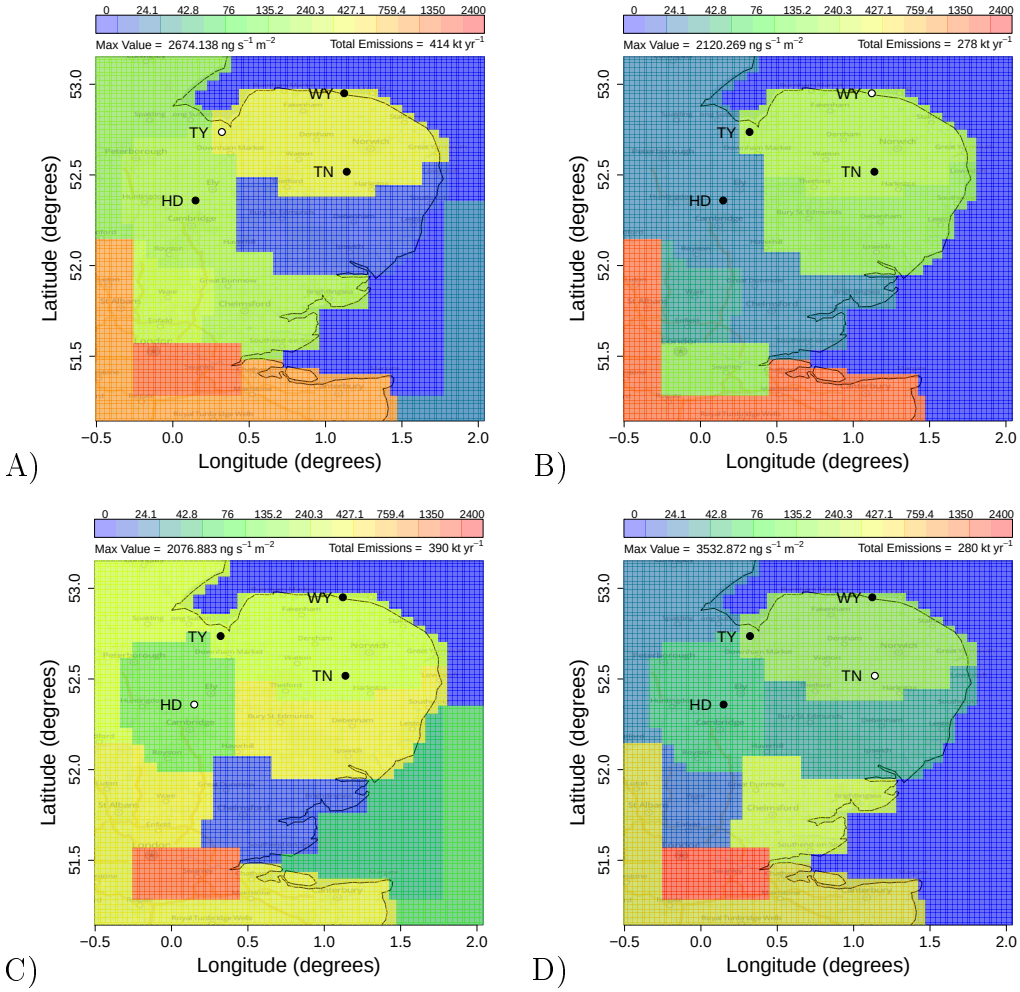

Figure 6.8: InTEM emission maps using single site observation data in the inversion setup for the one year period throughout June 2013 - May 2014. A) Tilney, B) Weybourne, C) Haddenham, D) Tacolneston. Regridded to the county scale regions. Site labelled for reference: HD = Haddenham, TN = Tacolneston, WY = Weybourne, TY = Tilney. Individual sites used within the InTEM setup is coloured white.

Table 6.4 shows the Weybourne and Tacolneston inversion estimates for Norfolk are within 10-15 % of the NAEI emission total. Surprisingly, Haddenham produces slightly lower estimates for Cambridgeshire compared to the NAEI, despite this site having large local point sources (Haddenham measured a higher distribution of methane concentrations compared to the other three sites). Instead, InTEM places higher emissions in the neighbouring counties, producing an overall estimate for the East Anglia region which is higher than the NAEI. Tilney estimates higher emissions for Norfolk than the NAEI (its occupying county) although this could due to its location being in the far western border of the county. Tilney produces an estimate for region 6 (Lincolnshire) which is similar to the NAEI equivalent. This region is directly upwind of

Tilney's prevailing wind direction and would have more information about surface influence calculated by NAME. This analysis suggests each single site inversion produces more reliable estimates for a specific 'footprint' region. These results suggest that future experiments should consider the size of the area of interest when deciding the appropriate number of measurement sites to be included.

Table 6.4: InTEM county emission totals (kt yr^{-1}) using single site observation data in the inversion setup. Counties where the measurement sites are close to or located within are highlighted in **bold**. Region label abbreviations: CBG - Cambridge, SFL - Suffolk, NFK - Norfolk, LDN - London, ESX - Essex, LCS - Lincolnshire, BHS - Bedfordshire / Hertfordshire, SW - Region to the south west (L-shaped). Regions 3, 7, 8 and 13 make up the border. Regions 9, 12 and 14 divide the sea. NSC = Norfolk (10) + Suffolk (4) + Cambridgeshire (15). Total does not include border regions.

	CBG	**NFK**	**SFK**	**LDN**	**ESX**	**LCS**	**Sea Regions**		
	15	**10**	**4**	**11**	**5**	**6**	**2**	**12**	**14**
NAEI	26.5	38.9	24.1	51.2	24.5	17.6	0.1	0.1	0.3
HD	**20.4**	66.9	87.8	51.3	2.2	45.1	11.3	0.2	8.4
sd	***2.7***	*3.5*	*5.1*	*23.0*	*2.2*	*4.2*	*20.4*	*0.6*	*8.4*
TN	7.0	**34.2**	6.6	85.0	41.8	3.9	26.4	1.2	43.5
sd	*4.1*	***2.9***	*1.7*	*29.8*	*13.9*	*3.1*	*45.0*	*4.5*	*80.9*
WY	4.8	**44.4**	44.4	11.20	4.3	3.7	0.3	0.6	0.6
sd	*5.6*	***5.4***	*6.5*	*12.9*	*9.8*	*9.4*	*1.1*	*3.1*	*2.5*
TY	**30.6**	91.6	2.8	58.2	28.8	**24.9**	3.1	0.2	0.2
sd	***2.6***	*6.8*	*2.8*	*26.3*	*19.8*	***17.0***	*5.0*	*0.3*	*0.3*
	BHS	**SW**	**Border Regions**				**Total**	**NSC**	**Cost**
	9	**1**	**3**	**7**	**8**	**13**			**Score**
NAEI	20.5	75.0	1.6	29.9	0.1	55.2	369.4	89.6	-
HD	29.2	77.6	181.3	207.0	70.9	253.2	400.5	175.1	7.5
sd	*6.4*	*48.6*	*5.8*	*5.0*	*27.5*	*42.0*	*59.1*	*6.8*	*0.0*
TN	1.3	99.6	182.0	352.0	110.9	500.0	350.6	47.9	20.3
sd	*2.2*	*62.2*	*13.2*	*7.3*	*4.1*	*70.0*	*116.5*	*5.3*	*0.0*
WY	3.0	173.9	94.6	211.3	9.2	398.6	291.3	93.7	12.0
sd	*6.2*	*92.7*	*8.8*	*28.8*	*6.7*	*85.7*	*95.4*	*10.1*	*0.0*
TY	19.3	154.8	24.1	266.4	31.8	130.6	414.4	125.0	7.8
sd	*6.6*	*77.4*	*2.7*	*28.4*	*20.2*	*91.4*	*86.5*	*7.8*	*0.0*

Figure 6.9 displays the regional totals for Norfolk, Suffolk and Cambridgeshire for all multiple site inversion runs. Only these three regions were used as previous analysis implied an increased confidence in these county estimates (Section 6.1). Figure 6.9 shows the added benefit of increasing the number of measurement sites to produce more concrete estimates of regional emissions. The x-axis indicates the number of observation sites used in an individual inversion run. The site(s) used in a particular inversion can be identified from the colour coding in the plot.

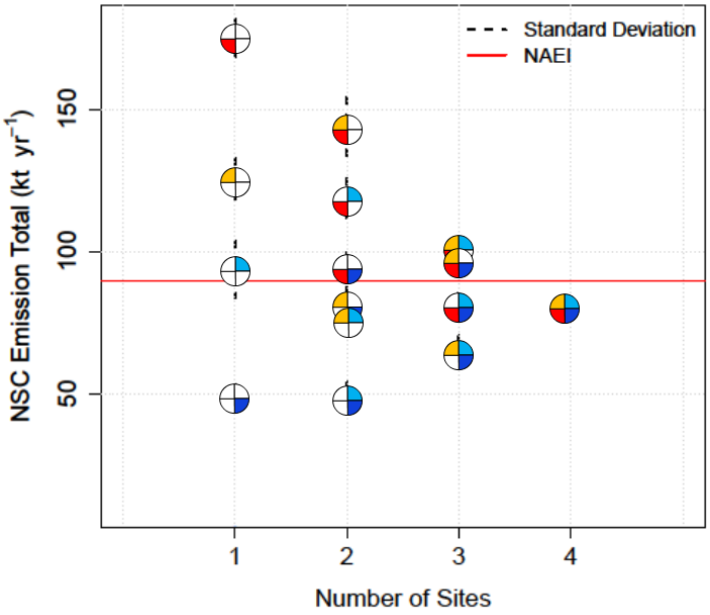

Figure 6.9: Multiple site InTEM emission totals (kt yr^{-1}) for the NSC region. x-axis shows number of observation sites used in each inversion run. The colours for Haddenham, Tacolneston, Weybourne and Tilney are red, dark blue, light blue and orange, respectively (similarly within Chapter 4). The position of the colour quarters within the circles refers to the site locations within the EA domain (Figure 2.1).

The sites which experience the lowest range of methane concentrations produce lower emission maps for the region. Similarly, sites with local point sources produce higher regional emissions maps. Figure 6.8 shows that single site inversions are able to produce emissions similar to the NAEI for their corresponding county, but emission estimates for the EA region seem to reflect the individual site's observations, i.e. sites which on average measure higher methane concentrations also produce higher EA emission estimates. The range within the NSC emissions in Figure 6.9 is reduced when multiple sites are incorporated within the inversion. Local biases are diminished but not removed entirely. Inversions using two or three sites show the incorporation of Haddenham always produces higher estimates within the resulting range of emissions. Similarly, Tacolneston always produces lower estimates of the emissions range. These results strengthen the argument for incorporating multiple sites within inversion analysis.

It also appears that the number of sites needed depends on the size of the desired domain. From Figure 6.9, several two or three site inversions produce results close to the NAEI and the four site inversion, but on the more local scale these emissions can still vary. Table 6.5 shows the individual county totals of the two or

three site inversions which produce similar NSC totals to the four site inversion. This table shows that, although the region is being well estimated, all three individual county totals still vary in their emission ranges. This is surprising as the single site inversion analysis showed local emissions can be reproduced well. It also seems that Cambridgeshire is more often underestimated (even in the four site inversion) whereas Norfolk and Suffolk are both under- and overestimated depending on the combination of sites used. Section 6.2 suggested that the NAEI is not representing methane wetland emissions within its 'Nature' source sector, for example, from the fenland north-east of Cambridge. Assuming that all other methane emissions within Cambridgeshire are accurate, this suggests InTEM should produce higher estimates than the NAEI. InTEM analysis has consistently produced lower estimates for this region within the multiple site analysis. This suggests the NAEI is failing to represent Cambridgeshire emissions correctly. This is assuming that NAEI values are absolute, whereas in reality there would be a reasonably large uncertainty associated with this region. It is difficult to ascertain the reason for this discrepancy at this spatial resolution.

Inversions using multiple sites produce regional emission totals (for the three EA counties) that seem to reflect a 'compromise' between the relative concentration ranges measured at each individual site. For example, the two site inversions which accurately recreate the NAEI NSC totals always have a combination of two sites which experience 'low' and 'high' methane variations, i.e. Haddenham and Tacolneston, or Tilney and Weybourne. Incorporating one 'high' site with another 'low' site produces an averaged emission estimate for the region. The addition of another 'low' or 'high' site adds biases again to the estimates. However, the overall range is still more constrained than the corresponding range of all two site inversions. If another site was added to produce a five-site inversion this would shift the region's estimates again. The resulting estimate range from the four site inversions combinations would be expected to be lower than the three site ranges. This analysis has shown there is a delicate balance between biases in the observational sites and the resolution / size of the domain of interest. In reality, InTEM can be run using only two sites and produce regional emission estimates for EA which are similar to the NAEI, but these sites must be carefully chosen so that they complement each other. For a detailed or local emission estimate more sites are required. Future site selection should involve identifying potential site biases, so they can be incorporated into the inversion process without hindering the setup.

Table 6.5: NSC regional emission totals and standard deviations for two and three site inversions. All values are in kt yr^{-1}. HD = Haddenham, TN = Tacolneston WY = Weybourne TY = Tilney.

	Suffolk	Norfolk	Cambridgeshire	Total
NAEI	24.1	38.9	26.5	89.6
HDTN	36.3	37.3	20.7	94.3
sd	*2.8*	*2.5*	*4.0*	*5.5*
TNTY	28.1	37.0	16.2	81.3
sd	*4.5*	*2.1*	*3.9*	*6.4*
WYTY	6.3	47.2	24.1	77.6
sd	*3.4*	*3.6*	*4.3*	*6.6*
HDTNWY	25.9	38.5	16.6	81.0
sd	*2.8*	*1.8*	*3.1*	*4.5*
HDTNTY	38.3	41.4	18.4	98.0
sd	*5.0*	*2.6*	*2.8*	*6.2*
HDWYTY	23.3	48.1	28.8	100.2
sd	*3.4*	*2.3*	*2.6*	*4.9*
TNWYTY	16.1	31.9	16.5	64.5
sd	*2.0*	*3.5*	*4.5*	*6.0*

6.4 Inversions throughout different time periods

This section looks into inversion results for different time periods as measurements within the two year data collection period (July 2012 - June 2014). Both Haddenham and Tacolneston recorded two full years of methane concentrations, whereas Weybourne and Tilney have shorter datasets (18 and 12 months, respectively). This section aims to assess results for the first year duration (2012-2013), and for the full duration period (2012-2014).

An inversion between 2012-2013 can only be run with Haddenham and Tacolneston data, for this reason the HDTN 2013-2014 inversion results should first be compared with the HDTNWYTY equivalent to see if any major differences occur. This can then help to identify possible reasons for differences in the 2012-2013 results. Section 6.3 showed that the HDTN emissions for NSC were relatively similar to the NAEI and four site emissions than to many of the two site combinations. Table 6.6 shows the regional emission totals for the four and two site inversions in 2013-2014. The discrepancy between the four and two site NSC totals lies solely in the Suffolk county (region 4), which has a higher value in the two site inversion than the four site. The other two regions (10 and 15) are nearly identical, although the finely resolved maps show differences in the emission

distributions, for example, the two site map shows higher emission north east of Haddenham and south of Weybourne but lower emissions from Norwich and to the east of Tacolneston (see Figure 6.10.B for the 2013-2014 two site emission map). These more finely resolved maps also show that these 'extra' emissions in region 4 originate from a coastal source directly to the east of Tacolneston. This area covers the Norfolk / Suffolk coastline and the Norfolk Broads. The four site inversion map (Figure 6.1) has a lower, more acutely resolved emission source which pinpoints more of a coastal emission rather than from the Norfolk Broads. Looking further afield, region 6 is not resolved at all with the two site inversion, and fails to pick up any emissions around the Wash or Boston, Lincolnshire. This area is located up wind of Tacolneston and Haddenham's prevailing wind direction, and a relatively great distance from the Haddenham observation site. It will therefore be less resolved than areas closer to the observation sites. This result allows for 2012-2013 inversions to be run with the knowledge that EA emissions should be reasonably robust compared to the four site equivalent when considering the county and regional totals.

Table 6.6: InTEM multiple year inversion county emission totals (kt yr^{-1}) from June 2012 to May 2014. Region label abbreviations: CBG - Cambridge, SFL - Suffolk, NFK - Norfolk, LDN - London, ESX - Essex, LCS - Lincolnshire, BHS - Bedfordshire / Hertfordshire, SW - Region to the south west (L-shaped). Regions 3, 7, 8 and 13 make up the border. Regions 9, 12 and 14 divide the sea. NSC = Norfolk (10) + Suffolk (4) + Cambridgeshire (15). Total does not include border regions.

	CBG	**NFK**	**SFK**	**LDN**	**ESX**	**LCS**	**Sea Regions**		
	15	**10**	**4**	**11**	**5**	**6**	**2**	**12**	**14**
NAEI	26.5	38.9	24.1	51.2	24.5	17.6	0.1	0.1	0.3
HDTNWYTY 2013-2014	20.5	37.1	22.8	45.7	19.6	9.1	0.2	0.1	0.4
sd	*2.1*	*1.7*	*1.9*	*18.0*	*8.1*	*4.1*	*0.6*	*0.1*	*1.2*
HDTN 2013-2014	20.7	37.3	36.3	88.3	13.8	3.4	0.1	0.4	0.1
sd	*4.0*	*2.5*	*2.8*	*24.6*	*9.0*	*3.9*	*0.2*	*0.5*	*0.2*
HDTN 2012-2013	24.6	19.5	41.1	123.5	6.2	0.2	0.5	0.3	28.1
sd	*3.6*	*2.4*	*3.6*	*15.5*	*6.5*	*0.4*	*0.1*	*0.9*	*42.4*
HDTNWYTY 2012-2014	21.5	30.0	33.7	71.4	14.5	9.2	0.2	0.1	0.1
sd	*3.1*	*2.0*	*4.5*	*27.6*	*6.9*	*11.7*	*1.1*	*0.2*	*0.1*
HDTN 2012-2014	24.5	24.8	37.8	105.4	7.9	0.5	0.5	1.8	0.1
sd	*3.9*	*2.8*	*4.2*	*26.7*	*7.2*	*1.0*	*2.7*	*10.9*	*0.2*

	BHS	**SW**	**Border Regions**				**Total**	**NSC**	**Cost Score**
	9	**1**	**3**	**7**	**8**	**13**			
NAEI	20.5	75.0	1.6	29.9	0.1	55.2	369.4	89.6	-
HDTNWYTY 2013-2014	30.6	124.5	116.1	240.0	53.6	294.9	310.5	80.4	12.5
sd	*7.3*	*59.2*	*1.0*	*7.1*	*16.1*	*43.1*	*63.0*	*3.3*	*0.0*
HDTN 2013-2014	29.4	98.0	191.8	279.2	115.4	328.6	327.8	94.3	14.7
sd	*2.5*	*51.6*	*6.9*	*8.2*	*7.3*	*46.4*	*59.2*	*5.5*	*0.0*
HDTN 2012-2013	33.4	132.2	256.3	301.5	22.6	159.7	460.8	85.2	15.2
sd	*7.7*	*33.8*	*5.7*	*7.8*	*9.9*	*36.3*	*115.7*	*5.7*	*0.0*
HDTNWYTY 2012-2014	29.6	113.9	129.8	247.1	46.0	284.3	324.0	85.2	13.3
sd	*6.4*	*56.8*	*3.0*	*21.2*	*8.7*	*47.7*	*65.2*	*5.8*	*0.0*
HDTN 2012-2014	32.0	82.0	226.9	292.7	91.6	271.0	317.4	87.2	13.3
sd	*6.6*	*40.8*	*22.0*	*5.8*	*15.8*	*29.9*	*51.4*	*6.4*	*0.0*

The region totals for the HDTN 2012-2013 inversion are found in Table 6.6. The overall NSC emissions have reduced by 10 % for the previous year

compared to 2013-2014, however the standard deviations do overlap. The county totals for 2012-2013 show a large decrease in Norfolk (region 10) whereas the Cambridgeshire and Suffolk differences (regions 15 and 4) are within their standard deviations. Figure 6.10.A shows the fine spatially resolved emission maps for the two site inversion during 2012-2013, and can identify where these changes have occurred. A decrease in emissions has occurred near Weybourne, Norwich, the Norfolk Broads, and King's Lynn (east of Tilney). It is difficult to identify whether this is a signal or arises from a methodological uncertainty.

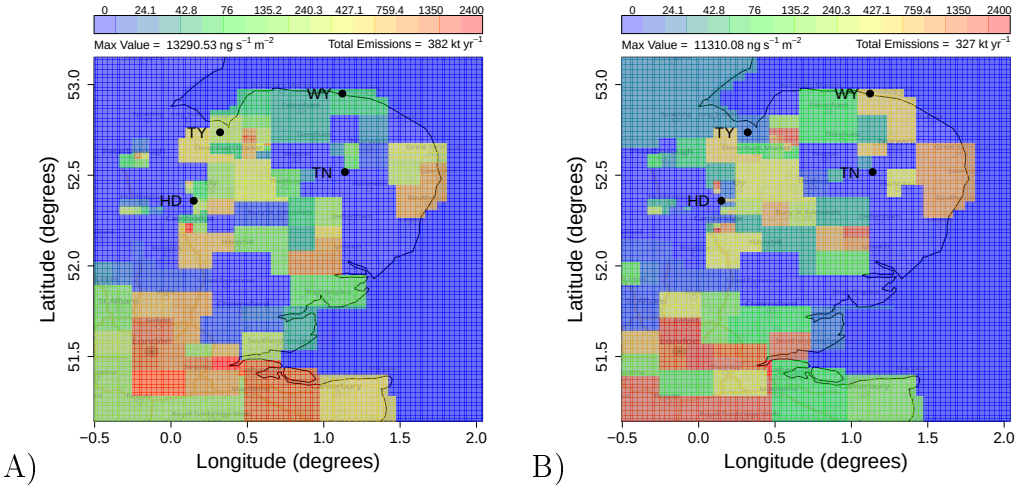

Figure 6.10: InTEM multiple year methane emission maps using Haddenham and Tacolneston observational data. A) June 2012 to May 2013, B) June 2013 to May 2014. Sites are labelled for reference: HD = Haddenham, TN = Tacolneston, WY = Weybourne, TY = Tilney.

Figure 6.11 shows histograms of different NAME meteorological variables normalised and separated into the two years for the Tacolneston site. The histograms show that 2012-2013 experienced colder temperatures and also slightly lower pressure values than 2013-2014. The average temperatures for 2012-2013 and 2013-2014 were 8.1 °C and 10.5 °C, respectively, with the average annual temperature of the EA region being between 9.5-10.5 °C (Met Office Website, 2015a). This 2012-2014 time period seems to compromise of an unusually cold year followed by a warmer than average year. Further analysis into temperature shows the differences observed between the two years were primarily in the winter and spring months. The winter of 2013-2014 saw an average temperature which was 2.6 °C warmer than the previous year (5.9 °C compared to 3.3 °C). Similarly, the spring of 2013-2014 saw an average temperature which was 1.6 °C warmer than the previous year (9.7 °C compared to 8.1 °C). The remaining seasons saw

an increase of 0.4 °C and 0.7 °C for Summer and Autumn, respectively. There is an increase in emissions from London (region 11) in the 2012-2013 compared to 2013-2014, which has a significant contribution from the 'offshore' source sector. As many methane sources are temperature dependent this could affect the emission values. A colder year would produce lower emissions in wetlands and possibly landfills. Conversely, colder years may also increase gas leakages from increased usage. Alternatively, a colder winter may have little impact on reducing biogenic sources as their productivity would be expected to be low already.

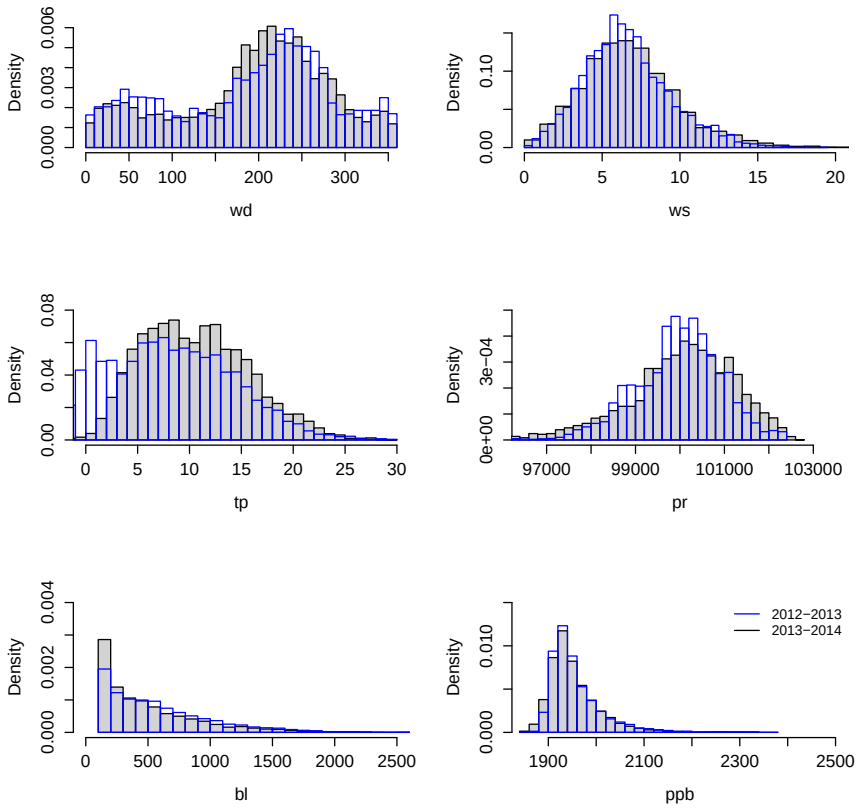

Figure 6.11: Histograms of the differences in meteorological data in 2012-2013 (blue line) and 2013-2014 (black line) for Tacolneston. wd = wind direction (°), ws = wind speed (m s^{-1}), tp = temperature (°C), pr = pressure (Pa), bl = boundary layer height (m)

The final part of this section describes resulting emission maps produced using the full two year dataset (2012-2014). These were run using both the two site and four site observations. The resulting county totals and emission maps are shown in Table 6.6 and Figure 6.12, respectively. The two and four site maps, both coarse and fine, show similar distributions and emission magnitudes in the

NSC region. This experiment assumes that emissions throughout this two year period are fixed. This is most-likely unrealistic but the aim of the experiment is to highlight any strengths and weaknesses to using two or four observation sites withing InTEM.

The limitation of using only two sites is highlighted in region 6 (Lincolnshire), which places near-zero methane emissions in this county. Interestingly, InTEM seems to require both Haddenham and Tilney data to resolve both Peterborough and Huntingdon emissions. Using just the Haddenham data produces much lower, more pinpointed emissions from these areas. This gives further evidence that London emissions are too distant from the measurement sites to be properly resolved and values remain too uncertain. The two year inversion NSC total, shown in Table 6.6, is higher than the four site 2013-2014 equivalents. These two year inversion maps distribute more emissions in Norfolk than in Suffolk, unlike what is seen in the 2013-2014 results (Figure 6.1). Although the NSC totals move closer to the NAEI emissions the individual county totals do not. The two year maps place lower emissions in Suffolk (region 4) and more in Norfolk (region 10). When looking at the more finely resolved maps in Figure 6.12 and Figure 6.1 these differences appear from a redistribution of emission from the east of Tacolneston to nearer the coast over Lowestoft, thus shifting from Norfolk to Suffolk. There is also an increase in emissions placed close to Ipswich. This area of emission is primarily dependent on observations from the Tacolneston site, as other sites are further away and up-wind from the prevailing wind direction. It would be interesting to analyse the influence of an additional site in south east EA on the resulting emissions in southern Suffolk. An observation site in this area would further resolve the eastern EA coast, as well as the London area (see further work Chapter 7 for more information). The differences observed in the individual year results shown above, and the two year inversion results could be driven by the different temperature ranges highlighted in Figure 6.11. However the complexity surrounding the methane sources' temperature dependance makes it difficult to determine this conclusively. Uncertainty associated with the inversion technique could also be driving these changes. Uncertainty and source sector issues could be analysed and addressed further with a longer dataset, as two years seems a prohibitively short period with which to make concrete conclusions about annual source variations.

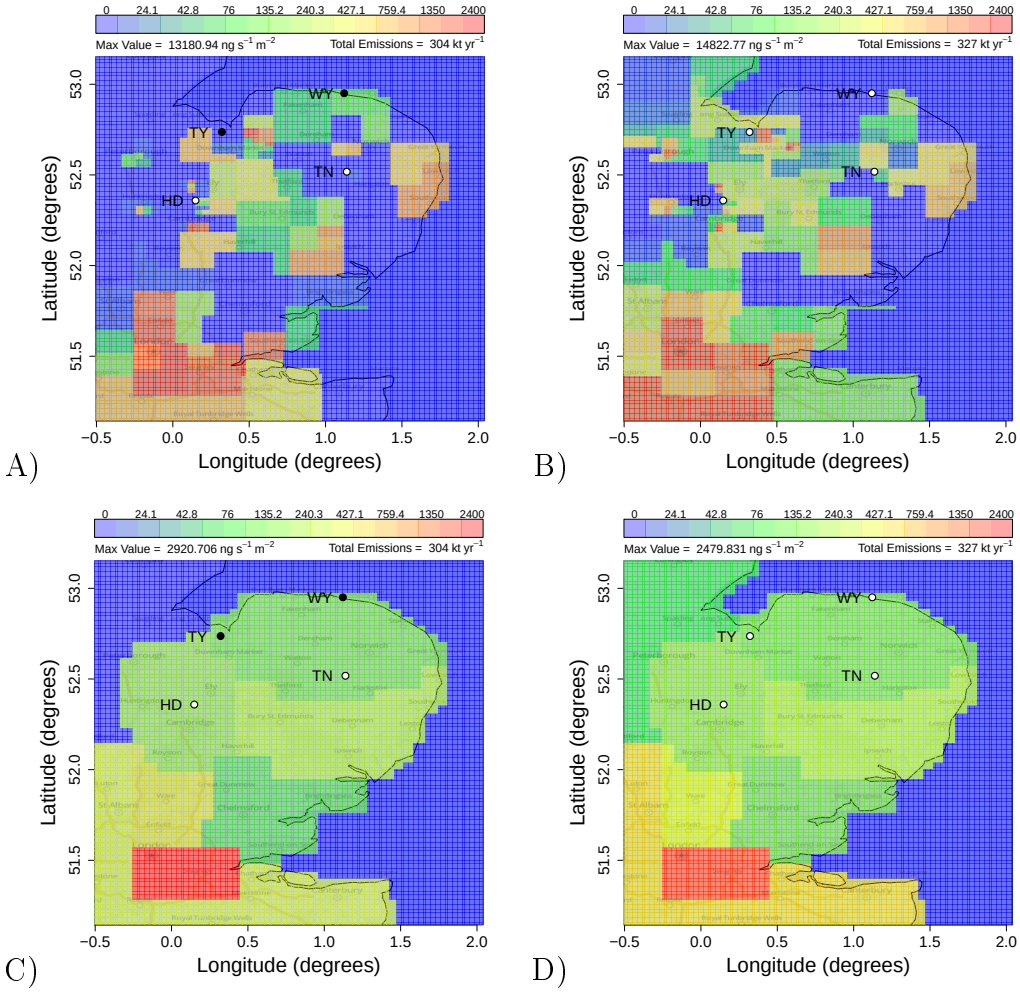

Figure 6.12: InTEM two year methane emission maps using Haddenham and Tacolneston observational data (A = fine, C = county resolution) and all four sites observational data (B = fine, D = county resolution). Sites are labelled for reference: HD = Haddenham, TN = Tacolneston, WY = Weybourne, TY = Tilney. Sites used within the InTEM setup is coloured white.

6.5 Sensitivity analysis of the Tacolneston site

This section looks at the sampling height at the Tacolneston site and its sensitivity on the inversion result. The primary motivation for this study was the significantly higher cost score that resulted from the single site inversion analysis in Section 6.3. The cost scores in Table 6.4 reflect a quantification of the difference between the pseudo- (modelled) and measured observations (Section 3.3.5). The two lowest scoring sites, Haddenham and Tilney, also have larger uncertainties associated with the measured concentrations. This is due to the impact of their local sources varying the hourly ppb standard deviations. The cost function used

in this analysis is an uncertainty-weighted function, which can produce lower cost scores when observations are more uncertain. The differences in the resulting cost scores could be an artifact of this cost function. An alternative reason could be that InTEM is failing to replicate the measured observations at Tacolneston. This could be due to the limited vertical transport representation within the NAME model. Tacolneston's measurement site is located higher than the other three sites (75 m compared to 15 - 25 m). This difference is incorporated into the NAME model and should be reflected in the resulting air history maps but the representation of vertical transportation within NAME's boundary layer scheme has been criticised (Meneguz and Thomson, 2014). For this reason the following sensitivity study was conducted.

6.5.1 Sensitivity of Tacolneston's sampling height

InTEM was run using NAME air history maps with a 150 m particle release height to assess the sensitivity of the sampling altitude in the NAME setup. This is double the altitude release height of the previous setup. The resulting regional totals for a Tacolneston-only and full four site inversion are shown in Table 6.7. This new setup produces higher methane emission estimates for NSC (regions 4, 10 and 15) but lower estimates for regions further away (regions 5, 6, 9 and 11). NSC emissions are 39 % higher than the equivalent single site InTEM run using the 75 m ±25 m particle release height at Tacolneston. This suggests the NAME air history maps have a more localised footprint when the sampling height is at a lower altitude. Increasing the NAME particle release height creates the assumption that the corresponding concentrations measured at Tacolneston have been diluted more from their emission source than for a particle release at 75 m. An increased emission rate would be a result from this increased dilution in order to still produce similar concentrations to what have been measured at Tacolneston.

The cost scores have slightly increased for both InTEM runs. This implies the observations are harder to be reproduced by InTEM than when the 75 m air history maps were used. This then suggests that the reported poor vertical transport setup in NAME is not responsible for the increased cost score seen in the Tacolneston-only inversion run. The reason why Tacolneston creates a higher cost score is therefore due to the lower uncertainty associated with its observations compared to other observation sites' equivalent values.

Table 6.7: InTEM regional emission totals (kt yr^{-1}) for a one year inversion from June 2013 to May 2014. Results compare the standard setup with an inversion using NAME air history maps released from Tacolneston at 150 m instead of 75 m. Region label abbreviations: CBG - Cambridge, SFL - Suffolk, NFK - Norfolk, LDN - London, ESX - Essex, LCS - Lincolnshire, BHS - Bedfordshire / Hertfordshire, SW - Region to the south west (L-shaped). Regions 3, 7, 8 and 13 make up the border. Regions 9, 12 and 14 divide the sea. NSC = Norfolk (10) + Suffolk (4) + Cambridgeshire (15). Total does not include border regions.

	CBG	**NFK**	**SFK**	**LDN**	**ESX**	**LCS**	**Sea Regions**		
	15	**10**	**4**	**11**	**5**	**6**	**2**	**12**	**14**
NAEI	26.5	38.9	24.1	51.2	24.5	17.6	0.1	0.1	0.3
TN	7.0	34.2	6.6	85.0	41.8	3.9	0.3	1.2	43.5
sd	*4.1*	*2.9*	*1.7*	*29.8*	*13.9*	*3.1*	*0.5*	*4.5*	*80.9*
TN (150 m)	8.2	47.0	11.4	47.8	34.0	1.6	0.7	5.7	0.1
sd	*8.0*	*2.6*	*4.1*	*23.1*	*10.5*	*2.3*	*4.0*	*19.1*	*0.2*
HDTNWYTY	20.5	37.1	22.8	45.7	19.6	9.1	0.2	0.1	0.4
sd	*2.1*	*1.7*	*1.9*	*18.0*	*8.1*	*4.1*	*0.6*	*0.1*	*1.2*
HDTNWYTY (150 m)	19.9	47.4	25.7	30.7	15.0	9.1	0.2	0.5	0.2
sd	*2.0*	*2.6*	*3.2*	*29.2*	*8.5*	*3.0*	*0.4*	*0.9*	*0.5*
	BHS	**SW**	**Border Regions**				**Total**	**NSC**	**Cost**
	9	**1**	**3**	**7**	**8**	**13**			**Score**
NAEI	20.5	75.0	1.6	29.9	0.1	55.2	369.4	89.6	-
TN	1.3	99.6	182.0	352.0	110.9	500.0	350.6	47.9	20.3
sd	*2.2*	*62.2*	*13.2*	*7.3*	*4.1*	*70.0*	*116.5*	*5.3*	*0.0*
TN (150 m)	0.7	142.2	150.5	374.7	104.2	0.6	299.2	66.6	21.9
sd	*0.7*	*76.1*	*38.2*	*9.3*	*12.9*	*0.07*	*83.1*	*9.4*	*0.0*
HDTNWYTY	30.6	124.5	116.1	240.0	53.6	294.9	310.5	80.4	12.5
sd	*7.3*	*59.2*	*1.0*	*7.1*	*16.1*	*43.1*	*63.0*	*3.3*	*0.0*
HDTNWYTY (150 m)	19.5	171.5	118.2	243.8	50.5	329.7	389.0	93.0	13.0
sd	*4.7*	*85.8*	*1.1*	*5.9*	*5.1*	*75.5*	*125.7*	*4.6*	*0.0*

The Tacolneston measurement site currently records methane concentrations at three altitudes: 54 m, 100 m and 150 m. As described in Chapter 2, this project used a combination of the two lower altitudes in its analysis. NAME released particles spanning these two heights averaging 75 m ±25 m. To investigate the sensitivity of the concentrations used within the inversion setup, InTEM was run using the 54 m and 100 m datasets with the 75 m NAME air history maps. Figure 6.13 shows the resulting fine resolution emission maps for these three datasets. Figure 6.14 shows the EA county totals plotted against sampling

altitude. The 54 m dataset is able to identify a more detailed local footprint than the other two sampling altitudes. There is also little difference between the regional totals of the 75 m and the 100 m emission maps in Figure 6.13. Figure 6.14 shows the NSC total divided into individual county estimates for the InTEM runs explained in this section, and mirrors the findings from Figure 6.13. NSC county totals are more similar in the 75 m and 100 m results, than the 54 m despite the 'merged' 75 m dataset having no bias towards either of the other values. Table 6.8 shows the concentration ranges in the three altitude datasets. The 'merged' 75 m dataset is almost a mean of the two other time series. The major difference for the NSC county estimates comes from the Suffolk country emissions, specifically on the East coast near Lowestoft and Southwold. The emission map of the 100 m dataset (Figure 6.13.C) shows a decrease in the spread of emissions compared to the other two maps (Figure 6.13.A and B). Interestingly, this altitude still produces very similar county totals to the 75 m results (Figure 6.14), however larger point-source emissions exist for the 100 m dataset. The 54 m results are most similar to the NAEI (EA total of 84 kt yr^{-1} compared to the NAEI's 89 kt yr^{-1}).

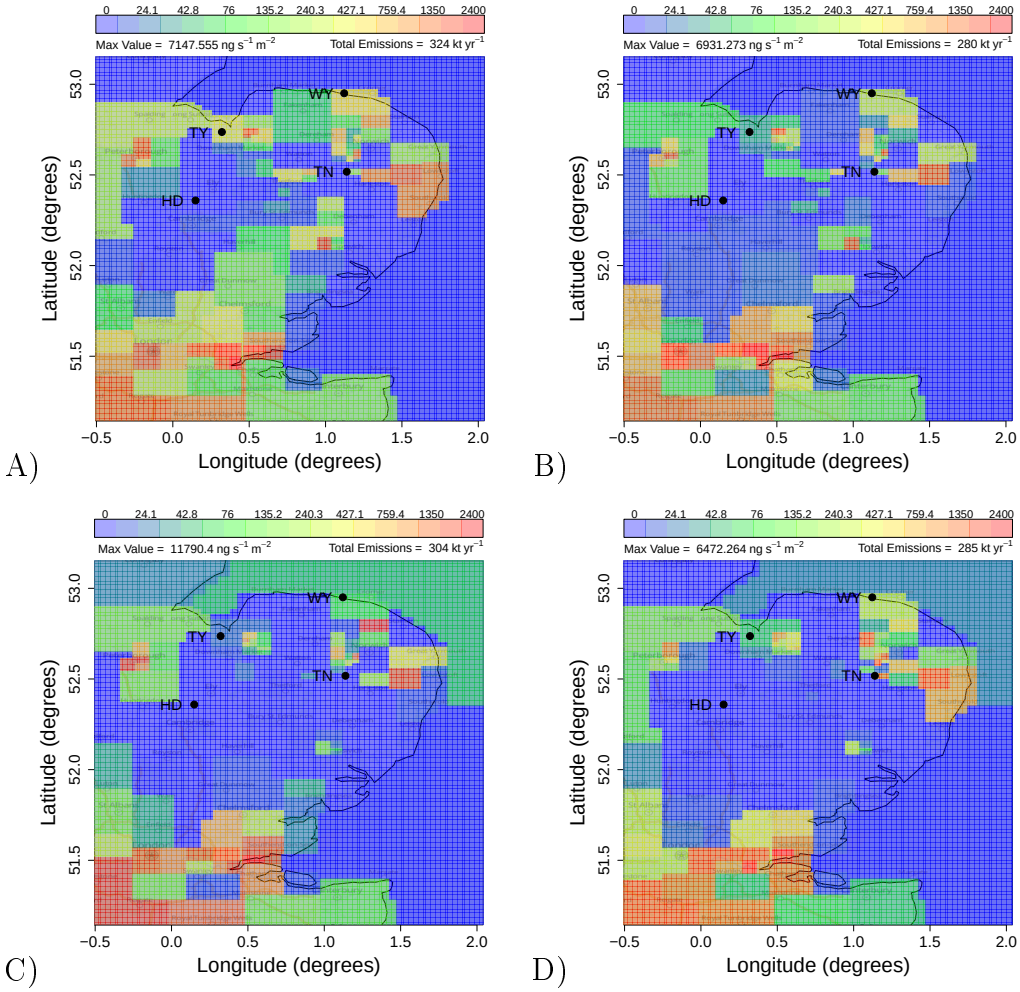

Figure 6.13: InTEM one year methane emission maps from June 2013 to May 2014 using different Tacolneston observational altitudes. A) 54 m, B) 75 m, C) 100 m, D) 100 m and NAME air history maps with a 150 m (±25 m) particle release height. Figures A-C use NAME air history maps with a 75 m (±25 m) particle release height. Sites are labelled for reference: HD = Haddenham, TN = Tacolneston, WY = Weybourne, TY = Tilney.

To estimate this sensitivity further, InTEM was run with the 100 m observations and the 150 m NAME air history maps. The resulting emission maps are shown in Figure 6.13.D which show similar aspects to both the 75 m and 100 m maps. Methane sources appear more dispersed and less localised (as seen in the 50 m map - Figure 6.13.A) but the emissions for Cambridge and Suffolk remain difficult to resolve (as seen in the 100 m map). The county totals for this final run in Figure 6.14 (labelled as 100b - Figure 6.13.C) shows that the increased altitude for the NAME air history maps has increased Suffolk emission estimates compared to the InTEM run using 100 m and 75 m NAME air history maps.

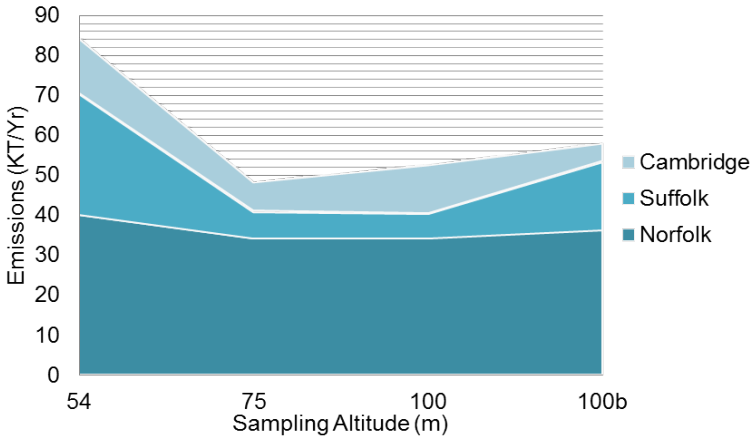

Figure 6.14: NSC emission totals split by county for InTEM emission estimates using Tacolneston observational data from different altitudes. 100b refers to InTEM run using the 100 m measurement dataset and NAME air history maps with a 150 m (±25 m) particle release height. The other three runs used NAME air history maps with a particle release height at Tacolneston of 75 m (±25 m).

Table 6.8: Concentration percentiles (ppb) for the three altitudes used in the Tacolneston analysis.

Altitude (m)	Percentile				
	5^{th}	25^{th}	50^{th}	75^{th}	95^{th}
54	1895	1920	1942	1980	2072
75	1894	1918	1940	1975	2062
100	1893	1917	1937	1970	2052
Average difference	0.8	1.5	2.5	5.1	10.2

This analysis suggests that tall tower measurement sites are somewhat limited at estimating regional emissions. The higher the sampling altitude, the more free tropospheric air, and therefore more air from further afield can be observed. It should be noted that consistent emission estimates for Norfolk were still produced using all three datasets but the sub-county emission distributions did vary.

6.5.2 Importance of boundary layer minimum height in NAME

A caveat of the above analysis lies in the default value assigned to the minimum boundary layer height in NAME. This is set to 100 m to be consistent with the defined 'surface influence' altitude range (0-100 m agl). 100 m was chosen to

de-weight local influences which occur on a sub-grid spatial scale within the UM meteorology (i.e. small-scale eddies). Below 100 m, local influences dominate on this scale. Relatively large errors in dispersion could propagate through to the trajectory and InTEM analysis as these influences are not fully represented in the UM meteorology. Areas of flat and low-lying topography can experience very low boundary layer heights (Stull, 1988). This is particularly prevalent at night when the boundary layer is already lower than during the day.

To assess the sensitivity of this minimum boundary layer height NAME analysis was rerun using a new minimum limit of 10 m. This recorded nocturnal boundary layer heights below 100 m were recorded 9 % of the time at Tacolneston during 2014. This accounted for 4 % of all observations at Tacolneston during this time period. With this NAME setup, datasets at 75 m and 100 m would experience more free tropospheric air, which could impact the InTEM results. If NAME underestimates the amount of free tropospheric air experienced at Tacolneston this could underestimate emissions inferred from this site's data. It is difficult to ascertain the impact this could have on results without running a full repeat of the Tacolneston analysis. This would have less of an impact at the other measurement sites as they rarely sample from above the boundary layer. Multiple site analysis has been proven to reduce individual site biases in Section 6.3, and thus any potential bias in Tacolneston's contribution to the four site estimates are hopefully minimised. To ensure this, it would be wise to rerun the NAME air history maps with a lower default minimum boundary layer height and the equivalent surface influence altitude range, however due to time constraints this was not possible for this thesis.

6.6 Summary

This chapter discussed the major results of this thesis. InTEM was run using the final setup described in Section 5.11 to estimate methane emissions for the East of England over various periods of time. Emission estimates were first produced using all four observation sites for a one year period between June 2013 and May 2014. These were compared to the 2012 NAEI which had been regridded onto the InTEM solution grid resolution. The fine resolution maps showed a similar distribution of methane emissions in both inventories but the individual magnitudes could vary, especially for point sources of methane, i.e. landfills. Particular differences between the InTEM and NAEI estimates

included the absence of emissions west of Haddenham in InTEM. This suggests the decommissioned landfills, which are estimated to still be high emitters of methane may not be as strong a source as the NAEI suggests. Emissions to the north east of Haddenham, which are present in the InTEM inventory but not the NAEI could also correspond to fenland emissions. These are not currently included in the NAEI. One final difference between the two inventories was a large source east of Tacolneston observed in InTEM but not the NAEI. This could correspond to biogenic emissions from the Norfolk Broads.

This section then regridded the fine spatial resolution emissions to the county-based regional estimates. This was to reduce uncertainties associated with the fine spatial resolution. The county regions showed that the two inventories complemented each other well in regions close to the observation sites. Regions further away from the observation sites produced estimates that were different to each other in InTEM and the NAEI. The Norfolk, Suffolk and Cambridge countries are estimated to produce 80.4 $\pm$3.3 kt yr^{-1} of methane for the period between June 2013 - May 2014 (NAEI equivalent of 89.6 kt yr^{-1}).

The following section (Section 6.2) assessed seasonal methane estimates, particularly focusing on the regions within EA (Norfolk, Suffolk and Cambridgeshire) and the London region. These regions showed opposing seasonal cycles which were thought to be due to the dominating source sectors within each region. The London region saw the most obvious seasonal cycle, with a maxima in winter and spring and a minima in summer.

Section 6.3 then focused on the sensitivity of the methane emission estimates when varying the number of sites included in the inversion setup. This section also focused its results mainly on the EA regions, which have been determined to be more robust and consistent throughout this analysis. Single site analysis showed each site had a 'footprint' which roughly corresponded to the county they were situated in. Relatively robust regional estimates of EA could be simulated using only two sites within InTEM but the individual county estimates could vary quite significantly. It also appeared that individual site biases would be reflected in the larger regional estimates. Care should be taken when choosing sites in future multiple site projects. Biases should be identified early so they can be taken into account in the analysis. The optimum number of sites was found to be dependent on the size of the region of interest.

Section 6.4 presented methane emission estimates for different periods of time. Estimates for the preceding year (June 2012 to May 2013) showed higher emissions

for EA. Estimates for a two year inversion from June 2012 to May 2014 showed estimates to be more similar to the 2012-2013 than the 2013-2014 emissions. Reasons for these differences were not easily identifiable. A longer dataset would possibly allow for a more thorough analysis of the interannual trends in methane emissions.

The final section (Section 6.5) of this chapter assessed the sensitivity of the Tacolneston sampling height in the InTEM setup. The Tacolneston only inversion produced much lower emission estimates than the other single site runs. A doubling of the sampling height in the NAME air history model runs produced emission estimates which were 39 % larger in the NSC region for the Tacolneston only InTEM estimates. This had a lower effect on the four site inversions which suggests that individual site biases are minimised when incorporated into a multiple site analysis. If the NAME vertical transport scheme can be trusted then this suggests that measurements taken at higher altitudes have a significantly lower footprint than sites at lower altitudes. The analysis within this section has the caveat that all NAME runs were conducted with a default minimum boundary layer height of 100 m. In this region of the UK the boundary layer height can reach lower levels, especially during the winter nocturnal hours. It was suggested that this analysis be rerun with a lower minimum boundary layer height for completeness, although little changes in the emission estimates from the four site InTEM run are expected.

7 Concluding discussion and further work

This chapter summarises the major results from this thesis. An overview of each chapter is discussed highlighting the main scientific findings. To conclude, this chapter then discusses the potential further work which could be conducted to develop the scientific findings from this thesis.

7.1 Overview

This thesis explains the development of a novel technique to estimate methane emissions at high spatial resolution. This inversion technique, named InTEM, incorporates in situ atmospheric methane measurements with computer dispersion modelling into a statistical method to infer methane emission estimates, via cost function analysis.

The first chapter gives an introduction to the atmosphere and the layers within it. Methane's major atmospheric chemical reactions are summarised and a detailed overview of its global sources and sinks is explained. The major techniques used to estimate regional and global methane budgets are divided into two distinct categories: bottom-up and top-down. Strengths and weaknesses exist for both techniques, which are described in Section 1.6. Chapter 1 concludes with a description of the UK National Atmospheric Emissions Inventory (NAEI) for methane.

Chapter 2 introduces the project upon which this thesis is based. Motivations for choosing East Anglia as a pilot region to develop this novel technique are explained, and the instrumental site locations are described. A detailed introduction to the methane sources within this region is then discussed. East Anglia is dominated by three main source sectors: waste, agriculture and offshore. The four sites are influenced by these sectors differently. Haddenham and Tilney

experience much large waste contributions whereas Tacolneston and Weybourne have a larger agricultural contribution.

Chapter 3 discusses in detail the instrumental setup and the modelling methods used throughout this project. Four measurement sites are used in the analysis of this thesis, which record atmospheric methane. All sites have GC-FID instruments installed with the exception of one, which uses a Picarro CRDS. A modelled representation of the physical atmospheric processes occurring at these sites is calculated using the UK Met Office's NAME model. So-called 'air history maps' are calculated for each instrument site for every hour observation throughout the measurement time period (July 2012 - June 2014). Both modelling data and measured observations are fed into the InTEM technique to produce the methane emission fields for the East of England. Strengths and weaknesses of InTEM's chosen cost function were also discussed in this chapter.

Chapter 4 is the first of the three results chapters. It gives a detailed analysis of the measured methane concentrations. Methane varies over different time frames and is dependent on numerous meteorological variables, particularly boundary layer height and wind speed. The NAEI emission can be converted to pseudo-observations using the NAME output. This analysis shows the NAEI has a reasonable distribution of methane emissions but the magnitudes do not directly compare to measured methane concentrations. The chapter concludes with a case study on the Haddenham site, which shows a comparison of modelled and measured meteorology using a SNAQ node. In addition, this section shows Haddenham is largely influenced by its local landfill sources. This is confirmed using correlation analysis with carbon dioxide, and isotopic analysis.

Chapter 5 focuses on the variables within the InTEM setup that influence the emission results. Sensitivity studies are conducted to ascertain the impact of these variables to establish a final setup. This final setup is formulated to ensure InTEM will produce robust and consistent emission estimates. Analysis shows that increasing the grid resolution improves the cost score but increases computer time. Chapter 5 highlights that care should be taken when considering an accurate estimation of uncertainty and how it varies temporally. Analysis shows that InTEM is sensitive to the starting regions defined before the solution grid is calculated. These sensitivities can be addressed, for example, ensuring regions of interest are central to the inversion domain and several 'buffer' regions exist to combat baseline issues.

The concluding results chapter applies a direct comparison of the final InTEM

emission results with the 2012 NAEI. County-scale methane emission estimates are produced for a one year period using all four observational sites. The methane emission estimates between the InTEM inventory and the NAEI are shown to be similar in regions close to the observation sites. The Norfolk, Suffolk and Cambridge counties are estimated to produce 80.4 ±3.3 kt yr^{-1} of methane for the period between June 2013 - May 2014 (NAEI equivalent of 89.6 kt yr^{-1}). Seasonal estimates are also estimated and qualitatively analysed. London is shown to have a seasonal cycle with a maxima in winter / spring, and a minima in summer. This could be due to the methane source sectors found in this region (large contributions from waste and the natural gas network). Multiple site sensitivity analysis shows that all four sites are necessary for the county methane estimates but regional estimates can be observed using a smaller selection of sites. Individual site biases were shown to have an impact on one-two site inversions but the four site results minimised these biases.

7.2 Further work

This section describes ways in which this study might have been improved or could be extended. It is split into two main areas of further work: the practical aspects of the project and the development of the scientific themes, which emerged during the analysis of this work.

7.2.1 Practical expansion of the network

The monitoring network is continuous and, to date, all four sites are still measuring atmospheric methane. This network can be expanded in several ways to develop our understanding of emissions in the East of England and beyond. Three main areas of development are listed and explained below.

- Longer measurement duration
- Increasing the number of measurement sites
- National scale inversions

The monitoring network at the date of this writing has three years of data from the Haddenham and Tacolneston sites. Weybourne and Tilney have been running for 28 and 25 months, respectively. The continual monitoring of these sites allows for future experiments to be conducted. Section 6.4 started to investigate

the inter-annual variability between methane emission estimates. Expanding the longevity of these measurements will enable this analysis to be developed further. Manning et al. (2011b) and DEFRA (2012) both report on the continuing decrease of UK methane emissions over the last two decades (-51 % relative to 1990). The continuation of this monitoring network will be able to serve as a verification for the conclusions drawn from this thesis.

Section 6.3 discussed the importance of the multiple site network in producing robust regional emission estimates. If fewer sites are included in the inversion then these estimates become less reliable. Similarly, estimates for areas further away from the full monitoring network proved less reliable and less consistent. This was highlighted with the estimates for central London (region 11). Figure 7.1 shows a map of the methane sites with two additional locations highlighted. Site 5, located to the south east of the map, shows a site installed on 14 November 2014 at Earl's Hall wind farm. The GC-FID instrument was installed in the base of the wind turbine with the inlet tube positioned half way up the turbine's shaft (~50 m). The close proximity to London would resolve emissions from this surrounding area. It would act as a verification or comparison to the current regional emissions. Site 6 in Figure 7.1 represents a fictional site whose installation would allow for further sensitivity analysis to be conducted in the NCS region. This site could help to ascertain a higher spatial resolution for this region. The current, four site network allows for local county scale estimates to be reported with confidence. Finer spatial resolution is less robust. The addition of this site would increase our understanding of this region's spatial resolution sensitivity as well as allowing a more quantified analysis to be conducted at this fine spatial resolution.

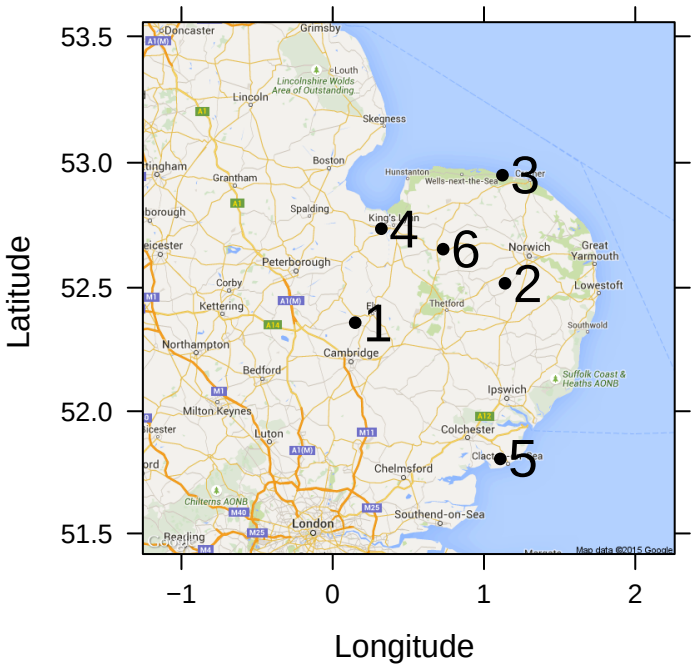

Figure 7.1: Map of the East of England methane monitoring network showing two additional sites. Site 5 is a GC-FID which was installed in Earl's Hall wind farm (November 2014). Site 6 represents a fictional location for an ideal future site to investigate further spatial sensitivity analysis. Original monitoring sites are 1) Haddenham 2) Tacolneston 3) Weybourne 4) Tilney.

A final way of expanding this network would be to increase the inversion to a national scale. Time constraints prevented national scale inversions to be estimated as this would have needed a reassessment of the baselines used to represent methane concentrations originating from outside the domain. Future work on this spatial scale could also incorporate other UK monitoring sites (for example, Ridgehill and Mace Head). These national estimates could then be directly compared to the equivalent results in the NAEI and Manning et al. (2011b). The EA region (including the county regions) could be compared to the regional estimates to see if any discrepancies are produced when the inversion domain size is changed.

7.2.2 Further development of the scientific investigation

This second section discussing future work concentrates on furthering the scientific investigation, which has been initially discussed in analysis throughout

this thesis. Figure 6.1 shows a potential source of methane from the fenland area north east of the Haddenham site. Haddenham, and to a lesser extent Tilney, experiences large influences from the local landfill point sources. Further analysis to more robustly identify and quantify these sources should be a future area of investigation. UK fenlands are not yet incorporated into the 'Nature' source sector in the NAEI. Landfills are also a highly uncertain and variable source of methane, which measurements at Haddenham have shown. The Haddenham site seems a prime location to further identify the emission strengths of these sources. One method of doing this would be to use longer datasets to constrain the inversion further and produce more robust emission estimates. Multiple years of data could also aid the seasonal analysis discussed in Section 6.2 to be more finely resolved.

Another method to identify these sources further would be to incorporate regular isotopic methane measurements at Haddenham (and ideally at all locations). The isotopic signatures of the landfills to the south of Haddenham were identified using whole air samples described in Section 4.6. If instruments capable of isotopic measurements with high temporal resolution could be installed at the sites then data could be filtered into different source sectors, for example, landfill and wetlands as they have different biogenic isotopic signals. Biogenic methane sources average between -55 to -70 ‰ (Dlugokencky et al., 2011). The landfills have been identified as having a signal at -58 ‰ whereas wetland signals are normally heavier (-60 ‰ to -65 ‰, Popp et al., 1999). InTEM could be run separately for each source sector to produce individual emission maps.

The final part of this section describes an alternative cost function which can be incorporated into InTEM to produce robust emission estimates for shorter time periods. The Bayesian approach incorporates the use of a prior emissions field to weight the calculated emission maps. The resulting cost function which is derived from Bayes' theorem is shown in Equation 7.2.1. Where x_a is the prior matrix, S_a is the error covariance matrix of the prior, K is the Jacobian matrix and S_ε is the error covariance matrix of all the observations

$$J(x) = (x - x_a)^T S_a^{-1}(x - x_a) + (y - Kx)^T S_\varepsilon^{-1}(y - Kx) \tag{7.2.1}$$

This thesis has shown the NAEI to be similar to our estimates on a county scale. The NAEI can therefore be 'trusted' to be used as a prior within this cost function. A Bayesian cost function can assign an estimation of uncertainty

to the prior emission field which constrains the inversion to within this range. This heightened constraint allows for shorter time periods of emissions to be estimated. Seasonal and even monthly emission estimates could be determined to analyse the intra-annual variability, which is currently unavailable with the NAEI. Areas where differences exist between the NAEI and InTEM estimates could be assigned larger uncertainties in the error covariance matrix of the prior (S_a), for example, the fenlands and the coastal area to the east of Tacolneston. Finally, further analysis into methane point sources, and their seasonality could be more thoroughly assessed through this cost function, i.e. landfills.

In addition to the Bayesian cost function, a hierarchical Bayesian inversion method has recently developed, where absolute uncertainty values associate with the priors and model are not needed and an assessment of the uncertainty is conducted within the inversion setup (Ganesan et al., 2014, 2015).

7.3 Summary

This final chapter gave a summary of the main highlights of this thesis. It then discussed potential areas of future work which could strengthen our current analysis and develop the scientific investigation. The areas for future work were divided into two sections: expanding the observation network and developing the scientific findings further.

Bibliography

AirLiquide: 2015, 'Air Liquide America Specialty Gases: Glossary'. `http://www.alspecialtygases.com/Rsc_glossary.aspx` [Accessed: 2015-06-15].

Ashfold, M. J., N. R. P. Harris, a. J. Manning, a. D. Robinson, N. J. Warwick, and J. a. Pyle: 2014, 'Estimates of tropical bromoform emissions using an inversion method'. *Atmospheric Chemistry and Physics* **14**(2), 979–994.

ATSDR: 2001, 'Landfill Gas Primer: An overview for Environmental Health Professionals'. Chapt. Chapter 2:, pp. 3–14.

Badr, O., S. Probert, and P. O'Callaghan: 1992, 'Methane: A greenhouse gas in the Earth's atmosphere'. *Applied Energy* **41**(2), 95–113.

Berchet, a., I. Pison, F. Chevallier, P. Bousquet, S. Conil, M. Geever, T. Laurila, J. Lavrič, M. Lopez, J. Moncrieff, J. Necki, M. Ramonet, M. Schmidt, M. Steinbacher, and J. Tarniewicz: 2013, 'Towards better error statistics for atmospheric inversions of methane surface fluxes'. *Atmospheric Chemistry and Physics* **13**(14), 7115–7132.

Bergamaschi, P., C. Frankenberg, J. F. Meirink, M. Krol, M. G. Villani, S. Houweling, F. Dentener, E. J. Dlugokencky, J. B. Miller, L. V. Gatti, A. Engel, and I. Levin: 2009, 'Inverse modeling of global and regional CH 4 emissions using SCIAMACHY satellite retrievals'. *Journal of Geophysical Research* **114**(D22), D22301.

Bergamaschi, P., M. Krol, F. Dentener, A. Vermeulen, F. Meinhardt, R. Graul, M. Ramonet, and W. Peters: 2005, 'Inverse modelling of national and European CH 4 emissions using the atmospheric zoom model TM5'. *Atmospheric Chemistry and Physics* **5**, 2431–2460.

Bergamaschi, P., M. Schupp, and G. W. Harris: 1994, 'High-precision direct measurements of and ratios in atmospheric methane sources by means of a long-path tunable diode laser absorption spectrometer'. *The Optical Society of America* **33**(33).

Bloss, W. J., M. J. Evans, J. D. Lee, R. Sommariva, D. E. Heard, and M. J. Pilling: 2005, 'The oxidative capacity of the troposphere: coupling of field measurements of OH and a global chemistry transport model.'. *Faraday discussions* **130**, 425–436; discussion 491–517, 519–524.

Bousquet, P., B. Ringeval, I. Pison, E. J. Dlugokencky, E.-G. Brunke, C. Carouge, F. Chevallier, A. Fortems-Cheiney, C. Frankenberg, D. a. Hauglustaine, P. B. Krummel, R. L. Langenfelds, M. Ramonet, M. Schmidt, L. P. Steele, S. Szopa, C. Yver, N. Viovy, and P. Ciais: 2011, 'Source attribution of the changes in atmospheric methane for 2006-2008'. *Atmospheric Chemistry and Physics* **11**(8), 3689–3700.

Bustamante, M., P. Smith, H. Ahammad, H. Clack, and H. Dong: 2014, 'IPCC WGIII: Chapter 11 Agriculture , Forestry and Other Land Use'.

Carslaw, D. and K. Ropkins: 2012, 'Openair - an R package for air quality data analysis.'. *Environmental Modelling & Software.* **27-28**(1364-8152), 52–61.

Chevillard, B. A., P. Ciais, U. T. E. Karstens, and M. Heimann: 2002, 'Transport of 222 Rn using the regional model REMO: a detailed comparison with measurements over Europe'. *Tellus* **54B**, 850–871.

Christensen, T. and N. Panikov: 2002, 'Biotic controls on CO2 and CH4 exchange in wetlands - a closed environment study'. *Biogeochemistry* pp. 337–354.

Christensen, T., I. Prentice, and J. Kaplan: 1996, 'Methane flux from northern wetlands and tundra'. *Tellus B*.

Christensen, T. R.: 2003, 'Factors controlling large scale variations in methane emissions from wetlands'. *Geophysical Research Letters* **30**(7), 1414.

Crutzen, P. and M. Andreae: 1990, 'Biomass Burning in the Tropics: Impact on Atmospheric Chemistry and Biogeochemical Cycles'. *Science (New York, N.Y.)* **250**(4988), 1669–1678.

Davies, T., M. J. P. Cullen, A. J. Malcolm, M. H. Mawson, A. Staniforth, A. A. White, and N. Wood: 2005, 'A new dynamical core for the Met Office's global and regional modelling of the atmosphere'. *Journal of Royal Meteorological Society* **131**(1), 1759–1782.

DEFRA: 2012, 'NAEI Pollutant information: Methane'. `http://naei.defra.gov.uk/overview/pollutants?pollutant_id=3` [Accessed: 2015-06-24].

DEFRA: 2015, 'NAEI Mapping Methodology'. `http://naei.defra.gov.uk/data/mapping` [Accessed: 2014-10-04].

Dlugokencky, E. J., E. G. Nisbet, R. Fisher, and D. Lowry: 2011, 'Global atmospheric methane: budget, changes and dangers.'. *Philosophical transactions. Series A, Mathematical, physical, and engineering sciences* **369**(1943), 2058–72.

Eggleston, S.: 2010, 'Expert Meeting on Uncertainty and Validation of Emission Inventories'. Utrecht, the Netherlands, Pub. IGES, Japan.

Eggleston, S., L. Buendia, and K. Miwa: 2006, 'IPCC guidelines for national greenhouse gas inventories'. *Institute for Global ...*.

Einola, J. K. M., R. H. Kettunen, and J. a. Rintala: 2007, 'Responses of methane oxidation to temperature and water content in cover soil of a boreal landfill'. *Soil Biology and Biochemistry* **39**(5), 1156–1164.

Elbern, H., A. Strunk, H. Schmidt, and O. Talagrand: 2007, 'Emission rate and chemical state estimation by 4-dimensional variational inversion'. *Atmospheric Chemistry and Physics* **7**, 3749–3769.

Ellutia: 2011a, '200 Series Gas Chromatograph'. `http://www.ellutia.com/200Series.html` [Accessed: 2012-06-20].

Ellutia: 2011b, '200 Series GC Manual: Cambridge University Special Engineered System'. Technical report.

Endresen, O. y.: 2003, 'Emission from international sea transportation and environmental impact'. *Journal of Geophysical Research* **108**(D17), 4560.

Environment Agency: 2015, 'What's in your backyard? Landfill Inventory'. `http://maps.environment-agency.gov.uk/wiyby/wiybyController?topic=waste&layerGroups=default&lang=_e&ep=map&scale=1&x=357683&y=355134` [Accessed: 2015-03-02].

EPA: 2006, 'Global Mitigation of Non-CO2 Greenhouse Gases'. Technical report, United States Environmental Protection Agency Office of Atmospheric Programs, Washington DC, USA.

EPA: 2008, 'Inventory of US Greenhouse Gas Emissions and Sinks 1990 to 2006'. Technical report, United States Environmental Protection Agency Office of Atmospheric Programs, Washington DC, USA.

Etiope, G., K. R. Lassey, R. W. Klusman, and E. Boschi: 2008, 'Reappraisal of the fossil methane budget and related emission from geologic sources'. *Geophysical Research Letters* **35**(9), L09307.

Etiope, G., G. Martinelli, A. Caracausi, and F. Italiano: 2007, 'Methane seeps and mud volcanoes in Italy: Gas origin, fractionation and emission to the atmosphere'. *Geophysical Research Letters* **34**(14), L14303.

European Environment Agency: 2012, 'Annual European Union greenhouse gas inventory 1990 - 2010 and inventory report 2012'. Technical Report 3, European Environment Agency, Brussels.

Fiore, A. M., J. J. West, L. W. Horowitz, V. Naik, and M. D. Schwarzkopf: 2008, 'Characterizing the tropospheric ozone response to methane emission controls and the benefits to climate and air quality'. *Journal of Geophysical Research: Atmospheres* **113**(8), 1–16.

Fischer, H., M. Behrens, M. Bock, U. Richter, J. Schmitt, L. Loulergue, J. Chappellaz, R. Spahni, T. Blunier, M. Leuenberger, and T. F. Stocker: 2008, 'Changing boreal methane sources and constant biomass burning during the last termination.'. *Nature* **452**(7189), 864–7.

Gabler, R. E., J. F. Petersen, M. Trapasso, and D. Sack: 2009, *Physical Geography*. Cengage Learning, 9th editio edition.

Ganesan, a. L., a. J. Manning, a. Grant, D. Young, D. E. Oram, W. T. Sturges, J. B. Moncrieff, and S. O'Doherty: 2015, 'Quantifying methane and nitrous oxide emissions from the UK and Ireland using a national-scale monitoring network'. *Atmospheric Chemistry and Physics* **15**(11), 6393–6406.

Ganesan, A. L., M. Rigby, A. J. Manning, R. G. Prinn, P. J. Fraser, and C. M. Harth: 2014, 'Characterization of uncertainties in atmospheric trace gas inversions using hierarchical Bayesian methods'. (1), 3855–3864.

Geels, C., M. Gloor, P. Ciais, P. Bousquet, P. Peylin, A. T. Vermeulen, R. Dargaville, T. Aalto, and J. Brandt: 2007, 'Comparing atmospheric transport models for future regional inversions over Europe-Part 1: mapping the atmospheric CO 2 signals'. *Atmospheric Chemistry and Physics* **7**, 3461–3479.

Grainger, C., T. Clarke, S. M. McGinn, M. J. Auldist, K. A. Beauchemin, M. C. Hannah, G. C. Waghorn, H. Clark, and R. J. Eckard: 2007, 'Methane Emissions from Dairy Cows Measured Using the Sulfur Hexafluoride (SF6) Tracer and Chamber Techniques'. *Journal of Dairy Science* **90**(6), 2755–2766.

Guinasso, N. and D. Schink: 1973, 'A simple physicochemical acoustic model of methane bubbles rising in the sea'. Technical report, Texas A and M University Technical Report, Dept. of Oceanography, Texas, USA.

Heard, I. P. C., A. J. Manning, J. M. Haywood, C. Witham, A. Redington, A. Jones, L. Clarisse, and A. Bourassa: 2012, 'and Sulphate Aerosol From Volcanic Eruptions'. *Journal of Geophysical Research* **117**, 1–15.

Hegde, U., T.-C. Chang, and S.-S. Yang: 2003, 'Methane and carbon dioxide emissions from Shan-Chu-Ku landfill site in northern Taiwan.'. *Chemosphere* **52**(8), 1275–85.

Herzberg, G.: 1945, *Molecular spectra and molecular structure. Vol.2: Infrared and Raman spectra of polyatomic molecules*. New York: Van Nostrand, Reinhold, 1 st edition.

Houweling, S. and F. Dentener: 2000, 'The modeling of tropospheric methane: How well can point measurements be reproduced by a global model?'. *Journal of ...* **105**(1999), 8981–9002.

Houweling, S., M. Krol, P. Bergamaschi, C. Frankenberg, E. J. Dlugokencky, I. Morino, J. Notholt, V. Sherlock, D. Wunch, V. Beck, C. Gerbig, H. Chen, E. a. Kort, T. Röckmann, and I. Aben: 2014, 'A multi-year methane inversion using SCIAMACHY, accounting for systematic errors using TCCON measurements'. *Atmospheric Chemistry and Physics* **14**(8), 3991–4012.

IPCC: 1996, 'Revised 1996 IPCC Guidelines for National Greenhouse Gas Inventories: Reference Manual'. Technical report, IPCC, Switzerland.

Jacob, D. J.: 2007, 'Lectures of Inverse modelling'.

Jacobson, M.: 2012, *Air Pollution and Global Warming. History, Science, and Solutions*. Cambridge University Press, 2nd editio edition.

Kaminski, T., P. J. Rayner, T. Kaminski, P. J. Rayner, M. Heimann, and I. G. Enting: 2001, 'On aggregation errors in atmospheric transport inversion On aggregation errors in atmospheric transport inversions'. *Journal of Geophysical Research: Letters* **106**, 4703–4715.

Keeling, D.: 1958, 'The concentration and isotopic abundances of atmospheric carbon dioxide in rural areas'. *Geochimica et Cosmochimica Acta* **13**(1), 322–334.

Keppler, F., M. Boros, C. Frankenberg, J. Lelieveld, A. McLeod, A. M. Pirttilä, T. Röckmann, and J.-P. Schnitzler: 2009, 'Methane formation in aerobic environments'. *Environmental Chemistry* **6**(6), 459.

Keppler, F., J. T. G. Hamilton, M. Brass, and T. Röckmann: 2006, 'Methane emissions from terrestrial plants under aerobic conditions.'. *Nature* **439**(7073), 187–91.

Kirschbaum, M. U. F. and A. Walcroft: 2008, 'No detectable aerobic methane efflux from plant material, nor from adsorption/desorption processes'. *Biogeosciences* **5**(6), 1551–1558.

Kirschke, S., P. Bousquet, P. Ciais, M. Saunois, J. G. Canadell, E. J. Dlugokencky, P. Bergamaschi, D. Bergmann, D. R. Blake, L. Bruhwiler, P. Cameron-Smith, S. Castaldi, F. Chevallier, L. Feng, A. Fraser, M. Heimann, E. L. Hodson, S. Houweling, B. Josse, P. J. Fraser, P. B. Krummel, J.-F. Lamarque, R. L. Langenfelds, C. Le Quéré, V. Naik, S. O'Doherty, P. I. Palmer, I. Pison, D. Plummer, B. Poulter, R. G. Prinn, M. Rigby, B. Ringeval, M. Santini, M. Schmidt, D. T. Shindell, I. J. Simpson, R. Spahni, L. P. Steele, S. a. Strode, K. Sudo, S. Szopa, G. R. van der Werf, A. Voulgarakis, M. van Weele, R. F. Weiss, J. E. Williams, and G. Zeng: 2013, 'Three decades of global methane sources and sinks'. *Nature Geoscience* **6**(10), 813–823.

Klauda, J. B. and S. I. Sandler: 2005, 'Global Distribution of Methane Hydrate in Ocean Sediment'. *Energy & Fuels* **19**(2), 459–470.

Kourtchev, I., S. Fuller, J. Aalto, T. M. Ruuskanen, M. W. McLeod, W. Maenhaut, R. Jones, M. Kulmala, and M. Kalberer: 2013, 'Molecular Composition of Boreal Forest Aerosol from Hyytiala, Finland, Using Ultrahigh Resolution Mass Spectrometry'. *Environmental Science & Technology* **47**(9), 4069–4079.

Kruger, M., H. Wolters, M. Gehre, S. B. Joye, and H.-h. Richnow: 2008, 'Tracing the slow growth of anaerobic methane-oxidizing communities by 15 N-labelling techniques'. *Federation of European Microbiological Societies* **63**, 401–411.

Kvenvolden, K. A.: 1988, 'Methane hydrates and global climate'. *Global Biogeochemical Cycles* **2**(3), 221–229.

Manning, A. and R. Derwent: 2006, 'Interpretation of longterm measurements of radiatively active trace gases and ozone depleting substances'. *Defra contract: CPEG1 quarterly report* (August).

Manning, A. C., E. G. Nisbet, R. F. Keeling, and P. S. Liss: 2011a, 'Greenhouse gases in the Earth system: setting the agenda to 2030.'. *Philosophical transactions. Series A, Mathematical, physical, and engineering sciences* **369**(1943), 1885–1890.

Manning, a. J.: 2003, 'Estimating European emissions of ozone-depleting and greenhouse gases using observations and a modeling back-attribution technique'. *Journal of Geophysical Research* **108**(D14), 4405.

Manning, A. J.: 2011, 'The challenge of estimating regional trace gas emissions from atmospheric observations.'. *Philosophical transactions. Series A, Mathematical, physical, and engineering sciences* **369**(1943), 1943–54.

Manning, a. J., S. O'Doherty, a. R. Jones, P. G. Simmonds, and R. G. Derwent: 2011b, 'Estimating UK methane and nitrous oxide emissions from 1990 to 2007 using an inversion modeling approach'. *Journal of Geophysical Research* **116**(D2), D02305.

Maryon, R. and F. Smith: 1991, 'The UK nuclear accident model'. *Progress in nuclear ...* **26**(2).

Mastepanov, M., C. Sigsgaard, E. J. Dlugokencky, S. Houweling, L. Ström, M. P. Tamstorf, and T. R. Christensen: 2008, 'Large tundra methane burst during onset of freezing.'. *Nature* **456**(7222), 628–30.

Maurice, C. and A. Lagerkvist: 2004, 'Assessment of the methane oxidation capacity of soil.'. *Waste management & research : the journal of the International Solid Wastes and Public Cleansing Association, ISWA* **22**(1), 42–48.

Mead, M., O. Popoola, G. Stewart, P. Landshoff, M. Calleja, M. Hayes, J. Baldovi, M. McLeod, T. Hodgson, J. Dicks, A. Lewis, J. Cohen, R. Baron, J. Saffell, and R. Jones: 2013, 'The use of electrochemical sensors for monitoring urban air quality in low-cost, high-density networks'. *Atmospheric Environment* **70**, 186–203.

Meirink, J. F., P. Bergamaschi, C. Frankenberg, M. T. S. D'Amelio, E. J. Dlugokencky, L. V. Gatti, S. Houweling, J. B. Miller, T. Röckmann, M. G. Villani, and M. C. Krol: 2008, 'Four-dimensional variational data assimilation for inverse modeling of atmospheric methane emissions: Analysis of SCIAMACHY observations'. *Journal of Geophysical Research* **113**(D17), D17301.

Meneguz, E. and D. J. Thomson: 2014, 'Parametrization of deep convection in NAME III'. Technical report, UK Met Office, Exeter.

Met.Office: 2015a, 'Eastern England: climate'. `http://www.metoffice.gov.uk/climate/uk/regional-climates/ee` [Accessed: 2015-06-12].

Met.Office: 2015b, 'Met Office Numerical Weather Prediction models'. `http://www.metoffice.gov.uk/research/modelling-systems/unified-model/weather-forecasting` [Accessed: 2015-06-02].

Milkov, A. V.: 2004, 'Global estimates of hydrate-bound gas in marine sediments: how much is really out there?'. *Earth-Science Reviews* **66**(3-4), 183–197.

Morgan, M. and M. Henrion: 1990, *Uncertainty: A Guide to Dealing with Uncertainty in Quantitative Risk and Policy Analysis*. New York, NY, USA.: Cambridge University Press.

NAEI: 2006, 'Greenhouse Gas Emissions Inventory Methodology'. `http://naei.defra.gov.uk/about/methodology` [Accessed: 2014-09-16].

ODoherty, S., A. Grant, A. Ganesan, D. Say, A. Stavert, R. G. Derwent, I. P. Simmonds, T. Modus, D. Young, U. E. A. S. Humphrey, D. Oram, B. Sturges, and A. J. Manning: 2014, 'Report to DECC: Long-term atmospheric measurements and interpretation (of radiatively active trace gases)'. Technical report, University of Bristol, Bristol.

Olivier, J. and J. Berdowski: 2014, 'Emission Database for Global Atmospheric Research (EDGAR), release version 4.1.'. `http://edgar.jrc.ec.europa.eu` [Accessed: 2015-02-02].

Pataki, D. E., J. R. Ehleringer, L. B. Flanagan, D. Yakir, D. R. Bowling, C. J. Still, N. Buchmann, J. O. Kaplan, and J. A. Berry: 2003, 'The application and interpretation of Keeling plots in terrestrial carbon cycle research'. *Global Biogeochemical Cycles* **17**(22), 1–14.

Patra, P. K., M. Krol, S. Montzka, T. Arnold, E. L. Atlas, B. R. Lintner, B. B. Stephens, B. Xiang, J. W. Elkins4, P. J. Fraser, A. Ghosh, E. J. Hintsa, D. F. Hurst, K. Ishijima, P. B. Krummel, K. M. B. R. Miller, F. L. Moore4, J. Muhle, S. O'Doherty, R. G. Prinn, L. P. Steele, M. Takigawa, R. F. W. , H. J. Wang, S. C. Wofsy, and D. Young: 2014, 'Observational evidence for interhemispheric hydroxyl-radical parity'. *Nature Letters* **513**, 219–223.

Popp, T. J., J. P. Chanton, G. J. Whiting, and N. Grant: 1999, 'Methane stable isotope distribution at a Carex dominated fen in north central Alberta'. *Global Biogeochemical Cycles* **13**(4), 1063–1077.

Prather, M., C. Holmes, and J. Hsu: 2012, 'Reactive greenhouse gas scenarios: Systematic exploration of uncertainties and the role of atmospheric chemistry'. *Geophysical Research Letters* **39**(9), L09803.

R Core Team: 2013, 'R: A Language and Environment for Statistical Computing'. R Foundation for Statistical Computing, Vienna, Austria. ISBN 3-900051-07-0.

Reay, D. S., P. Smith, and A. Van Amstel: 2010, *Methane and Climate Change*. London, Washington, DC: Earthscan, 1 st edition.

Reeburgh, W. S.: 2007, 'Oceanic methane biogeochemistry.'. *Chemical reviews* **107**(2), 486–513.

Riddick, S., S. Connors, A. Robbinson, and N. Harrie: 2015, 'Seasonality of methane emissions from landfill inferred using three emisison techniques.'. *In Preparation.*

Rigby, M., a. J. Manning, and R. G. Prinn: 2011, 'Inversion of long-lived trace gas emissions using combined Eulerian and Lagrangian chemical transport models'. *Atmospheric Chemistry and Physics* **11**(18), 9887–9898.

Rigby, M., R. G. Prinn, P. J. Fraser, P. G. Simmonds, R. L. Langenfelds, J. Huang, D. M. Cunnold, L. P. Steele, P. B. Krummel, R. F. Weiss, S. O'Doherty, P. K. Salameh, H. J. Wang, C. M. Harth, J. Mühle, and L. W. Porter: 2008, 'Renewed growth of atmospheric methane'. *Geophysical Research Letters* **35**(22), L22805.

Ringeval, B., N. de Noblet-Ducoudré, P. Ciais, P. Bousquet, C. Prigent, F. Papa, and W. B. Rossow: 2010, 'An attempt to quantify the impact of changes in wetland extent on methane emissions on the seasonal and interannual time scales'. *Global Biogeochemical Cycles* **24**(2), n/a–n/a.

Ryall, D. and R. Maryon: 1998, 'Validation of the UK Met Office NAME model against the ETEX dataset'. *Atmospheric Environment* **32**(24), 4265–4276.

Scheutz, C. and P. Kjeldsen: 2004, 'Environmental factors influencing attenuation of methane and hydrochlorofluorocarbons in landfill cover soils.'. *Journal of environmental quality* **33**(1), 72–79.

Scheutz, C., H. Mosbaek, and P. Kjeldsen: 2004, 'Attenuation of methane and volatile organic compounds in landfill soil covers.'. *Journal of environmental quality* **33**(1), 61–71.

Schmale, O.: 2005, 'Methane emission from high-intensity marine gas seeps in the Black Sea into the atmosphere'. *Geophysical Research Letters* **32**(7), L07609.

Schnell, R., A. Buggle, and R. Rosson: 2004, 'Climate Monitoring and Diagnostics Laboratory Summary Report No. 27'. Technical report, National Oceanic and Atmospheric Administration Oceanic and Atmospheric Research.

Smith, G. and B. Butcher: 2010, 'Greenhouse Gas Emissions Estimates for England's National Parks'. Technical report, English National Park Authorities Association.

Sneddon, S., N. Brophy, Y. Li, J. MacCarthy, C. Martinez, T. Murrels, N. Passant, J. Thomas, G. Thistlethwaite, I. Tsagatakis, H. Walker, A. Thomson,

and L. Cardenas: 2015, 'Greenhouse Gas Inventories for England, Scotland, Wales and Northern Ireland: 1990-2008'. Technical report, RICHARDO-AEA.

Solomon, S., D. Qin, M. Manning, Z. Chen, M. Marquis, K. Averyt, M. Tignor, and H. Miller: 2007, 'IPCC, 2007: Summary for Policymakers. Climate Change 2007: The Physical Science Basis. Contribution of Working Group I to the Fourth Assessment Report of the Intergovernmental Panel on Climate Change'. *Climate Change*.

Stocker, B. D., R. Roth, F. Joos, R. Spahni, M. Steinacher, S. Zaehle, L. Bouwman, and I. C. Prentice: 2013a, 'Multiple greenhouse-gas feedbacks from the land biosphere under future climate change scenarios'. *Nature Climate Change* **3**(7), 666–672.

Stocker, T., D. Qin, G.-K. Plattner, M. Tignor, S. K. Allen, J. Boschung, A. Nauels, Y. Xia, B. V., and Midgley P.M.: 2013b, 'IPCC, 2013: Summary for Policymakers. Climate Change 2013: The Physical Science Basis. Contribution of Working Group I to the Fifth Assessment Report of the Intergovernmental Panel on Climate Change'. *Climate Change*.

Stohl, A.: 1998, 'Computation, accuracy and applications of trajectories - A review and bibliography'. *Atmospheric Environment* **32**(6), 947–966.

Stull, R.: 1988, *An Introduction to Boundary Layer Meteorology*. Kluwer Academic Publishers.

Sugimoto, A., T. Inoue, N. Kirtibutr, and T. Abe: 1998, 'Methane oxidation by termite mounds estimated by the carbon isotopic composition of methane'. *Global Biogeochemical Cycles* **12**(4), 595–605.

Texier, J., J. Huxtable, E. Rhodes, D. Miallier, and M. Ousmoi: 1988, 'New data on the chronological situation of the Aterian of Morocco and their implications'. *Comptes rendus de l'Académie des sciences. Série 2, Mécanique, Physique, Chimie, Sciences de l'univers, Sciences de la Terre* **307**(7), 827–832.

Thompson, R. L., C. Gerbig, and C. Rödenbeck: 2011, 'A Bayesian inversion estimate of N2O emissions for western and central Europe and the assessment of aggregation errors'. *Atmospheric Chemistry and Physics* **11**(7), 3443–3458.

Turner, A. J. and D. J. Jacob: 2015, 'Balancing aggregation and smoothing errors in inverse models'. pp. 7039–7048.

Vigano, I., H. van Weelden, R. Holzinger, F. Keppler, A. McLeod, and T. Röckmann: 2008, 'Effect of UV radiation and temperature on the emission

of methane from plant biomass and structural components'. *Biogeosciences* **5**(3), 937–947.

Voulgarakis, a., V. Naik, J.-F. Lamarque, D. T. Shindell, P. J. Young, M. J. Prather, O. Wild, R. D. Field, D. Bergmann, P. Cameron-Smith, I. Cionni, W. J. Collins, S. B. Dalsø ren, R. M. Doherty, V. Eyring, G. Faluvegi, G. a. Folberth, L. W. Horowitz, B. Josse, I. a. MacKenzie, T. Nagashima, D. a. Plummer, M. Righi, S. T. Rumbold, D. S. Stevenson, S. a. Strode, K. Sudo, S. Szopa, and G. Zeng: 2013, 'Analysis of present day and future OH and methane lifetime in the ACCMIP simulations'. *Atmospheric Chemistry and Physics* **13**(5), 2563–2587.

Wassmann, R., H. U. Neue, R. S. Lantin, K. Makarim, N. Chareonsilp, L. V. Buendia, and H. Rennenberg: 2000, 'Characterization of methane emissions from rice fields in Asia . II . Differences among irrigated , rainfed , and deepwater rice'. *Nutrient Cycling in Agroecosystems* **58**, 13–22.

Wavemetrics: 2012, 'IGOR Pro Version6.3'.

Wayne, R.: 1991, *Chemistry of Atmospheres*. Oxford: Clarendon Press, Oxford (UK.

Webb, N., M. Broomfield, P. Brown, G. Buys, and L. Cardenas: 2014, 'UK greenhouse gas inventory 1990 to 2012: Report to UNFCCC'. Technical Report April.

Weller, R. and S. Stage: 1988, 'The Frontal Air-Sea Interaction Experiment(Fasinex)'. *... on Ocean-Atmosphere Interaction, 7 th, Anaheim, CA*.

Wetter Zentrale: 2015, 'Wetter Zentrale: Synotpic Weather Charts'.

Wilson, I. a. G., A. J. R. Rennie, Y. Ding, P. C. Eames, P. J. Hall, and N. J. Kelly: 2013, 'Historical daily gas and electrical energy flows through Great Britain's transmission networks and the decarbonisation of domestic heat'. *Energy Policy* **61**, 301–305.

Witham, C. and A. Manning: 2007, 'Impacts of Russian biomass burning on UK air quality'. *Atmospheric Environment* **41**(37), 8075–8090.

Wuebbles, D. J. and K. Hayhoe: 2002, 'Atmospheric methane and global change'. **57**(x), 177–210.

Zazzeri, G., D. Lowry, R. Fisher, J. France, M. Lanoisellé, and E. Nisbet: 2015, 'Plume mapping and isotopic characterisation of anthropogenic methane sources'. *Atmospheric Environment* **110**, 151–162.

Zimmerman, P. R.: 1982, 'Termites, a potentially large source of atmospheric methane'. *Science (New York, N.Y.)* **218**(4572), 563–565.